NASA / TM-2001-211046

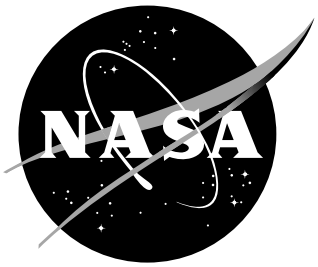

On Multifunctional Collaborative Methods in Engineering Science

Jonathan B. Ransom
Langley Research Center, Hampton, Virginia

September 2001

The NASA STI Program Office ... in Profile

Since its founding, NASA has been dedicated to the advancement of aeronautics and space science. The NASA Scientific and Technical Information (STI) Program Office plays a key part in helping NASA maintain this important role.

The NASA STI Program Office is operated by Langley Research Center, the lead center for NASA's scientific and technical information. The NASA STI Program Office provides access to the NASA STI Database, the largest collection of aeronautical and space science STI in the world. The Program Office is also NASA's institutional mechanism for disseminating the results of its research and development activities. These results are published by NASA in the NASA STI Report Series, which includes the following report types:

- TECHNICAL PUBLICATION. Reports of completed research or a major significant phase of research that present the results of NASA programs and include extensive data or theoretical analysis. Includes compilations of significant scientific and technical data and information deemed to be of continuing reference value. NASA counterpart of peer-reviewed formal professional papers, but having less stringent limitations on manuscript length and extent of graphic presentations.

- TECHNICAL MEMORANDUM. Scientific and technical findings that are preliminary or of specialized interest, e.g., quick release reports, working papers, and bibliographies that contain minimal annotation. Does not contain extensive analysis.

- CONTRACTOR REPORT. Scientific and technical findings by NASA-sponsored contractors and grantees.

- CONFERENCE PUBLICATION. Collected papers from scientific and technical conferences, symposia, seminars, or other meetings sponsored or co-sponsored by NASA.

- SPECIAL PUBLICATION. Scientific, technical, or historical information from NASA programs, projects, and missions, often concerned with subjects having substantial public interest.

- TECHNICAL TRANSLATION. English-language translations of foreign scientific and technical material pertinent to NASA's mission.

Specialized services that complement the STI Program Office's diverse offerings include creating custom thesauri, building customized databases, organizing and publishing research results ... even providing videos.

For more information about the NASA STI Program Office, see the following:

- Access the NASA STI Program Home Page at *http://www.sti.nasa.gov*

- E-mail your question via the Internet to help@sti.nasa.gov

- Fax your question to the NASA STI Help Desk at (301) 621-0134

- Phone the NASA STI Help Desk at (301) 621-0390

- Write to:
  NASA STI Help Desk
  NASA Center for AeroSpace Information
  7121 Standard Drive
  Hanover, MD 21076-1320

NASA / TM-2001-211046

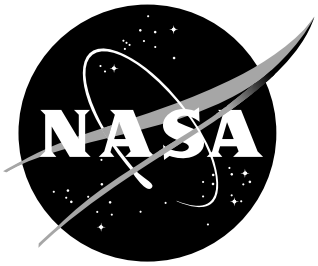

On Multifunctional Collaborative Methods in Engineering Science

Jonathan B. Ransom
Langley Research Center, Hampton, Virginia

National Aeronautics and
Space Administration

Langley Research Center
Hampton, Virginia 23681-2199

September 2001

Available from:

NASA Center for AeroSpace Information (CASI)
7121 Standard Drive
Hanover, MD 21076-1320
(301) 621-0390

National Technical Information Service (NTIS)
5285 Port Royal Road
Springfield, VA 22161-2171
(703) 605-6000

ABSTRACT

Engineers are challenged to produce better designs in less time and for less cost. Hence, to investigate novel and revolutionary design concepts, accurate, high-fidelity data must be assimilated rapidly into the design, analysis and simulation process. This data assimilation should consider diverse mathematical modeling and multi-discipline interactions necessitated by concepts exploiting advanced materials and structures. Integrated high-fidelity methods with diverse engineering applications provide the enabling technologies to assimilate these high-fidelity, multi-disciplinary data rapidly at an early stage in the design. These integrated methods must be multifunctional, collaborative and applicable to the general field of engineering science and mechanics.

Multifunctional methodologies and analysis procedures are formulated for interfacing diverse domain idealizations including multi-fidelity modeling methods and multi-discipline analysis methods. These methods, based on the method of weighted residuals, ensure accurate compatibility of primary and secondary variables across the domain interfaces. Methods are developed for scalar-field and vector-field problems in engineering science with extensions to multidisciplinary problems. Results are presented for the scalar- and vector-field developments using example patch test problems. In addition, results for torsion, thermal, and potential flow problems are presented to demonstrate further the effectiveness of the scalar-field development. Results for plane stress and plane flow problems are presented for the vector-field development. Results for all problems presented are in overall good agreement with the exact analytical solution or the reference numerical solution.

The multifunctional methodology presented provides an effective mechanism by which domains with diverse idealizations are interfaced. This capability rapidly provides the high-fidelity data needed in the early design phase. Moreover, the capability is applicable to the general field of engineering science and mechanics. Hence, it provides a collaborative capability that accounts for interactions among engineering analysis methods.

TABLE OF CONTENTS

Page

Page

Chapter

LIST OF TABLES

LIST OF FIGURES

Figure Page

Figure Page

CHAPTER I

INTRODUCTION

1.1. MOTIVATION

The analysis of revolutionary aerospace and ground vehicles relies heavily on accurate, efficient and robust computational methodologies such as the finite element and finite difference methods. To investigate novel and revolutionary design concepts, accurate, high-fidelity data must be assimilated rapidly into the design, analysis and simulation process. This data assimilation should consider mathematical modeling approximations ranging from simple handbook equations, empirically derived relations, spreadsheets, and design charts to complex continuous and discrete simulation models. In addition, the data assimilation needs to consider associated multi-discipline interactions necessitated by advanced design concepts exploiting multifunctional materials and leading to multifunctional structures. Rapid discipline-centric modeling techniques allow high-fidelity design trades between cost and performance, and based on the insight provided by these simulations, design uncertainties and risk assessment may be evaluated. Integrated multi-discipline analyses allow the assessment of the effects of multidisciplinary coupling on the system response. New computing systems and alternative computing strategies have presented new opportunities for optimal design, analysis, and simulation of aerospace systems. However, integrated high-fidelity methods with diverse engineering applications provide the enabling technologies to assimilate high-fidelity, multi-disciplinary data rapidly at an early stage in the design.

The journal model for this dissertation is the AIAA Journal.

These integrated methods must be multifunctional, collaborative and applicable to the general field of engineering science and mechanics.

To understand the impact of these integrated methods, the three concomitant attributes, namely, multifunctional, collaborative, and engineering science and mechanics, must be described. In the context of this work, multifunctional characterization has been adopted from the description of new and innovative materials and structures with multiple capabilities. These systems, referred to as multifunctional materials and structures, respectively, have several desirable simultaneous properties and many diverse disciplinary applications. The systems will adapt, react and evolve in changing environments, and their use will result in a combined system with enhanced capabilities at less cost and weight. Likewise, multifunctional methods refer to computational methodologies that have multiple capabilities such as multiple fidelity modeling, multiple approximation analysis and multidisciplinary analysis. The methods are computationally efficient while preserving solution accuracy and are applicable to a wide range of applications in engineering science. Their use in the combined analysis of complex configurations promises to provide enhanced computational and engineering capability at less cost and in less time. With these attributes, a multifunctional method may address the diverse modeling and analysis needs of evolving systems perhaps using a hierarchical approach including error analysis and risk assessment.

The collaborative aspect of the computational methods provides a mechanism by which two or more physical domains are integrated or interfaced and by which two or more methods or algorithms are shared or interfaced. It is through this interfacing that the diverse attributes create a unified framework that far exceeds the capability of an

individual method. Collaborative methods may integrate domains of different discretization fidelity, analysis approximations, or disciplines. An example of a collaborative method is adaptive dynamic relaxation. Explicit direct time integration algorithms are well-known for their computational efficient, low-memory requirements, low computational cost per solution step and direct mapping to massively parallel processing (MPP) systems. Adaptive dynamic relaxation techniques exploit these features to determine the quasi-static or steady-state response of a structure without relying on traditional methods requiring the solution of the large sparse matrices. Collaborative methods provide a mechanism by which the aggregate cost savings related to computational and modeling requirements are reduced, and analyses, previously intractable, may be performed. As in the case of the multifunctional materials or structures, these methods adapt, react and evolve in the changing environments of engineering science. Engineering science covers the broad perspective of engineering and includes the integrated application of engineering principles, science, mathematics, numerical analysis and non-deterministic methods. Problems in fluid flow, solid mechanics, thermal analysis, and constitutive modeling are representative of those in engineering science. Engineering science has a multidisciplinary emphasis, and future methods applicable to the field should possess multifunctional characteristics and a collaborative nature to further enhance their analysis capabilities and to advance the state-of-the-art in engineering design.

Multifunctional collaborative methods should address four typical steps of analysis and design, namely, (1) representation or modeling of the geometry, (2) knowledge-based selection and development of appropriate mathematical models (*i.e.*,

idealization/discretization), (3) solution of the mathematical model (continuous and/or discrete), and (4) interrogation/assessment of the results. These steps are briefly outlined in Appendix A. Methodology and analysis procedures that address these basic steps provide the foundation for enhanced integrated design and analysis tools within the realm of engineering science. Such multifunctional methodology should allow interaction between and collaboration with the analyst and designer, among different mathematical modeling approximations of the physical phenomena, and among multiple engineering disciplines. A major feature of the methodology is the transfer of data across the respective interface, whether the interface is one among diverse mathematical approximations or among diverse disciplines. Computational issues associated with individual modeling approaches and disciplines are magnified in number and significance due to the intricate couplings manifesting themselves as a by-product of their interfacing.

Multi-fidelity modeling approaches provide benefits in all of the major steps of analysis and simulation. These approaches are often characterized by the use of different approximations among multiple domains of the same continua and multiple domains involving different continua (*e.g.*, fluid-structure interaction). Analytical and closed-form solutions for specific geometries and configurations are often used to eliminate constraints placed on the analysis due to geometry considerations. Rapid modeling approaches facilitate the discretization of geometry by providing a capability to model regions of interest, independently, increasing the discretization fidelity or enhancing the mathematical approximation only in the desired domains. Thus, for multi-fidelity finite element modeling approaches, complex and often unsuitable mesh transitioning, generated manually or using automatic mesh generators, is limited. In addition, multi-

fidelity approaches have been developed that allow for the discretization of parts or components across geographically dispersed locations with minimal concern for the discretization of the parts along common boundaries or interfaces. Additional research has provided for accommodation of slight anomalies in the geometric representation provided by the independently discretized parts as well as parametric definition of the interface geometry between parts. Multi-fidelity modeling approaches benefit the solution of the discretized system in that the system size using a multi-domain approach for global/local modeling may be smaller for a given level of solution accuracy than the system obtained by standard practices. In addition, in component modeling, the associated matrices may be reduced by static condensation, which reduces the size and subsequent solution time of the overall system of equations. Multi-fidelity modeling approaches allow for the visualization and interrogation of the results only in regions of interest. Post-processing of secondary results such as stresses and failure parameters may be isolated to these regions and dynamically computed as the need arises. By reducing the modeling, computational and visualization time of simulations of aerospace structures, multi-fidelity modeling approaches promise to enhance the viability of high-fidelity analyses early in the design process.

Multidisciplinary coupling approaches involve the interfacing of different disciplines to account for their interactions and impact on the overall system response. There are myriad approaches, for example, any combination of approaches that couple the fluids, thermal, structures, and acoustic disciplines. The traditional independent approach for multidisciplinary analysis involves loosely coupling the disciplines through sequential execution of single discipline analyses. Typically this approach requires

several iterations among the different analysis methods and analysts and is relatively inefficient because the discipline specific models are generally incompatible and require extensive post-processing after each single discipline analysis to transfer (or interface) data to the next analysis model. Aeroelastic analysis as an interdisciplinary problem, requires the coupling of the aerodynamic and structural responses. The use of different spatial discretization procedures and potentially different mathematical modeling approximations for the aerodynamic model and the structures model gives rise to the interfacing problem of transferring computed data between the two grid systems. Moreover, the same issues are prevalent in fluid-thermal-structural analyses and structural-acoustic analyses. Suitable methodology for addressing these types of interfacing problems has been developed by many researchers.

The overarching purpose of this research is to investigate multifunctional collaborative methods, as described herein, that address the engineering design and analysis needs of multidisciplinary problems in engineering science. This research focuses on the fundamental relationships among underlying engineering science and mechanics principles, computational methods and multi-fidelity models, and methods using basic problems from continuum mechanics. Given its broad applicability with respect to the field of engineering science, continuum mechanics forms the foundation for the multifunctional collaborative methods developed in this work. Hence, for completeness and to establish notation, basic concepts of continuum mechanics are presented briefly in the next section.

1.2. CONTINUUM MECHANICS FOUNDATIONS

Continuum mechanics is the branch of physical sciences concerned with the deformations and motions of continuous material media under the influence of external effects[1]. The effects that influence the bodies appear in the form of forces, displacements, and velocities which arise from contact with other bodies, gravitational forces, thermal changes, chemical interactions, electromagnetic effects, and other environmental changes. In this work, bodies subject to forces of mechanical origin and/or thermal changes are of primary concern. General principles in the form of integral or differential equations govern the deformation and motion of the continuum. Hence, approximation methods and associated concepts are introduced in addition to the basic concepts of continuum mechanics.

1.2.1. General Principles of Continuous Media

A medium can be generally categorized as a fluid or a solid. A fluid can be loosely defined as a continuum that does not require external forces to maintain its deformed shape. When highly compressible it is called a gas and when essentially incompressible, it is called a liquid. A solid can be loosely defined as a continuum that requires external forces to maintain its deformed shape. According to its behavior, a solid may be called elastic, plastic, viscoelastic, thermoelastic, etc. Usually it is assumed to have a uniform density[2]. When a medium deforms, the small volumetric elements change position by moving along space curves. Their positions as functions of time can be specified either by the Lagrangian ($X_i = X_i(x_i, t)$ for i=1, 2, 3) or Eulerian description ($x_i = x_i(X_i, t)$). In the Lagrangian description, each particle is tracked in terms of its initial position with respect to a fixed reference system, X_i, and time. In the

Eulerian description, the motion is expressed in terms of the instantaneous position vector with respect to a moving reference system, x_i, and time.

Classical continuum mechanics rests upon equations expressing the balances of mass, linear momentum, angular momentum, energy, and entropy in a moving body[3]. These balance laws apply to all material bodies, whether fluid or solid in composition, and each gives rise to a field equation. These balance laws are as follows:

i. Principle of conservation of mass

ii. Principle of conservation of linear momentum

iii. Principle of conservation of angular momentum

iv. Principle of conservation of energy

v. Principle of entropy

The principle of conservation of mass states that when the total mass of the body is unchanged for an arbitrarily small neighborhood of each material point, the mass is considered to be conserved locally. The conservation of linear momentum represents Newton's second law and governs the motion of the continuum under the influence of the external effects. The principle of conservation of angular momentum is used to show symmetry of the stress tensor for many engineering materials, and the stress tensor describes the state of stress of the continuum. The principle of conservation of energy, also called the first law of thermodynamics, states that energy is conserved if the time rate of change of the kinetic and internal energy is equal to the sum of the rate of work of the external forces and all the other energies entering or leaving the body. The second law of thermodynamics is automatically satisfied and includes the change in entropy of

the continuum. More detailed descriptions of these balance laws are presented in Chapter III.

In deriving the governing equations, the starting point is a statement of the conservation principle applied to a "control volume" to develop the integral form of the equation and extract the differential form by using the divergence theorem. A control volume has a fixed volume in space; its boundary does not deform but allows mass transfer through it. In contrast, a material volume contains the same quantity of material at all times; its boundary can deform, and it does not allow mass transfer.

As the continuum moves, in general, properties change with time and space. The material derivative (substantial or total) must account for these changes depending on the method of description used. Consider the scalar property as ϕ, for the Lagrangian description, the material derivative is:

$$\frac{d\phi(X_j,t)}{dt} = \frac{\partial\phi}{\partial t} + \frac{\partial\phi}{\partial X_i}\frac{dX_i}{dt} = \frac{\partial\phi}{\partial t}$$

For the Eulerian description, the material derivative is:

$$\begin{aligned}\frac{d\phi(x_j,t)}{dt} &= \frac{\partial\phi}{\partial t} + \frac{\partial\phi}{\partial x_1}\frac{dx_1}{dt} + \frac{\partial\phi}{\partial x_2}\frac{dx_2}{dt} + \frac{\partial\phi}{\partial x_3}\frac{dx_3}{dt} \\ &= \frac{\partial\phi}{\partial t} + v_i\frac{\partial\phi}{\partial x_i} \\ &= \frac{\partial\phi}{\partial t} + \mathbf{v}\cdot\nabla\phi\end{aligned}$$

The general conservation equation may be written in integral form or differential form in conservative or divergence form. However, when considering the differential form, an equivalent representation is often obtained by working out the divergence operator and introducing the material derivative. This leads to a non-conservative form

of the differential equation. Although the conservative and non-conservative forms of the differential equations of the conservation principles are equivalent from a mathematical point of view, they will not necessarily remain so when a numerical discretization is performed. The general form of the conservation law is said to be written in conservative or divergence form. The importance of the conservative form in a numerical scheme lies in the fact that, if not properly taken into account, a discretization of the differential equations will lead to a numerical scheme in which all the mass fluxes through the mesh - cell boundaries will not cancel; hence, the numerical scheme will not keep the total mass constant[4].

1.2.2. Mathematical Approximations

Mathematical problems frequently encountered in engineering science may be classified as boundary-value and initial-value problems based upon the existence of one or more supplementary conditions. The differential equation describes a boundary-value problem if the dependent variable and possibly its derivative are required to have specified values on the domain boundary. The differential equation describes an initial-value problem if the dependent variable and possibly its derivative are specified initially (*i.e.*, t=0). Initial-value problems are generally time dependent.

Partial differential equations governing the motion of general continua are often of the canonical form $Au_{xx} + Bu_{xy} + Cu_{yy} = 0$ where the coefficients *A*, *B*, and *C* are real constants, *u* represents a field variable, and the subscripts, *x* and *y*, denote partial differentiation with respect to the independent variables, *x* and *y*. The character of this quasi-linear, second-order, partial differential equation is determined by the sign of the discriminant, $B^2 - 4AC$. The partial differential equation is

elliptic	for $B^2 - 4AC < 0$
hyperbolic	for $B^2 - 4AC > 0$
parabolic	for $B^2 - 4AC = 0$

The full significance of the classification of quasi-linear, second-order partial differential equations as elliptic, hyperbolic, or parabolic is beyond the scope of this work. However, this classification has proved important for an understanding of the kinds of initial and boundary conditions one must furnish along with the partial differential equation in order to determine a unique solution. Moreover, solution methods differ markedly from one classification to another, which is of particular importance in the field of fluid mechanics[6]. For example, boundary conditions are generally imposed all the way around a rectangular domain (the *x*-*y* region) of a two-dimensional flow when the equation is elliptic, and the solution must have no discontinuities in the second derivatives, except possibly at singular points where the differential equation is not applicable. Hyperbolic and parabolic equations, by contrast, have at least one open boundary; thus, boundary conditions are not usually imposed all around the domain under consideration. The boundary conditions for at least one variable, usually time, are specified at one end, and the system is integrated indefinitely. Certain kinds of discontinuities in the second derivatives are admissible across certain curves in such a way that the differential equation continues to be applicable in those regions.

Approximate solutions of differential equations (*e.g.*, Ritz, Galerkin, least-squares, collocation or in general weighted-residual methods) satisfy only part of the conditions of the problem. For example, either the governing equation or the boundary conditions may be satisfied only at a few positions rather than at each point. The

approximate solution is expanded in a set of known functions with arbitrary parameters. Two ways to determine the parameters are the method of weighted residuals (MWR) and the variational method. While the MWR and variational methods are only briefly discussed here, a more complete discussion of the approaches is given in the literature by Finlayson[7]. In MWR, one works directly with the differential equation and boundary conditions, whereas in the variational method one tries to satisfy the governing differential equation in an average sense using a functional related to the differential equations and/or the boundary conditions. MWR encompasses several methods (collocation, Galerkin, integral, etc.) and provides a framework to compare and contrast methods. Variational methods are not applicable to all problems, and thus suffer a lack of generality. MWR is easy to apply whereas variational methods require manipulation that can be more complex.

Variational methods provide a means for the determination of the governing equations. In solid mechanics, the principles of virtual work and stationary potential energy can be used to derive the governing equations and boundary conditions. The principle of virtual work demands that for the state of equilibrium, the work of the impressed forces is zero for any infinitesimal variation of the configuration of the system that is in harmony with the kinematic constraints. Hence, the variational statement implicitly imposes the natural boundary conditions. All work statements are derived from classical laws pertaining to the equilibrium of the particle. Moreover, the virtual work statement is simply the weak form of the equilibrium equations. For monogenic forces, this statement leads to the condition that for equilibrium, the potential energy shall be stationary with respect to all kinematically permissible variations.

The original differential equation is said to be the strong form of the problem while the integral form is typically referred to as the weak form. However, in the strict sense, particularly for approximation methods such as the Galerkin method, the weak form is obtained by transferring the differentiation from the dependent variable to the test functions, which includes the identification of the type of boundary conditions that the weak form can admit. The purpose of the transfer of differentiation is to equalize the continuity requirements on the dependent variable and the test function. This results in a weaker continuity requirement on the solution in the weak form than in the original equation. In the process of transferring the differentiation, boundary terms that determine the nature of the natural or essential boundary conditions in the solution are obtained.

The classification of boundary conditions as natural and essential boundary conditions plays a crucial role in the derivation of the approximate functions. From variational calculus, consider a partial differential equation in the form,

$$\frac{\partial F}{\partial u} - \frac{\partial}{\partial x}\left(\frac{\partial F}{\partial u_x}\right) - \frac{\partial}{\partial y}\left(\frac{\partial F}{\partial u_y}\right) = 0 \quad \text{in } \Omega$$

where $F = F(x, y, u, u_x, u_y)$, $u_x = \partial u / \partial x$ and $u_y = \partial u / \partial y$. Transferring the differentiation from the dependent variable, *u*, to the test function, *v*, yields the weak form of the differential equations in the form

$$\int_{\Omega}\left[v\frac{\partial F}{\partial u} + \frac{\partial v}{\partial x}\frac{\partial F}{\partial u_x} + \frac{\partial v}{\partial y}\frac{\partial F}{\partial u_y}\right]\mathrm{dxdy} - \oint_{\Gamma} v\left(\frac{\partial F}{\partial u_x}n_x + \frac{\partial F}{\partial u_y}n_x\right)\mathrm{ds} = 0$$

It is at this point that the natural and essential boundary conditions are readily identified. Generally, specifying coefficients of *v* and its derivative in the boundary integral constitute the natural boundary condition. That is,

$$\frac{\partial F}{\partial u_x} n_x + \frac{\partial F}{\partial u_y} n_x = \hat{q} \quad \text{on } \Gamma$$

is the natural boundary condition. Specification of the dependent variable in the same form as the arbitrary test function constitutes the essential boundary condition. In the case presented above, only *v* appears in the boundary integral. Hence, specifying *u* on Γ is the essential boundary condition. The variables involved in the essential boundary conditions of the problem are identified as primary variables and those in the natural boundary conditions as the secondary variables in the formulation. The primary variables are required to be continuous, whereas the secondary variables may be discontinuous in a problem.

The differential equation is said to describe a scalar-field problem if the dependent variable is a scalar and requires only the specification of magnitude for a complete description. A vector-field problem is one that requires the specification of magnitude and direction. The Poisson equation is an example of a differential equation describing a scalar-field problem that arises in many fields of engineering science such as elasticity, heat transfer, fluid mechanics, and electrostatics. The equation of motion is an example of a differential equation describing the vector-field problem that governs the motion of general continua. Each of these categories of differential equations will be discussed in more detail and the concomitant formulations presented in Chapters II and III.

The basic concepts of continuum mechanics and the ancillary fundamental concepts of mathematical approximation methods outlined in this section form the basis for the methodologies developed in this work. In subsequent chapters, the concepts are

described further as they relate to the development of multifunctional approaches for scalar-field and vector-field problems in engineering science.

1.3. LITERATURE REVIEW FOR COLLABORATIVE METHODS

This section includes a literature review of topics related to collaborative methods for multi-fidelity modeling and analysis. Review of approaches for collaborative modeling of multiple domains is presented. This review is not intended to be an exhaustive review of the subject matter but rather to provide sufficient background of the fundamental concepts applicable to collaborative methods for engineering science. For more detailed discussions on any of the topics reviewed, the reader is directed to the referenced reports.

Multi-fidelity modeling, as referred to herein, entails the use of diverse approximations among multiple domains. Numerous approaches for multi-fidelity modeling have been developed over the last several decades. Many of these approaches are commonplace in the analysis and design of aerospace structures. Generally, these methods focus on modeling to obtain accurate stress data, and they have been used primarily in an analysis framework rather than as an integral part of the design process. With the development of rapid equation solvers and fast computer systems with enormous storage capacities, these methods have the potential for impacting the preliminary design stage. Research directly applicable to multi-fidelity modeling based upon the finite element method continues to flourish. Developments pertinent to this research include substructuring, global/local methods, model synthesis methods (*i.e.*, multiple method approaches), submodeling, and finite element interface methods. While

all of these methods can be used in a global/local analysis, in general, they provide a diverse capability for modeling multiple subdomains.

Substructuring, submodeling, and general global/local methods have been highlighted, for example, by Ransom[8] and Ransom and Knight[9] and have been further elaborated on by Rose[10]. One notable application of substructuring related to recent advances in computational strategies is the use of neural networks to synthesize or combine substructures[11]. In reference 11, substructures are modeled individually with computational neural networks, and the response of the assembled substructure is predicted by synthesizing the neural networks. Statically determinant substructures and statically indeterminate substructures were assembled using a superposition approach and a displacement collocation approach. Typically, substructuring and submodeling approaches either require that the finite element nodes along the interdomain boundaries coincide or make use of restrictive interpolations of displacements to the boundaries of the local models. The global/local method proposed in reference 8 alleviates the requirement for nodal compatibility along the local model boundary by introducing a surface spline interpolation of the displacements from an independent global model to the boundary of a more refined local model. This uncoupled approach was further extended to provide global/local model interaction in an iterative approach proposed by Whitcomb et al.[12,13] In addition, global/local methodology for two- and three-dimensional stress analysis of composite structures has been developed within a common framework by Knight et al.[14]

In the context of this work, model synthesis refers to collaborative methodology that couples or synthesizes two or more dissimilar mathematical models of multiple

subdomains. Myriad methods fall into this category. Examples of these methods and representative references include, but are not limited to, synthesis of finite element and boundary element methods[15,16,17], finite element and Rayleigh-Ritz approximations[18], finite element and finite difference methods[19,20], finite element and analytical solutions[21], and finite element and equivalent plate solutions[22]. Furthermore, an extensive review of coupling the finite element method and boundary solution procedures has been given by Zienkiewicz[23]. In reference 23, the finite element method is generalized to encompass both the finite difference and the finite volume approaches.

A new era of multi-fidelity modeling was introduced through the development of an alternative approach for combining finite element models with different levels of fidelity, which is referred to in the literature as interface technology. The concept of interface technology is the genesis for the multifunctional capability presented in this work. As such, a more extensive review of the literature is presented and the notable contributions are outlined. The basic concept of the interface technology was discussed by Housner and Aminpour[24]. In this work, the fundamental approaches were discussed for mathematically coupling multiple subdomains whose grid points along common boundaries did not coincide. Subsequent developments performed by Aminpour et al.[25] implemented the basic concepts, extended the work to alternative approximations, and compared the results for representative benchmark applications. Ransom et al.[26] advanced further the technology by recasting the interface technology in the form of an element, thus facilitating the use of the method for more than two subdomains. Moreover, the implementation of the method as an element facilitated the inclusion of the technology into standard commercially available finite element software codes[27]. Davilá

et al.[28] extended further the capability for coupling not only along finite element edges as originally implemented but across finite element faces as well. Rose[10] extended the concept of interface technology to include geometric incompatibility as well as nodal incompatibility. In this work, the geometry of the subdomains is automatically adjusted to account for an inaccurate geometry description along the common subdomain boundaries and for gaps in the boundary definition, which allows for enhanced modeling flexibility. In addition, extensions have been developed to include geometrically nonlinear analysis[29]. The technology has been developed to provide dimensionality reduction for integrating three-dimensional finite element models within two-dimensional finite element models[26]. All of the aforementioned interface technology developments have focused on a one-dimensional interface along a curve or line. Aminpour et al.[30] and Schiermeier et al.[31] have extended the work to a two-dimensional surface interface for coupling three-dimensional finite element models.

1.4. OBJECTIVES AND SCOPE

The overall objective of this research is to formulate multifunctional methodologies and analysis procedures for interfacing diverse domain idealizations including multi-fidelity modeling methods and multi-discipline analysis methods. Specific goals of this research include:

1. To formulate general methodology providing capability for multifunctional modeling, analysis, and solution.
2. To identify computational aspects and related algorithms for this methodology.
3. To apply the formulation to scalar- and vector-field applications in engineering science.

The scope of the present work includes the multi-fidelity modeling and analysis of interfaced domains within the same discipline as well as among multiple disciplines. The analysis capabilities are limited to scalar- and vector-field problems using both single and multiple approximation methods within a given domain. The capabilities are developed considering discrete changes in domain characteristics across the interfaced boundaries, compatibility with general-purpose finite element codes, applicability for a wide range of discretization methods and engineering disciplines, and cost-effectiveness related to both modeling and analysis time. To accomplish the objectives of the present work, numerical studies are performed to gain insight into the interactions among the interfaced domains and the computational strategies for the modeling and analysis. Prior to applying the method to vector-field problems, the proposed method is evaluated with regard to accuracy and computational implications on representative scalar-field problems.

The organization of the remainder of the dissertation is as follows. A multifunctional approach for scalar-field problems is presented in Chapter II. Single- and multiple-domain formulations are presented in the chapter along with a discussion of the spatial modeling and the computational implications, and numerical results for a verification test case are presented. The multifunctional approach for vector-field problems is presented in Chapter III. Single- and multiple-domain formulations are presented in this chapter along with a discussion of the spatial modeling and the computational implications, and numerical results for a verification test case are presented. Numerical results for representative scalar-field problems in engineering science are presented in Chapter IV, while results for vector-field problems are presented in Chapter V. In addition, a discussion of extensions of the methodology to multiple

discipline coupling is given in Chapter V. Conclusions and recommendations are presented in Chapter VI. An overview of the steps in analysis and simulation is given in Appendix A. A derivation of the cubic spline interpolation matrices used in the multifunctional approach is presented in Appendix B. Details of the geometry representation along the subdomain interface are given in Appendix C.

CHAPTER II

MULTIFUNCTIONAL APPROACH FOR SCALAR-FIELD PROBLEMS

2.1. GENERAL

The motivation for the consideration of multifunctional approaches for scalar-field problems comes from the fact that methods of approximation such as Ritz, Galerkin, and other weighted residual methods are based on weak statements of the differential equations governing the system response. The differential equation is said to describe a scalar-field problem if the dependent variable is a scalar and requires only the specification of magnitude for a complete description. The scalar-field problem is a basic form of the governing differential equations and thus lends itself to forming the mathematical foundation for the general methodology developed herein. Representative examples of the scalar-field differential equations in two dimensions are considered herein, and the mathematical statement is formulated. The concepts developed here are directly applicable to one-dimensional scalar-field problems; however, the development is not included in the interest of brevity. The general form of the differential equation describing a scalar-field problem for domain Ω (see Figure 2.1) is given by the Poisson equation, which is of the form

$$-\nabla \cdot (k \nabla u) = Q \quad \text{in } \Omega \tag{2.1}$$

subject to the natural boundary condition, $k\dfrac{du}{dn} + h(u - u_\infty) = q$ on Γ^s, and essential boundary condition, $u = \tilde{u}$ on Γ^p. The normal derivative, $\dfrac{du}{dn} = \dfrac{\partial u}{\partial x} n_x + \dfrac{\partial u}{\partial y} n_y$, and n_x

and n_y are the components of the outward normal vector, $\boldsymbol{n}$, to the bounding surface, Γ, of domain, Ω. In Eq. (2.1), the variables k and Q are known coefficients, and the primary variable or dependent variable is u, which is a function of the independent variables x and y. In the natural boundary condition, the variables, h and u_∞, are the convection coefficient, and the far-field value of the primary variable, respectively. The terms, q, $k\frac{\partial u}{\partial x}$, and $k\frac{\partial u}{\partial y}$ are the secondary variables that may be described on a portion of the boundary, Γ^s. The primary variable, u, is specified on the boundary, Γ^p, and its prescription to the boundary value, $\bar{u}$, constitutes the essential boundary condition. The complete boundary is defined as $\Gamma = \Gamma^p + \Gamma^s$.

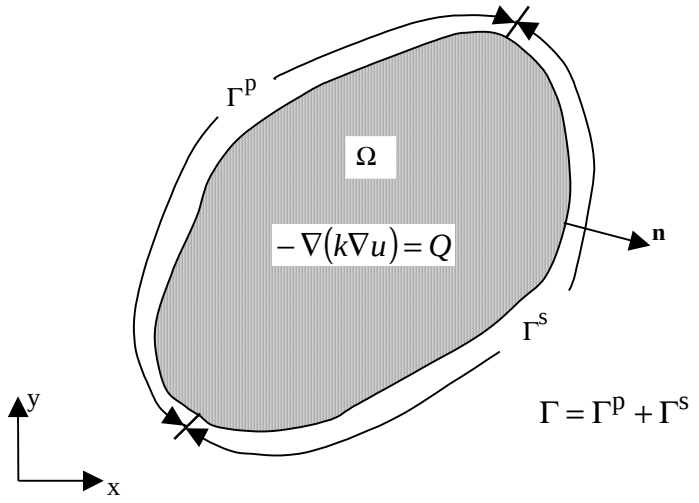

Figure 2.1. Geometric Representation of Two-Dimensional Domain.

2.2. DISCIPLINE SPECIFICS

Equations of the type of Eq. (2.1) arise in many fields of engineering science such as elasticity, heat transfer, fluid mechanics, and electrostatics. Reddy[32] has tabulated several examples. In this work, the Poisson equation is applied to problems in the solid mechanics and fluid mechanics disciplines.

2.2.1. Solid Mechanics

For applicability of the Eq. (2.1) in solid mechanics, consider a prismatic bar of constant cross section subjected to equal and opposite twisting moments at the ends as shown in Figure 2.2(a).

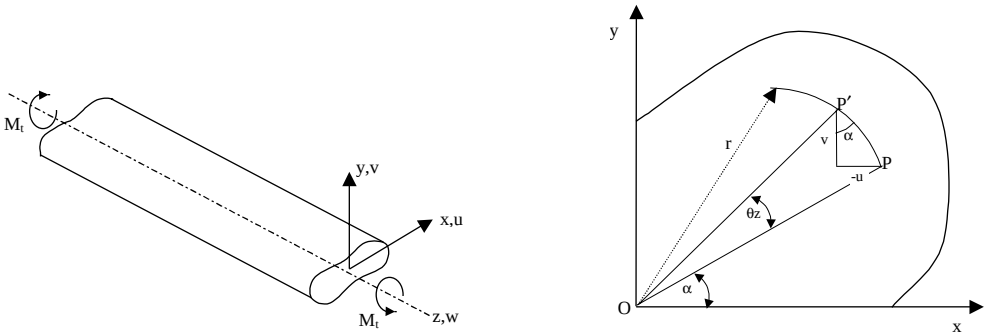

(a) Geometry (b) Partial End View

Figure 2.2. Geometric Configuration of Prismatic Bar.

In general, the cross sections normal to the axis of the bar warp. As a fundamental assumption, the warping deformation is taken to be independent of the axial location and is given by

$$w = w(x, y)$$

Assuming that that no rotation occurs at the end z=0 and that the angle of rotation, θ, is small, the displacement components, u and v, in the x and y coordinate directions, of an arbitrary point, P, $P(x, y)$, in a plane for constant z, are respectively,

$$u = -(r\theta z)\sin\alpha = -y\theta z$$

$$v = (r\theta z)\cos\alpha = x\theta z \qquad (2.2)$$

where the angular displacement of a line segment, *OP*, from the origin, *O*, to an arbitrary point, *P*, is θz and α is the angle between *OP* and the *x* axis (See Figure 2.2(b)). By substituting Eq. (2.2) into the strain-displacement relations, the following are obtained

$$\varepsilon_x = \gamma_{xy} = \varepsilon_y = \varepsilon_z = 0$$

$$\gamma_{zx} = \frac{\partial w}{\partial x} - y\theta \quad ; \quad \gamma_{zy} = \frac{\partial w}{\partial y} + x\theta \tag{2.3}$$

The three-dimensional stress-strain relations given in terms of Lame's constants for a linear isotropic solid are given by

$$\begin{aligned} \sigma_x &= 2G\varepsilon_x + \lambda e \quad ; \quad \tau_{xy} = G\gamma_{xy} \\ \sigma_y &= 2G\varepsilon_y + \lambda e \quad ; \quad \tau_{yz} = G\gamma_{yz} \\ \sigma_z &= 2G\varepsilon_z + \lambda e \quad ; \quad \tau_{xz} = G\gamma_{xz} \end{aligned}$$

where $e = \varepsilon_x + \varepsilon_y + \varepsilon_z$, $\lambda = \dfrac{\nu E}{(1+\nu)(1-2\nu)}$, and $G = \dfrac{E}{2(1+\nu)}$.

The shear modulus, *G*, and the quantity, λ, are referred to as the Lame's constants, and the modulus of elasticity, *E*, and the Poisson's ratio, ν, are material properties. Substituting the strain-displacement relations of Eqs. (2.3) into the stress-strain relations gives

$$\sigma_x = \tau_{xy} = \sigma_y = \sigma_z = 0$$

$$\tau_{zx} = G\left(\frac{\partial w}{\partial x} - y\theta\right) \quad ; \quad \tau_{zy} = G\left(\frac{\partial w}{\partial y} + x\theta\right) \tag{2.4}$$

Then, the three-dimensional equations of equilibrium,

$$\begin{aligned}
\frac{\partial \sigma_x}{\partial x} + \frac{\partial \tau_{xy}}{\partial y} + \frac{\partial \tau_{xz}}{\partial z} + F_x &= 0 \\
\frac{\partial \tau_{xy}}{\partial x} + \frac{\partial \sigma_y}{\partial y} + \frac{\partial \tau_{yz}}{\partial z} + F_y &= 0 \\
\frac{\partial \tau_{xz}}{\partial x} + \frac{\partial \tau_{yz}}{\partial y} + \frac{\partial \sigma_z}{\partial z} + F_z &= 0
\end{aligned} \tag{2.5}$$

with negligible body forces, simplify to the following equations:

$$\frac{\partial \tau_{zx}}{\partial z} = 0, \quad \frac{\partial \tau_{zy}}{\partial z} = 0, \quad \frac{\partial \tau_{zx}}{\partial x} + \frac{\partial \tau_{zy}}{\partial y} = 0 \tag{2.6}$$

First, note that the stresses in Eq. (2.4) satisfy exactly the first two equilibrium equations above (see Eq. (2.5)). Next, Eq. (2.4) can be combined into a single equation by differentiating the expressions for τ_{zx} and τ_{zy} by y and x, respectively, and subtracting the resulting equations. These operations yield the compatibility equation given by

$$\frac{\partial \tau_{zx}}{\partial y} - \frac{\partial \tau_{zy}}{\partial x} = -2G\theta\,. \tag{2.7}$$

The stress in a bar of arbitrary cross section may thus be determined by solving the third equation of equilibrium given in Eq. (2.6) along with the equations of compatibility given in Eq. (2.7) and the given boundary conditions.

This torsion problem is commonly solved by introducing a single stress function. If such a function, $\phi(x, y)$, the so-called Prandtl stress function, is assumed to exist, such that

$$\tau_{zx} = \frac{\partial \phi}{\partial y} \quad ; \quad \tau_{zy} = -\frac{\partial \phi}{\partial x}\,,$$

then, the equations of equilibrium are automatically satisfied. The equation of compatibility becomes, upon substituting these expressions for the shear stress,

$$\frac{\partial^2 \phi}{\partial x^2} + \frac{\partial^2 \phi}{\partial x^2} = -2G\theta$$

Therefore, if the compatibility requirement is to be satisfied, the stress function, ϕ, must satisfy Poisson's equation, Eq. (2.1). The primary variable, *u*, the constant, *k*, and the source variable, *Q*, are represented by the stress function, ϕ, the inverse of the shear modulus, *G*, and twice the angle of twist per unit length, θ, respectively. Moreover, the stress function, ϕ=constant on the surface of the bar.

2.2.2. Fluid Mechanics

For a two-dimensional incompressible irrotational flow, expressions are given for the velocity components, v_x and v_y, in terms of the *x* and *y* coordinate directions, respectively. The velocity components should satisfy the continuity condition

$$\nabla \cdot \mathbf{v} = \frac{\partial v_x}{\partial x} + \frac{\partial v_y}{\partial y} = 0 \tag{2.8}$$

and the irrotational flow condition

$$\nabla \times \mathbf{v} = \frac{\partial v_y}{\partial x} - \frac{\partial v_x}{\partial y} = 0\,. \tag{2.9}$$

In terms of the stream function, ψ, the components are given by

$$v_x = \frac{\partial \Psi}{\partial y} \quad \text{and} \quad v_y = -\frac{\partial \Psi}{\partial x} \tag{2.10}$$

and in terms of the velocity potential, Φ, the components are

$$v_x = -\frac{\partial \Phi}{\partial x} \quad \text{and} \quad v_y = -\frac{\partial \Phi}{\partial y} \quad . \tag{2.11}$$

Substituting the velocity components, v_x and v_y, from Eq. (2.10) into the irrotational flow condition Eq. (2.9), one obtains

$$\frac{\partial^2 \Psi}{\partial x^2} + \frac{\partial^2 \Psi}{\partial y^2} = 0 \,. \tag{2.12}$$

Note that the velocity components in terms of the stream function given in Eq. (2.10) satisfy the continuity condition, Eq. (2.8) identically. Hence, Eq. (2.12) governs the flow in terms of the stream function, ψ, and is in the form of the Poisson Equation, Eq. (2.1) where the primary variable, u, the constant, k, and the source variable, Q, are represented by the stream function, ψ, the density, ρ, and the mass production, σ (normally zero), respectively.

Substituting the velocity components, v_x and v_y, from Eq. (2.11) into the continuity equation, one obtains

$$\frac{\partial^2 \Phi}{\partial x^2} + \frac{\partial^2 \Phi}{\partial y^2} = 0 \,. \tag{2.13}$$

Note that the velocity components in terms of the velocity potential given in Eq. (2.11) satisfy the irrotational flow condition, Eq. (2.9), identically. Eq. (2.13) governs the flow in terms of the velocity potential, Φ, and is in the form of the Poisson Equation, Eq. (2.1), where the primary variable, u, the material constant, k, and the source variable, Q, are represented by the velocity potential, Φ, the density, ρ, and the mass production, σ (normally zero), respectively.

2.3. SINGLE-DOMAIN FORMULATION

In this section, multifunctional methodology for a scalar-field problem over a single domain is presented in terms of weighted residuals. The method of weighted residuals is used extensively in fluid mechanics and thus the potential problem is formulated from this perspective. While the intent of this work is to develop general

methodology for multiple domains, the salient features of the weighted residual method formulation may be investigated and discussed using the single domain. Consider the general Poisson equation for a two-dimensional domain for field variable, u

$$-k\nabla^2 u = Q \tag{2.14}$$

in a domain, Ω, bounded by Γ. In general, the boundary, Γ, can have mixed boundary conditions with the primary variable, u, prescribed on Γ^p and the secondary variable, the flux, q, prescribed on the remaining part of the boundary, Γ^s (see Figure 2.1).

In the method of weighted residuals, an approximate solution, $\tilde{u}$, is used in expressing $\nabla^2 u$, then the differential equation, Eq. (2.14), will no longer be satisfied, and this lack of equality is a measure of the departure of $\tilde{u}$ from the exact solution. The lack of equality is called the residual, R, and is written as

$$R = -k\nabla^2 u - Q \neq 0 .$$

The residual is orthogonalized by a set of weight functions, Φ_i and averaged over the domain. This residual may be written as

$$\int_{\Omega} \left(-k\nabla^2 \tilde{u} - Q\right)\Phi_i \, d\Omega = 0 . \tag{2.15}$$

The solution for $\tilde{u}$ is sought in the form $\tilde{u} = \sum_{i=1}^{n} a_i \Psi_i + \Psi_0$. The functions, Ψ_i, are usually called trial functions, and a_i are arbitrary constants. The trial functions satisfy the homogeneous boundary conditions, while Ψ_0 satisfies the nonhomogeneous boundary conditions. Posing the problem to be solved in a generalized weighted residual form[33,34] and relaxing the requirement for the approximate solution to satisfy all boundary conditions, the weighted residual statement may be written in the form

$$\int_{\Omega} \mathbf{\Phi A}(\tilde{\mathbf{u}})\,\mathrm{d}\Omega + \oint_{\Gamma} \overline{\mathbf{\Phi}}\mathbf{B}(\tilde{\mathbf{u}})\,\mathrm{d}\Gamma = 0$$

where the residual in the satisfaction of the boundary conditions is orthogonalized by a secondary set of weight functions, $\overline{\mathbf{\Phi}}$, and the differential equation set is represented by

$$\mathbf{A}(\mathbf{u}) = \begin{Bmatrix} A_1(u) \\ A_2(u) \\ \vdots \end{Bmatrix} = \mathbf{0}$$

in the domain, Ω, together with the boundary conditions

$$\mathbf{B}(\mathbf{u}) = \begin{Bmatrix} B_1(u) \\ B_2(u) \\ \vdots \end{Bmatrix} = \mathbf{0}$$

on the boundary, Γ, of the domain. As implied by the matrix notation used previously, the solution sought may represent a scalar quantity or a vector of several variables. Similarly, the differential equation may be a single equation or a set of simultaneous equations. For the system at hand, a scalar quantity is sought and the differential equation is a single equation. Here, $\mathbf{A}(\mathbf{u}) = -\nabla^2 u - Q = 0$, and the essential and natural boundary conditions, respectively, are represented by

$$B_1(u) = u - \bar{u} = 0 \qquad \text{on } \Gamma^{\mathrm{p}}$$

and

$$B_2(u) = k\frac{\partial u}{\partial n} - \bar{q} = 0 \qquad \text{on } \Gamma^{\mathrm{s}}.$$

Therefore, considering the approximate solution, $\tilde{u}$, we may write the general integral form of the differential equation governing the potential flow as

$$\int_{\Omega} \mathbf{\Phi}\left(-k\nabla^2\tilde{u} - Q\right)\mathrm{d}\Omega + \int_{\Gamma^p} \overline{\mathbf{\Phi}}_1(\tilde{u}\text{-}\bar{u})\,\mathrm{d}\Gamma^p + \int_{\Gamma^s} \overline{\mathbf{\Phi}}_2\left(k\frac{\mathrm{d}\tilde{u}}{\mathrm{d}n} - \bar{q}\right)\mathrm{d}\Gamma^s = 0 \qquad (2.16)$$

Note that the trial function may be selected so as to satisfy the essential and the natural boundary conditions; thus, the boundary integrals in Eq. (2.16) are identically zero. In this formulation, only the essential boundary conditions, *i.e.*,

$$\tilde{u} - \bar{u} = 0 \qquad \text{on } \Gamma^{\mathrm{p}}$$

are assumed to be automatically satisfied by the choice of the trial functions. Therefore, Eq. (2.16) is rewritten as

$$\int_{\Omega} \boldsymbol{\Phi}\left(-k\nabla^2\tilde{u} - Q\right)\mathrm{d}\Omega + \int_{\Gamma^s} \overline{\boldsymbol{\Phi}}\left(k\frac{\mathrm{d}\tilde{u}}{\mathrm{d}n} - \bar{q}\right)\mathrm{d}\Gamma^s = 0 \tag{2.17}$$

or

$$\int_{\Omega} \boldsymbol{\Phi}\left[-k\left(\frac{\partial^2\tilde{u}}{\partial x^2} + \frac{\partial^2\tilde{u}}{\partial y^2}\right) - Q\right]\mathrm{d}\Omega + \int_{\Gamma^s} \overline{\boldsymbol{\Phi}}\left(k\frac{\mathrm{d}\tilde{u}}{\mathrm{d}n} - \bar{q}\right)\mathrm{d}\Gamma^s = 0$$

where $\dfrac{\mathrm{d}\tilde{u}}{\mathrm{d}n} = \dfrac{\partial\tilde{u}}{\partial x}n_x + \dfrac{\partial\tilde{u}}{\partial y}n_y$ and $\boldsymbol{\Phi}_2 = \overline{\boldsymbol{\Phi}}$.

In general, the method of weighted residuals does not strictly require the incorporation of natural boundary conditions into the weak formulation, as in the Ritz method. However, if the operator permits the weak formulation, continuity requirements on the primary variable and its derivatives may be relaxed. Moreover, if integration by parts is possible, one may reduce the order of the highest derivative in the integral form to eliminate the difficulty of selecting the appropriate weight functions. Thus, in the formulation herein, the order of differentiation on the primary variable in the integral equation, Eq. (2.17), is reduced to obtain the weak formulation. In addition, acknowledging that the primary variable, *u*, is approximated by $\tilde{u}$, for simplicity, the subsequent development is presented in terms of *u*. Application of the divergence theorem to Eq. (2.17) yields

$$\int_{\Omega} k\left(\frac{\partial u}{\partial x}\frac{\partial \boldsymbol{\Phi}}{\partial x}+\frac{\partial u}{\partial y}\frac{\partial \boldsymbol{\Phi}}{\partial y}\right)\mathrm{d}\Omega-\oint_{\Gamma} k\left(\frac{\partial u}{\partial x}n_x+\frac{\partial u}{\partial y}n_y\right)\boldsymbol{\Phi}\,\mathrm{d}\Gamma - \int_{\Omega} Q\boldsymbol{\Phi}\mathrm{d}\Omega+\int_{\Gamma^s}\left(k\frac{\mathrm{d}u}{\mathrm{d}n}-\bar{q}\right)\overline{\boldsymbol{\Phi}}\,\mathrm{d}\Gamma^s=0 \tag{2.18}$$

Note that the boundary is presumed to consist of boundaries on which the primary variable is specified and boundaries on which the secondary variable is specified, and $\Gamma=\Gamma^p+\Gamma^s$. Therefore, the boundary integral on Γ, may be expressed as

$$\oint_{\Gamma} k\left(\frac{\partial u}{\partial x}n_x+\frac{\partial u}{\partial y}n_y\right)\boldsymbol{\Phi}\,\mathrm{d}\Gamma=\int_{\Gamma^p} k\left(\frac{\partial u}{\partial x}n_x+\frac{\partial u}{\partial y}n_y\right)\boldsymbol{\Phi}\mathrm{d}\Gamma^p+\int_{\Gamma s} k\left(\frac{\partial u}{\partial x}n_x+\frac{\partial u}{\partial y}n_y\right)\boldsymbol{\Phi}\mathrm{d}\Gamma^s$$

Noting that, in the method of weighted residuals, the weight function, **Φ**, satisfies the homogeneous boundary conditions for the primary variable (*i.e.*, essential boundary conditions). Thus, $\boldsymbol{\Phi}=\mathbf{0}$ on Γ^p. Therefore, the boundary integral on Γ^p is identically zero and Eq. (2.18) may be rewritten as

$$\int_{\Omega} k\left(\frac{\partial u}{\partial x}\frac{\partial \boldsymbol{\Phi}}{\partial x}+\frac{\partial u}{\partial y}\frac{\partial \boldsymbol{\Phi}}{\partial y}\right)\mathrm{d}\Omega-\oint_{\Gamma^s} k\frac{\mathrm{d}u}{\mathrm{d}n}\boldsymbol{\Phi}\,\mathrm{d}\Gamma^s-\int_{\Omega} Q\boldsymbol{\Phi}\mathrm{d}\Omega+\oint_{\Gamma^s}\left(k\frac{\mathrm{d}u}{\mathrm{d}n}-\bar{q}\right)\overline{\boldsymbol{\Phi}}\,\mathrm{d}\Gamma^s=0$$

Since the weight functions, $\boldsymbol{\Phi}$ and $\overline{\boldsymbol{\Phi}}$, are arbitrary, they may be chosen, without loss of generality, such that, $\boldsymbol{\Phi}=\overline{\boldsymbol{\Phi}}$. Therefore,

$$\int_{\Omega} k\left(\frac{\partial u}{\partial x}\frac{\partial \boldsymbol{\Phi}}{\partial x}+\frac{\partial u}{\partial y}\frac{\partial \boldsymbol{\Phi}}{\partial y}\right)\mathrm{d}\Omega-\int_{\Omega} Q\boldsymbol{\Phi}\mathrm{d}\Omega-\oint_{\Gamma^s}\bar{q}\boldsymbol{\Phi}\,\mathrm{d}\Gamma^s=0$$

or

$$\int_{\Omega} k\left(\frac{\partial u}{\partial x}\frac{\partial \boldsymbol{\Phi}}{\partial x}+\frac{\partial u}{\partial y}\frac{\partial \boldsymbol{\Phi}}{\partial y}\right)\mathrm{d}\Omega=\int_{\Omega} Q\boldsymbol{\Phi}\mathrm{d}\Omega+\oint_{\Gamma^s}\bar{q}\boldsymbol{\Phi}\,\mathrm{d}\Gamma^s \tag{2.19}$$

The integral form of Eq. (2.19) forms the basis of finite element approximations, which is summarized in a subsequent section.

2.4. MULTIPLE-DOMAIN FORMULATION

In the multiple domain method, the domain of the problem is subdivided into a number of smaller subdomains. The method is quite similar to the subdomain collocation method, which is another weighted residual method. In the subdomain collocation approach, the domain is divided into as many subdomains as there are adjustable parameters. These parameters are then determined by making the residual orthogonal to a weight function in an integral sense over each subdomain. Here, as in the single-domain formulation, methodology is presented formulating the general method of weighted residuals for multiple domains by considering the Poisson equation for a two-dimensional domain for a field variable, u. Then,

$$-k\nabla^2 u = Q \tag{2.20}$$

in the entire domain, Ω, bounded by Γ. For simplicity, the multiple-domain formulation is presented for two subdomains, Ω_1 and Ω_2 (see Figure 2.3). Independent approximations and weight functions are assumed in each of the subdomains and continuity conditions are used to provide for a continuous solution across the subdomain interfaces. Thus, Eq. (2.20) is satisfied in each subdomain, independently, *i.e.*,

$$-k_1\nabla^2 u_1 = Q_1 \quad \text{in } \Omega_1 \quad \text{and} \quad -k_2\nabla^2 u_2 = Q_2 \quad \text{in } \Omega_2$$

subject to the boundary conditions on the subdomain boundaries, Γ_1 and Γ_2. Although Eq. (2.20) is assumed for uniform constant, k, throughout the domain, it is permitted to be different in each subdomain. That is, constants, k_1 and k_2, are used for subdomains Ω_1 and Ω_2, respectively, to allow for the general case of nonhomogeneous material.

At this point, differences between the single- and multiple-domain approaches become evident. First, the domain, Ω, is now represented by the union of *ns* subdomains, Ω_i, such that

$$\Omega = \sum_{i=1}^{ns} \Omega_i \, .$$

Second, the bounding surface, Γ, of the domain, Ω, is the union of the exterior surfaces, Γ_i^{E}, of the *ns* subdomains, Ω_i, such that

$$\Gamma = \sum_{i=1}^{ns} \Gamma_i^{\mathrm{E}}$$

In general, these exterior surfaces, Γ_i^{E}, may involve mixed boundary conditions with the primary variable, *u*, prescribed on Γ_i^{p} and the secondary variable, the flux, *q*, prescribed on Γ_i^{s} such that

$$\Gamma_i^{\mathrm{E}} = \Gamma_i^{p} + \Gamma_i^{s} \, .$$

Finally, as a result of the subdomain modeling, the collaborative effort to solve the problem involves an interior surface interface boundary, Γ_i^{I}, and the information transfer across the boundary. Hence, the boundary surface for the i^{th} subdomain is given by

$$\Gamma_i = \Gamma_i^{\mathrm{p}} + \Gamma_i^{\mathrm{s}} + \Gamma_i^{\mathrm{I}}$$

The boundary conditions may be written as

$$u_1 - \bar{u}_1 = 0 \quad \text{on } \Gamma_1^{p} \quad \text{and} \quad k_1 \frac{\mathrm{d}u_1}{\mathrm{d}n} - \bar{q}_1 = 0 \quad \text{on } \Gamma_1^{s}$$

and

$$u_2 - \bar{u}_2 = 0 \quad \text{on } \Gamma_2^p \quad \text{and} \quad k_2 \frac{\mathrm{d}u_2}{\mathrm{d}n} - \bar{q}_2 = 0 \quad \text{on } \Gamma_2^s .$$

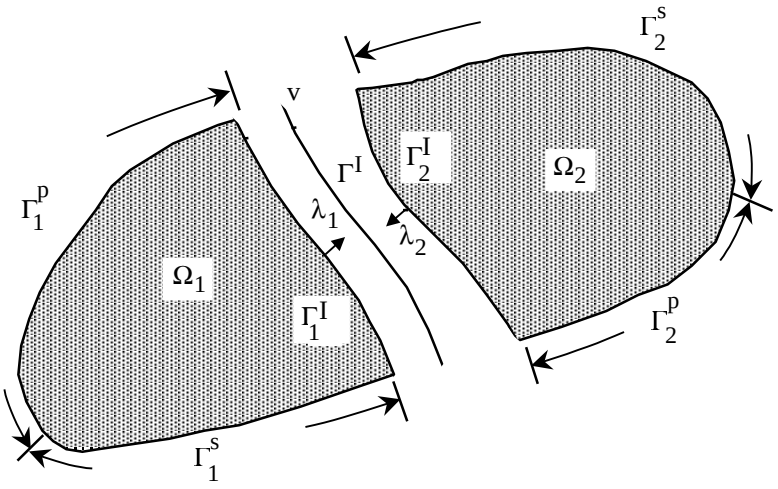

Figure 2.3. Boundary Definitions for Two-Dimensional Subdomains.

The residual for each domain is orthogonalized by a set of weight functions, Φ_i and is written as

$$\int_{\Omega_1} \left(-k_1 \nabla^2 u_1 - Q_1 \right) \mathbf{\Phi}_1 \, \mathrm{d}\Omega_1 = 0$$

and

$$\int_{\Omega_2} \left(-k_2 \nabla^2 u_2 - Q_2 \right) \mathbf{\Phi}_2 \, \mathrm{d}\Omega_2 = 0$$

where the approximate solution is sought in the form $\tilde{u}_1 = \sum_1^n a_{1i} \Psi_{1i} + \Psi_{0i}$ and

$\tilde{u}_2 = \sum_1^n a_{2i} \Psi_{2i} + \Psi_{0i}$. The functions, Ψ_{0i} ,Ψ_{1i}, and Ψ_{2i}, are trial functions, and a_{1i} and a_{2i}

are sets of arbitrary constants. Using the general form outlined in the single-domain formulation (*i.e.*, $\int_{\Omega} \mathbf{\Phi A}(\tilde{\mathbf{u}})\,d\Omega + \oint_{\Gamma} \overline{\mathbf{\Phi}}\mathbf{B}(\tilde{\mathbf{u}})\,d\Gamma = 0$), for each subdomain, one may write

$$\int_{\Omega_i} \mathbf{\Phi}_i \mathbf{A}(\tilde{\mathbf{u}}_i)\,d\Omega + \oint_{\Gamma_i} \overline{\mathbf{\Phi}}_i \mathbf{B}(\tilde{\mathbf{u}}_i)\,d\Gamma_i = 0 \qquad \text{for } i = 1,2$$

where the residual in the satisfaction of the boundary conditions is orthogonalized by a secondary set of weight functions, $\overline{\mathbf{\Phi}}_i$, for subdomain *i*. Therefore, considering the approximate solution, $\tilde{u}_1$ and $\tilde{u}_2$, we may write the general integral form of the differential equation governing the potential flow for subdomain 1 as

$$\int_{\Omega_1} \mathbf{\Phi}_1\left(-k_1\nabla^2\tilde{u}_1 - Q_1\right)d\Omega_1 + \int_{\Gamma_1^p} \overline{\mathbf{\Phi}}_{11}(\tilde{u}_1 - \bar{u}_1)\,d\Gamma_1^p + \int_{\Gamma_1^s} \overline{\mathbf{\Phi}}_{12}\left(k_1\frac{d\tilde{u}_1}{dn} - \bar{q}_1\right)d\Gamma_1^s = 0 \quad (2.21)$$

and for subdomain 2 as

$$\int_{\Omega_2} \mathbf{\Phi}_2\left(-k_2\nabla^2\tilde{u}_2 - Q_2\right)d\Omega_2 + \int_{\Gamma_2^p} \overline{\mathbf{\Phi}}_{21}(\tilde{u}_2 - \bar{u}_2)\,d\Gamma_2^p + \int_{\Gamma_2^s} \overline{\mathbf{\Phi}}_{22}\left(k_2\frac{d\tilde{u}_2}{dn} - \bar{q}_2\right)d\Gamma_2^s = 0 \quad (2.22)$$

Again, we will presume that the essential boundary conditions, *i.e.*,

$$\tilde{u}_1 - \bar{u}_1 = 0 \qquad \text{on } \Gamma_1^p$$

and

$$\tilde{u}_2 - \bar{u}_2 = 0 \qquad \text{on } \Gamma_2^p$$

are automatically satisfied by the choice of the functions, $\tilde{u}_1$ and $\tilde{u}_2$. Therefore, for subdomain 1, Eq. (2.21) is rewritten as

$$\int_{\Omega_1} \mathbf{\Phi}_1\left(-k_1\nabla^2\tilde{u}_1 - Q_1\right)d\Omega_1 + \int_{\Gamma_1^s} \overline{\mathbf{\Phi}}_{12}\left(k_1\frac{d\tilde{u}_1}{dn} - \bar{q}_1\right)d\Gamma_1^s = 0 \quad (2.23)$$

or in its expanded form

$$\int_{\Omega_1} \mathbf{\Phi}_1 \left[-k_1 \left(\frac{\partial^2 \tilde{u}_1}{\partial x^2} + \frac{\partial^2 \tilde{u}_1}{\partial y^2} \right) - Q_1 \right] \mathrm{d}\Omega_1 + \int_{\Gamma_1^s} \overline{\mathbf{\Phi}}_1 \left(k_1 \frac{\mathrm{d}\tilde{u}_1}{\mathrm{d}n} - \bar{q}_1 \right) \mathrm{d}\Gamma_1^s = 0 \qquad (2.24)$$

where $\frac{\partial \tilde{u}_i}{\partial n} = \frac{\partial \tilde{u}_i}{\partial x} n_{x_i} + \frac{\partial \tilde{u}_i}{\partial y} n_{y_i}$ and $\overline{\mathbf{\Phi}}_{12} = \overline{\mathbf{\Phi}}_1$ and $\overline{\mathbf{\Phi}}_{22} = \overline{\mathbf{\Phi}}_2$. Similarly, the weighted residual form for subdomain 2,

$$\int_{\Omega_2} \mathbf{\Phi}_2 \left[-k_2 \left(\frac{\partial^2 \tilde{u}_2}{\partial x^2} + \frac{\partial^2 \tilde{u}_2}{\partial y^2} \right) - Q_2 \right] \mathrm{d}\Omega_2 + \int_{\Gamma_2^s} \overline{\mathbf{\Phi}}_2 \left(k_2 \frac{\mathrm{d}\tilde{u}_2}{\mathrm{d}n} - \bar{q}_2 \right) \mathrm{d}\Gamma_2^s = 0 \qquad (2.25)$$

The order of differentiation on the primary variable in the integral equations, Eq. (2.24) and (2.25), is reduced to obtain the weak formulation. In addition, acknowledging that the primary variables, u_1 and u_2, are approximated by $\tilde{u}_1$ and $\tilde{u}_2$, for simplicity, the subsequent development is presented in terms of u_1 and u_2. Utilizing the divergence theorem, Eq. (2.24), can be rewritten, for subdomain 1, yields,

$$\begin{aligned} \int_{\Omega_1} k_1 \left(\frac{\partial u_1}{\partial x} \frac{\partial \mathbf{\Phi}_1}{\partial x} + \frac{\partial u_1}{\partial y} \frac{\partial \mathbf{\Phi}_1}{\partial y} \right) \mathrm{d}\Omega_1 - \oint_{\Gamma_1} k_1 \left(\frac{\partial u_1}{\partial x} n_{x_1} + \frac{\partial u_1}{\partial y} n_{y_1} \right) \mathbf{\Phi}_1 \mathrm{d}\Gamma_1 - \int_{\Omega_1} Q_1 \mathbf{\Phi}_1 \mathrm{d}\Omega_1 \\ + \int_{\Gamma_1^s} \left(k_1 \frac{\mathrm{d}u_1}{\mathrm{d}n} - \bar{q}_1 \right) \overline{\mathbf{\Phi}}_1 \mathrm{d}\Gamma_1^s = 0 \end{aligned} \qquad (2.26)$$

and similarly, for subdomain 2,

$$\begin{aligned} \int_{\Omega_2} k_2 \left(\frac{\partial u_2}{\partial x} \frac{\partial \mathbf{\Phi}_2}{\partial x} + \frac{\partial u_2}{\partial y} \frac{\partial \mathbf{\Phi}_2}{\partial y} \right) \mathrm{d}\Omega_2 - \oint_{\Gamma_2} k_2 \left(\frac{\partial u_2}{\partial x} n_{x_2} + \frac{\partial u_2}{\partial y} n_{y_2} \right) \mathbf{\Phi}_2 \mathrm{d}\Gamma_2 - \int_{\Omega_2} Q_2 \mathbf{\Phi}_2 \mathrm{d}\Omega_2 \\ + \int_{\Gamma_2^s} \left(k_2 \frac{\mathrm{d}u_2}{\mathrm{d}n} - \bar{q}_2 \right) \overline{\mathbf{\Phi}}_2 \mathrm{d}\Gamma_2^s = 0 \end{aligned} \qquad (2.27)$$

Note that the domain boundary is presumed to consist of boundaries on which the primary variable is specified, boundaries on which the secondary variable is specified,

and boundaries at the subdomain interface. Thus, for subdomain *i*, $\Gamma_i = \Gamma_i^p + \Gamma_i^s + \Gamma_i^{\mathrm{I}}$. Here, the boundary on the interface is assumed to be conforming (*i.e.*, represents same geometry) and $\Gamma_i^{\mathrm{I}} = \Gamma^{\mathrm{I}}$. Therefore, the boundary integral on Γ_i, may be expressed as

$$\oint_{\Gamma_i}\left(\frac{\partial u_i}{\partial x}n_{x_i}+\frac{\partial u_i}{\partial y}n_{y_i}\right)\boldsymbol{\Phi}_i\,\mathrm{d}\Gamma_i = \int_{\Gamma_i^p}\left(\frac{\partial u_i}{\partial x}n_{x_i}+\frac{\partial u_i}{\partial y}n_{y_i}\right)\boldsymbol{\Phi}_i\mathrm{d}\Gamma_i^p$$
$$+\int_{\Gamma_i^s}\left(\frac{\partial u_i}{\partial x}n_{x_i}+\frac{\partial u_i}{\partial y}n_{y_i}\right)\boldsymbol{\Phi}_i\mathrm{d}\Gamma_i^s+\int_{\Gamma^{\mathrm{I}}}\left(\frac{\partial u_i}{\partial x}n_{x_i}+\frac{\partial u_i}{\partial y}n_{y_i}\right)\boldsymbol{\Phi}_i\,\mathrm{d}\Gamma^{\mathrm{I}}$$

Note that $\boldsymbol{\Phi}_i = \mathbf{0}$ on Γ_i^p. Eq. (2.27) can be rewritten, for subdomain 1, as

$$\int_{\Omega_1}k_1\left(\frac{\partial u_1}{\partial x}\frac{\partial \boldsymbol{\Phi}_1}{\partial x}+\frac{\partial u_1}{\partial y}\frac{\partial \boldsymbol{\Phi}_1}{\partial y}\right)\mathrm{d}\Omega_1-\int_{\Gamma_1^s}k_1\frac{\mathrm{d}u_1}{\mathrm{d}n}\boldsymbol{\Phi}_1\mathrm{d}\Gamma_1^s-\int_{\Gamma^{\mathrm{I}}}k_1\frac{\mathrm{d}u_1}{\mathrm{d}n}\boldsymbol{\Phi}_1\mathrm{d}\Gamma^{\mathrm{I}}$$
$$+\int_{\Gamma_1^s}\left(k_1\frac{\mathrm{d}u_1}{\mathrm{d}n}-\bar{q}_1\right)\overline{\boldsymbol{\Phi}}_1\mathrm{d}\Gamma_1^s-\int_{\Omega_1}Q_1\boldsymbol{\Phi}_1\mathrm{d}\Omega_1=0$$

Since the weight functions, $\boldsymbol{\Phi}_1$ and $\overline{\boldsymbol{\Phi}}_1$, are arbitrary, they may be chosen, such that, $\boldsymbol{\Phi}_1 = \overline{\boldsymbol{\Phi}}_1$. Therefore,

$$\int_{\Omega_1}k_1\left(\frac{\partial u_1}{\partial x}\frac{\partial \boldsymbol{\Phi}_1}{\partial x}+\frac{\partial u_1}{\partial y}\frac{\partial \boldsymbol{\Phi}_1}{\partial y}\right)\mathrm{d}\Omega_1-\int_{\Gamma^{\mathrm{I}}}k_1\frac{\mathrm{d}u_1}{\mathrm{d}n}\boldsymbol{\Phi}_1\mathrm{d}\Gamma^{\mathrm{I}}-\int_{\Gamma_1^s}\bar{q}_1\boldsymbol{\Phi}_1\mathrm{d}\Gamma_1^s$$
$$-\int_{\Omega_1}Q_1\boldsymbol{\Phi}_1\mathrm{d}\Omega_1=0 \qquad (2.28)$$

Similarly, for subdomain, Ω_2,

$$\int_{\Omega_2}k_2\left(\frac{\partial u_2}{\partial x}\frac{\partial \boldsymbol{\Phi}_2}{\partial x}+\frac{\partial u_2}{\partial y}\frac{\partial \boldsymbol{\Phi}_2}{\partial y}\right)\mathrm{d}\Omega_2-\int_{\Gamma^{\mathrm{I}}}k_2\frac{\mathrm{d}u_2}{\mathrm{d}n}\boldsymbol{\Phi}_2\,\mathrm{d}\Gamma^{\mathrm{I}}-\int_{\Gamma_2^s}\bar{q}_2\boldsymbol{\Phi}_2\mathrm{d}\Gamma_2^s$$
$$-\int_{\Omega_2}Q_2\boldsymbol{\Phi}_2\mathrm{d}\Omega_2=0 \qquad (2.29)$$

In general, for the multiple domain case, the approximation for the primary variable (*e.g.*, the potential field) must satisfy the following conditions:

i. The primary variable must be continuous and single valued in the subdomain.

ii. The primary variable must be continuous across the interdomain boundary.

iii. The primary variable on the subdomain boundary must satisfy the boundary conditions.

If the requirement to satisfy interdomain continuity is relaxed, an additional boundary condition is used, namely,

$$u_1 - u_2 = 0 \quad \text{on} \quad \Gamma^{\mathrm{I}}.$$

This constraint can be satisfied in the integral sense as

$$\int_{\Gamma_{\mathrm{I}}} \lambda(u_1 - u_2)\mathrm{d}\Gamma = 0 \quad \text{on} \quad \Gamma^{\mathrm{I}} \tag{2.30}$$

where λ is a Lagrange multiplier associated with the secondary variable along the common subdomain boundary. Therefore, combining Eqs. (2.28) and (2.29) for the entire domain, and including the continuity integral at the interdomain boundary yields

$$\begin{aligned} &\int_{\Omega_1} k_1\left(\frac{\partial u_1}{\partial x}\frac{\partial \boldsymbol{\Phi}_1}{\partial x} + \frac{\partial u_1}{\partial y}\frac{\partial \boldsymbol{\Phi}_1}{\partial y}\right)\mathrm{d}\Omega_1 + \int_{\Omega_2} k_2\left(\frac{\partial u_2}{\partial x}\frac{\partial \boldsymbol{\Phi}_2}{\partial x} + \frac{\partial u_2}{\partial y}\frac{\partial \boldsymbol{\Phi}_2}{\partial y}\right)\mathrm{d}\Omega_2 - \int_{\Omega_1} Q_1\boldsymbol{\Phi}_1\mathrm{d}\Omega_1 \\ &\quad - \int_{\Omega_2} Q_2\boldsymbol{\Phi}_2\mathrm{d}\Omega_2 - \oint_{\Gamma_1^s} \bar{q}_1\boldsymbol{\Phi}_1\,\mathrm{d}\Gamma_1^s - \int_{\Gamma_2^s} \bar{q}_2\boldsymbol{\Phi}_2\mathrm{d}\Gamma_2^s - \int_{\Gamma^{\mathrm{I}}} \hat{q}_1\boldsymbol{\Phi}_1\,\mathrm{d}\Gamma^{\mathrm{I}} - \int_{\Gamma^{\mathrm{I}}} \hat{q}_2\boldsymbol{\Phi}_2\mathrm{d}\Gamma^{\mathrm{I}} \\ &\quad + \int_{\Gamma^{\mathrm{I}}} \lambda(u_1 - u_2)\mathrm{d}\Gamma^{\mathrm{I}} = 0 \end{aligned} \tag{2.31}$$

where for subdomain, i, $\hat{\mathbf{q}}_i$, are the secondary variables along the interdomain boundary, $\hat{\mathbf{q}}_i = \dfrac{\mathrm{d}u_i}{\mathrm{d}n} = \dfrac{\partial u_i}{\partial x}n_{x_i} + \dfrac{\partial u_i}{\partial y}n_{y_i}$. Note that the normals on the interdomain

boundary are equal and opposite (see Figure 2.3). That is, $\mathbf{n}_1 = -\mathbf{n}_2$ where $\mathbf{n}_i = n_{x_i}\mathbf{i} + n_{y_i}\mathbf{j}$, and it follows that, $\hat{\mathbf{q}}_1 = -\hat{\mathbf{q}}_2 = \hat{\mathbf{q}}$. Therefore,

$$\int_{\Omega_1} k_1\left(\frac{\partial u_1}{\partial x}\frac{\partial \mathbf{\Phi}_1}{\partial x} + \frac{\partial u_1}{\partial y}\frac{\partial \mathbf{\Phi}_1}{\partial y}\right)\mathrm{d}\Omega_1 + \int_{\Omega_2} k_2\left(\frac{\partial u_2}{\partial x}\frac{\partial \mathbf{\Phi}_2}{\partial x} + \frac{\partial u_2}{\partial y}\frac{\partial \mathbf{\Phi}_2}{\partial y}\right)\mathrm{d}\Omega_2 - \int_{\Omega_1} Q_1\mathbf{\Phi}_1\mathrm{d}\Omega_1$$
$$- \int_{\Omega_2} Q_2\mathbf{\Phi}_2\mathrm{d}\Omega_2 - \int_{\Gamma_1^s} \bar{q}_1\mathbf{\Phi}_1\mathrm{d}\Gamma_1^s - \int_{\Gamma_2^s} \bar{q}_2\mathbf{\Phi}_2\mathrm{d}\Gamma_2^s - \int_{\Gamma^{\mathrm{I}}} \hat{q}\left(\mathbf{\Phi}_1 - \mathbf{\Phi}_2\right)\mathrm{d}\Gamma^{\mathrm{I}}$$
$$+ \int_{\Gamma^{\mathrm{I}}} \lambda\left(u_1 - u_2\right)\mathrm{d}\Gamma^{\mathrm{I}} = 0$$

or rearranging

$$\left[\int_{\Omega_1} k_1\left(\frac{\partial u_1}{\partial x}\frac{\partial \mathbf{\Phi}_1}{\partial x} + \frac{\partial u_1}{\partial y}\frac{\partial \mathbf{\Phi}_1}{\partial y}\right)\mathrm{d}\Omega_1 - \oint_{\Gamma^{\mathrm{I}}} \hat{q}\mathbf{\Phi}_1\,\mathrm{d}\Gamma^{\mathrm{I}} - \int_{\Omega_1} Q_1\mathbf{\Phi}_1\mathrm{d}\Omega_1 - \int_{\Gamma_1^s} \bar{q}_1\mathbf{\Phi}_1\,\mathrm{d}\Gamma_1^s\right] +$$
$$\left[\int_{\Omega_2} k_2\left(\frac{\partial u_2}{\partial x}\frac{\partial \mathbf{\Phi}_2}{\partial x} + \frac{\partial u_2}{\partial y}\frac{\partial \mathbf{\Phi}_2}{\partial y}\right)\mathrm{d}\Omega_2 + \oint_{\Gamma^{\mathrm{I}}} \hat{q}\mathbf{\Phi}_2\,\mathrm{d}\Gamma^{\mathrm{I}} - \int_{\Omega_2} Q_2\mathbf{\Phi}_2\mathrm{d}\Omega_2 - \int_{\Gamma_2^s} \bar{q}_2\mathbf{\Phi}_2\,\mathrm{d}\Gamma_2^s\right] \qquad (2.32)$$
$$+\left[\int_{\Gamma^{\mathrm{I}}} \lambda\left(u_1 - u_2\right)\mathrm{d}\Gamma^{\mathrm{I}}\right] = 0\,.$$

Note that Eq. (2.32) is written as a single equation for convenience and represents the sum of terms related to the residual in the governing differential equation within each subdomain and the continuity constraint for the primary variables along the common subdomain boundary. However, each of the bracketed terms in Eq. (2.32) must equal zero individually. These bracketed terms are identical to Eqs. (2.28), (2.29), and (2.30) which must be satisfied independently.

In this formulation, the two primary field variables, u_1 and u_2 are approximated independently, and continuity requirements between these two approximations are satisfied along the subdomain interface boundary. The use of these approximations and

the associated continuity requirements gives rise to the classification of the formulation as a two-approximation approach.

Now consider a configuration that makes use of a third approximation for the primary variable along the subdomain interface boundary in addition to the approximations given along the boundary of each of the subdomains. This primary variable, v, along the interface is assumed to be independent of the primary variables, u_1 and u_2, of the subdomains to which it is attached. These independent approximations give rise to continuity requirements along the interface of the form

$$v - u_1 = 0 \quad \text{on} \quad \Gamma^{\mathrm{I}}$$

$$v - u_2 = 0 \quad \text{on} \quad \Gamma^{\mathrm{I}}$$

These constraints can be satisfied in the integral sense as

$$\int_{\Gamma^{\mathrm{I}}} \lambda_1 (v - u_1) \mathrm{d}\Gamma^{\mathrm{I}} = 0 \quad \text{on} \quad \Gamma^{\mathrm{I}} \tag{2.33}$$

$$\int_{\Gamma^{\mathrm{I}}} \lambda_2 (v - u_2) \mathrm{d}\Gamma^{\mathrm{I}} = 0 \quad \text{on} \quad \Gamma^{\mathrm{I}} \tag{2.34}$$

where λ_1 and λ_2 are Lagrange multipliers or weight functions in the form of the secondary variable along the interface. An additional continuity requirement in terms of the secondary variable along the common subdomain boundary is required. These secondary variables, $\hat{q}_1$ and $\hat{q}_2$, are assumed to be independent of each other. These independent approximations give rise to continuity requirements along the interface of the form

$$\hat{q}_1 + \hat{q}_2 = 0 \quad \text{on} \quad \Gamma^{\mathrm{I}}$$

These constraints can be satisfied in the integral sense as

$$\int_{\Gamma^I} \hat{\lambda}(\hat{q}_1 + \hat{q}_2)\, d\Gamma^I = 0 \quad \text{on} \quad \Gamma^I \tag{2.35}$$

where $\hat{\lambda}$ is a Lagrange multiplier or weight function of the form of the primary variable along the interface. Combining Eqs. (2.28) and (2.29) for the entire domain and including the three continuity integrals along the interdomain boundary, Eqs. (2.33), (2.34), and (2.35), yields

$$\int_{\Omega_1} k_1 \left(\frac{\partial u_1}{\partial x}\frac{\partial \boldsymbol{\Phi}_1}{\partial x} + \frac{\partial u_1}{\partial y}\frac{\partial \boldsymbol{\Phi}_1}{\partial y} \right) d\Omega_1 + \int_{\Omega_2} k_2 \left(\frac{\partial u_2}{\partial x}\frac{\partial \boldsymbol{\Phi}_2}{\partial x} + \frac{\partial u_2}{\partial y}\frac{\partial \boldsymbol{\Phi}_2}{\partial y} \right) d\Omega_2 -$$
$$\int_{\Gamma^I} \hat{q}_1 \boldsymbol{\Phi}_1\, d\Gamma^I - \int_{\Gamma^I} \hat{q}_2 \boldsymbol{\Phi}_2\, d\Gamma^I + \int_{\Gamma^I} \lambda_1 (v - u_1) d\Gamma^I + \int_{\Gamma^I} \lambda_2 (v - u_2) d\Gamma^I + \int_{\Gamma^I} \hat{\lambda}(\hat{q}_1 + \hat{q}_2) d\Gamma^I$$
$$= \int_{\Omega_1} Q_1 \boldsymbol{\Phi}_1 d\Omega_1 + \int_{\Gamma_1^s} \bar{q}_1 \boldsymbol{\Phi}_1\, d\Gamma_1^s + \int_{\Omega_2} Q_2 \boldsymbol{\Phi}_2 d\Omega_2 + \int_{\Gamma_2^s} \bar{q}_2 \boldsymbol{\Phi}_2\, d\Gamma_2^s$$

or rearranging

$$\left[\int_{\Omega_1} k_1 \left(\frac{\partial u_1}{\partial x}\frac{\partial \boldsymbol{\Phi}_1}{\partial x} + \frac{\partial u_1}{\partial y}\frac{\partial \boldsymbol{\Phi}_1}{\partial y} \right) d\Omega_1 - \int_{\Gamma^I} \hat{q}_1 \boldsymbol{\Phi}_1\, d\Gamma^I - \int_{\Omega_1} Q_1 \boldsymbol{\Phi}_1 d\Omega_1 - \int_{\Gamma_1^s} \bar{q}_1 \boldsymbol{\Phi}_1\, d\Gamma_1^s \right] +$$
$$\left[\int_{\Omega_2} k_2 \left(\frac{\partial u_2}{\partial x}\frac{\partial \boldsymbol{\Phi}_2}{\partial x} + \frac{\partial u_2}{\partial y}\frac{\partial \boldsymbol{\Phi}_2}{\partial y} \right) d\Omega_2 - \int_{\Gamma^I} \hat{q}_2 \boldsymbol{\Phi}_2\, d\Gamma^I - \int_{\Omega_2} Q_2 \boldsymbol{\Phi}_2 d\Omega_2 - \int_{\Gamma_2^s} \bar{q}_2 \boldsymbol{\Phi}_2\, d\Gamma_2^s \right] \tag{2.36}$$
$$+ \left[\int_{\Gamma^I} \lambda_1 (v - u_1) d\Gamma^I \right] + \left[\int_{\Gamma^I} \lambda_2 (v - u_2) d\Gamma^I \right] + \left[\int_{\Gamma^I} \hat{\lambda}(\hat{q}_1 + \hat{q}_2) d\Gamma^I \right] = 0$$

Again, note that Eq. (2.36) is written as a single equation for convenience and represents the sum of terms related to the residual in the governing differential equation within each subdomain and the continuity constraints for the primary and secondary variables along the common subdomain boundary. Each of the bracketed terms in Eq. (2.36) must equal zero individually. These bracketed terms are identical to Eqs. (2.28), (2.29), (2.33), (2.34), and (2.35), which must be satisfied independently.

The integral form of Eqs. (2.32) and (2.36) forms the basis for the subsequent spatial modeling approximations. The spatial modeling approximations are discussed in detail in the next section. Eqs. (2.32) and (2.36) may be generalized for more than two subdomains and for multiple interfaces by

$$\sum_{m=1}^{N_{ss}}\left[\int_{\Omega_m} k_m\left(\frac{\partial u_m}{\partial x}\frac{\partial \mathbf{\Phi}_m}{\partial x}+\frac{\partial u_m}{\partial y}\frac{\partial \mathbf{\Phi}_m}{\partial y}\right)\mathrm{d}\Omega_m\right]$$
$$+\sum_{i=1}^{N_I}\sum_{j=1}^{n_{ss}(i)}\left[(-1)^{j+1}\left(\int_{\Gamma_i^{\mathrm{I}}}\lambda_i u_{ij}\,\mathrm{d}\Gamma_{ij}^{\mathrm{I}}-\oint_{\Gamma_i^{\mathrm{I}}}\hat{q}_i\mathbf{\Phi}_{ij}\,\mathrm{d}\Gamma_{ij}^{\mathrm{I}}\right)\right]=\sum_{m=1}^{N_{ss}}\left[\int_{\Omega_m}Q_m\mathbf{\Phi}_m\mathrm{d}\Omega_m+\int_{\Gamma_m^s}\bar{q}_m\mathbf{\Phi}_m\,\mathrm{d}\Gamma_m^s\right] \tag{2.37}$$

and

$$\sum_{m=1}^{N_s}\left[\int_{\Omega_m} k_m\left(\frac{\partial u_m}{\partial x}\frac{\partial \mathbf{\Phi}_m}{\partial x}+\frac{\partial u_m}{\partial y}\frac{\partial \mathbf{\Phi}_m}{\partial y}\right)\mathrm{d}\Omega_m\right]$$
$$+\sum_{i=1}^{N_I}\sum_{j=1}^{n_{ss}(i)}\left[\int_{\Gamma_i^{\mathrm{I}}}\lambda_{ij}\left(v_i-u_{ij}\right)\mathrm{d}\Gamma_{ij}^{\mathrm{I}}-\int_{\Gamma_i^{\mathrm{I}}}\hat{q}_{ij}\mathbf{\Phi}_{ij}\,\mathrm{d}\Gamma_{ij}^{\mathrm{I}}+\int_{\Gamma_i^{\mathrm{I}}}\hat{\lambda}_i\hat{q}_{ij}\,\mathrm{d}\Gamma_{ij}^{\mathrm{I}}\right] \tag{2.38}$$
$$=\sum_{m=1}^{N_s}\left[\int_{\Omega_m}Q_m\mathbf{\Phi}_m\mathrm{d}\Omega_m+\int_{\Gamma_m^s}\bar{q}_m\mathbf{\Phi}_m\,\mathrm{d}\Gamma_m^s\right]$$

where N_{ss} is the number of subdomains in which the entire domain is subdivided, N_I is the number of interfaces connecting the N_{ss} subdomains and $n_{ss}(i)$ are the number of subdomains attached to interface i. For example, for one interface connecting two subdomains, Eq. (2.38) yields in its expanded form

$$\left[\int_{\Omega_1} k_1\left(\frac{\partial u_1}{\partial x}\frac{\partial \Phi_1}{\partial x}+\frac{\partial u_1}{\partial y}\frac{\partial \Phi_1}{\partial y}\right)d\Omega_1+\int_{\Omega_2} k_2\left(\frac{\partial u_2}{\partial x}\frac{\partial \Phi_2}{\partial x}+\frac{\partial u_2}{\partial y}\frac{\partial \Phi_2}{\partial y}\right)d\Omega_2\right]$$
$$+\int_{\Gamma_1^I}\lambda_{11}(v_1-u_{11})d\Gamma_1^I-\int_{\Gamma_1^I}\hat{q}_{11}\Phi_{11}\,d\Gamma_1^I+\int_{\Gamma_1^I}\lambda_{12}(v_1-u_{12})d\Gamma_1^I-\int_{\Gamma_1^I}\hat{q}_{12}\Phi_{12}\,d\Gamma_1^I+$$
$$\int_{\Gamma_1^I}\hat{\lambda}_1\hat{q}_{11}\,d\Gamma_1^I+\int_{\Gamma_1^I}\hat{\lambda}_1\hat{q}_{12}\,d\Gamma_1^I=\int_{\Omega_1}Q_1\Phi_1 d\Omega_1+\int_{\Gamma_1^s}\bar{q}_1\Phi_1\,d\Gamma_1^s+\int_{\Omega_2}Q_2\Phi_2 d\Omega_2+\int_{\Gamma_2^s}\bar{q}_2\Phi_2\,d\Gamma_2^s$$

which is identical to Eq. (2.36).

2.5. SPATIAL MODELING FOR MULTIPLE DOMAINS

Although this section is focused on spatial modeling of multiple domains using a multifunctional development, a brief discussion of spatial modeling for a single domain is given first, followed by a more detailed discussion for multiple domains. Thus far, a multifunctional approach based on weighted residuals has been formulated. This approximation technique provides a mechanism for finding approximate solutions to problems in mathematical physics and engineering science such as those represented by the Poisson problem. Selection of the approximating and weighting functions for complex geometrical shapes and boundary conditions poses a major difficulty for weighted residual methods. In addition, the methods were generally not regarded as being computationally competitive compared to the traditional finite difference method. However, weighted residual methods offer a versatile means by which to formulate finite element equations where no functional is available. Hence, many of the difficulties associated with this class of methods are alleviated. The derivation of discrete equations is an essential component of the approximation technique. Thus, several discretization approaches are outlined in the next section.

2.5.1. Overview of Discretization Methods

Various forms of spatial modeling or discretization of the continuum problem defined by the differential equations can be used. These forms include, but are not limited to, the finite difference method, the finite volume method, the finite element method, and the boundary element method. In such spatial modeling, the infinite set of numbers, representing the unknown function or functions is replaced by a finite number of unknown parameters. A brief discussion of each of the aforementioned modeling methods is given here to provide the foundation for discussion of interfacing such diverse methods, which is presented in subsequent subsections.

The finite difference method

Of the various forms of spatial modeling, one of the simplest is the finite difference method. The finite difference method gives a pointwise approximation to the governing equations. In the finite difference approximation of a differential equation, the derivatives in the equation are replaced by differential quotients that involve the values of the solution at discrete mesh points of the domain. The resulting discrete equations are solved for values of the solution at the mesh points, after imposing the boundary conditions. While finite difference techniques are widely used in fluid dynamics and heat transfer and can treat fairly difficult problems, they become hard to use when irregular geometrical shapes or unusual boundary conditions are encountered. In addition, because it is difficult to vary the size of different cells in particular regions, the method is not suitable for problems of rapidly changing variables, such as stress concentration problems. These adverse attributes are particularly significant in structural analysis.

The finite volume method

The finite volume method evolved in the early seventies via the finite difference approximations and has many proponents in the field of fluid mechanics. The method takes as its starting point the physical conservation laws in integral form written for small control volumes around every discrete point. Modifying the shape and location of the control volumes associated with a given discrete point, as well as varying the rules and accuracy for the evaluation of the fluxes through the control volume, gives the method considerable flexibility. Unlike the finite difference method, the finite volume method can readily handle arbitrary mesh orientation thus making it more amenable to problems of rapidly changing variables. In addition, by direct discretization of the integral form of the conservation laws, the basic quantities (*e.g.*, mass, momentum, and energy) will be conserved at the discrete level. Like the finite difference method, the finite volume method has been shown to be a special case of the finite element method with non-Galerkin weight functions[35].

The finite element method

The finite element method consists of representing a given domain by an assembly of smaller, geometrically simple subdomains or elements over which the approximation functions are systematically derived. Then, Ritz-Galerkin approximations of the governing equations are developed over each element. Finally, the equations over all elements of the collection are connected by continuity of the primary variables. In the mathematical literature, the names Petrov-Galerkin are often associated with the use of weighting functions such that $\mathbf{\Phi} \neq \mathbf{N}$, and the names Bubnov-Galerkin are often associated with the use of weighting functions such that $\mathbf{\Phi} = \mathbf{N}$, where in the finite

element method **N** are the element shape functions. The latter method is often referred to as the Galerkin method. The resulting system of equations is sparse, banded, symmetric, and positive definite. The finite element method is especially well suited for handling arbitrary shapes or domains. To obtain good accuracy in regions of rapidly changing variables a large number of small elements must be used. Furthermore, the method is widely used for the analysis of many engineering problems involving static, dynamic, and thermal stresses of structures.

The boundary element method

The boundary element method is an alternative to the finite element method. Like the finite element method, the boundary element method uses nodes and elements to discretize the boundary of the domain. Thus, compared to the finite element method, the dimensionality is reduced by one. The governing differential equations are transformed into integral identities, which are applicable over a surface or boundary. These integrals are numerically integrated over the boundary, which is divided into small boundary segments. The method may be used to model accurately the response in the domain bounded by its mesh. The method can easily accommodate geometrically complex boundaries. Furthermore, since all the approximations are restricted to the surface, the method can be used to model regions with rapidly changing variables with better accuracy than the finite element method. Complex kernel routines are required to determine the response for the interior of the domain. Hence, the computational expense increases quickly if the response at several interior locations is needed. In addition, for nonlinear problems, the interior must be modeled; thus losing the advantage of reduction

in dimensionality. Unlike the finite element system matrix, the analogous boundary element matrix is small, fully populated, and unsymmetric.

Each of the aforementioned discretization approaches has advantages and disadvantages specific to the domain of the physical problem or the discipline within which it is applied. To overcome the disadvantages of the individual methods, coupled or collaborative methods have been developed. Collaborative methods couple two or more discretization approaches and make use of a given approach when and where it is best suited. The interaction between the methods is an essential feature related to the robustness and accuracy of the combined methods and is a subject of discussion herein. Moreover, this work focuses on the application of the multifunctional method developed here to the finite difference and finite element methods and their coupling. Computational methods using finite-differences for fluids experiencing field discontinuities such as shock-waves and flow separations have been proven to be efficient solution techniques. The finite element method has proven to be efficient in solving for the response of complex aerospace structures, which may contain internal discontinuous members such as spars, ribs, and bulkheads found in fuselage and wing structures. In addition, coupled finite difference/finite element methods have been proposed that make use of the strengths of the each of the modeling methods in the solution of the aeroelastic problem and elasticity problems in references 36 and 19, respectively. Thus, both spatial modeling approaches and their coupling will be discussed in turn.

2.5.2. Overview of Single-Domain Spatial Modeling

Finite element discretization

For a single domain, the finite element equations may be obtained by rewriting Eq. (2.19) over an element domain as

$$\int_{\Omega^e} k\left(\frac{\partial u}{\partial x}\frac{\partial \mathbf{\Phi}}{\partial x}+\frac{\partial u}{\partial y}\frac{\partial \mathbf{\Phi}}{\partial y}\right)\mathrm{d}\Omega^e = \int_{\Omega^e} Q\mathbf{\Phi}\mathrm{d}\Omega^e + \int_{\Gamma^{s\,e}} \bar{q}\mathbf{\Phi}\,\mathrm{d}\Gamma^{s\,e} \tag{2.39}$$

where superscripts on the domain, Ω, and boundary surface, Γ^s, integrals denote integration over the element. In later sections, numeric subscripts will be used to denote element integration within the specified subdomain. The primary variable is approximated over the element domain by $u = \mathbf{N}\mathbf{u}_e$, and using the Galerkin method, the vector of weight functions is given by $\mathbf{\Phi} = \mathbf{N}$. Substituting approximations into the integral equation given in Eq. (2.39) yields

$$\left[\int_{\Omega^e} k\left(\frac{\partial \mathbf{N}^{\mathrm{T}}}{\partial x}\frac{\partial \mathbf{N}}{\partial x}+\frac{\partial \mathbf{N}^{\mathrm{T}}}{\partial y}\frac{\partial \mathbf{N}}{\partial y}\right)\mathrm{d}\Omega^e\right]\mathbf{u}_e = \int_{\Omega^e} \mathbf{N}^{\mathrm{T}} Q\mathrm{d}\Omega^e + \int_{\Gamma^{s\,e}} \mathbf{N}^{\mathrm{T}}\bar{q}\,\mathrm{d}\Gamma^{s\,e}$$

or

$$\mathbf{k}_e\mathbf{u}_e = \mathbf{f}_e$$

where $\mathbf{k}_e$ is the element stiffness matrix, $\mathbf{u}_e$ is the vector containing the generalized primary variables, and $\mathbf{f}_e$ is the element force vector containing the generalized secondary variables. The element field quantities, **k**, **u**, and **f**, are denoted by a subscript, *e*. Assembling these element equations over the entire domain and enforcing continuity of the primary variable at the interelement boundaries yields the system of equations given by

$$\mathbf{K}\mathbf{u} = \mathbf{F}$$

where $\mathbf{K} = \sum_{e=1}^{nelem} \int_{\Omega^e} k\left(\frac{\partial \mathbf{N}^{\mathrm{T}}}{\partial x}\frac{\partial \mathbf{N}}{\partial x} + \frac{\partial \mathbf{N}^{\mathrm{T}}}{\partial y}\frac{\partial \mathbf{N}}{\partial y}\right)\mathrm{d}\Omega^e$; **u** is the assembly of all of the nodal degrees of freedom associated with the primary variables; and

$$\mathbf{F} = \sum_{1}^{nnodes} \int_{\Omega^e} \mathbf{N}^{\mathrm{T}} Q \mathrm{d}\Omega^e + \int_{\Gamma^{s\,e}} \mathbf{N}^{\mathrm{T}} \bar{q} \mathrm{d}\Gamma^{s\,e}$$

Finite difference discretization

In the finite difference methods, derivatives are approximated by difference expressions that transform the derivatives appearing in the partial differential equations to algebraic equations. For an elliptic partial differential equation, usually time-independent, the methods result in a system of algebraic equations that are solved using a direct or iterative solution technique. For hyperbolic and parabolic partial differential equations, a set of algebraic equations is obtained. These equations are solved either explicitly or implicitly. For the explicit solution, each equation will yield one unknown. The matrix of unknown variables is a diagonal matrix and the right-hand-side vector of the system is dependent on the variables at previous times. For the implicit solution, the equations are coupled and must be solved simultaneously. Since the system equations are coupled and more than one set of variables is unknown at the same level, the matrix to be inverted is non-diagonal. In most cases, however, the structure of the matrix will be rather simple, such as a block pentadiagonal, block tridiagonal, or block bidiagonal. The truncation errors, stability and consistency of the numerical scheme are aspects that must be considered in the development of the methods. The difference expressions are obtained by Taylor series expansion, using forward, backward or central expansions. Zienkiewicz and Morgan[37] have shown that the finite difference method of approximation

is a particular case of collocation with locally defined basis functions. In the collocation method, the unknown weight function parameters are determined by forcing the residual in the approximation to vanish at *N* selected points in the domain. Upon substitution of the approximation function into the differential equation, the equations can be recast in weighted residual form by selecting $\Phi_i = \delta(x - x_i)$. The weighted form of the residual reduces to the evaluation of the partial differential equations using the approximate solution evaluated at the *N* selected mesh points. For a second-order ordinary differential equation, the approximate solution, $\tilde{u}$, may be given as a function of the solution at neighboring points (see Figure 2.4) as

$$\tilde{u} = u_{i-1}N_{i-1}^e + u_i N_i^e + u_{i+1}N_{i+1}^e$$

where N_i^e are locally defined quadratic basis functions represented by

$$N_{i-1}^e = -\frac{x(h^e - x)}{2(h^e)^2}; \quad N_i^e = \frac{(h^e - x)(h^e + x)}{(h^e)^2}; \quad N_{i+1}^e = \frac{x(h^e + x)}{2(h^e)^2}.$$

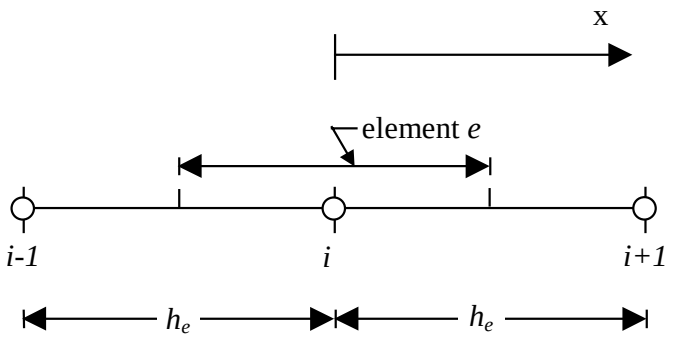

Figure 2.4. One-Dimensional Finite Difference Element Configuration.

The locally defined quadratic basis functions, N_i^e, given here in the Cartesian coordinate system, may be written in the element natural coordinate system, ξ, as

$$N_{i-1}^e = -\frac{1}{2}\xi(1-\xi); \quad N_i^e = (1-\xi^2); \quad N_{i+1}^e = \frac{1}{2}\xi(1+\xi)$$

where $\xi = x/h^e$. Note that $-1 \le \xi \le 1$. These basis functions are the standard Lagrangian shape functions for three-node one-dimensional finite elements. This derivation for one-dimensional problems may be extended to two- and three-dimensional problems. The derivation is given for two-dimensional problems considering the bi-quadratic shape functions for a nine-node two-dimensional finite element. A schematic of the finite difference template and the associated finite element are shown in Figure 2.5 where the open circles represent grid points in the five-point finite difference template used to represent second-order derivatives.

The shape functions for a nine-node quadrilateral[34] are given in Table 2.1. For example, the shape function at point i,j-1 is given by

$$N_{i,j-1} = \frac{1}{2}(1-\xi^2)(1-\eta) - \frac{1}{2}(1-\xi^2)(1-\eta^2).$$

Similarly,

$$N_{i+1,j} = \frac{1}{2}(1+\xi)(1-\eta^2) - \frac{1}{2}(1-\xi^2)(1-\eta^2),$$

$$N_{i,j+1} = \frac{1}{2}(1-\xi^2)(1+\eta) - \frac{1}{2}(1-\xi^2)(1-\eta^2),$$

$$N_{i-1,j} = \frac{1}{2}(1-\xi)(1-\eta^2) - \frac{1}{2}(1-\xi^2)(1-\eta^2),$$

and

$$N_{i,j} = (1-\xi^2)(1-\eta^2).$$

Then,

$$\frac{\partial^2 N_{i-1,j}}{\partial x^2} = \frac{1}{\left(h^e\right)^2}\frac{\partial^2 N_{i-1,j}}{\partial \xi^2} = \frac{1}{\left(h^e\right)^2}\left[\left(1-\eta^2\right)\Big|_{\eta=0}\right] = \frac{1}{\left(h^e\right)^2} = \frac{\partial^2 N_{i+1,j}}{\partial x^2},$$

$$\frac{\partial^2 N_{i,j}}{\partial x^2} = \frac{1}{\left(h^e\right)^2}\frac{\partial^2 N_{i,j}}{\partial \xi^2} = \frac{1}{\left(h^e\right)^2}\left[-2\left(1-\eta^2\right)\Big|_{\eta=0}\right] = \frac{-2}{\left(h^e\right)^2},$$

$$\frac{\partial^2 N_{i,j-1}}{\partial y^2} = \frac{1}{\left(h^e\right)^2}\frac{\partial^2 N_{i,j-1}}{\partial \eta^2} = \frac{1}{\left(h^e\right)^2}\left[\left(1-\xi^2\right)\Big|_{\eta=0}\right] = \frac{1}{\left(h^e\right)^2} = \frac{\partial^2 N_{i,j+1}}{\partial x^2}, \quad (2.40)$$

and

$$\frac{\partial^2 N_{i,j}}{\partial y^2} = \frac{1}{\left(h^e\right)^2}\frac{\partial^2 N_{i,j}}{\partial \eta^2} = \frac{1}{\left(h^e\right)^2}\left[-2\left(1-\xi^2\right)\Big|_{\xi=0}\right] = \frac{-2}{\left(h^e\right)^2}.$$

The standard finite difference representation follows by direct substitution. This specialization of the finite difference method as a form of the generalized method of weighted residuals forms the basis for its inclusion in this multifunctional derivation.

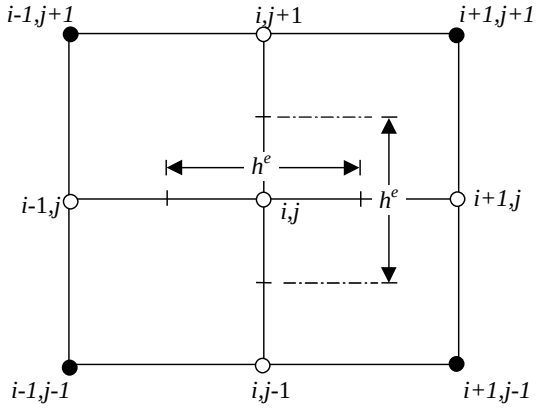

Figure 2.5. Two-Dimensional Finite Difference Element Configuration.

For a single domain, as in the finite element method, the finite difference equations may be obtained by interrogating the weighted residual equations over an element domain where the element, *e*, surrounds node *i* (see Figure 2.5). The approximate solution for the primary variable is given by

$$\tilde{u} = \sum_{m=1}^{M} N_m u_m \quad \text{or} \quad \mathbf{u} = \mathbf{N}\mathbf{u}_e$$

where *M* is the number of shape functions over the element, and the weight function, Φ_i, is given by the Dirac delta function, $\delta(x - x_i, y - y_i) = \delta(x_i, y_i)$. Note that the subscript *i* on the weight function is used to denote the subdomain, while the subscript *i* on the coordinate values, *x* and *y*, is used to represent the point in the physical domain at which the Dirac delta function is evaluated. Therefore, Eq. (2.39) becomes

$$\left[\int_{\Omega^e} k \left(\frac{\partial \mathbf{N}}{\partial x} \frac{\partial \delta(x_i, y_i)}{\partial x} + \frac{\partial \mathbf{N}}{\partial y} \frac{\partial \delta(x_i, y_i)}{\partial y} \right) d\Omega^e \right] \mathbf{u}_e = \int_{\Omega^e} Q \delta(x_i, y_i) d\Omega^e + \int_{\Gamma^{s^e}} \bar{q} \delta(x_i, y_i) d\Gamma^{s^e}$$

Using the identities $\int_{-\infty}^{\infty} f(x) \delta(x - x_i) dx = f(x_i)$ and $\int_{-\infty}^{\infty} f(x) \frac{d\delta(x - x_i)}{dx} dx = \left. \frac{df(x)}{dx} \right|_{x=x_i}$

(See Bracewell[38]), the element equation reduces to

$$-k \left[\left. \frac{\partial^2 N}{\partial x^2} \right|_{\substack{x=x_i \\ y=y_i}} + \left. \frac{\partial^2 N}{\partial y^2} \right|_{\substack{x=x_i \\ y=y_i}} \right] \mathbf{u}_e = Q(x_i, y_i) + \bar{q}(x_i, y_i)$$

For the second derivative difference approximation, the number of shape functions of an element, *M*=3 and $\mathbf{u}_e^T = \{u_{i-1} \quad u_i \quad u_{i+1}\}$. Therefore, as in the finite element method, the resulting finite difference equations may be written in matrix form as

$$\mathbf{k}_e \mathbf{u}_e = \mathbf{f}_e$$

where $\mathbf{k}_e$ is the finite difference "element stiffness" matrix, $\mathbf{u}_e$ is the vector of generalized primary variables and $\mathbf{f}_e$ is the finite difference generalized force vector. Assembling the element equations yields

$$\mathbf{Ku} = \mathbf{F}$$

where $\mathbf{u}$ contains all of the nodal degrees of freedom associated with the primary variables,

$$\mathbf{K} = \sum_{1}^{Nelem} -k\left[\left.\frac{\partial^2 N}{\partial x^2}\right|_{\substack{x=x_i \\ y=y_i}} + \left.\frac{\partial^2 N}{\partial y^2}\right|_{\substack{x=x_i \\ y=y_i}}\right],$$

and

$$\mathbf{F} = \sum_{1}^{Nnodes}\left[Q(x_i, y_i) + \bar{q}(x_i, y_i)\right].$$

While a single spatial modeling approach (*i.e.*, the finite element method or the finite difference method) is used for the single domain formulation, subdomain modeling permits multiple discretization strategies to be used in a collaborative manner. These discretization strategies include homogeneous approaches in which the same discretization method is used in each subdomain and heterogeneous approaches in which different discretization methods are used amongst the subdomains. Each of these discretization strategies is discussed in the following sections.

Table 2.1. Shape Functions for a Nine-Node Quadrilateral Finite Element.

Primary Terms	Secondary Terms of Shape Functions				
$N_{i-1,j-1} = \frac{1}{4}(1-\xi)(1-\eta)$	$-\frac{1}{2}N_{i,j-1}$			$-\frac{1}{2}N_{i-1,j}$	$+\frac{1}{4}N_{i,j}$
$N_{i+1,j-1} = \frac{1}{4}(1+\xi)(1-\eta)$	$-\frac{1}{2}N_{i,j-1}$	$-\frac{1}{2}N_{i+1,j}$			$+\frac{1}{4}N_{i,j}$
$N_{i+1,j+1} = \frac{1}{4}(1+\xi)(1+\eta)$		$-\frac{1}{2}N_{i+1,j}$	$-\frac{1}{2}N_{i,j+1}$		$+\frac{1}{4}N_{i,j}$
$N_{i-1,j+1} = \frac{1}{4}(1-\xi)(1+\eta)$			$-\frac{1}{2}N_{i,j+1}$	$-\frac{1}{2}N_{i-1,j}$	$+\frac{1}{4}N_{i,j}$
$N_{i,j-1} = \frac{1}{2}(1-\xi^2)(1-\eta)$					$+\frac{1}{2}N_{i,j}$
$N_{i+1,j} = \frac{1}{2}(1+\xi)(1-\eta^2)$					$+\frac{1}{2}N_{i,j}$
$N_{i,j} = \frac{1}{2}(1-\xi^2)(1+\eta)$					$+\frac{1}{2}N_{i,j}$
$N_{i-1,j} = \frac{1}{2}(1-\xi)(1-\eta^2)$					$+\frac{1}{2}N_{i,j}$
$N_{i,j} = (1-\xi^2)(1-\eta^2)$					

2.5.3. Multiple-Domain Modeling - Homogeneous Discretization

In this context, homogeneous discretization approaches are applicable to multiple subdomain discretization. These approaches make use of a single discretization method among all subdomains in which the domain is subdivided. Of the many spatial modeling approaches, this work will focus on the finite element and the finite difference methods.

Two-approximation interface modeling

For homogeneous domain discretization developed herein, Eq. (2.32) is used to provide the mathematical basis. The two-approximation formulation, for both the finite element (FE) and finite difference (FD) methods, may be obtained by rewriting Eq. (2.32) over an element domain as

$$\int_{\Omega_1^e} k_1\left(\frac{\partial u_1}{\partial x}\frac{\partial \Phi_1}{\partial x}+\frac{\partial u_1}{\partial y}\frac{\partial \Phi_1}{\partial y}\right)d\Omega_1^e + \int_{\Omega_2^e} k_2\left(\frac{\partial u_2}{\partial x}\frac{\partial \Phi_2}{\partial x}+\frac{\partial u_2}{\partial y}\frac{\partial \Phi_2}{\partial y}\right)d\Omega_2^e$$
$$- \int_{\Gamma^{I^e}} \hat{q}(\Phi_1-\Phi_2)\,d\Gamma^{I^e} + \int_{\Gamma^{I^e}} \lambda(u_1-u_2)\,d\Gamma^{I^e} = \int_{\Omega_1^e} Q_1\Phi_1 d\Omega_1^e + \int_{\Gamma_1^{s^e}} \bar{q}_1\Phi_1\,d\Gamma_1^{s^e} \quad (2.41)$$
$$+ \int_{\Omega_2^e} Q_2\Phi_2 d\Omega_2^e + \int_{\Gamma_2^{s^e}} \bar{q}_2\Phi_2\,d\Gamma_2^{s^e}$$

Note that the integration over the common subdomain boundary, Γ^I, is considered only for element edges along that boundary.

The form of Eq. (2.41) for the two (FE and FD) methods differs by the form of the element shape functions and the approximation selected for the weight functions, Φ. For the generalized element expansion of subdomain *i*, the independent approximations for the element generalized primary variables, (*i.e.*, displacements or velocities), interface secondary variables (*i.e.*, tractions or fluxes), and the weight functions associated with the secondary variables, are, respectively

$$\mathbf{u}_i = \mathbf{N}_i\mathbf{u}_{e_i} \quad ; \quad \hat{\mathbf{q}} = \mathbf{R}_i\boldsymbol{\alpha} \quad \text{and} \quad \boldsymbol{\lambda}_i = \mathbf{R}_i$$

where $\boldsymbol{\alpha}$ is a vector of unknown coefficients associated with secondary variable, $\hat{\mathbf{q}}$, and **N** and **R** are matrices of interpolation functions for the element primary and secondary variables, respectively. The interpolation functions in the matrix **R** are assumed to be constants for linear finite elements and linear functions for quadratic finite elements.

Substituting these approximations into Eq. (2.41) yields an integral equation in terms of the weight function, $\mathbf{\Phi}$, which is given by

$$\left[\int_{\Omega_1^e} k_1\left(\frac{\partial \mathbf{N}_1^{\mathrm{T}}}{\partial x}\frac{\partial \mathbf{\Phi}_1}{\partial x}+\frac{\partial \mathbf{N}_1^{\mathrm{T}}}{\partial y}\frac{\partial \mathbf{\Phi}_1}{\partial y}\right)\mathrm{d}\Omega_1^e\right]\mathbf{u}_{e_1}+\left[\int_{\Omega_2^e} k_2\left(\frac{\partial \mathbf{N}_2^{\mathrm{T}}}{\partial x}\frac{\partial \mathbf{\Phi}_2}{\partial x}+\frac{\partial \mathbf{N}_2^{\mathrm{T}}}{\partial y}\frac{\partial \mathbf{\Phi}_2}{\partial y}\right)\mathrm{d}\Omega_2^e\right]\mathbf{u}_{e_2}$$
$$-\left[\int_{\Gamma^{\mathrm{I}^e}} \mathbf{\Phi}_1^{\mathrm{T}}\mathbf{R}_1\,\mathrm{d}\Gamma^{\mathrm{I}^e}\right]\boldsymbol{\alpha}+\left[\int_{\Gamma^{\mathrm{I}^e}} \mathbf{\Phi}_2^{\mathrm{T}}\mathbf{R}_2\,\mathrm{d}\Gamma^{\mathrm{I}^e}\right]\boldsymbol{\alpha}+\left[\int_{\Gamma^{\mathrm{I}^e}} \mathbf{R}_1^{\mathrm{T}}\mathbf{N}_1\,\mathrm{d}\Gamma^{\mathrm{I}^e}\right]\mathbf{u}_{e_1}-\left[\int_{\Gamma^{\mathrm{I}^e}} \mathbf{R}_2^{\mathrm{T}}\mathbf{N}_2\,\mathrm{d}\Gamma^{\mathrm{I}^e}\right]\mathbf{u}_{e_2}$$
$$=\int_{\Omega_1^e}\mathbf{\Phi}_1^{\mathrm{T}}Q_1\mathrm{d}\Omega_1+\int_{\Gamma_1^{s^e}}\mathbf{\Phi}_1^{\mathrm{T}}\bar{q}_1\mathrm{d}\Gamma_1^{s^e}+\int_{\Omega_2^e}\mathbf{\Phi}_2^{\mathrm{T}}Q_2\mathrm{d}\Omega_2^e+\int_{\Gamma_2^{s^e}}\mathbf{\Phi}_2^{\mathrm{T}}\bar{q}_2\,\mathrm{d}\Gamma_2^{s^e}$$

where for i=1,2

$$\mathbf{k}_{\mathbf{e}_i}=\int_{\Omega_i^e} k_i\left(\frac{\partial \mathbf{N}_i^{\mathrm{T}}}{\partial x}\frac{\partial \mathbf{\Phi}_i}{\partial x}+\frac{\partial \mathbf{N}_i^{\mathrm{T}}}{\partial y}\frac{\partial \mathbf{\Phi}_i}{\partial y}\right)\mathrm{d}\Omega_i^e\,,$$

$$\mathbf{k}_{\mathbf{p}_i}=(-1)^{i+1}\int_{\Gamma^{\mathrm{I}^e}}\mathbf{R}_i^{\mathrm{T}}\mathbf{N}_i\,\mathrm{d}\Gamma^{\mathrm{I}^e}\,,$$

$$\mathbf{k}_{\mathbf{s}_i}=(-1)^{i}\int_{\Gamma^{\mathrm{I}^e}}\mathbf{\Phi}_i^{\mathrm{T}}\mathbf{R}_i\,\mathrm{d}\Gamma^{\mathrm{I}^e}\,,$$

and

$$\mathbf{f}_{\mathbf{e}i}=\int_{\Omega_i^e}\mathbf{\Phi}_i^{\mathrm{T}}Q_i\mathrm{d}\Omega_i^e+\int_{\Gamma_i^{s^e}}\mathbf{\Phi}_i^{\mathrm{T}}\bar{q}_i\,\mathrm{d}\Gamma_i^{s^e}$$

Assembling the element equations over the entire domain, enforcing continuity of the primary variable only within each subdomain and assembling the contributions along the element edges on the common subdomain boundary, and noting that $\mathbf{u}_{\mathbf{e}_1}$ and $\mathbf{u}_{\mathbf{e}_2}$ and $\mathbf{f}_{\mathbf{e}_1}$ and $\mathbf{f}_{\mathbf{e}_2}$ are completely uncoupled, yields the system of equations given by

$$\begin{bmatrix} \mathbf{K}_1 & \mathbf{0} & \mathbf{K}_{s_1} \\ \mathbf{0} & \mathbf{K}_2 & \mathbf{K}_{s_2} \\ \mathbf{K}_{p_1} & \mathbf{K}_{p_2} & \mathbf{0} \end{bmatrix} \begin{Bmatrix} \mathbf{u}_1 \\ \mathbf{u}_2 \\ \boldsymbol{\alpha} \end{Bmatrix} = \begin{Bmatrix} \mathbf{f}_1 \\ \mathbf{f}_2 \\ \mathbf{0} \end{Bmatrix} \tag{2.42}$$

The system of equations given in Eq. (2.42) is obtained based on the initial development of the weighted residual statement, from Eqs. (2.28) and (2.29),

$$\int_{\Omega_i} k_i \left(\frac{\partial u_i}{\partial x} \frac{\partial \boldsymbol{\Phi}_i}{\partial x} + \frac{\partial u_i}{\partial y} \frac{\partial \boldsymbol{\Phi}_i}{\partial y} \right) \mathrm{d}\Omega_i - \int_{\Gamma^{\mathrm{I}}} k_i \frac{\mathrm{d}u_i}{\mathrm{d}n} \boldsymbol{\Phi}_i \, \mathrm{d}\Gamma^{\mathrm{I}} = \int_{\Omega_i} Q_i \boldsymbol{\Phi}_i \mathrm{d}\Omega_i + \int_{\Gamma_i^s} \bar{q}_i \boldsymbol{\Phi}_i \mathrm{d}\Gamma_i^s$$

subject to the constraint equation, Eq. (2.30),

$$\int_{\Gamma^{\mathrm{I}}} \lambda (u_1 - u_2) \, \mathrm{d}\Gamma^{\mathrm{I}} = 0 \quad \text{on} \quad \Gamma^{\mathrm{I}} \ .$$

Here, the first two matrix equations in Eq. (2.42) are obtained from the weighted residual statement for each subdomain, Eqs. (2.28) and (2.29), and the third matrix equation is obtained from the constraint on the primary variables along the common subdomain boundary, Eq. (2.30).

For the finite element modeling, the weight functions are taken to be the finite element shape functions. That is, $\boldsymbol{\Phi}_i = \mathbf{N}_i$, and thus, for i=1,2

$$\mathbf{k}_{\mathbf{e}_i} = \int_{\Omega_i^e} k_i \left(\frac{\partial \mathbf{N}_i^{\mathrm{T}}}{\partial x} \frac{\partial \mathbf{N}_i}{\partial x} + \frac{\partial \mathbf{N}_i^{\mathrm{T}}}{\partial y} \frac{\partial \mathbf{N}_i}{\partial y} \right) \mathrm{d}\Omega_i^e \ ,$$

$$\mathbf{k}_{\mathbf{p}_i} = (-1)^{i+1} \int_{\Gamma^{\mathrm{I}^e}} \mathbf{R}_i^{\mathrm{T}} \mathbf{N}_i \, \mathrm{d}\Gamma^{\mathrm{I}^e} \ ,$$

$$\mathbf{k}_{\mathbf{s}_i} = (-1)^{i} \int_{\Gamma^{\mathrm{I}^e}} \mathbf{N}_i^{\mathrm{T}} \mathbf{R}_i \, \mathrm{d}\Gamma^{\mathrm{I}^e} \ , \tag{2.43}$$

and

$$\mathbf{f}_{\mathbf{e}i} = \int_{\Omega_i^e} \mathbf{N}_i^{\mathrm{T}} Q_i \mathrm{d}\Omega_i^e + \int_{\Gamma_i^{s^e}} \mathbf{N}_i^{\mathrm{T}} \bar{q}_i \, \mathrm{d}\Gamma_i^{s^e}$$

Here, note that at the element level, $\mathbf{k}_{\mathbf{p}_i} = \mathbf{k}_{\mathbf{s}_i}^{\mathrm{T}}$, and consequently, at the global system level, $\mathbf{K}_{\mathbf{p}_i} = \mathbf{K}_{\mathbf{s}_i}^{\mathrm{T}}$.

For the finite difference modeling, the weight functions are taken to be the Dirac delta function. That is, $\mathbf{\Phi}_i = \delta_i(x - x_i, y - y_i) = \delta_i(x_i, y_i)$, and thus, for i=1,2

$$\mathbf{k}_{\mathbf{e}_i} = \int_{\Omega_i^e} k_i \left(\frac{\partial \mathbf{N}_i}{\partial x} \frac{\partial \delta_i(x_i, y_i)}{\partial x} + \frac{\partial \mathbf{N}_i}{\partial y} \frac{\partial \delta_i(x_i, y_i)}{\partial y} \right) \mathrm{d}\Omega_i^e = k_i \left(\left. \frac{\partial^2 \mathbf{N}_i}{\partial x^2} \right|_{\substack{x=x_i \\ y=y_i}} + \left. \frac{\partial^2 \mathbf{N}_i}{\partial y^2} \right|_{\substack{x=x_i \\ y=y_i}} \right),$$

$$\mathbf{k}_{\mathbf{p}_i} = (-1)^{i+1} \int_{\Gamma^{\mathrm{I}^e}} \mathbf{R}_i^{\mathrm{T}} \mathbf{N}_i \, \mathrm{d}\Gamma^{\mathrm{I}^e},$$

$$\mathbf{k}_{\mathbf{s}_i} = (-1)^i \int_{\Gamma^{\mathrm{I}^e}} \delta_i(x_i, y_i) \mathbf{R}_i \, \mathrm{d}\Gamma^{\mathrm{I}^e} = (-1)^i \mathbf{R}_i(x_i, y_i), \tag{2.44}$$

and

$$\mathbf{f}_{\mathbf{e}i} = \int_{\Omega_i^e} \delta_i(x_i, y_i) Q_i \mathrm{d}\Omega_i^e + \int_{\Gamma_i^{s^e}} \delta_i(x_i, y_i) \bar{q}_i \, \mathrm{d}\Gamma_i^{s^e} = Q_i(x_i, y_i) + \bar{q}_i(x_i, y_i).$$

Three-approximation interface modeling

For the three-approximation formulation, Eq. (2.36) is used to provide the mathematical basis for the development. In previous work by Aminpour et al.[25], a similar formulation based on the principle of minimum potential energy is implemented in the form of an element. In that work as is the case in this study, the interdomain interface boundary is discretized with a mesh of evenly-spaced pseudo-nodes (open

circles in Figure 2.6) that need not be coincident with any of the interface nodes (filled circles in the figure) of any of the subdomains.

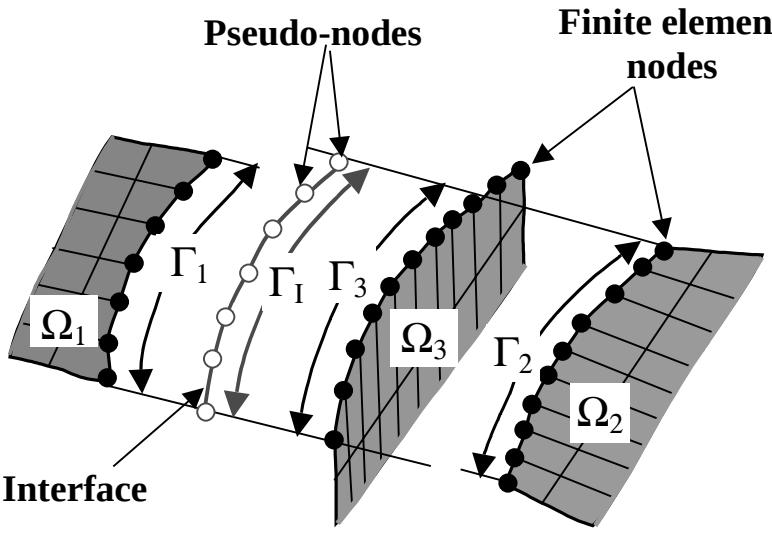

Figure 2.6. Interface Definition.

The generalized element equations may be obtained by introducing the continuity requirements into the weighted residual statement. Eq. (2.36) can be rewritten over an element domain as

$$\int_{\Omega_1^e} k_1\left(\frac{\partial u_1}{\partial x}\frac{\partial \Phi_1}{\partial x}+\frac{\partial u_1}{\partial y}\frac{\partial \Phi_1}{\partial y}\right)d\Omega_1^e+\int_{\Omega_2^e} k_2\left(\frac{\partial u_2}{\partial x}\frac{\partial \Phi_2}{\partial x}+\frac{\partial u_2}{\partial y}\frac{\partial \Phi_2}{\partial y}\right)d\Omega_2^e-\int_{\Gamma^{I^e}}\hat{q}_1\Phi_1\,d\Gamma^{I^e}$$
$$-\int_{\Gamma^{I^e}}\hat{q}_2\Phi_2\,d\Gamma^{I^e}+\int_{\Gamma^{I^e}}\lambda_1(v-u_1)\,d\Gamma^{I^e}+\int_{\Gamma^{I^e}}\lambda_2(v-u_2)\,d\Gamma^{I^e}+\int_{\Gamma^{I^e}}\hat{\lambda}(\hat{q}_1+\hat{q}_2)\,d\Gamma^{I^e} \qquad (2.45)$$
$$=\int_{\Omega_1^e} Q_1\Phi_1 d\Omega_1^e+\int_{\Gamma_1^{s^e}}\bar{q}_1\Phi_1\,d\Gamma_1^{s^e}+\int_{\Omega_2^e} Q_2\Phi_2 d\Omega_2^e+\int_{\Gamma_2^{s^e}}\bar{q}_2\Phi_2\,d\Gamma_2^{s^e}\ .$$

Note that in the potential energy formulation[25], the continuity of the secondary variables was satisfied through the subsidiary conditions obtained through the minimization of the potential energy. In this weighted residual formulation, the continuity of the secondary

variables is satisfied in a weighted residual sense and the Lagrange multipliers, λ_i and $\hat{\lambda}$, are represented by weight functions in the form of the secondary and primary variables, respectively.

The form of the equations for the finite element and finite difference applications differs by the form of the element shape functions and the approximation selected for the weight functions, $\mathbf{\Phi}$. For the generalized element expansion of subdomain *i*, the independent approximations for the element generalized primary variables, (*i.e.*, displacements or velocities), interface secondary variables (*i.e.*, tractions or fluxes), the weight functions associated with the secondary and primary variables, and the interface variables, are, respectively

$$\mathbf{u}_i = \mathbf{N}_i \mathbf{u}_{e_i} \quad ; \quad \hat{\mathbf{q}}_i = \mathbf{R}_i \boldsymbol{\alpha}_i \quad ; \quad \boldsymbol{\lambda}_i = \mathbf{R}_i \ ; \ \hat{\boldsymbol{\lambda}} = \mathbf{T} \ \text{ and } \ \mathbf{v} = \mathbf{T}\mathbf{u}_{\mathrm{I}}$$

where $\boldsymbol{\alpha}$ is a vector of unknown coefficients associated with the secondary variables, $\hat{\mathbf{q}}$, and **N**, **R**, and **T** are matrices of interpolation functions for the element primary and secondary variables, and primary variables along the interface, respectively. The interpolation functions in the matrix **R** are assumed to be constants for linear elements and linear functions for quadratic elements. The interpolation functions in the matrix **T** are cubic spline functions. The derivation of this interpolation matrix is given in Appendix B, and the derivation of the geometry representation, Γ^{I}, is given in Appendix C. Substituting these approximations into Eq. (2.45) yields an integral equation in terms of the weight function, Φ, which is given by

$$\left[\int_{\Omega_1^e} k_1\left(\frac{\partial \mathbf{N}_1^{\mathrm{T}}}{\partial x}\frac{\partial \mathbf{\Phi}_1}{\partial x}+\frac{\partial \mathbf{N}_1^{\mathrm{T}}}{\partial y}\frac{\partial \mathbf{\Phi}_1}{\partial y}\right)\mathrm{d}\Omega_1^e\right]\mathbf{u}_{e_1}+\left[\int_{\Omega_2^e} k_2\left(\frac{\partial \mathbf{N}_2^{\mathrm{T}}}{\partial x}\frac{\partial \mathbf{\Phi}_2}{\partial x}+\frac{\partial \mathbf{N}_2^{\mathrm{T}}}{\partial y}\frac{\partial \mathbf{\Phi}_2}{\partial y}\right)\mathrm{d}\Omega_2^e\right]\mathbf{u}_{e_2}$$
$$-\left[\int_{\Gamma^{\mathrm{I}^e}}\mathbf{\Phi}_1^{\mathrm{T}}\mathbf{R}_1\,\mathrm{d}\Gamma^{\mathrm{I}^e}\right]\boldsymbol{\alpha}_1-\left[\int_{\Gamma^{\mathrm{I}^e}}\mathbf{\Phi}_2^{\mathrm{T}}\mathbf{R}_2\,\mathrm{d}\Gamma^{\mathrm{I}^e}\right]\boldsymbol{\alpha}_2+\left[\int_{\Gamma^{\mathrm{I}^e}}\mathbf{T}^{\mathrm{T}}\mathbf{R}_1\,\mathrm{d}\Gamma^{\mathrm{I}^e}\right]\boldsymbol{\alpha}_1+\left[\int_{\Gamma^{\mathrm{I}^e}}\mathbf{T}^{\mathrm{T}}\mathbf{R}_2\,\mathrm{d}\Gamma^{\mathrm{I}^e}\right]\boldsymbol{\alpha}_2+$$
$$\left[\int_{\Gamma^{\mathrm{I}^e}}\mathbf{R}_1{}^{\mathrm{T}}\mathbf{T}\,\mathrm{d}\Gamma^{\mathrm{I}^e}\right]\mathbf{u}_{\mathrm{I}}-\left[\int_{\Gamma^{\mathrm{I}^e}}\mathbf{R}_1{}^{\mathrm{T}}\mathbf{N}_1\,\mathrm{d}\Gamma^{\mathrm{I}^e}\right]\mathbf{u}_{e_1}+\left[\int_{\Gamma^{\mathrm{I}^e}}\mathbf{R}_2{}^{\mathrm{T}}\mathbf{T}\,\mathrm{d}\Gamma^{\mathrm{I}^e}\right]\mathbf{u}_{\mathrm{I}}-\left[\int_{\Gamma^{\mathrm{I}^e}}\mathbf{R}_2{}^{\mathrm{T}}\mathbf{N}_2\,\mathrm{d}\Gamma^{\mathrm{I}^e}\right]\mathbf{u}_{e_2}$$
$$=\int_{\Omega_1^e}\mathbf{\Phi}_1^{\mathrm{T}}Q_1\mathrm{d}\Omega_1^e+\int_{\Gamma_1^{s^e}}\mathbf{\Phi}_1^{\mathrm{T}}\bar{q}_1\,\mathrm{d}\Gamma_1^{s^e}+\int_{\Omega_2^e}\mathbf{\Phi}_2^{\mathrm{T}}Q_2\mathrm{d}\Omega_2^e+\int_{\Gamma_2^{s^e}}\mathbf{\Phi}_2^{\mathrm{T}}\bar{q}_2\,\mathrm{d}\Gamma_2^{s^e}$$

where, for i=1,2

$$\mathbf{k}_{\mathbf{e}_i}=\int_{\Omega_i^e} k_i\left(\frac{\partial \mathbf{N}_i^{\mathrm{T}}}{\partial x}\frac{\partial \mathbf{\Phi}_i}{\partial x}+\frac{\partial \mathbf{N}_i^{\mathrm{T}}}{\partial y}\frac{\partial \mathbf{\Phi}_i}{\partial y}\right)\mathrm{d}\Omega_i^e$$

$$\mathbf{k}_{\mathbf{p}_i}=-\int_{\Gamma^{\mathrm{I}^e}}\mathbf{R}_i^{\mathrm{T}}\mathbf{N}_i\mathrm{d}\Gamma^{\mathrm{I}^e}\ ,$$

$$\mathbf{k}_{\mathbf{s}_i}=-\int_{\Gamma^{\mathrm{I}^e}}\mathbf{\Phi}_i^{\mathrm{T}}\mathbf{R}_i\,\mathrm{d}\Gamma^{\mathrm{I}^e},$$

$$\mathbf{k}_{\mathrm{I}_i}=\int_{\Gamma^{\mathrm{I}^e}}\mathbf{T}^{\mathrm{T}}\mathbf{R}_i\mathrm{d}\Gamma^{\mathrm{I}^e}\ ,$$

and

$$\mathbf{f}_{\mathbf{e}i}=\int_{\Omega_i^e}\mathbf{\Phi}_i^{\mathrm{T}}Q_i\mathrm{d}\Omega_i^e+\int_{\Gamma_i^{s^e}}\mathbf{\Phi}_i^{\mathrm{T}}\bar{q}_i\,\mathrm{d}\Gamma_i^{s^e}$$

where integration over the common subdomain boundary, Γ^{I}, is considered only for element edges along that boundary.

Note that all of the element submatrices in the three-approximation formulation except for the $\mathbf{k}_{\mathrm{I}_i}$ matrix are identical to those obtained in the two-approximation formulation. The submatrix, $\mathbf{k}_{\mathrm{I}_i}$, does not exist in the two-approximation formulation but is included in the three-field formulation. This submatrix is associated with the coupling of the primary variables along the subdomain interface boundaries to those along the interface.

Assembling the element equations over the entire domain, enforcing continuity of the primary and secondary variables only within each subdomain and assembling the contributions along the element edges on the common subdomain boundary, and noting that $\mathbf{u}_{\mathbf{e}_1}$ and $\mathbf{u}_{\mathbf{e}_2}$, and $\mathbf{f}_{\mathbf{e}_1}$ and $\mathbf{f}_{\mathbf{e}_2}$, and $\boldsymbol{\alpha}_1$ and $\boldsymbol{\alpha}_2$ are completely uncoupled, yields the system of equations given by

$$\begin{bmatrix} \mathbf{K}_1 & \mathbf{0} & \mathbf{0} & \mathbf{K}_{\mathrm{s}_1} & \mathbf{0} \\ \mathbf{0} & \mathbf{K}_2 & \mathbf{0} & \mathbf{0} & \mathbf{K}_{\mathrm{s}_2} \\ \mathbf{0} & \mathbf{0} & \mathbf{0} & \mathbf{K}_{\mathrm{I}_1} & \mathbf{K}_{\mathrm{I}_2} \\ \mathbf{K}_{\mathrm{p}_1} & \mathbf{0} & \mathbf{K}_{\mathrm{I}_1}^{\mathrm{T}} & \mathbf{0} & \mathbf{0} \\ \mathbf{0} & \mathbf{K}_{\mathrm{p}_2} & \mathbf{K}_{\mathrm{I}_2}^{\mathrm{T}} & \mathbf{0} & \mathbf{0} \end{bmatrix} \begin{Bmatrix} \mathbf{u}_1 \\ \mathbf{u}_2 \\ \mathbf{u}_{\mathrm{I}} \\ \boldsymbol{\alpha}_1 \\ \boldsymbol{\alpha}_2 \end{Bmatrix} = \begin{Bmatrix} \mathbf{f}_1 \\ \mathbf{f}_2 \\ \mathbf{0} \\ \mathbf{0} \\ \mathbf{0} \end{Bmatrix} \tag{2.46}$$

or in a symbolic manner

$$\begin{bmatrix} \mathbf{K} & \mathbf{0} & \mathbf{K}_{\mathrm{s}} \\ \mathbf{0} & \mathbf{0} & \mathbf{K}_{\mathrm{I}} \\ \mathbf{K}_{\mathrm{p}} & \mathbf{K}_{\mathrm{I}} & \mathbf{0} \end{bmatrix} \begin{Bmatrix} \mathbf{u} \\ \mathbf{u}_{\mathrm{I}} \\ \boldsymbol{\alpha} \end{Bmatrix} = \begin{Bmatrix} \mathbf{f} \\ \mathbf{0} \\ \mathbf{0} \end{Bmatrix}$$

where **K**, **u**, and **f** are the assembled stiffness matrix, displacement vector and force vector for the entire structure, and $\mathbf{K}_{\mathrm{p}}$, $\mathbf{K}_{\mathrm{s}}$, $\mathbf{K}_{\mathrm{I}}$, $\mathbf{u}_{\mathrm{I}}$, and α are the assembled $\mathbf{K}_{\mathrm{p}_i}$, $\mathbf{K}_{\mathrm{s}_i}$, $\mathbf{K}_{\mathrm{I}_i}$, $\mathbf{u}_{\mathrm{I}}$, and $\boldsymbol{\alpha}_i$ for all interfaces.

While it is convenient to represent the weighted residual form over the domain using a single equation, the system of equations, Eq. (2.46) is obtained from the individual weighted residual expressions over each of the subdomains and the constraint integrals. The first two matrix equations of the system of equations, Eq. (2.46) are derived from the weighted residual statement for subdomain *i*. That is,

$$\int_{\Omega_i} k_i \left(\frac{\partial u_i}{\partial x} \frac{\partial \mathbf{\Phi}_i}{\partial x} + \frac{\partial u_i}{\partial y} \frac{\partial \mathbf{\Phi}_i}{\partial y} \right) \mathrm{d}\Omega_1 - \int_{\Gamma^{\mathrm{I}}} k_i \frac{\partial u_i}{\partial n} \mathbf{\Phi}_i \, \mathrm{d}\Gamma^{\mathrm{I}} = \int_{\Omega_i} Q_i \mathbf{\Phi}_i \mathrm{d}\Omega_i + \int_{\Gamma_i^s} \overline{q}_i \mathbf{\Phi}_i \, \mathrm{d}\Gamma_i^s$$

The third matrix equation of the system results from the reciprocity statement of the secondary variables. That is,

$$\int_{\Gamma^{\mathrm{I}}} \hat{\lambda} (\hat{q}_1 + \hat{q}_2) \, \mathrm{d}\Gamma^{\mathrm{I}} = 0 \quad \text{on} \quad \Gamma^{\mathrm{I}}.$$

The fourth and fifth matrix equations result from the continuity requirement for the primary variables, which is given by

$$\int_{\Gamma^{\mathrm{I}}} \lambda_1 (u_{\mathrm{I}} - u_1) \, \mathrm{d}\Gamma^{\mathrm{I}} = 0 \quad \text{on} \quad \Gamma^{\mathrm{I}}$$

$$\int_{\Gamma^{\mathrm{I}}} \lambda_2 (u_{\mathrm{I}} - u_2) \, \mathrm{d}\Gamma^{\mathrm{I}} = 0 \quad \text{on} \quad \Gamma^{\mathrm{I}}$$

For the finite element development, the weight functions are taken to be the finite element shape functions (*i.e.*, $\mathbf{\Phi}_i = \mathbf{N}_i$). For the finite difference development, the weight functions are taken to be the Dirac delta function (*i.e.*, $\mathbf{\Phi}_i = \delta_i (x - x_i, y - y_i) = \delta_i (x_i, y_i)$). Thus, for *i*=1,2, the finite element and finite difference stiffness matrices and force vector, $\mathbf{k}_{\mathbf{e}_i}$, $\mathbf{k}_{\mathbf{p}_i}$, $\mathbf{k}_{\mathbf{s}_i}$, and $\mathbf{f}_{\mathbf{e}_i}$, for the three-approximation formulation are identical to those obtained for the two-approximation formulation for the respective discretization approaches.

Note that, for both of the discretization methods, the form of the coupling element matrices that are not in terms of the weight functions are independent of the method of discretization. That is,

$$\mathbf{k}_{\mathbf{p}_i} = -\int_{\Gamma^{I^e}} \mathbf{R}_i^{\mathrm{T}} \mathbf{N}_i \, d\Gamma^{I^e} ,$$

and

$$\mathbf{k}_{\mathrm{I}_i} = \int_{\Gamma^{I^e}} \mathbf{T}^{\mathrm{T}} \mathbf{R}_i \, d\Gamma^{I^e}$$

are of the same form for the finite element and finite difference discretizations. However, since the element shape functions, $\mathbf{N}_i$, differ for the two methods, the interface matrices, $\mathbf{k}_{\mathbf{p}_i}$, in general, are not identical. Moreover, in the finite element development, the weight functions, $\mathbf{\Phi}_i$, are taken to be the finite element shape functions, $\mathbf{N}_i$; thus, at the element level $\mathbf{k}_{\mathrm{s}_i} = \mathbf{k}_{\mathrm{p}_i}^{\mathrm{T}}$, and at the global system level $\mathbf{K}_{\mathrm{s}_i} = \mathbf{K}_{\mathrm{p}_i}^{\mathrm{T}}$.

The three-approximation derivation is more general as it allows for the coupling of the primary variables to an independent approximation. This attribute is particularly important in the heterogeneous discretization approach described in the next section.

2.5.4. Multiple-Domain Modeling - Heterogeneous Discretization

Heterogeneous discretization approaches make use of different discretization methods for at least two of the subdomains in which the domain is subdivided. There are many combinations of spatial modeling approaches; however, this work will focus on the coupling of the finite element and finite difference methods.

Both the two- or three-approximation multifunctional formulations, discussed for the homogeneous discretization approach, are applicable to heterogeneous discretization.

However, as noted earlier, the three-approximation approach provides additional flexibility for the interface definition. Thus, only the three-approximation approach is presented. Hence, the multifunctional weighted residual formulation of Eq. (2.46) is used. Considering the two domains, upon which this discussion is based, one subdomain is discretized using the finite element method, and the other subdomain is discretized using the finite difference method. As before, for the finite element development, the weight functions are taken to be the finite element shape functions (*i.e.*, $\mathbf{\Phi}_i = \mathbf{N}_i$), and for the finite difference development, the weight functions are taken to be the Dirac delta function (*i.e.*, $\mathbf{\Phi}_i = \delta_i(x - x_i, y - y_l) = \delta_i(x_i, y_i)$). As expected, the set of element matrices becomes a hybrid of the matrices from the finite element method and the finite difference method. For completeness, these matrices are repeated here considering subdomain 1 as the finite element subdomain and subdomain 2 as the finite difference subdomain, and

$$\mathbf{k}_{\mathbf{e}_1} = \int_{\Omega_1^e} k_1 \left(\frac{\partial \mathbf{N}_1^{\mathrm{T}}}{\partial x}\frac{\partial \mathbf{N}_1}{\partial x} + \frac{\partial \mathbf{N}_1^{\mathrm{T}}}{\partial y}\frac{\partial \mathbf{N}_1}{\partial y} \right) \mathrm{d}\Omega_1^e \text{ and } \mathbf{k}_{\mathbf{e}_2} = k_2 \left(\left.\frac{\partial^2 \mathbf{N}_2^{\mathrm{T}}}{\partial x^2}\right|_{\substack{x=x_i \\ y=y_i}} + \left.\frac{\partial^2 \mathbf{N}_2^{\mathrm{T}}}{\partial y^2}\right|_{\substack{x=x_i \\ y=y_i}} \right),$$

$$\mathbf{k}_{\mathbf{s}_1} = -\int_{\Gamma^{\mathrm{I}^e}} \mathbf{N}_1^{\mathrm{T}} \mathbf{R}_1 \, \mathrm{d}\Gamma^{\mathrm{I}^e} \quad \text{and} \quad \mathbf{k}_{\mathbf{s}_2} = -\mathbf{R}_2(x_i, y_i) \,, \tag{2.47}$$

and

$$\mathbf{f}_{\mathbf{e}1} = \int_{\Omega_1^e} \mathbf{N}_1^{\mathrm{T}} Q_1 \mathrm{d}\Omega_1^e + \int_{\Gamma_1^{s^e}} \mathbf{N}_1^{\mathrm{T}} \bar{q}_1 \mathrm{d}\Gamma_1^{s^e} \quad \text{and} \quad \mathbf{f}_{\mathbf{e}2} = Q_2(x_i, y_i) + \bar{q}_2(x_i, y_i),$$

and for the two domains, i=1,2,

$$\mathbf{k}_{\mathbf{p}_i} = -\int_{\Gamma^{I^e}} \mathbf{R}_i^{\mathrm{T}} \mathbf{N}_i \, d\Gamma^{I^e} \quad ,$$

and

$$\mathbf{k}_{\mathrm{I}_i} = \int_{\Gamma^{I^e}} \mathbf{T}^{\mathrm{T}} \mathbf{R}_i \, d\Gamma^{I^e} \quad .$$

2.6. COMPUTATIONAL IMPLICATIONS

The two- and three-approximation multifunctional modeling approaches have been generalized such that they are applicable to both homogeneous and heterogeneous discretization approaches. Computational implications are presented in this section for the generalized system of equations, Eqs. (2.42) and (2.46). Implications specific to a discretization approach are highlighted, where appropriate.

The assembled stiffness matrix **K** is a block diagonal matrix containing the stiffness matrices $\mathbf{K}_i$ of each of the subdomains along its block diagonal. The interface "stiffness" matrix thus contains coupling terms that augment the stiffness matrices of the subdomains along the interface. The two- and three-approximation approaches yield systems of equations (see Eqs. (2.42) and (2.46)) of similar form and with the same attributes. Due to the use of Lagrange multipliers in the constraint conditions, the systems are neither banded nor positive definite. Therefore, standard Cholesky solvers can not be used, unless full pivoting is performed to obtain the solution. In addition, due to the generalization for the finite difference approximations, the system of equations is not necessarily symmetric due to different off-diagonal submatrices, $\mathbf{K}_{\mathrm{p}}$ and $\mathbf{K}_{\mathrm{s}}$. The system unknowns in Eq. (2.46) consist of both primary and secondary variables given by

the potential function, u, and the secondary variable coefficients, α, respectively. Generally, the coupling matrices, $\mathbf{K}_{s_i}$, are of the order of the length of the interdomain boundary, which results in a marked difference in the magnitude of the off-diagonal terms of the system matrix compared to its diagonal terms. This characteristic produces an ill-conditioned matrix whose solution can cause difficulties for some general-purpose solvers. Hence, the coupling matrix should be scaled such that it is of the same order as the subdomain stiffness. The upper diagonal submatrix blocks contain uncoupled subdomain stiffness matrices. The symmetry of the subdomain matrix is determined by the choice of the weight function, Φ. For the finite element discretization, the subdomain matrices are symmetric. However, due to the elimination of fictitious nodes for the imposition of boundary conditions and loads in the finite difference discretization, the subdomain stiffness matrices, $\mathbf{K}_i$, generally are not symmetric, but they are positive definite and sparse. The coupling is accomplished through the introduction of the coupling terms in the matrices, $\mathbf{K}_{p_i}$ and $\mathbf{K}_{s_i}$, for both approaches. The three-approximation approach requires an additional matrix, $\mathbf{K}_I$. For the three-approximation approach, the number of additional degrees of freedom associated with the interface is generally small in comparison with the total number of degrees of freedom in the subdomains. Thus, modeling flexibility is provided at a relatively small computational expense. The computational expense in this study may be reduced additionally as the efficiency of new solution algorithms for the system of equations in Eqs. (2.42) and (2.46) is increased.

The load transfer mechanism for finite element multiple-domain discretizations presented by Aminpour et al.[25] is generalized for the multifunctional approach, herein.

This load transfer mechanism may be interrogated for the two- and three-approximation formulations by considering the first and second rows of Eqs. (2.42) and (2.46), respectively. For the three-approximation approach, the matrix equations of interest are given by

$$\mathbf{K}_1\mathbf{u}_1 + \mathbf{K}_{s_1}\boldsymbol{\alpha}_1 = \mathbf{f}_1$$
$$\mathbf{K}_2\mathbf{u}_2 + \mathbf{K}_{s_2}\boldsymbol{\alpha}_2 = \mathbf{f}_2$$

These equations can be partitioned such that they correspond only to the primary variables, $\bar{\mathbf{u}}_i$ on the interdomain boundaries. That is, $\bar{\mathbf{u}}_i$ represents a subset of $\mathbf{u}_i$; hence,

$$\begin{aligned} \overline{\mathbf{K}}_1\bar{\mathbf{u}}_1 + \mathbf{K}_{s_1}\boldsymbol{\alpha}_1 &= \mathbf{0} \\ \overline{\mathbf{K}}_2\bar{\mathbf{u}}_2 + \mathbf{K}_{s_2}\boldsymbol{\alpha}_2 &= \mathbf{0} \end{aligned} \tag{2.48}$$

where $\overline{\mathbf{K}}_i$ denotes interdomain boundary stiffness terms related to $\bar{\mathbf{u}}_i$, and there are no forces on the interdomain boundary. The expressions given by the product term, $\overline{\mathbf{K}}_i\bar{\mathbf{u}}_i$, represent the internal fluxes at the i^{th} interdomain boundary, and thus Eq. (2.48) may be written as

$$\bar{\mathbf{f}}_1 = -\mathbf{K}_{s_1}\boldsymbol{\alpha}_1 \quad \text{and} \quad \bar{\mathbf{f}}_2 = -\mathbf{K}_{s_2}\boldsymbol{\alpha}_2 . \tag{2.49}$$

For homogeneous discretization using the finite element method, substituting for $\mathbf{K}_{s_i}$ from Eq. (2.43) into Eq. (2.49) gives

$$\bar{\mathbf{f}}_1 = -\int_{\Gamma^{I^e}} \mathbf{N}_1^{\mathrm{T}}\mathbf{R}_1 \, d\Gamma^{I^e} \; \boldsymbol{\alpha}_1 = -\int_{\Gamma^{I^e}} \mathbf{N}_1^{\mathrm{T}}\hat{\mathbf{q}}_1 \, d\Gamma^{I^e} \tag{2.50}$$

$$\bar{\mathbf{f}}_2 = -\int_{\Gamma^{I^e}} \mathbf{N}_2^{\mathrm{T}}\mathbf{R}_2 \, d\Gamma^{I^e} \; \boldsymbol{\alpha}_2 = -\int_{\Gamma^{I^e}} \mathbf{N}_2^{\mathrm{T}}\hat{\mathbf{q}}_2 \, d\Gamma^{I^e}$$

Examining Eq. (2.50) indicates that the evaluation of the internal fluxes is consistent with the evaluation of equivalent nodal fluxes in the presence of applied fluxes on the boundary. In addition, Eq. (2.50) substantiates that the secondary variables along the interface are represented by distributed fluxes for each of the subdomains.

For homogeneous discretization using the finite difference method, substituting for $\mathbf{K}_{s_i}$ from Eq. (2.44) into Eq. (2.49) gives

$$\bar{\mathbf{f}}_1 = -\mathbf{R}_1\boldsymbol{\alpha}_1 = -\hat{\mathbf{q}}_1 \tag{2.51}$$

$$\bar{\mathbf{f}}_2 = -\mathbf{R}_2\boldsymbol{\alpha}_2 = -\hat{\mathbf{q}}_2$$

Examining Eq. (2.51) indicates that the evaluation of the internal fluxes is consistent with nodal fluxes evaluated at points in the presence of applied fluxes on the boundary. In addition, Eq. (2.50) substantiates that the secondary variables along the interface for this approach are represented by nodal fluxes for each of the subdomains.

For heterogeneous discretization using the combined finite element and finite difference methods, substituting for $\mathbf{K}_{s_i}$ from Eq. (2.47) into Eq. (2.49) gives

$$\bar{\mathbf{f}}_1 = -\int_{\Gamma^{\mathrm{I}^e}} \mathbf{N}_1^{\mathrm{T}}\mathbf{R}_1 \, \mathrm{d}\Gamma^{\mathrm{I}^e} \; \boldsymbol{\alpha}_1 = -\int_{\Gamma^{\mathrm{I}^e}} \mathbf{N}_1^{\mathrm{T}}\hat{\mathbf{q}}_1 \, \mathrm{d}\Gamma^{\mathrm{I}^e} \tag{2.52}$$

$$\bar{\mathbf{f}}_2 = -\mathbf{R}_2\boldsymbol{\alpha}_2 = -\hat{\mathbf{q}}_2$$

Examining Eq. (2.52) indicates for subdomain 1 (the finite element subdomain), that the evaluation of the internal fluxes is consistent with the evaluation of equivalent nodal fluxes in the presence of applied fluxes on the boundary. Meanwhile, for subdomain 2 (the finite difference subdomain), the evaluation of the internal fluxes is consistent with nodal fluxes evaluated at points. This reveals that for this multiple-domain approach, the secondary variables along the interface for subdomain 1 are represented by distributed

fluxes, while for subdomain 2 the secondary variables along the interface are represented by nodal fluxes. Thus, for this heterogeneous modeling approach, it is required to transform the interface secondary variables into equivalent quantities.

2.7. VERIFICATION TEST CASE

In this section, the multifunctional methodology for the scalar-field problem is demonstrated on a verification test case. The application is described, and the associated results and salient features are discussed. This application is considered a patch test for the formulation and verifies the applicability of the method for a configuration for which the solutions are known. Finite difference and finite element solutions for single- and multiple-domain configurations are presented to provide benchmark solutions for the multifunctional approach using homogeneous and heterogeneous discretization. Representative applications from the field of engineering science are presented in Chapter IV.

2.7.1. Patch Test Problems

The patch test has proven to be a useful discriminator of the convergence properties of finite elements and other discretization approaches. A patch test refers to any problem with an exact solution as a constant state for which the approximating primary variable is capable of reproducing. The fundamental concept of the patch test for the scalar-field problem herein is to subject a domain to boundary conditions that engender a linear or quadratic primary variable field and a constant or linear secondary variable field throughout the domain. For the governing differential equation of the form of Eq. (2.1), boundary conditions that serve this purpose are:

i. Specified primary variable on Γ^p which emanate from a linear field as

$$u = a_1 x + a_2 y + a_0$$

or quadratic field as

$$u = a_1\left(x^2 - y^2\right) + a_2 x + a_3 y + a_0$$

where a_1, a_2, a_3,and a_0 are arbitrary constants.

ii. Constant or linear secondary variable on Γ^s

$$q = b_1 x + b_2 y + b_0$$

Given these boundary conditions, a solution is sought to the Laplace's equation. This governing equation is applicable to a variety of problems in engineering science. For example, consider the solution for the primary variable, $u(x,y)$, in a rectangular domain (see Figure 2.7) with boundary conditions of the forms indicated which yield the exact solution.

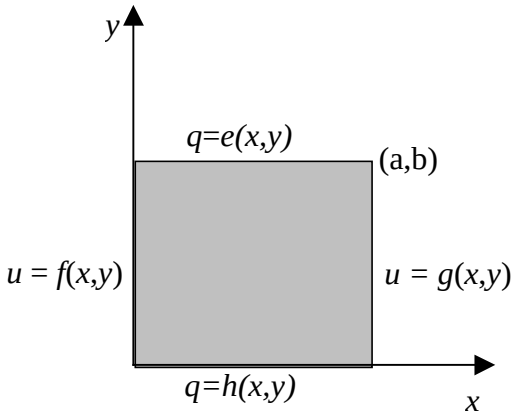

Figure 2.7. Two-Dimensional Rectangular Domain.

The problem is given by

$$\frac{\partial^2 u}{\partial x^2} + \frac{\partial^2 u}{\partial y^2} = 0, \qquad 0 < x < a, \qquad 0 < y < b$$

which is known as Laplace's equation for a planar domain.

Results of the analyses performed have been compared to appropriate reference solutions and are summarized in Table 2.2 using normalized values. A value of unity implies perfect agreement with the reference solution. Specified boundary conditions representing linear, bilinear, and quadratic potential functions are applied to the square domain. For all cases, the reference solution is the exact solution. For the linear case, a specified boundary condition of the form

$$u(0, y) = 2, \quad u(a, y) = a + 2, \text{ and } q_n(x,0) = q_n(x,b) = 0$$

has been imposed. For the bilinear case, a specified boundary condition of the form

$$u(0, y) = y, \quad u(a, y) = a + y, \text{ and } q_n(x,0) = -1 \text{ and, } q_n(x,b) = 1$$

has been imposed. For the quadratic case, a specified boundary condition of the form

$$u(0, y) = -y^2, \text{ and } u(a, y) = a^2 - y^2, \; q_n(x,0) = 0, \text{ and } q_n(x,b) = -2b$$

has been imposed. Several analyses have been performed namely, (1) two single-domain analyses with individual finite element and finite difference discretizations, respectively, (2) two multiple-domain analyses with homogeneous modeling with individual finite element and finite difference discretizations, respectively, and (3) one multiple-domain analysis with heterogeneous modeling with combined finite element and finite difference discretizations. Results from these analyses are summarized in Table 2.2. In this work, a five-node central difference template and four-node quadrilateral finite elements are used to form the models. Spatial modeling is used consistent with single-domain modeling approaches with a (5×5) mesh and a (9×9) mesh. The coarse and fine models, shown in Figure 2.8, are used in the finite element homogeneous modeling. For the finite difference homogeneous modeling and the heterogeneous modeling, a finite difference

mesh is used that has the same number of mesh points as the finite element mesh in the respective domain.

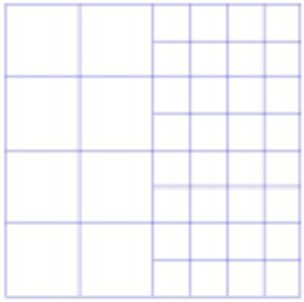

Figure 2.8. Spatial Discretization for Two-Dimensional Rectangular Domain.

For boundary conditions consistent with linear and bilinear potential functions, the computed potential and flux results are exact for all analysis types. For boundary conditions consistent with a quadratic potential function, the error in the computed potential and flux is approximately 3% for the multiple-domain homogeneous finite element (MDFE) spatial modeling, and the error is approximately 1% for the multiple-domain heterogeneous modeling (MD/HM) with finite difference and finite element discretization. For the given boundary conditions and element configuration (*i.e.*, square or rectangular elements), the single-domain finite element (SD/FE) model reproduces the exact solution using the bilinear finite element. However, for a general element orientation (*i.e.*, quadrilateral elements), the bilinear element used does not reproduce the exact solution. Moreover, for the multiple-domain analysis, error is introduced when combining finite element models of different discretization along the boundary. This error is due to the use of a higher-order interpolation function (*i.e*., cubic spline) on the interface than that used to represent the potential on the finite element edges. The error

obtained using the heterogeneous model is smaller than that obtained for the homogeneous finite element model. This attribute is due to the ability of the finite difference model to represent accurately the potential function on the interface based on the higher-order shape function used in the generalization of the finite difference method.

Table 2.2. Results of the Multifunctional Approach for the Patch Test Problems.

Analysis Type*	Normalized Potential Function, u			Normalized Flux, q_x		
	Order of Potential function			Order of Potential Function		
	Linear	Bilinear	Quadratic	Linear	Bilinear	Quadratic
SD/FE	1.0	1.0	1.0	1.0	1.0	1.0
SD/FD	1.0	1.0	1.0	1.0	1.0	1.0
MD/FE	1.0	1.0	1.03125	1.0	1.0	1.03125
MD/FD	1.0	1.0	1.0	1.0	1.0	1.0
MD/HM	1.0	1.0	.98958	1.0	1.0	.98958

* SD/FE: Single-Domain with Finite Element discretization
SD/FD: Single-Domain with Finite Difference discretization
MD/FE: Multiple-Domain with Finite Element discretization
MD/FD: Multiple-Domain with Finite Difference discretization
MD/HM: Multiple-Domain with Heterogeneous Modeling (combined finite difference and finite element discretizations)

CHAPTER III

MULTIFUNCTIONAL APPROACH FOR VECTOR-FIELD PROBLEMS

3.1. GENERAL

While a scalar-field problem is one in which the dependent variable is a scalar and requires only the specification of magnitude for a complete description, a vector-field problem is one in which the dependent variable is a vector of components and requires the specification of magnitude and direction. Many of the concepts outlined for the scalar-field problem in the previous chapter are readily extendable to the vector-field problem, which allows further generalization of the multifunctional approach developed herein. A representative example of the vector-field differential equation in two dimensions is considered, and the mathematical statement is formulated. The concepts developed here are directly applicable to one-, two-, and three-dimensional vector-field problems; however, only the two-dimensional development is included in the interest of brevity. The general form of the differential equation describing the vector-field problem governing the motion of a continuum is given by the equilibrium equation

$$\rho\mathbf{b} + \nabla \cdot \mathbf{T} = \frac{\mathrm{d}(\rho\mathbf{v})}{\mathrm{d}t} \tag{3.1}$$

where the variables ρ, **b**, **T** and **v** are the material mass density, the body force per unit volume, the stress tensor and the velocity vector, respectively. Eq. (3.1) is subject to the natural boundary condition, $\mathbf{t} = \mathbf{T} \cdot \mathbf{n} = \bar{\mathbf{t}}$ on Γ^s, and essential boundary conditions, $\mathbf{u} = \bar{\mathbf{u}}$, on Γ^p where the normal vector to the boundary Γ is given by $\mathbf{n} = n_x\hat{\boldsymbol{i}} + n_y\hat{\boldsymbol{j}}$, and

n_x and n_y are direction cosines of the unit normals, $\hat{\boldsymbol{i}}$ and $\hat{\boldsymbol{j}}$. In addition, $\bar{\mathbf{t}}$, and $\bar{\mathbf{u}}$ are applied tractions, and prescribed displacements, respectively, and $\bar{\mathbf{v}}$ is the initial velocity vector. The equilibrium equations must be satisfied within the domain. Note that instead of prescribing the tractions on the boundary, boundary conditions may be given in terms of displacement or velocity components. Furthermore, boundary conditions on Γ may be mixed (*i.e.*, surface forces, **t**, may be prescribed on one part of the boundary and displacements or velocities may be prescribed on another). The equilibrium equation and other governing equations of continuum mechanics are discussed in more detail in the following section.

3.2. CONTINUUM MECHANICS FOUNDATIONS

The conservation of mass, linear momentum, angular momentum, energy, and entropy give rise to field equations that govern the deformation and motion of a continuum, and these equations are given in the form of integral or differential equations. In deriving the governing equations, the starting point is a statement of the conservation principle applied to a "control volume" to develop the integral form of the equation and extract the differential form by using the divergence theorem.

3.2.1. Principle of Conservation of Mass

The principle of conservation of mass states that when the total mass of the body is unchanged for an arbitrarily small neighborhood of each material point, the mass is considered to be conserved locally. Hence, the rate of increase of the mass inside the control volume is equal to the net inflow of mass through the control surface. Mathematically, this principle is given by

$$\int_V \left(\frac{\partial \rho}{\partial t} + \nabla \cdot (\rho \mathbf{v}) \right) \mathrm{dV} = 0$$

Since the integral is equal to zero for arbitrary respective volumes, *V*, the integrand must be equal to identically zero everywhere in the domain. The resulting equation, known as the continuity equation, is well known in fluid dynamics and is given in a conservative form by

$$\frac{\partial \rho}{\partial t} + \nabla \cdot (\rho \mathbf{v}) = 0 \quad \text{or} \quad \frac{\partial \rho}{\partial t} + \frac{\partial (\rho v_i)}{\partial x_i} = 0 \tag{3.2}$$

The differential equation takes on a slightly different form when the derivatives of products are expanded and the definition of the material derivative is considered. The resulting non-conservative form is given by

$$\frac{\mathrm{d}\rho}{\mathrm{d}t} + \rho \nabla \cdot \mathbf{v} = 0 \quad \text{or} \quad \frac{\mathrm{d}\rho}{\mathrm{d}t} + \rho \frac{\partial v_i}{\partial x_i} = 0$$

If the material is incompressible so that the density in the neighborhood of each material particle remains constant as it moves, the continuity equation takes the simpler form

$$\nabla \cdot \mathbf{v} = 0 \quad \text{or} \quad \frac{\partial v_i}{\partial x_i} = 0 \tag{3.3}$$

This is known as the condition of incompressibility, which is important in classical hydrodynamics and plasticity theories. The continuity equation is an important partial differential equation in all branches of continuum mechanics and the discipline-specific aspects are discussed in the next section.

3.2.2. Conservation of Linear Momentum

The equations of motion, valid in all branches of mechanics, are partial differential equations derived from the momentum principles of a collection of particles.

In this case, it is easier to use integrals over a given mass of material (the material volume, V') rather than over a given spatial volume (the control volume, V). The Reynolds transport theorem is used to replace the material volume with the control volume. The conservative form of this theorem is given by

$$\frac{\mathrm{d}}{\mathrm{d}t}\int_{V'}\phi\rho\,\mathrm{d}V' = \frac{\partial}{\partial t}\int_{V}\phi\rho\,\mathrm{d}V + \oint_{S}\phi\rho\mathbf{v}\cdot\mathbf{n}\,\mathrm{d}S$$

where ϕ is the continuum property per unit mass and $\oint_{S}\rho\mathbf{v}\cdot\mathbf{n}\,\mathrm{d}S$ is recognized as the mass flux. The conservation of linear momentum represents Newton's second law and governs the motion of the continuum under the influence of the external effects. This principle states that the time rate of change of momentum is equal to the resultant force, **F**, acting on the body. Thus, $\mathbf{F} = \frac{\mathrm{d}\mathbf{L}}{\mathrm{d}t}$ where **F** is the resultant of all external forces and is given acting on a material volume as $\mathbf{F} = \int_{V'}\rho\mathbf{b}\,\mathrm{d}V' + \oint_{S'}\mathbf{t}\,\mathrm{d}S'$, and **L** is the linear momentum vector on a material volume given by $\mathbf{L} = \int_{V'}\mathbf{v}\rho\,\mathrm{d}V'$. First, expressing the conservation of linear momentum over the material volume and then using the Reynolds transport theorem to express the equation in terms of the control volume yields the integral conservative momentum equation given by

$$\int_{V}\rho\mathbf{b}\,\mathrm{d}V + \oint_{S}\mathbf{t}\,\mathrm{d}S = \frac{\partial}{\partial \mathrm{t}}\int_{V}\mathbf{v}\rho\,\mathrm{d}V + \oint_{S}\mathbf{v}\rho\mathbf{v}\cdot\mathbf{n}\,\mathrm{d}S$$

Using the divergence theorem and Cauchy's formula, the conservative differential form may be obtained as

$$\rho\mathbf{b} + \nabla\cdot\mathbf{T} = \frac{\partial(\rho\mathbf{v})}{\partial \mathrm{t}} + \nabla\cdot(\rho\mathbf{v}\mathbf{v})$$

The non-conservative form of the differential equations is obtained by expanding the divergence operator, $\nabla \cdot (\rho \mathbf{v}\mathbf{v})$, and making use of the continuity equation, Eq. (3.3), yielding

$$\rho \mathbf{b} + \nabla \cdot \mathbf{T} = \frac{\mathrm{d}(\rho \mathbf{v})}{\mathrm{d}t} \quad \text{or} \quad \rho b_i + \frac{\partial T_{ij}}{\partial x_j} = \frac{\mathrm{d}(\rho v_i)}{\mathrm{d}t}$$

3.2.3. Conservation of Angular Momentum

The principle of conservation of angular momentum is used to show symmetry of the stress tensor, which is used to describe the state of stress of the continuum. In a collection of particles whose interactions are equal, opposite and collinear forces, the time rate of change of the total moment of momentum for the given collection of particles is equal to the vector sum of the moments of the external forces acting on the system. In the absence of distributed couples, the same principle for a continuum is postulated. Thus,

$$\int_S (\mathbf{r} \times \mathbf{t})\,\mathrm{d}S + \int_V (\mathbf{r} \times \rho \mathbf{b})\,\mathrm{d}V = \frac{\mathrm{d}}{\mathrm{d}t} \int_V (\mathbf{r} \times \rho \mathbf{v})\,\mathrm{d}V$$

where $\times$ denotes the vector cross-product operation. Upon expressing the cross products in indicial notation, transforming the surface integral to a volume integral (using the divergence theorem), and using the expression for the material derivative of a volume integral, the moment of momentum equation is reduced to

$$e_{krs} T_{sr} = 0$$

at each point where e_{krs} is the permutation operator. This yields

For r=1 $\qquad\qquad$ $T_{32} - T_{23} = 0$

For r=2 $\quad T_{31} - T_{13} = 0$

For r=3 $\quad T_{12} - T_{21} = 0$

establishing the symmetry of the stress tensor in general without any assumption of equilibrium or of uniformity of the stress distribution. However, the balance of the couple stresses is assumed. In reference 39, a proof is given for symmetry of the stress tensor involving the condition that the rates of change of the components of stress remain finite.

3.2.4. Conservation of Energy

The principle of conservation of energy states that energy is conserved if the time rate of change of the kinetic and internal energy is equal to the sum of the rate of work of the external forces and all the other energies that enter or leave the body per unit time. Such energies supplied may include thermal energy, chemical energy, or electromagnetic energy. Herein, only mechanical and thermal energies are considered, and the energy principle takes the form of the well-known first law of thermodynamics. Since the energy equation involves an additional unknown quantity, the internal energy, the equation is a useful addition to the equations of continuum mechanics only when it is possible to relate the internal energy to the other state variables; in traditional thermodynamics an equation of state furnishes the required relation. The first law of thermodynamics applied to a material volume may be written as

$$\dot{K} + \dot{U} = W + Q$$

where the superscripted dot, $(\dot{})$, represents the derivative with respect to time, and $\dot{K}$ is the rate of increase of the kinetic energy of the material volume , $\dot{U}$ is the rate of increase of the internal energy of the material volume, W is the rate of work done by the external

forces on the material volume, and Q is the rate of heat added to the material volume. The individual variables are defined as follows:

$$\dot{K} = \frac{d}{dt}\int_{V'} \frac{1}{2}\rho \mathbf{v}\cdot\mathbf{v}\,\mathrm{d}V'$$

$$\dot{U} = \frac{d}{dt}\int_{V'} \rho\hat{u}\,\mathrm{d}V'$$

$$W = \int_{V'} \rho\mathbf{b}\cdot\mathbf{v}\,\mathrm{d}V' + \int_{S'} \mathbf{T}\mathbf{v}\cdot\mathbf{n}\,\mathrm{d}S'$$

$$Q = -\int_{S'} \mathbf{q}\cdot\mathbf{n}\,\mathrm{d}S' + \int_{V'} \rho r\,\mathrm{d}V'$$

where $\hat{u}$ is the specific internal energy, $\mathbf{q}$ is the heat flux vector and r is the radiative heat transfer per unit mass. Upon using Reynolds transport theorem to convert the material volume to the control volume and the divergence theorem to convert the surface integrals to volume integrals, and performing further algebraic manipulation, the energy takes the form

$$\int_V \rho\frac{\mathrm{d}\hat{u}}{\mathrm{d}t}\,\mathrm{d}V = -\int_V \nabla\cdot\mathbf{q}\,\mathrm{d}V + \int_V \rho r\,\mathrm{d}V + \int_V \mathbf{T}\!:\!\mathbf{D}\,\mathrm{d}V$$

where the stress power, $\mathbf{T}\!:\!\mathbf{D}$, is the scalar product of the stress tensor, $\mathbf{T}$, and the rate of deformation tensor, $\mathbf{D}$. The differential forms are given by

$$\rho\frac{\mathrm{d}\hat{u}}{\mathrm{d}t} = -\nabla\cdot\mathbf{q} + \rho r + \mathbf{T}\!:\!\mathbf{D}$$

or

$$\rho\frac{\mathrm{d}\hat{u}}{\mathrm{d}t} = -\frac{\partial\mathbf{q}}{\partial x_i} + \rho r + T_{ij}D_{ij}$$

If only mechanical quantities are considered, the principle of conservation of energy for the continuum may be derived directly from the equation of motion. This equation, referred to as the conservation of mechanical energy, states that the rate of increase of the internal energy equals the heat added per unit time plus the stress power that is not contributing to the kinetic energy. The equation is given by

$$\rho \frac{\mathrm{d}\hat{\mathbf{u}}}{\mathrm{d}t} = -\nabla \cdot \mathbf{q} + \rho r + \mathbf{T} : \mathbf{D} \tag{3.4}$$

3.2.5. Second Law of Thermodynamics

The second law of thermodynamics is automatically satisfied and includes the change in entropy of the continuum. The entropy is regarded as a measure of change of energy dissipation with respect to temperature. The relationship expressing conversion of heat and work into kinetic and internal energies during a thermodynamic process is set forth in the energy equation. The first law, however, leaves unanswered the question of the extent to which the conversion process is reversible or irreversible. The basic criterion for irreversibility is given by the second law of thermodynamics through the statement on the limitations of entropy production. For a general process, the energy equation and the second law of thermodynamics are combined yielding

$$\frac{\mathrm{d}\hat{s}}{\mathrm{d}t} = \frac{1}{T}\frac{\bar{\mathrm{d}}q}{\mathrm{d}t} + \frac{Q}{\rho T}$$

where $\mathrm{d}\hat{s}$ is the change in the entropy per unit mass, T is the absolute temperature, $\frac{\bar{\mathrm{d}}q}{\mathrm{d}t}$ is the heat transferred per unit time per unit mass, Q is the dissipative function obtained from $Q = T_{ij}^{D} D_{ij}$ using the dissipative or deviatoric stress tensor $\mathbf{T}^{\mathrm{D}}$, and the notation $\bar{\mathrm{d}}$ is used to indicate that the quantity is not an exact differential. The deviatoric stress

tensor is defined by $T_{ij}^{D} = T_{ij} - \bar{p}\delta_{ij}$ where $-\bar{p}$ is the hydrostatic pressure. For a general process, $Q \geq 0$

$$\frac{\mathrm{d}\hat{s}}{\mathrm{d}t} \geq \frac{1}{T}\frac{\bar{\mathrm{d}}q}{\mathrm{d}t}$$

and for an adiabatic process,

$$\frac{\mathrm{d}\hat{s}}{\mathrm{d}t} \geq 0$$

where in each of the above equations, the equality condition holds for a reversible process and the inequality condition holds for an irreversible process.

The general principles of continuum mechanics have been outlined in this section to provide a foundation for the basic equations governing the motion of general continua. In the derivation of the balance laws, no differentiation has been made between various types of substances. The character of the material is brought into the formulation through appropriate constitutive equations for each material with the constitutive variables being restricted in their regions of definitions. These and other discipline-specific attributes are outlined in the following section.

3.3. DISCIPLINE SPECIFICS

The constitutive equations characterize the individual material and its reactions to applied loads. Hence, in the following section, the discipline-specific attributes of solid and fluid continua and their impact on the general principles of continuum mechanics are reviewed. In addition, other salient characteristics of the governing equations for solids and fluids are discussed.

All constitutive equations must be consistent with the general principles of continuum mechanics. While impact of the constitution of the continua is discussed for

all of the balance laws, emphasis is placed on the principle of conservation of linear momentum. This principle is the basis for the governing equations of the multifunctional approach presented herein. This law states that the sum of the body forces together with the sum of the contact forces is equal to the change of the linear momentum of the material. The law is used as the basis for describing the motion in both solid mechanics and fluid mechanics.

3.3.1. Solid Mechanics

The field of solid mechanics has traditionally been characterized by well-formulated analysis of mechanical phenomena occurring in engineering systems, combined with experiments that explore the basic concepts[40]. Herein, elasticity theory is the primary field of solid mechanics discussed. In classical linear elasticity theory, it is assumed that displacements and displacement gradients are sufficiently small such that no distinction need be made between the Lagrangian and Eulerian descriptions. It is further assumed that the deformation processes are adiabatic (no heat loss or gain) and isothermal (constant temperature). The conservation of mass states that the mass of a deformed piece of material is the same as the mass of the undeformed material. In elasticity, based on the small strain assumption, the density, ρ, in the deformed state may be approximated by the density, ρ_0, in the undeformed state, and the conservation of mass is identically satisfied.

Moreover, it is convenient to identify a material particle of the continuous body by giving its initial coordinates. The position coordinates, *x*, *y*, *z* appearing in the partial derivatives and the integrals in the foregoing derivatives are, however, the instantaneous positions. For an elastic body in equilibrium, they represent the coordinates of a particle

in its new position in the deformed body. When the strains and displacements are small, it may be possible that the equilibrium conditions are satisfied in the undeformed configuration of the body. The equilibrium differential equations are strictly applicable and the stress tensor is strictly symmetric for the nonpolar case only when defined in the instantaneous deformed position. Even in small strain theory of elasticity, it is necessary to take account of this attribute in applications where the instability may occur, as in the buckling of a column or a shell. Asymmetry of the stress tensor also occurs when there is distributed couple stress[6].

In ideal elasticity, heat transfer is considered insignificant, and all of the input work is assumed to be converted into internal energy in the form of recoverable stored elastic strain energy, which can be recovered as work when the body is unloaded. In general, however, the major part of the input work into a deforming material is not recoverable energy stored, but dissipated by the deformation process, causing an increase in the body's temperature and eventually being conducted away as heat. When thermal effects are neglected, the energy balance equation may be written as

$$\frac{\mathrm{d}\hat{u}}{\mathrm{d}t} = \frac{1}{\rho} T_{ij} D_{ij} = \frac{1}{\rho} T_{ij} \varepsilon_{ij}$$

The internal energy, $\hat{u}$, in this case is purely mechanical and is called the strain energy density (per unit mass)

$$\mathrm{d}\hat{u} = \frac{1}{\rho} T_{ij} \mathrm{d}\varepsilon_{ij}$$

A material body is said to be ideally elastic when the body recovers (under isothermal conditions) its original form completely upon removal of the forces causing deformation, and there is a one-to-one relationship between the state of stress and state of

strain. The generalized Hooke's law relates the nine components of stress to the nine components of strain

$$\sigma_{ij} = C_{ijkl}\varepsilon_{kl}$$

Symmetry of stress and strain reduces the number of material constants in the fourth-order tensor, C_{ijkl}, from 81 to 36. The existence of the strain energy density functional further reduces the number of constants to 21. The existence of three mutually orthogonal planes of symmetry reduces the number of constants to nine. Isotropy reduces the number of constants to two.

For this special case, Hooke's law reduces to

$$\sigma_{ij} = \left[\lambda\delta_{ij}\delta_{kl} + \mu\left(\delta_{ik}\delta_{jl} + \delta_{il}\delta_{jk}\right)\right]\varepsilon_{kl} \tag{3.5}$$

where

$$\mu = G = \frac{E}{2(1+\nu)} \quad ; \quad \lambda = \frac{\nu E}{(1+\nu)(1-2\nu)}$$

For i=j=1, the second and third terms of Eq. (3.5) are nonzero if k=1 and l=1. Thus,

$$\sigma_{11} = \lambda e + 2\mu\varepsilon_{11}$$

where $e = \varepsilon_{11} + \varepsilon_{22} + \varepsilon_{33}$. For i=1 and j=2, the second term of Eq. (3.5) is nonzero if k=1 and l=2 and the third term is nonzero if k=2 and l=1. Thus,

$$\sigma_{12} = \mu\varepsilon_{12} + \mu\varepsilon_{21} = 2\mu\varepsilon_{12}.$$

Similarly, other components of stress may be defined.

Noting that the linear strain-displacement relationship is given by

$$\varepsilon_{ij} = \frac{1}{2}\left(u_{i,j} + u_{j,i}\right)$$

One method of solution of the problems of elasticity is to eliminate the stress components in the equilibrium equations given in indicial notation as

$$\sigma_{ij,j} + \rho(b_i - \dot{v}_i) = 0\,,$$

and using Hooke's law to express the strain components in terms of the displacements. Eq. (3.5) may be written, with no loss of generality, as

$$\sigma_{ij} = \lambda\varepsilon_{ll}\delta_{ij} + 2\mu\varepsilon_{ij}$$

Solving the boundary-value problem involving 15 equations for 15 unknowns is a formidable task. There are several ways of formulating the problem in terms of fewer unknowns and fewer equations. The most straightforward method is to obtain the stresses in terms of displacement gradients, and then substitute into the equilibrium equations to obtain three second-order partial differential equations for the three displacement components. Therefore, in terms of displacements,

$$\sigma_{ij} = \lambda u_{l,l}\delta_{ij} + \mu(u_{i,j} + u_{j,i})$$

and

$$\dot{v}_i = \ddot{u}_i = \frac{\partial^2 u_i}{\partial t^2}$$

Substituting these expressions into the equilibrium equation yields

$$\lambda u_{l,lj}\delta_{ij} + \mu(u_{i,jj} + u_{j,ij}) + \rho(b_i - \ddot{u}_i) = 0$$

or

$$\lambda u_{l,li} + \mu(u_{i,jj} + u_{j,ij}) + \rho(b_i - \ddot{u}_i) = 0$$

Noting that l is a dummy index in the term $u_{l,li}$. The equation may be written as

$$\lambda u_{j,ji} + \mu(u_{i,jj} + u_{j,ij}) + \rho(b_i - \ddot{u}_i) = 0$$

This leads to the field equations of Navier

$$(\lambda+\mu)u_{j,ji}+\mu u_{i,jj}+\rho(b_i-\ddot{u}_i)=0$$

or

$$\mu\nabla^2 u_i+(\lambda+\mu)u_{j,ji}+\rho(b_i-\ddot{u}_i)=0 \tag{3.6}$$

The conditions for the static equilibrium of an elastic body are described by an elliptic system of nine partial differential equations for the displacements and stresses.

3.3.2. Fluid Mechanics

Fluids whose constitution is described by linear constitutive relations are called Newtonian fluids. The subject of Newtonian fluids is generally referred to as fluid mechanics, which encompasses widely diverse topics including, but not limited to, motion of airplanes and missiles through the atmosphere, the flow of liquids and gases through ducts, and the transfer of heat and mass by fluid motion. The constitutive equations for these fluids are given by

$$\sigma_{ij}=-P\delta_{ij}+C_{ijkl}D_{kl}$$

where P is the thermodynamic pressure and D_{kl} are the components of the rate of deformation tensor

$$D_{kl}=\frac{1}{2}(v_{k,l}+v_{l,k})$$

For isotropic fluids, the last term in the constitutive equations may be written as

$$C_{ijkl}D_{kl}=\lambda D_{rr}\delta_{ij}+2\mu D_{ij}$$

or

$$C_{ijkl}D_{kl}=\lambda[\delta_{ij}\delta_{kl}+\mu(\delta_{ik}\delta_{jl}+\delta_{il}\delta_{jk})]D_{kl}$$

Therefore,

$$\sigma_{ij} = -P\delta_{ij} + \lambda\left[\delta_{ij}\delta_{kl} + \mu\left(\delta_{ik}\delta_{jl} + \delta_{il}\delta_{jk}\right)\right]D_{kl}$$

and by evaluating the Kronecka delta parameters,

$$\sigma_{ij} = -P\delta_{ij} + \lambda D_{kk}\delta_{ij} + 2\mu D_{ij} \tag{3.7}$$

This is the Navier-Poisson law for a Newtonian fluid.

As in linear elasticity, substituting the constitutive equation into the equation of motion yields

$$-P_{,j}\delta_{ij} + \lambda v_{k,kj}\delta_{ij} + \mu\left(v_{i,jj} + v_{j,ij}\right) + \rho(b_i - \dot{v}_i) = 0$$

expanding gives

$$-P_{,i} + (\lambda + \mu)v_{j,ji} + \mu v_{i,jj} + \rho(b_i - \dot{v}_i) = 0$$

or

$$\rho\dot{v}_i = -P_{,i} + (\lambda + \mu)v_{j,ji} + \mu v_{i,jj} + \rho b_i$$

or in vector form

$$\rho\frac{d\mathbf{v}}{dt} = -\nabla\mathbf{P} + (\lambda + \mu)\nabla(\nabla\cdot\mathbf{v}) + \mu\nabla^2\mathbf{v} + \rho\mathbf{b}$$

Using the Stokes condition, $\lambda = -\frac{2}{3}\mu$, the equations reduce to the Navier-Stokes equations and are given by

$$\rho\dot{v}_i = -P_{,i} + \frac{\mu}{3}v_{j,ji} + \mu v_{i,jj} + \rho b_i \tag{3.8}$$

or

$$\rho\frac{d\mathbf{v}}{dt} = -\nabla\mathbf{P} + \frac{\mu}{3}\nabla(\nabla\cdot\mathbf{v}) + \mu\nabla^2\mathbf{v} + \rho\mathbf{b} \tag{3.9}$$

In this form, the difference between the Navier equations of solid mechanics, Eq. (3.6) and the Navier-Stokes equations of fluid mechanics, Eq. (3.8) or (3.9), can be readily

considered. In Navier-Stokes equations, there is not only an additional pressure term but also the equations are nonlinear; this can be seen by examining the acceleration, $\dot{v}_i = \frac{dv_i}{dt} = \frac{\partial v_i}{\partial t} + v_{i,j} v_j$, and from the products of the density, ρ, and the acceleration, $\dot{v}$, present in the equation. Additional nonlinearities are evident in the continuity equation given by $v_{k,k}=0$ ($\nabla \cdot \mathbf{v}=0$). In the linear theory of elasticity, this situation does not occur since $\dot{v}_i \approx \frac{\partial^2 u}{\partial t^2}$ and ρ is taken as a constant. The Navier-Stokes equations together with the continuity equation form a complete set of four equations and four unknowns: the pressure, P, and the three velocity components, v_i.

For steady and low-speed flow of an incompressible fluid ($\nabla \cdot \mathbf{v}=D_{kk}=0$), for constant ρ and by making use of the divergence-free condition in Eq. (3.8) or (3.9), the governing equations take the form

$$D_{kk} = 0$$

$$-P_{,i} + \mu v_{i,jj} + \rho b_i = 0$$

However, these equations, often referred to as Stokes equations, may be written for two-dimensions in the most general form without using the divergence-free condition to simplify the equations. In so doing, the physical form of the natural boundary conditions is preserved. The form of these equations is given by

$$\frac{\partial v_1}{\partial x_1} + \frac{\partial v_2}{\partial x_2} = 0 \tag{3.10}$$

$$-\mu\left[2\frac{\partial^2 v_1}{\partial x_1^2}+\frac{\partial}{\partial x_2}\left(\frac{\partial v_1}{\partial x_2}+\frac{\partial v_2}{\partial x_1}\right)\right]+\frac{\partial P}{\partial x_1}=\rho b_1$$

$$-\mu\left[\frac{\partial}{\partial x_1}\left(\frac{\partial v_1}{\partial x_2}+\frac{\partial v_2}{\partial x_1}\right)+2\frac{\partial^2 v_2}{\partial x_2^2}\right]+\frac{\partial P}{\partial x_2}=\rho b_2$$

Fluids often behave as though they are inviscid or frictionless. Therefore, it is useful to investigate the dynamics of an ideal fluid that is incompressible and has zero viscosity. For frictionless flow of an incompressible fluid, the equations, called Euler's equations, may be obtained from the general Navier-Stokes equations. Since in a frictionless flow, there can be no shear stress present and the normal stress is the negative of the thermodynamic pressure, the equations of motion are

$$\rho\dot{v}_i = -P_{,i} + \rho b_i$$

or

$$\rho\frac{\partial \mathbf{v}}{\partial t} = -\nabla\mathbf{P} + \rho\mathbf{b}$$

For a general fluid, the character (*e.g.*, elliptic, hyperbolic, or parabolic) of these equations of motion is determined by the sign of the discriminant. The Navier-Stokes system of equations, in general, is considered as mixed elliptic, parabolic and hyperbolic equations. The system of time-dependent Navier-Stokes equations is essentially parabolic in time and space, although the continuity equation has a hyperbolic structure. Therefore, they are considered a parabolic hyperbolic system. For the same reason, the steady-state form of the Navier-Stokes equations leads to elliptic-hyperbolic properties. In addition, the classification of the differential equation changes with the flow

characteristics (*i.e.*, subsonic, supersonic, or transonic), which may create great difficulties in solution where part of the flow is supersonic and part of it is subsonic.

3.4. SINGLE-DOMAIN FORMULATION

As in the scalar-field problem, methodology for the vector-field problem is presented formulating the general method of weighted residuals for a single domain. Consider the equilibrium equation governing the motion, *u*, of a continuum

$$\rho\mathbf{b} + \nabla \cdot \mathbf{T} = \rho \frac{\partial \mathbf{v}}{\partial t}$$

or in indicial notation

$$\sigma_{ij,j} + \rho(b_i - \dot{v}_i) = 0 \quad \text{in } \Omega \qquad \text{for } i, j = 1,2,3 \tag{3.11}$$

in a domain, Ω, bounded by Γ. In this work, the equilibrium equations of Eq. (3.11) describe the motion of a three-dimensional continuum. Hence, the indices, *i* and *j* range from the value of unity to three (*i.e.*, *i*,*j* = 1,2,3). This range will apply throughout this development unless otherwise specified. In general, the boundary, Γ, can have mixed boundary conditions with the primary variables, **u**, prescribed on Γ^p and the secondary variable, the traction, **t**, prescribed on the remaining part of the boundary, Γ^s. In solid mechanics, the six stress components will be some general functions of the components of the generalized displacement

$$\mathbf{u}^{\mathrm{T}} = \begin{bmatrix} u & v & w & \theta_x & \theta_y & \theta_z \end{bmatrix}$$

where *u*, *v*, and *w* are translational components and θ_x, θ_y and θ_z are rotational components. In fluid mechanics, the stress components will be functions of the velocity vector

$$\mathbf{u}^{\mathrm{T}} = \begin{bmatrix} v_1 & v_2 & v_3 \end{bmatrix},$$

which has similar components to those of the displacement vector. Thus, Eq. (3.11) can be considered as a general equation of the form of $\mathbf{A}(\mathbf{u}) = 0$.

The method of weighted residuals is applied to the vector-field problem in this chapter in the same way as for the scalar-field problem of Chapter II. Hence, an approximate solution, $\tilde{\mathbf{u}}$, is used in expressing $\sigma_{ij,j}$ through the use of stress-strain and strain-displacement (or stress-rate of strain) relations, then the differential equation, Eq. (3.11), will no longer be satisfied, and this lack of equality is a measure of the departure of $\tilde{\mathbf{u}}$ from the exact solution. The lack of equality is called the residual, **R**, and is written as

$$R_i = \sigma_{ij,j} + \rho(b_i - \dot{v}_i) \neq 0 \qquad \text{for } i,j = 1,2,3 .$$

The residual is orthogonalized by a set of weight functions, Φ_i and may be written as

$$\int_{\Omega} R_i \, \Phi_i \, \mathrm{d}\Omega = \int_{\Omega} \left(\sigma_{ij,j} + \rho(b_i - \dot{v}_i)\right)\Phi_i \, \mathrm{d}\Omega = 0 \tag{3.12}$$

where the approximate solution is given by $\tilde{\mathbf{u}} = \Psi_0 + \sum_{m=1}^{n} a_m \Psi_m$. As defined before, the functions, Ψ_m, are trial functions, and a_m are arbitrary coefficients. The trial functions satisfy the homogeneous part of the essential boundary conditions, while Ψ_0 satisfies the nonhomogeneous part. Using the general weighted residual form outlined in Chapter II,

$$\int_{\Omega} \mathbf{\Phi A}(\tilde{\mathbf{u}}) \, \mathrm{d}\Omega + \oint_{\Gamma} \overline{\mathbf{\Phi}} \mathbf{B}(\tilde{\mathbf{u}}) \, \mathrm{d}\Gamma = 0 .$$

where the residual in the satisfaction of the boundary conditions is orthogonalized by a secondary weight function, $\overline{\mathbf{\Phi}}$. For the system at hand, a vector quantity is sought and the differential equation is a simultaneous system of equations. Here,

$\mathbf{A}(\mathbf{u}) = \sigma_{ij,j} + \rho(b_i - \dot{v}_i) = 0$, and the essential and natural boundary conditions are represented by

$$B_1(\mathbf{u}) = \mathbf{u} - \bar{\mathbf{u}} = \mathbf{0} \text{ or } u_i - \bar{u}_i = 0 \qquad \text{on } \Gamma^p$$

and

$$B_2(\mathbf{u}) = \mathbf{t} - \bar{\mathbf{t}} = \mathbf{0} \text{ or } t_i - \bar{t}_i = 0 \qquad \text{on } \Gamma^s,$$

respectively. Therefore, considering the approximate solution, $\tilde{\mathbf{u}}$, we may write the general integral form of the differential equation governing the continuum motion as

$$\int_\Omega \Phi_i \left(\sigma_{ij,j} + \rho(b_i - \dot{v}_i)\right) d\Omega + \int_{\Gamma^p} \overline{\Phi}_{i1} (\tilde{u}_i - \bar{u}_i)\, d\Gamma^p + \int_{\Gamma^s} \overline{\Phi}_{i2} (t_i - \bar{t}_i)\, d\Gamma^s = 0 \qquad (3.13)$$

Note that the approximate solution may be selected to satisfy the essential and the natural boundary conditions and thus the boundary integral equations in Eq. (3.13) are identically zero. In this formulation, we will presume that the essential boundary conditions, *i.e.*,

$$\tilde{\mathbf{u}} - \bar{\mathbf{u}} = \mathbf{0} \text{ or } \tilde{u}_i - \bar{u}_i = 0 \qquad \text{on } \Gamma^p$$

are automatically satisfied by the choice of the function, $\tilde{\mathbf{u}}$. Therefore, Eq. (3.13) is rewritten as

$$\int_\Omega \Phi_i \left(\sigma_{ij,j} + \rho(b_i - \dot{v}_i)\right) d\Omega + \int_{\Gamma^s} \overline{\Phi}_i (t_i - \bar{t}_i)\, d\Gamma^s = 0 \qquad (3.14)$$

where $\overline{\Phi}_{i2} = \overline{\Phi}_i$.

In the formulation herein, the order of differentiation on the stress term in the integral equation, Eq. (3.14), is reduced to obtain the weak formulation. Recognizing that the stress components are functions of the primary variable, **u**, which is approximated by $\tilde{\mathbf{u}}$. For simplicity, the subsequent development is presented in terms of **u**. Application of the divergence theorem to Eq. (3.14) yields

$$-\int_{\Omega}\sigma_{ij}\Phi_{i,j}\,d\Omega+\oint_{\Gamma}(\sigma_{ij}n_j)\Phi_i\,d\Gamma+\int_{\Omega}\rho(b_i-\dot{v}_i)\Phi_i\,d\Omega+\int_{\Gamma^s}(t_i-\bar{t}_i)\overline{\Phi}_i d\Gamma^s=0\,. \quad (3.15)$$

Note that the domain boundary is presumed to consist of boundaries on which the primary variable is specified and boundaries on which the secondary variable is specified, and $\Gamma=\Gamma^p+\Gamma^s$. Therefore, the boundary integral on Γ, may be expressed as

$$\oint_{\Gamma}(\sigma_{ij}n_j)\Phi_i\,d\Gamma=\int_{\Gamma^p}(\sigma_{ij}n_j)\Phi_i\,d\Gamma^p+\int_{\Gamma^s}(\sigma_{ij}n_j)\Phi_i\,d\Gamma^s\,.$$

In the method of weighted residuals, the weight functions, Φ, satisfy the homogeneous boundary conditions for the primary variable, and thus, $\mathbf{\Phi=0}$ on Γ^p. Therefore, the boundary integral on Γ^p is identically zero and Eq. (3.15) may be rewritten as

$$-\int_{\Omega}\sigma_{ij}\Phi_{i,j}\,d\Omega+\int_{\Gamma^s}(\sigma_{ij}n_j)\Phi_i\,d\Gamma^s+\int_{\Omega}\rho(b_i-\dot{v}_i)\Phi_i\,d\Omega+\int_{\Gamma^s}(t_i-\bar{t}_i)\overline{\Phi}_i d\Gamma^s=0\,.$$

Since the weight functions, $\mathbf{\Phi}$ and $\overline{\mathbf{\Phi}}$, are arbitrary, they may be chosen, without loss of generality, such that, $\overline{\mathbf{\Phi}}=-\mathbf{\Phi}$, and using the Cauchy formula, $t_i=\sigma_{ij}n_j$,

$$-\int_{\Omega}\sigma_{ij}\Phi_{i,j}\,d\Omega+\int_{\Omega}\rho(b_i-\dot{v}_i)\Phi_i\,d\Omega+\int_{\Gamma^s}\bar{t}_i\,\Phi_i d\Gamma^s=0 \quad (3.16)$$

or

$$\int_{\Omega}\sigma_{ij}\Phi_{i,j}\,d\Omega=\int_{\Omega}\rho(\dot{v}_i-b_i)\Phi_i\,d\Omega+\int_{\Gamma^s}\bar{t}_i\,\Phi_i d\Gamma^s\,.$$

The integral form of Eq. (3.16) is given for a general continuum. If the weight functions, Φ_i, are selected to be virtual displacements or velocities, δu_i, then Eq. (3.16) is given by

$$-\int_{\Omega}\sigma_{ij}\delta u_{i,j}\,d\Omega+\int_{\Omega}\rho(b_i-\dot{v}_i)\delta u_i\,d\Omega+\int_{\Gamma^s}\bar{t}_i\,\delta u_i d\Gamma^s=0\,. \quad (3.17)$$

The term $\delta u_{i,j}$ can be expanded to

$$\delta u_{i,j} = \delta\left(u_{i,j} \right) = \delta\left(\varepsilon_{ij} + \omega_{ij} \right)$$

where ε_{ij} and ω_{ij} are symmetric and skew-symmetric tensors, respectively. These tensors are given by

$$\varepsilon_{ij} = \frac{1}{2}\left(u_{i,j} + u_{j,i} \right) \quad \text{and} \quad \omega_{ij} = \frac{1}{2}\left(u_{i,j} - u_{j,i} \right).$$

In solid mechanics, these tensors represent the linear infinitesimal strain-displacement and linear infinitesimal rotation tensors, respectively. In fluid mechanics, the tensors represent the linear infinitesimal strain-rate of deformation and vorticity tensors, respectively. Noting that σ_{ij} is a symmetric tensor and that the product of a symmetric tensor and a skew-symmetric tensor is zero, Eq. (3.17) may be rewritten as

$$-\int_{\Omega} \sigma_{ij}\delta\varepsilon_{ij}\, \mathrm{d}\Omega + \int_{\Omega} \rho(b_i - \dot{v}_i)\delta u_i\, \mathrm{d}\Omega + \int_{\Gamma^S} \bar{t}_i\, \delta u_i \mathrm{d}\Gamma^S = 0 \qquad (3.18)$$

Eq. (3.18) represents the principle of virtual work where the first integral term represents the internal virtual work, the second and third terms represents the external virtual work due to body forces, inertial forces and surface tractions.

In the virtual work development, the term virtual work is loosely used for fluid mechanics and has been included here to highlight the similarities between solid and fluid mechanics. Variational techniques for perfect fluids, non-Newtonian fluids and general Navier-Stokes equations are discussed in Finlayson[7]. In this work, concentration is given to the general weighted residual equations, Eq. (3.16), and these equations form the basis of finite element approximations, which will be presented briefly in a subsequent section.

Thus far, the single domain formulation has been developed for the vector-field problem focussing on the momentum equation, which is applicable to general continua.

However, the motion of a fluid is governed by the conservation laws of mass, momenta, and energy. In general, these equations consist of a set of coupled nonlinear, partial differential equations in terms of the velocity components, temperature, and pressure. When the Reynolds number for the flow is very low, the nonlinear terms due to inertial effects can be neglected, resulting in a linear boundary value problem. Such a flow is called Stokes flow[41] (see Eq. (3.10)). When temperature effects are not important, the energy equations are uncoupled from the momentum (*i.e.*, Navier-Stokes) equations.

Thus, for isothermal flows, only the Navier-Stokes, Eq. (3.8), and continuity, Eq. (3.2), need to be solved. Hence, an additional equation expressing the continuity condition is included in the weighted residual formulation. In the interest of completeness, the formulation herein is described using a Newtonian fluid. The laws governing the flow of Newtonian fluids were reviewed in Section 3.3.2 in which the equations were specialized to viscous fluids that are subject to the assumption of incompressibility. Under these conditions, the weighted residual statement of the equation of continuity, Eq. (3.3), is given by

$$\int_{\Omega} u_{i,j} \hat{\Phi} \, d\Omega = 0 \tag{3.19}$$

where the residual in the continuity condition is orthogonalized by the weight function, $\hat{\Phi}$, and $u_{i,j} = \nabla \cdot \mathbf{u} = \dfrac{\partial v_j}{\partial x_j}$. Hence, for fluid mechanics, both Eqs. (3.16) and (3.19) are the weighted residual statements required to approximate the continuum motion. While for solid mechanics, since the continuity condition, Eq. (3.3) and likewise Eq. (3.19) are automatically satisfied, Eq. (3.16) is the only weighted residual statement required to approximate the continuum motion.

3.5. MULTIPLE-DOMAIN FORMULATION

As in the case of the scalar-field problem of Chapter II, the domain of the problem is subdivided into smaller subdomains. Consider the equilibrium equation governing the motion, **u**, of a continuum

$$\sigma_{ij,j} + \rho(b_i - \dot{v}_i) = 0 \text{ in } \Omega \quad \text{for } i, j = 1,2,3 \tag{3.20}$$

in the entire domain, Ω, bounded by Γ. For simplicity, the multiple-domain formulation is presented for only two subdomains, Ω_1 and Ω_2 (see Figure 2.3) with a single interface boundary. Independent approximations and weight functions are assumed in each of the subdomains and continuity conditions are used to provide for a continuous solution across the domain. Thus, Eq. (3.20) is satisfied in each subdomain, independently, *i.e.*,

$$\sigma^{(1)}_{ij,j} + \rho_1(b^{(1)}_i - \dot{v}^{(1)}_i) = 0 \text{ in } \Omega_1 \quad \text{and} \quad \sigma^{(2)}_{ij,j} + \rho_1(b^{(2)}_i - \dot{v}^{(2)}_i) = 0 \text{ in } \Omega_2$$

subject to the boundary conditions on the subdomain boundaries, Γ_1 and Γ_2, and the superscripted numbers enclosed by parentheses denote the subdomain. In general, the boundaries can have mixed boundary conditions with the primary variable, **u**, prescribed on Γ^p and the secondary variable, the traction, **t**, prescribed on Γ^s. These boundary conditions may be written as

$$\mathbf{u}_1 - \bar{\mathbf{u}}_1 = \mathbf{0} \text{ or } u^{(1)}_i - \bar{u}^{(1)}_i = 0 \quad \text{on } \Gamma^p_1 \quad \text{and} \quad \mathbf{t} - \bar{\mathbf{t}}_1 = \mathbf{0} \text{ or } t^{(1)}_i - \bar{t}^{(1)}_i = 0 \quad \text{on } \Gamma^s_1$$

and

$$\mathbf{u}_2 - \bar{\mathbf{u}}_2 = \mathbf{0} \text{ or } u^{(2)}_i - \bar{u}^{(2)}_i = 0 \quad \text{on } \Gamma^p_2 \quad \text{and} \quad \mathbf{t} - \bar{\mathbf{t}}_2 = \mathbf{0} \text{ or } t^{(2)}_i - \bar{t}^{(2)}_i = 0 \quad \text{on } \Gamma^s_2 .$$

For the multiple domain case, the boundary at the interface between the two subdomains is denoted Γ^{I}. Hence, the subdomain boundaries, Γ_k, are presumed to include three boundary types, and these boundaries are given by

$$\Gamma_k = \Gamma_k^p + \Gamma_k^s + \Gamma_k^{\mathrm{I}} \qquad \text{for } k = 1,2\,.$$

Here, the boundary on the subdomain common boundary is assumed to represent the same geometry and thus, $\Gamma_k^{\mathrm{I}} = \Gamma^{\mathrm{I}}$. The residual for each domain is orthogonalized by a set of weight functions, $\Phi_i^{(\mathrm{k})}$ and is written as

$$\int_{\Omega_1} \left(\sigma_{ij,j}^{(1)} + \rho_1 (b_i^{(1)} - \dot{v}_i^{(1)})\right) \Phi_i^{(1)} \, \mathrm{d}\Omega_1 = 0$$

and

$$\int_{\Omega_2} \left(\sigma_{ij,j}^{(2)} + \rho_1 (b_i^{(2)} - \dot{v}_i^{(2)})\right) \Phi_i^{(2)} \, \mathrm{d}\Omega_2 = 0$$

where the approximate solution is given by $\tilde{u}_1 = \sum_{m=1}^{n} a_{1m} \Psi_{1m}$ and $\tilde{u}_2 = \sum_{m=1}^{n} a_{2m} \Psi_{2m}$. The functions, Ψ_{1m} and Ψ_{2m}, are the trial functions, and a_{1m} and a_{2m} are sets of arbitrary coefficients. Using the general form outlined previously, (*i.e.*, $\int_{\Omega} \mathbf{\Phi A}(\tilde{\mathbf{u}})\, \mathrm{d}\Omega + \oint_{\Gamma} \overline{\mathbf{\Phi}} \mathbf{B}(\tilde{\mathbf{u}})\, \mathrm{d}\Gamma = 0$), for each subdomain, one may write

$$\int_{\Omega_k} \mathbf{\Phi}^{(k)} \mathbf{A}\left(\tilde{\mathbf{u}}^{(k)}\right) \mathrm{d}\Omega + \oint_{\Gamma_k} \overline{\mathbf{\Phi}}^{(k)} \mathbf{B}\left(\tilde{\mathbf{u}}^{(k)}\right) \mathrm{d}\Gamma_k = 0 \qquad \text{for } k = 1,2$$

Therefore, considering the approximate solutions, $\tilde{\mathbf{u}}^{(1)}$ and $\tilde{\mathbf{u}}^{(2)}$, the general integral form of the differential equation governing the motion for subdomain 1 is given by

$$\int_{\Omega_1} \Phi_i^{(1)}\left(\sigma_{ij,j}^{(1)} + \rho_1(b_i^{(1)} - \dot{v}_i^{(1)})\right)\mathrm{d}\Omega_1 + \int_{\Gamma_1^p} \overline{\Phi}_{i1}^{(1)}\left(\tilde{u}_i^{(1)} - \bar{u}_i^{(1)}\right)\mathrm{d}\Gamma_1^p + \int_{\Gamma_1^s} \overline{\Phi}_{i2}^{(1)}\left(\tilde{t}_i^{(1)} - \bar{t}_i^{(1)}\right)\mathrm{d}\Gamma_1^s = 0 \tag{3.21}$$

and for subdomain 2 as

$$\int_{\Omega_2} \Phi_i^{(2)}\left(\sigma_{ij,j}^{(2)} + \rho_2(b_i^{(2)} - \dot{v}_i^{(2)})\right)\mathrm{d}\Omega_2 + \int_{\Gamma_2^p} \overline{\Phi}_{i1}^{(2)}\left(\tilde{u}_i^{(2)} - \bar{u}_i^{(2)}\right)\mathrm{d}\Gamma_2^p + \int_{\Gamma_2^s} \overline{\Phi}_{i2}^{(2)}\left(\tilde{t}_i^{(2)} - \bar{t}_i^{(2)}\right)\mathrm{d}\Gamma_2^s = 0 \tag{3.22}$$

Again, the essential boundary conditions, *i.e.*,

$$\tilde{\mathbf{u}}_1 - \bar{\mathbf{u}}_1 = \mathbf{0} \quad \text{or} \quad \tilde{u}_i^{(1)} - \bar{u}_i^{(1)} = 0 \qquad \text{on} \quad \Gamma_1^p$$

and

$$\tilde{\mathbf{u}}_2 - \bar{\mathbf{u}}_2 = \mathbf{0} \quad \text{or} \quad \tilde{u}_i^{(2)} - \bar{u}_i^{(2)} = 0 \qquad \text{on} \quad \Gamma_2^p$$

are identically satisfied by the choice of the functions, $\tilde{\mathbf{u}}_1$ and $\tilde{\mathbf{u}}_2$. Therefore, for subdomain 1, Eq. (3.21) is rewritten as

$$\int_{\Omega_1} \Phi_i^{(1)}\left(\sigma_{ij,j}^{(1)} + \rho_1(b_i^{(1)} - \dot{v}_i^{(1)})\right)\mathrm{d}\Omega_1 + \int_{\Gamma_1^s} \overline{\Phi}_i^{(1)}\left(t_i^{(1)} - \bar{t}_i^{(1)}\right)\mathrm{d}\Gamma_1^s = 0 \tag{3.23}$$

where $\overline{\Phi}_{i2}^{(1)} = \overline{\Phi}_i^{(1)}$. Similarly, for subdomain 2,

$$\int_{\Omega_2} \Phi_i^{(2)}\left(\sigma_{ij,j}^{(2)} + \rho_2(b_i^{(2)} - \dot{v}_i^{(2)})\right)\mathrm{d}\Omega_2 + \int_{\Gamma_2^s} \overline{\Phi}_i^{(2)}\left(t_i^{(2)} - \bar{t}_i^{(2)}\right)\mathrm{d}\Gamma_2^s = 0 \tag{3.24}$$

where $\overline{\Phi}_{i2}^{(2)} = \overline{\Phi}_i^{(2)}$.

The order of differentiation on the primary variable in the integral equations, Eq. (3.23) and (3.24), is reduced to obtain the weak formulation. Using the divergence theorem Eq. (3.23) can be rewritten, for subdomain 1, as

$$
\begin{aligned}
&-\int_{\Omega_1} \Phi^{(1)}_{i,j}\sigma^{(1)}_{ij}\,\mathrm{d}\Omega_1 + \oint_{\Gamma_1}\left(\sigma^{(1)}_{ij}n^{(1)}_j\right)\Phi^{(1)}_i\,\mathrm{d}\Gamma_1 + \int_{\Omega_1}\rho_1(b^{(1)}_i-\dot{v}^{(1)}_i)\,\Phi^{(1)}_i\,\mathrm{d}\Omega_1 \\
&+\int_{\Gamma^s_1}\overline{\Phi}^{(1)}_i\left(t^{(1)}_i-\bar{t}^{(1)}_i\right)\mathrm{d}\Gamma^s_1 = 0
\end{aligned}
\tag{3.25}
$$

and similarly, for subdomain 2,

$$
\begin{aligned}
&-\int_{\Omega_2} \Phi^{(2)}_{i,j}\sigma^{(2)}_{ij}\,\mathrm{d}\Omega_2 + \oint_{\Gamma_2}\left(\sigma^{(2)}_{ij}n^{(2)}_j\right)\Phi^{(2)}_i\,\mathrm{d}\Gamma_2 + \int_{\Omega_2}\rho_2(b^{(2)}_i-\dot{v}^{(2)}_i)\,\Phi^{(2)}_i\,\mathrm{d}\Omega_2 \\
&+\int_{\Gamma^s_2}\overline{\Phi}^{(2)}_i\left(t^{(2)}_i-\bar{t}^{(2)}_i\right)\mathrm{d}\Gamma^s_2 = 0
\end{aligned}
\tag{3.26}
$$

Recall that the boundary Γ is presumed to consist of boundaries on which the primary variable is specified and of boundaries on which the secondary variable is specified, and boundaries at the subdomain interface, and for subdomain k, $\Gamma_k = \Gamma^p_k + \Gamma^s_k + \Gamma^{\mathrm{I}}$.

Therefore, the boundary integral on Γ_k may be expressed as

$$
\begin{aligned}
\oint_{\Gamma_k}\left(\sigma^{(k)}_{ij}n^{(k)}_j\right)\Phi^{(k)}_i\,\mathrm{d}\Gamma_k = &\int_{\Gamma^p_k}\left(\sigma^{(k)}_{ij}n^{(k)}_j\right)\Phi^{(k)}_i\,\mathrm{d}\Gamma^p_k + \int_{\Gamma^s_k}\left(\sigma^{(k)}_{ij}n^{(k)}_j\right)\Phi^{(k)}_i\,\mathrm{d}\Gamma^s_k \\
&+\int_{\Gamma^{\mathrm{I}}}\left(\sigma^{(k)}_{ij}n^{(k)}_j\right)\Phi^{(k)}_i\,\mathrm{d}\Gamma^{\mathrm{I}}
\end{aligned}
$$

Noting that, $\Phi^k_i = 0$ on Γ^p_k. Therefore, the boundary integral on Γ^p_k is identically zero, and Eq. (3.25) can be rewritten, for subdomain 1, as

$$-\int_{\Omega_1}\Phi^{(1)}_{i,j}\sigma^{(1)}_{ij}\,d\Omega_1+\int_{\Gamma_1^s}\left(\sigma^{(1)}_{ij}n^{(1)}_j\right)\Phi^{(1)}_i\,d\Gamma_1^s+\int_{\Gamma^I}\left(\sigma^{(1)}_{ij}n^{(1)}_j\right)\Phi^{(1)}_i\,d\Gamma^I$$
$$+\int_{\Gamma_1^s}\overline{\Phi}^{(1)}_i\left(t^{(1)}_i-\bar{t}^{(1)}_i\right)d\Gamma_1^s+\int_{\Omega_1}\rho_1(b^{(1)}_i-\dot{v}^{(1)}_i)\,\Phi^{(1)}_i\,d\Omega_1=0$$

Since the weight functions, $\Phi^{(1)}_i$ and $\overline{\Phi}^{(1)}_i$, are arbitrary, they may chosen such that $\overline{\Phi}^{(1)}_i=-\Phi^{(1)}_i$, and using the Cauchy formula, $t^{(1)}_i=\sigma^{(1)}_{ij}n^{(1)}_j$,

$$-\int_{\Omega_1}\Phi^{(1)}_{i,j}\sigma^{(1)}_{ij}\,d\Omega_1+\int_{\Gamma^I}\left(\sigma^{(1)}_{ij}n^{(1)}_j\right)\Phi^{(1)}_i\,d\Gamma^I+\int_{\Gamma_1^s}\bar{t}^{(1)}_i\Phi^{(1)}_i\,d\Gamma_1^s$$
$$+\int_{\Omega_1}\rho_1(b^{(1)}_i-\dot{v}^{(1)}_i)\,\Phi^{(1)}_i\,d\Omega_1=0 \qquad (3.27)$$

Similarly, for subdomain, Ω_2,

$$-\int_{\Omega_2}\Phi^{(2)}_{i,j}\sigma^{(2)}_{ij}\,d\Omega_2+\int_{\Gamma^I}\left(\sigma^{(2)}_{ij}n^{(2)}_j\right)\Phi^{(2)}_i\,d\Gamma^I+\int_{\Gamma_2^s}t^{(2)}_i\Phi^{(2)}_i\,d\Gamma_2^s$$
$$+\int_{\Omega_2}\rho_2(b^{(2)}_i-\dot{v}^{(2)}_i)\,\Phi^{(2)}_i\,d\Omega_2=0 \qquad (3.28)$$

In the two-approximation formulation for the scalar-field problem, the two primary field variables, $\mathbf{u}_1$ and $\mathbf{u}_2$ are approximated independently, and continuity requirements between these two fields are satisfied at the subdomain interface boundary. The three-approximation approach, which makes use of a third approximation field for the primary variables along the subdomain interface boundary in addition to the approximations given along the boundary of the subdomains, is most general. Hence, only the three-approximation approach will be discussed for the vector-field problem. This primary variable, **v**, along the interface is assumed to be independent of the primary

variables, $\mathbf{u}_1$ and $\mathbf{u}_2$, of the subdomains to which it is attached. These independent approximations give rise to continuity requirements along the interface of the form

$$\mathbf{v}-\mathbf{u}_1=\mathbf{0} \text{ or } v_i-u_i^{(1)}=0 \quad \text{on} \quad \Gamma^{\mathrm{I}}$$

$$\mathbf{v}-\mathbf{u}_2=\mathbf{0} \text{ or } v_i-u_i^{(2)}=0 \quad \text{on} \quad \Gamma^{\mathrm{I}}$$

These constraints can be satisfied in the integral sense as

$$\int_{\Gamma_{\mathrm{I}}}\boldsymbol{\lambda}_1(\mathbf{v}-\mathbf{u}_1)\,\mathrm{d}\Gamma^{\mathrm{I}}=0 \text{ or } \int_{\Gamma_{\mathrm{I}}}\lambda_i^{(1)}\left(v_i-u_i^{(1)}\right)\mathrm{d}\Gamma^{\mathrm{I}}=0 \quad \text{on} \quad \Gamma^{\mathrm{I}} \tag{3.29}$$

$$\int_{\Gamma_{\mathrm{I}}}\boldsymbol{\lambda}_2(\mathbf{v}-\mathbf{u}_2)\,\mathrm{d}\Gamma^{\mathrm{I}}=0 \text{ or } \int_{\Gamma_{\mathrm{I}}}\lambda_i^{(2)}\left(v_i-u_i^{(2)}\right)\mathrm{d}\Gamma^{\mathrm{I}}=0 \quad \text{on} \quad \Gamma^{\mathrm{I}} \tag{3.30}$$

where $\lambda_i^{(1)}$ and $\lambda_i^{(2)}$ are Lagrange multipliers or weight functions in the form of the secondary variable along the interface. An additional continuity requirement in terms of the secondary variable along the common subdomain boundary is required. These secondary variables, $\hat{t}_i^{(1)}$ and $\hat{t}_i^{(2)}$, are assumed to be independent of each other. These independent approximations give rise to continuity requirements along the interface of the form

$$\hat{t}_i^{(1)}+\hat{t}_i^{(2)}=0 \quad \text{on} \quad \Gamma^{\mathrm{I}}$$

These constraints can be satisfied in the integral sense as

$$\int_{\Gamma^{\mathrm{I}}}\hat{\lambda}_i\left(\hat{t}_i^{(1)}+\hat{t}_i^{(2)}\right)\mathrm{d}\Gamma^{\mathrm{I}}=0 \quad \text{on} \quad \Gamma^{\mathrm{I}} \tag{3.31}$$

where $\hat{\lambda}_i$ is a Lagrange multiplier or weight function of the form of the primary variable along the interface. Combining Eqs. (3.27) and (3.28) for the entire domain, including

the three continuity integrals at the interdomain boundary, Eqs. (3.29), (3.30), and (3.31), and recognizing that $\hat{t}_i^{(1)} = \left(\sigma_{ij}^{(1)} n_j^{(1)}\right)$ and $\hat{t}_i^{(2)} = \left(\sigma_{ij}^{(2)} n_j^{(2)}\right)$ yields

$$
\begin{aligned}
&- \int_{\Omega_1} \left(\Phi_{i,j}^{(1)} \sigma_{ij}^{(1)}\right) \mathrm{d}\Omega_1 - \int_{\Omega_2} \left(\Phi_{i,j}^{(2)} \sigma_{ij}^{(2)}\right) \mathrm{d}\Omega_2 - \int_{\Gamma^{\mathrm{I}}} \hat{t}_i^{(1)} \Phi_i^{(1)} \, \mathrm{d}\Gamma^{\mathrm{I}} - \int_{\Gamma^{\mathrm{I}}} \hat{t}_i^{(2)} \Phi_i^{(2)} \, \mathrm{d}\Gamma^{\mathrm{I}} \\
&\quad + \int_{\Gamma^{\mathrm{I}}} \lambda_i^{(1)} \left(v_i - u_i^{(1)}\right) \mathrm{d}\Gamma^{\mathrm{I}} + \int_{\Gamma^{\mathrm{I}}} \lambda_i^{(2)} \left(v_i - u_i^{(2)}\right) \mathrm{d}\Gamma^{\mathrm{I}} + \int_{\Gamma^{\mathrm{I}}} \hat{\lambda}_i \left(\hat{t}_i^{(1)} + \hat{t}_i^{(2)}\right) \mathrm{d}\Gamma^{\mathrm{I}} \\
&\qquad = \int_{\Omega_1} \rho_1 (b_i^{(1)} - \dot{v}_i^{(1)}) \Phi_i^{(1)} \, \mathrm{d}\Omega_1 + \oint_{\Gamma_1^s} \bar{t}_i^{(1)} \Phi_i^{(1)} \, \mathrm{d}\Gamma_1^s + \\
&\qquad \int_{\Omega_2} \rho_2 (b_i^{(2)} - \dot{v}_i^{(2)}) \Phi_i^{(2)} \, \mathrm{d}\Omega_2 + \oint_{\Gamma_2^s} \bar{t}_i^{(2)} \Phi_i^{(2)} \, \mathrm{d}\Gamma_2^s
\end{aligned}
\tag{3.32}
$$

In addition, for fluid mechanics, the continuity equation is given and satisfied independently over each domain as

$$u_{i,j}^{(1)} = 0 \text{ in } \Omega_1 \quad \text{and} \quad u_{i,j}^{(2)} = 0 \text{ in } \Omega_2$$

The weighted residual statements over the domains are given by

$$\int_{\Omega_1} u_{i,j}^{(1)} \hat{\Phi}_i^{(1)} \, \mathrm{d}\Omega_1 = 0 \quad \text{and} \quad \int_{\Omega_2} u_{i,j}^{(2)} \hat{\Phi}_i^{(2)} \, \mathrm{d}\Omega_2 = 0 \ . \tag{3.33}$$

Here, note that no integration by parts is used on the continuity equations, and no relaxation of the differentiability on **u** can be accomplished since the resulting boundary conditions would not be physical. Combining Eqs. (3.33) yields

$$\int_{\Omega_1} u_{i,j}^{(1)} \hat{\Phi}_i^{(1)} \, \mathrm{d}\Omega_1 + \int_{\Omega_2} u_{i,j}^{(2)} \hat{\Phi}_i^{(2)} \, \mathrm{d}\Omega_2 = 0 \ . \tag{3.34}$$

The integral form of Eq. (3.32) forms the basis of finite element approximations for solid mechanics, and both Eqs. (3.32) and (3.34) form the basis for fluid mechanics. These finite element approximations as well as other approximations will be discussed in more detail in the next section.

3.6. SPATIAL MODELING FOR MULTIPLE DOMAINS

Spatial modeling for multiple domains using the finite element and finite difference methods for the approximation of the vector-field problem is outlined in this section. A brief overview of discretization methods is given followed by spatial modeling for solid and fluid mechanics domains.

3.6.1. Overview of Discretization Methods

Finite element and finite difference discretization methods for the vector-field problem are outlined in this subsection. For a more detailed discussion the reader should consult the literature.

The finite element method

The finite element method for the vector-field problem is developed in the same manner as for the scalar-field problem. In the vector-field problem, the dependent variable in the integral equations is a vector of components. In general, the inplane vector components (*e.g.*, displacements parallel to the *x* and *y* axes) are approximated by the same shape functions. For isoparametric elements, this approximation is the same as that taken for the shape. For the elasticity problem, the consideration for the strain-displacement relation, the Jacobian transformation, and the displacement gradient interpolation results in a more complex (the product of three matrices) set of equations than for the scalar field.

The finite difference method

The finite difference method is ideal for solving the governing partial differential equations of a continuum. It represents a variety of equations in engineering science;

however, the method has not been used in solid mechanics to the same degree as the finite element method[42]. The decline in the use of the finite difference method in solid mechanics is largely due to the limited flexibility of its treatment of boundary conditions. Most finite difference developments avoid the general problem of boundary conditions in one of the following ways: (1) a scalar problem, such as those of the previous chapter, is solved as an example and the boundary conditions are incorporated in the analysis using arguments based on symmetry of the independent variables in the derivative approximations or (2) an example is chosen with fixed boundaries to eliminate the presence of fictitious points. The lack of an intuitive procedure for elimination of the fictitious or external grid points introduced when a central difference operator is applied to a boundary point is one cause of the deficiency in the method. For the vector-field problem discussed herein, a 3×3 central difference template is used to evaluate the momentum equation, Eq. (3.20). An approach for eliminating the fictitious points based on physical arguments is presented in reference 43. The fictitious nodes are replaced by boundary tractions using a set of constitutive equations and the primary variables in the continuum. These points can then be eliminated, and the boundary tractions are introduced into the finite difference model. An alternative approach is to construct special forms of the difference equations for grid points at or near the boundaries[44]. These forms make use of forward or backward difference operators to express differential forms. In general, standard forward or backward difference operators have higher-order truncation error than the central difference operators used for the differential equation. Hence, special forms using additional interior grid points are constructed such that the operators have the same order of truncation error as those operators used for the

differential equation. The latter approach is used in this work and will be discussed in some detail in the discussions of the patch test application given in this chapter.

3.6.2. Overview of Single-Domain Spatial Modeling

For a single domain, the finite element equations may be obtained by rewriting and manipulating slightly Eq. (3.16) over an element domain as

$$\int_{\Omega^e} \Phi_{i,j}\, \sigma_{ij}\, \mathrm{d}\Omega^e - \int_{\Omega^e} \Phi_i \rho(b_i - \dot{v}_i)\, \mathrm{d}\Omega^e - \int_{\Gamma^{s^e}} \Phi_i \bar{t}_i\, \mathrm{d}\Gamma^{s^e} = 0 \tag{3.35}$$

where σ_{ij} are the approximate stress fields produced by the stress-strain and strain-displacement (or rate of deformation) relations and approximating the primary variable over the element domain by $\mathbf{u} = \mathbf{N}\mathbf{u}_e$.

General finite element development

Using the Galerkin method, the weight function is given by $\mathbf{\Phi} = \mathbf{N}$. Substituting these approximations into the integral equation given in Eq. (3.35) and writing in matrix form yields

$$\int_{\Omega^e} \partial\mathbf{N}^{\mathrm{T}}\boldsymbol{\sigma}\, \mathrm{d}\Omega^e - \int_{\Omega^e} \mathbf{N}^{\mathrm{T}} \rho(\mathbf{b} - \dot{\mathbf{v}})\, \mathrm{d}\Omega^e - \int_{\Gamma^{s^e}} \mathbf{N}^{\mathrm{T}}\bar{\mathbf{t}}\, \mathrm{d}\Gamma^{s^e} = 0 \tag{3.36}$$

where ∂ is the operator matrix defined, in general, by

$$\partial = \begin{bmatrix} \frac{\partial}{\partial x} & 0 & 0 \\ 0 & \frac{\partial}{\partial y} & 0 \\ 0 & 0 & \frac{\partial}{\partial z} \\ \frac{\partial}{\partial y} & \frac{\partial}{\partial x} & 0 \\ 0 & \frac{\partial}{\partial z} & \frac{\partial}{\partial y} \\ \frac{\partial}{\partial z} & 0 & \frac{\partial}{\partial x} \end{bmatrix},$$

and the stress vector $\boldsymbol{\sigma}$ is given by

$$\boldsymbol{\sigma} = [\sigma_{11} \quad \sigma_{22} \quad \sigma_{33} \quad \sigma_{12} \quad \sigma_{23} \quad \sigma_{13}]^{\mathrm{T}}$$

General finite difference development

Recall that in the finite difference methods, derivatives are approximated by difference expressions that transform the derivatives and consequently the partial differential equation to algebraic expressions and equations, respectively. Upon substitution of the approximation function into the differential equation, the equations can be recast in weighted residual form by selecting $\boldsymbol{\Phi}_i = \delta(x - x_i, y - y_i)$. Note that the subscript *i* on the weight function is used to denote the subdomain, while the subscript *i* on the coordinate values, *x* and *y*, is used to represent the point in the physical domain at which the Dirac delta function is evaluated. This nomenclature is used throughout the mathematical formulation presented here. The weighted form of the residual reduces to the evaluation of the partial differential equations using the approximate solution evaluated at the *N* selected mesh points

For a single domain, as in the finite element method, the finite difference equations may be obtained by interrogating the weighted residual equations over an

element domain where the element, *e*, surrounds grid point *i* (see Figure 2.5). The approximate solution for the primary variable is given by

$$\tilde{u} = \sum_{m=1}^{M} N_m u_m \quad \text{or} \quad \mathbf{u} = \mathbf{N}\mathbf{u}_e$$

where *M* is the number of shape functions over the element. The weight function, Φ, is given by the Dirac delta function, $\delta(x - x_i, y - y_i) = \delta(x_i, y_i)$. Therefore, Eq. (3.35) becomes

$$\int_{\Omega^e} \delta(x_i, y_i)_{,j}\, \sigma_{ij}\, \mathrm{d}\Omega^e - \int_{\Omega^e} \delta(x_i, y_i)\rho(b_i - \dot{v}_i)\, \mathrm{d}\Omega^e - \int_{\Gamma^{s^e}} \delta(x_i, y_i)\bar{t}_i\, \mathrm{d}\Gamma^{s^e} = 0$$

and upon making use of properties of the Dirac delta function,

$$\sigma_{ij,j}\Big|_{\substack{x=xi \\ y=y_i}} - \rho[b_i(x_i, y_i) - \dot{v}_i(x_i, y_i)] - \bar{t}_i(x_i, y_i) = 0\,. \tag{3.37}$$

This equation and the equations related to the finite difference formulation that follow are evaluated at point (x_i,y_i) where *i* denotes a point in the physical domain, and no summation is implied over the x_i terms. Eqs. (3.36) and (3.37) are applicable to a general continuum irrespective of its physical constitution. Discipline-specific constitutive relations are considered at this point to continue with the finite element and finite difference developments specific to solid and fluid mechanics. Each of these developments will be discussed in turn.

Solid mechanics - finite element discretization

For solid mechanics, the constitutive relation relating stress and strain is given by

$$\boldsymbol{\sigma} = \mathbf{E}(\boldsymbol{\varepsilon} - \boldsymbol{\varepsilon}_0) + \boldsymbol{\sigma}_0$$

where the strain vector

$$\boldsymbol{\varepsilon} = \begin{bmatrix} \varepsilon_{11} & \varepsilon_{22} & \varepsilon_{33} & 2\varepsilon_{12} & 2\varepsilon_{23} & 2\varepsilon_{13} \end{bmatrix}^{\mathrm{T}},$$

E is a matrix of material stiffnesses, and $\boldsymbol{\sigma}_0$ and $\boldsymbol{\varepsilon}_0$ are initial stress and strain quantities, respectively. The strain-displacement relation is given by

$$\boldsymbol{\varepsilon} = \partial \mathbf{u} = \partial \mathbf{N} \mathbf{u}_{\mathbf{e}} = \mathbf{B} \mathbf{u}_{\mathbf{e}}.$$

Implicit in the definition of **B** is the use of the Jacobian matrix to transform from Cartesian coordinates to element natural coordinates used in the shape function development. In addition, in solid mechanics, the acceleration of the continuum is given by $\dot{\mathbf{v}} = \ddot{\mathbf{u}} = \dfrac{\partial^2 \mathbf{u}}{\partial t^2}$. Moreover, the second time derivative of the primary variable over the element domain is approximated by $\ddot{\mathbf{u}} = \mathbf{N} \ddot{\mathbf{u}}_e$. Substituting the stress-strain, strain-displacement relations and the acceleration into Eq. (3.36) yields

$$\begin{aligned} \left(\int_{\Omega^e} \mathbf{B}^{\mathrm{T}} \mathbf{E} \mathbf{B} \, \mathrm{d}\Omega^e \right) \mathbf{u}_e + \left(\int_{\Omega^e} \rho \mathbf{N}^{\mathrm{T}} \mathbf{N} \, \mathrm{d}\Omega^e \right) \ddot{\mathbf{u}}_e = & \int_{\Omega^e} \mathbf{B}^{\mathrm{T}} \mathbf{E} \boldsymbol{\varepsilon}_0 \, \mathrm{d}\Omega^e - \int_{\Omega^e} \mathbf{B}^{\mathrm{T}} \boldsymbol{\sigma}_0 \, \mathrm{d}\Omega^e \\ & + \int_{\Omega^e} \mathbf{N}^{\mathrm{T}} \rho \mathbf{b} \, \mathrm{d}\Omega^e + \int_{\Gamma^{s^e}} \mathbf{N}^{\mathrm{T}} \bar{\mathbf{t}} \, \mathrm{d}\Gamma^{s^e} \end{aligned} \tag{3.38}$$

or

$$\mathbf{k}_e \mathbf{u}_e + \mathbf{m}_e \ddot{\mathbf{u}}_e = \mathbf{f}_e$$

where $\mathbf{k}_e$ is the element stiffness matrix, $\mathbf{m}_e$ is the element mass matrix, $\mathbf{u}_e$ is the vector containing the generalized primary variables, $\ddot{\mathbf{u}}_e$ is the vector containing the second time derivative of the generalized primary variables, and $\mathbf{f}_e$ is the element force vector containing the generalized secondary variables. Note that the acceleration term can be considered as an inertial force and included as part of the element force vector.

Assembling these element equations over the entire domain and enforcing continuity of the primary variable at the interelement boundaries yields the system of equations given by

$$\mathbf{M}\ddot{\mathbf{u}} + \mathbf{K}\mathbf{u} = \mathbf{F}$$

where $\mathbf{K} = \sum_{1}^{nelem} \int_{\Omega^e} \mathbf{B}^{\mathrm{T}}\mathbf{E}\mathbf{B}\mathrm{d}\Omega^e$; $\mathbf{M} = \sum_{1}^{nelem} \int_{\Omega^e} \rho\mathbf{N}^{\mathrm{T}}\mathbf{N}\mathrm{d}\Omega^e$; $\mathbf{u}$ is the assembly of all of the nodal degrees of freedom associated with the primary variables; $\ddot{\mathbf{u}}$ is the assembly of all of the nodal degrees of freedom associated with time derivative of the primary variables, and $\mathbf{F} = \sum_{1}^{nnodes} \int_{\Omega^e} \mathbf{B}^{\mathrm{T}}\mathbf{E}\boldsymbol{\varepsilon}_0 \, \mathrm{d}\Omega^e - \int_{\Omega^e} \mathbf{B}^{\mathrm{T}}\boldsymbol{\sigma}_0 \, \mathrm{d}\Omega^e + \int_{\Omega^e} \mathbf{N}^{\mathrm{T}}\rho(\mathbf{b} - \ddot{\mathbf{u}}) \, \mathrm{d}\Omega^e + \int_{\Gamma^{s^e}} \mathbf{N}^{\mathrm{T}}\bar{\mathbf{t}} \, \mathrm{d}\Gamma^{s^e}$

Solid mechanics - finite difference discretization

For solid mechanics, making use of the stress-strain and strain-displacement relations, and substitution of the primary variable approximations into Eq. (3.37), the element equation becomes

$$\left[\partial^{\mathrm{T}}\mathbf{E}\mathbf{B}\Big|_{\substack{x=x_i \\ y=y_i}}\right]\mathbf{u}_e + \left[\rho\mathbf{N}\Big|_{\substack{x=x_i \\ y=y_i}}\right]\ddot{\mathbf{u}}_e = \partial^{\mathrm{T}}\mathbf{E}\boldsymbol{\varepsilon}_0\Big|_{\substack{x=x_i \\ y=y_i}} - \partial^{\mathrm{T}}\boldsymbol{\sigma}_0\Big|_{\substack{x=x_i \\ y=y_i}} + \rho\mathbf{b}(x_i, y_i) + \bar{\mathbf{t}}(x_i, y_i)$$

For the second derivative difference approximation, the number of shape functions, *M*=3 and $\mathbf{u}_e^T = \{u_{i-1} \quad u_i \quad u_{i+1}\}$.

Therefore, as in the finite element method the difference equations may be written in the form

$$\mathbf{m}_e\ddot{\mathbf{u}}_e + \mathbf{k}_e\mathbf{u}_e = \mathbf{f}_e$$

where $\mathbf{k}_e$ and $\mathbf{m}_e$ are the finite difference "element mass and stiffness" matrices, $\mathbf{u}_e$ is the vector of generalized primary variables, $\ddot{\mathbf{u}}_e$ is the vector of time derivatives of the

generalized primary variables, and $\mathbf{f}_e$ is the finite difference generalized force vector. Assembling the element equations yields

$$\mathbf{M}\ddot{\mathbf{u}} + \mathbf{K}\mathbf{u} = \mathbf{F}$$

where

$\mathbf{K} = \sum_{1}^{Nelem}\left[\partial^{\mathrm{T}}\mathbf{E}\mathbf{B}\Big|_{\substack{x=x_i \\ y=y_i}}\right]$, $\mathbf{M} = \sum_{1}^{Nelem}\left[\rho\mathbf{N}\Big|_{\substack{x=x_i \\ y=y_i}}\right]$, $\mathbf{u}$ and $\ddot{\mathbf{u}}_e$ contain all of the nodal degrees of freedom associated with the primary variables and its time derivative, and

$$\mathbf{F} = \sum_{1}^{Nnodes}\left[\partial^{\mathrm{T}}\mathbf{E}\boldsymbol{\varepsilon}_0\Big|_{\substack{x=x_i \\ y=y_i}} - \partial^{\mathrm{T}}\boldsymbol{\sigma}_0\Big|_{\substack{x=x_i \\ y=y_i}} + \rho\mathbf{b}(x_i, y_i) + \bar{\mathbf{t}}(x_i, y_i)\right].$$

Fluid mechanics- finite element discretization

For fluid mechanics, the constitutive relation relating stress and the rate of deformation, Eq. (3.7), for an incompressible fluid is given by

$$\boldsymbol{\sigma} = \boldsymbol{\tau} - P\mathbf{I}$$

where the viscous stress vector, $\boldsymbol{\tau}$, is given by

$$\boldsymbol{\tau} = [\tau_{11} \quad \tau_{22} \quad \tau_{33} \quad \tau_{12} \quad \tau_{23} \quad \tau_{13}]^{\mathrm{T}},$$

$\mathbf{u}$ denotes the velocity vector, P is the pressure, and $\mathbf{I}$ is the identity matrix. The viscous stress is given by $\boldsymbol{\tau} = 2\mu\mathbf{D}$ where μ is the shear viscosity of the fluid and $\mathbf{D}$ is the rate of deformation tensor whose components are given by

$$D_{ij} = \frac{1}{2}\left(u_{i,j} + u_{j,i}\right) \tag{3.39}$$

Hence, the rate of deformation is related to the deformation and may be expressed in the same form as the strain-displacement relation as

$$\boldsymbol{D} = \partial_{\mathrm{f}}\mathbf{u} = \partial_{\mathrm{f}}\mathbf{N}\mathbf{u}_{\mathbf{e}} = \mathbf{B}_{\mathrm{f}}\mathbf{u}_{\mathbf{e}}$$

where ∂_{f} is a differential operator defined by $\partial_{\mathrm{f}} = \mathbf{T}\partial$ and $\mathbf{B}_{\mathrm{f}} = \mathbf{T}\partial\mathbf{N}$. The transformation matrix, **T**, is used to introduce the scalar multiple of the shear components of the rate of deformation (see Eq. (3.39)) and is symbolically defined as

$$\mathbf{T} = \begin{bmatrix} 1 & 0 & 0 & 0 & 0 & 0 \\ 0 & 1 & 0 & 0 & 0 & 0 \\ 0 & 0 & 1 & 0 & 0 & 0 \\ 0 & 0 & 0 & \frac{1}{2} & 0 & 0 \\ 0 & 0 & 0 & 0 & \frac{1}{2} & 0 \\ 0 & 0 & 0 & 0 & 0 & \frac{1}{2} \end{bmatrix} = \begin{bmatrix} \mathbf{I} & \mathbf{0} \\ \mathbf{0} & \frac{1}{2}\mathbf{I} \end{bmatrix}$$

In addition, in fluid mechanics, the acceleration of the continuum is given by $\dot{\mathbf{v}} = \dfrac{\mathrm{d}\mathbf{v}}{\mathrm{dt}} = \dfrac{\partial \mathbf{v}}{\partial t} + \mathbf{v}\cdot\nabla\mathbf{v}$. Moreover, the time derivative of the primary variable over the element domain is approximated by $\dot{\mathbf{v}} = \dot{\mathbf{u}} = \mathbf{N}\dot{\mathbf{u}}_e$ and $\mathbf{P} = \hat{\mathbf{N}}\mathbf{P}_e$. Substituting the constitutive and rate of deformation relations along with the acceleration into Eq. (3.36) and rearranging yields

$$\begin{aligned} \left(\int_{\Omega^e} \rho\mathbf{N}^{\mathrm{T}}\mathbf{N}\,\mathrm{d}\Omega^e\right)\dot{\mathbf{u}}_e + \left(\int_{\Omega^e} \rho\mathbf{N}^{\mathrm{T}}(\mathbf{N}\mathbf{u}_e)\mathbf{N}\,\mathrm{d}\Omega^e\right)\mathbf{u}_e + \left(\int_{\Omega^e} 2\mu\mathbf{B}^{\mathrm{T}}\mathbf{B}_{\mathrm{f}}\,\mathrm{d}\Omega^e\right)\mathbf{u}_e \\ -\left(\int_{\Omega^e} \mathbf{B}^{\mathrm{T}}\hat{\mathbf{N}}\mathbf{I}\,\mathrm{d}\Omega^e\right)\mathbf{P}_e = \int_{\Omega^e} \mathbf{N}^{\mathrm{T}}\rho\mathbf{b}\,\mathrm{d}\Omega^e + \int_{\Gamma^{s^e}} \mathbf{N}^{\mathrm{T}}\bar{\mathbf{t}}\,\mathrm{d}\Gamma^{s^e} \end{aligned} \tag{3.40}$$

or

$$\mathbf{m}_e\dot{\mathbf{u}}_e + \mathbf{c}_e\mathbf{u}_e + \mathbf{k}_e\mathbf{u}_e - \mathbf{q}_e\mathbf{P}_e = \mathbf{f}_e$$

where the element matrices $\mathbf{k}_e$ and $\mathbf{m}_e$ and the element force vector, $\mathbf{f}_e$, are of similar form as those obtained in the solid mechanics development, $\mathbf{c}_e$, is a nonlinear element matrix

resulting from the total derivative of the velocity, $\mathbf{u}_e$ is the vector containing the generalized primary variables, $\mathbf{P}_e$ is the vector containing the element pressure variables, and $\dot{\mathbf{u}}_e$ is the vector containing the time derivative of the generalized primary variables. Hence, in the fluid mechanics development, the rate of change of the velocity - $\dot{\mathbf{u}}$ is analogous to the second derivative with respect to time of the displacement ($\ddot{\mathbf{u}}$ in the solid mechanics development). Moreover, the first integral term of Eq. (3.40) can be thought of as an inertial force. Assembling these element equations over the entire domain and enforcing continuity of the primary variable at the interelement boundaries yields the system of equations given by

$$\mathbf{M}\dot{\mathbf{u}} + \mathbf{C(u)u} + \mathbf{Ku} - \mathbf{QP} = \mathbf{F} \tag{3.41}$$

where $\mathbf{K} = \sum_{1}^{nelem} \int_{\Omega^e} 2\mu \mathbf{B}^{\mathrm{T}} \mathbf{B}_{\mathrm{f}} \, \mathrm{d}\Omega^e$; $\mathbf{M} = \sum_{1}^{nelem} \int_{\Omega^e} \rho \mathbf{N}^{\mathrm{T}} \mathbf{N} \mathrm{d}\Omega^e$;

$\mathbf{C} = \sum_{1}^{nelem} \int_{\Omega^e} \rho \mathbf{N}^{\mathrm{T}} (\mathbf{N}\mathbf{u}_e) \mathbf{N} \, \mathrm{d}\Omega^e$; $\mathbf{Q} = \sum_{1}^{nelem} \int_{\Omega^e} \mathbf{B}^{\mathrm{T}} \hat{\mathbf{N}} \mathbf{I} \, \mathrm{d}\Omega^e$; $\mathbf{u}$ is the assembled vector of all nodal degrees of freedom associated with the primary variables; $\mathbf{P}$ is the assembled vector of all nodal degrees of freedom associated with the pressure, $\dot{\mathbf{u}}$ is the assembled vector of all nodal degrees of freedom associated with the time derivative of the primary variables and $\mathbf{F} = \sum_{1}^{nnodes} \int_{\Omega^e} \mathbf{N}^{\mathrm{T}} \rho \mathbf{b} \, \mathrm{d}\Omega^e + \int_{\Gamma^{s^e}} \mathbf{N}^{\mathrm{T}} \bar{\mathbf{t}} \, \mathrm{d}\Gamma^{s^e}$.

In addition to the element equations for momentum, Eq. (3.40), the element equations for continuity must also be developed from Eq. (3.19). Using the Galerkin method, the weight function corresponding to the continuity equation is given by $\hat{\Phi} = \hat{\mathbf{N}}$.

Substituting the approximation for the weight function and the primary variable into Eq. (3.19) and writing the equation over the element yields

$$\left(\int_{\Omega^e} \mathbf{B}^{\mathrm{T}} \hat{\mathbf{N}} \, \mathrm{d}\Omega^e \right) \mathbf{u}_e = 0$$

or

$$\mathbf{q}_e^{\mathrm{T}} \mathbf{u}_e = 0$$

Assembling these element equations yields

$$-\mathbf{Q}^{\mathrm{T}} \mathbf{u} = 0 \tag{3.42}$$

Equations (3.41) and (3.42) can be combined into one system of equations and written in matrix form as

$$\begin{bmatrix} \mathbf{M} & \mathbf{0} \\ \mathbf{0} & \mathbf{0} \end{bmatrix} \begin{Bmatrix} \dot{\mathbf{u}} \\ \mathbf{P} \end{Bmatrix} + \begin{bmatrix} \mathbf{C(u)} + \mathbf{K} & -\mathbf{Q} \\ -\mathbf{Q}^{\mathrm{T}} & \mathbf{0} \end{bmatrix} \begin{Bmatrix} \mathbf{u} \\ \mathbf{P} \end{Bmatrix} = \begin{Bmatrix} \mathbf{F} \\ \mathbf{0} \end{Bmatrix} \tag{3.43}$$

or in a more symbolic form as

$$\overline{\mathbf{M}} \dot{\mathbf{U}} + \overline{\mathbf{K}} \mathbf{U} = \overline{\mathbf{F}}$$

where $\mathbf{U} = \{ \mathbf{u}_1 \quad \mathbf{u}_2 \quad \mathbf{u}_3 \quad \mathbf{P} \}^{\mathrm{T}}$. Hence, the equations for fluid mechanics may be expressed in the same form as the equations for solid mechanics. Note that the system of equations, Eq. (3.43), is referred to as the primitive-variable model, the pressure-velocity model, or the mixed model[32]. This mixed model results in a system that is nonpositive definite because of the zeros appearing on the main diagonal. In addition, the interpolation used for the pressure should be one order less than those that appear for the velocity field[41]. Furthermore, the pressure approximation may be discontinuous across interelement boundaries. In addition, because different orders of approximation are typically used for the velocity and pressure fields, the pressure may not appear at every

node of an element, which can complicate the assembly process. An alternative formulation, called the penalty function formulation[32,41], circumvents this situation by treating the continuity equation as a constraint among the velocity components. This formulation is developed here for finite element discretization.

From the weak form in Eq. (3.16), a functional describing the continuum motion can be obtained. The linear and bilinear forms of the functional over an element when the two-dimensional velocity field, (v_1, v_2), satisfies the continuity constraint, Eq. (3.19), is given by

$$L(\Phi_1,\Phi_2) = \int_{\Omega^e} \rho(b_1 - \dot{v}_1)\Phi_1 \, d\Omega^e + \int_{\Omega^e} \rho(b_2 - \dot{v}_2)\Phi_2 \, d\Omega^e + \int_{\Gamma^{s^e}} t_1 \, \Phi_1 d\Gamma^{s^e} + \int_{\Gamma^{s^e}} t_2 \, \Phi_2 d\Gamma^{s^e}$$

$$B((\Phi_1,\Phi_2),(v_1,v_2)) = \mu \int_{\Omega^e} 2\left(\frac{\partial\Phi_1}{\partial x_1}\frac{\partial v_1}{\partial x_1} + \frac{\partial\Phi_2}{\partial x_2}\frac{\partial v_2}{\partial x_2}\right) d\Omega^e + \mu \int_{\Omega^e} \left(\frac{\partial\Phi_1}{\partial x_2} + \frac{\partial\Phi_2}{\partial x_1}\right)\left(\frac{\partial v_1}{\partial x_2} + \frac{\partial v_2}{\partial x_1}\right) d\Omega^e .$$

Note that the pressure does not appear explicitly in the bilinear form. The quadratic functional is given by

$$\begin{aligned} I(v_1,v_2) &= \frac{1}{2} B((v_1,v_2),(v_1,v_2)) - L(v_1,v_2) \\ &= \mu \int_{\Omega^e} \left[\left(\frac{\partial v_1}{\partial x_1}\right)^2 + \left(\frac{\partial v_1}{\partial x_2}\right)^2 + \frac{1}{2}\left(\frac{\partial v_1}{\partial x_2} + \frac{\partial v_2}{\partial x_1}\right)^2\right] d\Omega^e \\ &\quad - \int_{\Omega^e} \rho(b_1 - \dot{v}_1)v_1 \, d\Omega^e - \int_{\Omega^e} \rho(b_2 - \dot{v}_2)v_2 \, d\Omega^e - \int_{\Gamma^{s^e}} t_1 \, v_1 d\Gamma^{s^e} \\ &\quad - \int_{\Gamma^{s^e}} t_2 \, v_2 d\Gamma^{s^e} \end{aligned} \tag{3.44}$$

The equations governing the flow of viscous incompressible fluids, Eqs. (3.16), and (3.19), are equivalent to minimizing of Eq. (3.44) subject to the constraint

$$G(v_1, v_2) = \frac{\partial v_1}{\partial x_2} + \frac{\partial v_2}{\partial x_1} = 0 .$$

In the penalty function method, the constrained problem is reformulated as an unconstrained problem by minimizing the modified functional

$$I_m(v_1, v_2) = I(v_1, v_2) + \frac{1}{2}\gamma_e \int_{\Omega^e} \left[G(v_1, v_2)^2 \right] \mathrm{d}\Omega^e$$

where the penalty parameter, γ_e, can be chosen for each element. The necessary conditions for the minimum of I_m is $\delta I_m = 0$ or $\delta_{v_1} I_m = 0$ and $\delta_{v_2} I_m = 0$.

where δv_1 and δv_2 denote the first variation with respect to the velocity components, v_1 and v_2, respectively. Therefore,

$$\begin{aligned} \delta_{v_1} I_m &= \delta_{v_1} I + \gamma_e \int_{\Omega^e} G(v_1, v_2) \delta_{v_1} G(v_1, v_2) \mathrm{d}\Omega^e \\ &= \int_{\Omega^e} \left[2\mu \frac{\partial \delta v_1}{\partial x_1} \frac{\partial v_1}{\partial x_1} + \mu \frac{\partial \delta v_1}{\partial x_2} \left(\frac{\partial v_1}{\partial x_2} + \frac{\partial v_2}{\partial x_1} \right) \right] \mathrm{d}\Omega^e \\ &\quad - \int_{\Omega^e} \rho(b_1 - \dot{v}_1) \delta v_1 \, \mathrm{d}\Omega^e - \int_{\Gamma^{s^e}} t_1 \delta v_1 \mathrm{d}\Gamma^{s^e} \\ &\quad + \gamma_e \int_{\Omega^e} \frac{\partial \delta v_1}{\partial x_1} \left(\frac{\partial v_1}{\partial x_1} + \frac{\partial v_2}{\partial x_2} \right) \mathrm{d}\Omega = 0 \end{aligned} \tag{3.45}$$

and

$$
\begin{aligned}
\delta_{v_2} I_m &= \delta_{v_2} I + \gamma_e \int_{\Omega^e} G(v_1, v_2)\delta_{v_2} G(v_1, v_2)\mathrm{d}\Omega^e \\
&= \int_{\Omega^e} \left[2\mu \frac{\partial \delta v_2}{\partial x_2}\frac{\partial v_2}{\partial x_2} + \mu \frac{\partial \delta v_2}{\partial x_1}\left(\frac{\partial v_1}{\partial x_2} + \frac{\partial v_2}{\partial x_1} \right) \right] \mathrm{d}\Omega^e \\
&\quad - \int_{\Omega^e} \rho(b_2 - \dot{v}_2)\delta v_2 \, \mathrm{d}\Omega^e - \int_{\Gamma^{s^e}} t_2 \delta v_2 \mathrm{d}\Gamma^{s^e} \\
&\quad + \gamma_e \int_{\Omega^e} \frac{\partial \delta v_2}{\partial x_2}\left(\frac{\partial v_1}{\partial x_1} + \frac{\partial v_2}{\partial x_2} \right) \mathrm{d}\Omega = 0
\end{aligned}
\tag{3.46}
$$

These two statements, Eqs. (3.45) and (3.46), provide the weak forms for the penalty finite element model. While, the pressure does not appear in the weak forms explicitly, it is part of the boundary tractions, t_1 and t_2. The penalty finite element model is obtained using Eqs. (3.45) and (3.46), the approximations for the primary variable and the time rate of change of the primary variable, $\mathbf{v} = \mathbf{u} = \mathbf{N}\mathbf{u}_e$ and $\dot{\mathbf{v}} = \dot{\mathbf{u}} = \mathbf{N}\dot{\mathbf{u}}_e$, respectively, and by choosing $\delta v_1 = \delta v_2 = \mathbf{N}$. Assembling these element equations over the entire domain and enforcing continuity of the primary variable at the interelement boundaries yields the system of equations given by

$$
\mathbf{M}\dot{\mathbf{u}} + \mathbf{C(u)u} + \mathbf{Ku} + \mathbf{Su} = \mathbf{F} \tag{3.47}
$$

where $\mathbf{K} = \sum_{1}^{nelem} \int_{\Omega^e} 2\mu \mathbf{B}^{\mathrm{T}} \mathbf{B}_{\mathrm{f}} \, \mathrm{d}\Omega^e$; $\mathbf{M} = \sum_{1}^{nelem} \int_{\Omega^e} \rho \mathbf{N}^{\mathrm{T}} \mathbf{N} \mathrm{d}\Omega^e$;

$\mathbf{C} = \sum_{1}^{nelem} \int_{\Omega^e} \rho \mathbf{N}^{\mathrm{T}} (\mathbf{N}\mathbf{u}_e) \mathbf{N} \, \mathrm{d}\Omega^e$; $\mathbf{S} = \sum_{1}^{nelem} \gamma \int_{\Omega^e} \mathbf{N}_{,x_1}{}^{\mathrm{T}} \mathbf{N}_{,x_2} \, \mathrm{d}\Omega^e$; $\mathbf{u}$ is the assembled vector of all nodal degrees of freedom associated with the primary variables; $\dot{\mathbf{u}}$ is the assembled vector of all nodal degrees of freedom associated with the time derivative of

the primary variables, $\mathbf{F} = \sum_{1}^{nnodes} \int_{\Omega^e} \mathbf{N}^{\mathrm{T}} \rho \mathbf{b} \, \mathrm{d}\Omega^e + \int_{\Gamma^{s^e}} \mathbf{N}^{\mathrm{T}} \bar{\mathbf{t}} \, \mathrm{d}\Gamma^{s^e}$, and $\mathbf{N}_{,x_i}$ denotes differentiation with respect to the independent variable, x_i, i=1, 2.

Eq. (3.47) may be represented in a more symbolic form as

$$\mathbf{M}\dot{\mathbf{U}} + \overline{\overline{\mathbf{K}}}\mathbf{U} = \mathbf{F}$$

where $\overline{\overline{\mathbf{K}}} = \mathbf{C(u)u} + \mathbf{K} + \mathbf{S}$. Note that this penalty finite element method yields a system of equations in terms of the primary variables, **u**, and does not include the pressures, **P**. The pressures may be obtained from the computed velocity field by

$$-\mathbf{P}_\gamma^e = \gamma G\left(v_{1\gamma}, v_{2\gamma}\right) = \gamma\left(\frac{\partial v_{1\gamma}}{\partial x_1}, \frac{\partial v_{2\gamma}}{\partial x_1}\right)$$

where $\left(v_{1\gamma}, v_{2\gamma}\right)$ is the finite element solution of Eq. (3.47).

Fluid mechanics - finite difference discretization

For fluid mechanics, making use of the stress-rate of deformation constitutive relation, and substitution of the primary variable approximations along with the acceleration into Eq. (3.37), the element equation becomes

$$\left[\rho \mathbf{N}\Big|_{\substack{x=x_i \\ y=y_i}}\right]\dot{\mathbf{u}}_e + \left[\rho\left(\mathbf{N}\mathbf{u}_e\right)\mathbf{N}\Big|_{\substack{x=x_i \\ y=y_i}}\right]\mathbf{u}_e + \left[2\mu\partial^{\mathrm{T}}\mathbf{T}\partial\mathbf{N}\Big|_{\substack{x=x_i \\ y=y_i}}\right]\mathbf{u}_e - \left[\partial^{\mathrm{T}}\mathbf{I}\hat{\mathbf{N}}\Big|_{\substack{x=x_i \\ y=y_i}}\right]\mathbf{P}_e = \rho\mathbf{b}\left(x_i, y_i\right) + \bar{\mathbf{t}}\left(x_i, y_i\right)$$

Also, considering continuity,

$$\left[\partial^{\mathrm{T}}\mathbf{I}\hat{\mathbf{N}}\Big|_{\substack{x=x_i \\ y=y_i}}\right]\mathbf{u}_e = \mathbf{0}$$

The difference equations may be written in the form

$$\mathbf{m}_e\dot{\mathbf{u}}_e + \mathbf{c}_e\mathbf{u}_e + \mathbf{k}_e\mathbf{u}_e - \mathbf{q}_e\mathbf{P}_e = \mathbf{f}_e$$

and

$$\mathbf{q}_e\mathbf{u}_e = \mathbf{0}$$

where $\mathbf{k}_e$, $\mathbf{c}_e$, $\mathbf{q}_e$, and $\mathbf{m}_e$ are finite difference "element" matrices, $\mathbf{u}_e$ is the vector of generalized primary variables, $\dot{\mathbf{u}}_e$ is the vector of time derivatives of the generalized primary variables, and $\mathbf{f}_e$ is the finite difference generalized force vector. Assembling the element equations yields

$$\mathbf{M}\dot{\mathbf{u}} + \mathbf{C}(\mathbf{u})\mathbf{u} + \mathbf{K}\mathbf{u} - \mathbf{Q}\mathbf{P} = \mathbf{F} \tag{3.48}$$

$$-\mathbf{Q}^{\mathrm{T}}\mathbf{u} = \mathbf{0} \tag{3.49}$$

where

$$\mathbf{K} = \sum_{1}^{nelem}\left[2\mu\partial^{\mathrm{T}}\mathbf{T}\partial\mathbf{N}\Big|_{\substack{x=x_i\\y=y_i}}\right],\ \mathbf{M} = \sum_{1}^{nelem}\left[\rho\mathbf{N}\Big|_{\substack{x=x_i\\y=y_i}}\right],\ \mathbf{C} = \sum_{1}^{nelem}\left[\rho(\mathbf{N}\mathbf{u}_e)\mathbf{N}\Big|_{\substack{x=x_i\\y=y_i}}\right]$$

$\mathbf{Q} = \sum_{1}^{nelem}\left[\partial^{\mathrm{T}}\mathbf{I}\hat{\mathbf{N}}\Big|_{\substack{x=x_i\\y=y_i}}\right]$, $\mathbf{u}$ and $\dot{\mathbf{u}}_e$ are vectors that contain all nodal degrees of freedom associated with the primary variables and its time derivative, and

$\mathbf{F} = \sum_{1}^{nnodes}\left[\rho\mathbf{b}(x_i, y_i) + \bar{\mathbf{t}}(x_i, y_i)\right]$. As in the finite element method, Eq. (3.48) and (3.49) can be combined into one system of equations and written in matrix form as

$$\begin{bmatrix}\mathbf{M} & \mathbf{0}\\ \mathbf{0} & \mathbf{0}\end{bmatrix}\begin{Bmatrix}\dot{\mathbf{u}}\\ \mathbf{P}\end{Bmatrix} + \begin{bmatrix}\mathbf{C(u)} + \mathbf{K} & -\mathbf{Q}\\ -\mathbf{Q}^{\mathrm{T}} & \mathbf{0}\end{bmatrix}\begin{Bmatrix}\mathbf{u}\\ \mathbf{P}\end{Bmatrix} = \begin{Bmatrix}\mathbf{F}\\ \mathbf{0}\end{Bmatrix}$$

or in a more symbolic form as

$$\overline{\mathbf{M}}\dot{\mathbf{U}} + \overline{\mathbf{K}}\mathbf{U} = \overline{\mathbf{F}}$$

where $\mathbf{U} = \{\mathbf{u}_1 \quad \mathbf{u}_2 \quad \mathbf{u}_3 \quad \mathbf{P}\}^{\mathrm{T}}$.

As in the case for the scalar-field formulation, the shape functions for a nine-node quadrilateral finite element are used (see Table 2.1). The shape function at point i-1,j-1 is given by

$$N_{i-1,j-1} = \frac{1}{4}(1-\xi)(1-\eta) - \frac{1}{2}\left(1-\xi^2\right)(1-\eta) - \frac{1}{2}(1-\xi)\left(1-\eta^2\right) + \frac{1}{4}\left(1-\xi^2\right)\left(1-\eta^2\right).$$

Similarly,

$$N_{i+1,j-1} = \frac{1}{4}(1+\xi)(1-\eta) - \frac{1}{2}\left(1-\xi^2\right)(1-\eta) - \frac{1}{2}(1+\xi)\left(1-\eta^2\right) + \frac{1}{4}\left(1-\xi^2\right)\left(1-\eta^2\right),$$

$$N_{i+1,j+1} = \frac{1}{4}(1+\xi)(1+\eta) - \frac{1}{2}(1+\xi)\left(1-\eta^2\right) - \frac{1}{2}\left(1-\xi^2\right)(1+\eta) + \frac{1}{4}\left(1-\xi^2\right)\left(1-\eta^2\right),$$

and

$$N_{i-1,j+1} = \frac{1}{4}(1-\xi)(1+\eta) - \frac{1}{2}\left(1-\xi^2\right)(1+\eta) - \frac{1}{2}(1-\xi)\left(1-\eta^2\right) + \frac{1}{4}\left(1-\xi^2\right)\left(1-\eta^2\right),$$

Then, for a square element

$$\frac{\partial^2 N_{i-1,j-1}}{\partial x \partial y} = \frac{1}{\left(h^e\right)^2}\frac{\partial^2 N_{i-1,j-1}}{\partial \xi \partial \eta} = \frac{1}{\left(h^e\right)^2}\left[\left(\frac{1}{4} - \frac{1}{2}\xi - \frac{1}{2}\eta + \xi\eta\right)_{\xi=0,\eta=0}\right] = \frac{1}{4\left(h^e\right)^2}$$
$$= \frac{\partial^2 N_{i+1,j+1}}{\partial x^2}$$

$$\frac{\partial^2 N_{i+1,j-1}}{\partial x \partial y} = \frac{1}{\left(h^e\right)^2}\frac{\partial^2 N_{i+1,j-1}}{\partial \xi \partial \eta} = \frac{1}{\left(h^e\right)^2}\left[\left(-\frac{1}{4} - \frac{1}{2}\xi + \frac{1}{2}\eta + \xi\eta\right)_{\xi=0,\eta=0}\right] = -\frac{1}{4\left(h^e\right)^2}$$
$$= \frac{\partial^2 N_{i-1,j+1}}{\partial x^2} \tag{3.50}$$

The standard finite difference representation follows by direct substitution of Eqs. (3.50) for the cross-derivative terms of the momentum equation along with Eqs. (2.40) for the

second-order terms. As noted previously, a single spatial modeling approach (*i.e.*, the finite element method or the finite difference method) is used for the single-domain formulation. While for multiple domains, homogeneous approaches and heterogeneous approaches are available. That is, the same method in each domain (homogeneous approach) or different methods in different domains (heterogeneous approach) are possible combinations of spatial modeling.

3.6.3. Multiple-Domain Modeling - Homogeneous Discretization

These homogeneous approaches make use of a single discretization method among all subdomains in which the domain is subdivided. The focus of this work is on the finite element and the finite difference methods as the spatial discretization methods. For homogeneous domain discretization developed herein, Eq. (3.32) is used to provide the mathematical basis for the three-approximation formulation. The generalized element equations, for both the finite element and finite difference methods, may be obtained by rewriting Eq. (3.32) over an element domain as

$$
\begin{aligned}
&-\int_{\Omega_1^e}\left(\Phi_{i,j}^{(1)}\sigma_{ij}^{(1)}\right)\mathrm{d}\Omega_1^e-\int_{\Omega_2^e}\left(\Phi_{i,j}^{(2)}\sigma_{ij}^{(2)}\right)\mathrm{d}\Omega_2^e-\int_{\Gamma^{I^e}}\hat{t}_i^{(1)}\Phi_i^{(1)}\,\mathrm{d}\Gamma^{I^e}-\int_{\Gamma^{I^e}}\hat{t}_i^{(2)}\Phi_i^{(2)}\,\mathrm{d}\Gamma^{I^e}\\
&\quad+\int_{\Gamma^{I^e}}\lambda_i^{(1)}\left(v_i-u_i^{(1)}\right)\mathrm{d}\Gamma^{I^e}+\int_{\Gamma^{I^e}}\lambda_i^{(2)}\left(v_i-u_i^{(2)}\right)\mathrm{d}\Gamma^{I^e}+\int_{\Gamma^{I^e}}\hat{\lambda}_i\left(\hat{t}_i^{(1)}+\hat{t}_i^{(2)}\right)\mathrm{d}\Gamma^{I^e}\\
&\qquad=\int_{\Omega_1^e}\rho_1(b_i^{(1)}-\dot{v}_i^{(1)})\Phi_i^{(1)}\,\mathrm{d}\Omega_1^e+\oint_{\Gamma_1^{s^e}}\bar{t}_i^{(1)}\Phi_i^{(1)}\,\mathrm{d}\Gamma_1^{s^e}\\
&\qquad+\int_{\Omega_2^e}\rho_2(b_i^{(2)}-\dot{v}_i^{(2)})\Phi_i^{(2)}\,\mathrm{d}\Omega_2^e+\oint_{\Gamma_2^{s^e}}\bar{t}_i^{(2)}\Phi_i^{(2)}\,\mathrm{d}\Gamma_2^{s^e}
\end{aligned}
\tag{3.51}
$$

Note that in the potential energy formulation[25], the continuity of the secondary variables was satisfied through the subsidiary conditions obtained through the minimization of the

potential energy. In this weighted residual formulation, the continuity of the secondary variables is satisfied in a weighted residual sense and the Lagrange multipliers, $\lambda_i^{(k)}$ and $\hat{\lambda}_i$, are represented by weight functions in the form of the secondary and primary variables, respectively.

The form of the equations for the finite element and finite difference applications differs by the form of the element shape functions and the approximation selected for the weight functions, Φ. The formulation for solid mechanics and fluid mechanics differs by the constitutive relations. For the generalized element expansion of subdomain *i*, the independent approximations for the element generalized primary variables, (*i.e.*, displacements or velocities), interface secondary variables (*i.e.*, tractions or fluxes), the weight functions associated with the secondary and primary variables, and the interface variables, are, respectively

$$\mathbf{u}_k = \mathbf{N}_k \mathbf{u}_{e_k} \; ; \; \hat{\mathbf{t}}_k = \mathbf{R}_k \boldsymbol{\alpha}_k \quad ; \quad \boldsymbol{\lambda}_k = \mathbf{R}_k \; ; \; \hat{\boldsymbol{\lambda}} = \mathbf{T} \quad \text{and} \quad \mathbf{v} = \mathbf{T}\mathbf{u}_{\mathrm{I}} \tag{3.52}$$

Both the solid and fluid mechanics derivations may be developed from Eq. (3.51), given the approximations of Eq. (3.52), the appropriate constitutive relation, and the choice of weight function. Each derivation is presented in turn in the following work.

Solid Mechanics- finite element discretization

Substituting the approximations of Eq. (3.52) into Eq. (3.51) along with the constitutive equations and using the Galerkin method in which $\boldsymbol{\Phi} = \mathbf{N}$, yields

$$\left[\int_{\Omega_1^e}\mathbf{B}_1^{\mathrm{T}}\mathbf{E}_1\mathbf{B}_1\,\mathrm{d}\Omega_1^e\right]\mathbf{u}_{e_1}+\left[\int_{\Omega_2^e}\mathbf{B}_2^{\mathrm{T}}\mathbf{E}_2\mathbf{B}_2\,\mathrm{d}\Omega_2^e\right]\mathbf{u}_{e_2}+\left[\int_{\Omega_1^e}\rho\mathbf{N}_1^{\mathrm{T}}\mathbf{N}_1\,\mathrm{d}\Omega_1^e\right]\ddot{\mathbf{u}}_{e_1}+\left[\int_{\Omega_2^e}\rho\mathbf{N}_2^{\mathrm{T}}\mathbf{N}_2\,\mathrm{d}\Omega_2^e\right]\ddot{\mathbf{u}}_{e_2}$$
$$-\left[\int_{\Gamma^{\mathrm{I}^e}}\mathbf{N}_1^{\mathrm{T}}\mathbf{R}_1\,\mathrm{d}\Gamma^{\mathrm{I}^e}\right]\boldsymbol{\alpha}_1-\left[\int_{\Gamma^{\mathrm{I}^e}}\mathbf{N}_2^{\mathrm{T}}\mathbf{R}_2\,\mathrm{d}\Gamma^{\mathrm{I}^e}\right]\boldsymbol{\alpha}_2+\left[\int_{\Gamma^{\mathrm{I}^e}}\mathbf{T}^{\mathrm{T}}\mathbf{R}_1\,\mathrm{d}\Gamma^{\mathrm{I}^e}\right]\boldsymbol{\alpha}_1+\left[\int_{\Gamma^{\mathrm{I}^e}}\mathbf{T}^{\mathrm{T}}\mathbf{R}_2\,\mathrm{d}\Gamma^{\mathrm{I}^e}\right]\boldsymbol{\alpha}_2+$$
$$\left[\int_{\Gamma^{\mathrm{I}^e}}\mathbf{R}_1^{\mathrm{T}}\mathbf{T}\,\mathrm{d}\Gamma^{\mathrm{I}^e}\right]\mathbf{u}_{\mathrm{I}}-\left[\int_{\Gamma^{\mathrm{I}^e}}\mathbf{R}_1^{\mathrm{T}}\mathbf{N}_1\,\mathrm{d}\Gamma^{\mathrm{I}^e}\right]\mathbf{u}_{e_1}+\left[\int_{\Gamma^{\mathrm{I}^e}}\mathbf{R}_2^{\mathrm{T}}\mathbf{T}\,\mathrm{d}\Gamma^{\mathrm{I}^e}\right]\mathbf{u}_{\mathrm{I}}-\left[\int_{\Gamma^{\mathrm{I}^e}}\mathbf{R}_2^{\mathrm{T}}\mathbf{N}_2\,\mathrm{d}\Gamma^{\mathrm{I}^e}\right]\mathbf{u}_{e_2}$$
$$=\int_{\Omega_1^e}\mathbf{B}_1^{\mathrm{T}}\mathbf{E}_1\boldsymbol{\varepsilon}_0^{(1)}\,\mathrm{d}\Omega_1^e-\int_{\Omega_1^e}\mathbf{B}_1^{\mathrm{T}}\boldsymbol{\sigma}_0^{(1)}\,\mathrm{d}\Omega_1^e+\int_{\Omega_1^e}\mathbf{N}_1^{\mathrm{T}}\rho\mathbf{b}_1\mathrm{d}\Omega_1^e+\int_{\Gamma_1^{s^e}}\mathbf{N}_1^{\mathrm{T}}\bar{\mathbf{t}}_1\,\mathrm{d}\Gamma_1^{s^e}$$
$$+\int_{\Omega_2^e}\mathbf{B}_2^{\mathrm{T}}\mathbf{E}_2\boldsymbol{\varepsilon}_0^{(2)}\,\mathrm{d}\Omega_2^e-\int_{\Omega_2^e}\mathbf{B}_2^{\mathrm{T}}\boldsymbol{\sigma}_0^{(2)}\,\mathrm{d}\Omega_2^e+\int_{\Omega_2^e}\mathbf{N}_2^{\mathrm{T}}\rho\mathbf{b}_2\mathrm{d}\Omega_2^e+\int_{\Gamma_2^{s^e}}\mathbf{N}_2^{\mathrm{T}}\bar{\mathbf{t}}_2\,\mathrm{d}\Gamma_2^{s^e} \tag{3.53}$$

where $\mathbf{B}_k=\partial\mathbf{N}_k$ for k=1,2 and for the k^{th} subdomain, the element matrices are

$$\mathbf{k}_{\mathbf{e}_k}=\int_{\Omega_k^e}\mathbf{B}_k^{\mathrm{T}}\mathbf{E}_k\mathbf{B}_k\,\mathrm{d}\Omega_k^e\;;\;\mathbf{m}_{\mathbf{e}_k}=\int_{\Omega_k^e}\rho\mathbf{N}_k^{\mathrm{T}}\mathbf{N}_k\,\mathrm{d}\Omega_k^e$$

$$\mathbf{k}_{\mathbf{p}_k}=-\int_{\Gamma^{\mathrm{I}^e}}\mathbf{R}_k^{\mathrm{T}}\mathbf{N}_k\,\mathrm{d}\Gamma^{\mathrm{I}^e},$$

$$\mathbf{k}_{\mathbf{s}_k}=-\int_{\Gamma^{\mathrm{I}^e}}\mathbf{N}_k^{\mathrm{T}}\mathbf{R}_k\,\mathrm{d}\Gamma^{\mathrm{I}^e}, \tag{3.54}$$

$$\mathbf{k}_{\mathrm{I}_k}=\int_{\Gamma^{\mathrm{I}^e}}\mathbf{T}^{\mathrm{T}}\mathbf{R}_k\,\mathrm{d}\Gamma^{\mathrm{I}^e},$$

and

$$\mathbf{f}_{ek}=\int_{\Omega_k^e}\mathbf{B}_k^{\mathrm{T}}\mathbf{E}_k\boldsymbol{\varepsilon}_0^{(k)}\,\mathrm{d}\Omega_k^e-\int_{\Omega_k^e}\mathbf{B}_k^{\mathrm{T}}\boldsymbol{\sigma}_0^{(k)}\,\mathrm{d}\Omega_k^e+\int_{\Omega_k^e}\mathbf{N}_k^{\mathrm{T}}\rho\mathbf{b}_k\mathrm{d}\Omega_i^e+\int_{\Gamma_k^{s^e}}\mathbf{N}_k^{\mathrm{T}}\bar{\mathbf{t}}_k\,\mathrm{d}\Gamma_k^{s^e}.$$

Solid Mechanics- finite difference discretization

Substituting the approximations of Eq. (3.52) into Eq. (3.51) along with the constitutive equations and using the Dirac delta function as the weight function,

$$\mathbf{\Phi}_k = \delta(x - x_i, y - y_i) = \delta(x_i, y_i),$$

$$\begin{aligned}
&\left[\partial^{\mathrm{T}}\mathbf{E}_1\partial\mathbf{N}_1\Big|_{\substack{x=x_i\\y=y_i}}\right]\mathbf{u}_{e_1} + \left[\partial^{\mathrm{T}}\mathbf{E}_2\partial\mathbf{N}_2\Big|_{\substack{x=x_i\\y=y_i}}\right]\mathbf{u}_{e_2} + \left[\rho\mathbf{N}_1\Big|_{\substack{x=x_i\\y=y_{il}}}\right]\ddot{\mathbf{u}}_{e_1} + \left[\rho\mathbf{N}_2\Big|_{\substack{x=x_i\\y=y_i}}\right]\ddot{\mathbf{u}}_{e_2} \\
&\quad - \left[\mathbf{R}_1\Big|_{\substack{x=x_i\\y=y_i}}\right]\boldsymbol{\alpha}_1 - \left[\mathbf{R}_2\Big|_{\substack{x=x_i\\y=y_i}}\right]\boldsymbol{\alpha}_2 + \left[\int_{\Gamma^{\mathrm{I}^e}}\mathbf{T}^{\mathrm{T}}\mathbf{R}_1\,\mathrm{d}\Gamma^{\mathrm{I}^e}\right]\boldsymbol{\alpha}_1 + \left[\int_{\Gamma^{\mathrm{I}^e}}\mathbf{T}^{\mathrm{T}}\mathbf{R}_2\,\mathrm{d}\Gamma^{\mathrm{I}^e}\right]\boldsymbol{\alpha}_2 \\
&\qquad + \left[\int_{\Gamma^{\mathrm{I}^e}}\mathbf{R}_1^{\mathrm{T}}\mathbf{T}\,\mathrm{d}\Gamma^{\mathrm{I}^e}\right]\mathbf{u}_{\mathrm{I}} - \left[\int_{\Gamma^{\mathrm{I}^e}}\mathbf{R}_1^{\mathrm{T}}\mathbf{N}_1\,\mathrm{d}\Gamma^{\mathrm{I}^e}\right]\mathbf{u}_{e_1} \\
&\qquad + \left[\int_{\Gamma^{\mathrm{I}^e}}\mathbf{R}_2^{\mathrm{T}}\mathbf{T}\,\mathrm{d}\Gamma^{\mathrm{I}^e}\right]\mathbf{u}_{\mathrm{I}} - \left[\int_{\Gamma^{\mathrm{I}}}\mathbf{R}_2^{\mathrm{T}}\mathbf{N}_2\,\mathrm{d}\Gamma^{\mathrm{I}^e}\right]\mathbf{u}_{e_2} \\
&\quad = \partial^{\mathrm{T}}\mathbf{E}_1\boldsymbol{\varepsilon}_0^{(1)}\Big|_{\substack{x=x_i\\y=y_i}} - \partial^{\mathrm{T}}\boldsymbol{\sigma}_0^{(1)}\Big|_{\substack{x=x_i\\y=y_i}} + \rho\mathbf{b}_1\Big|_{\substack{x=x_i\\y=y_i}} + \bar{\mathbf{t}}_1\Big|_{\substack{x=x_i\\y=y_i}} \\
&\quad + \partial^{\mathrm{T}}\mathbf{E}_2\boldsymbol{\varepsilon}_0^{(2)}\Big|_{\substack{x=x_i\\y=y_i}} - \partial^{\mathrm{T}}\boldsymbol{\sigma}_0^{(2)}\Big|_{\substack{x=x_i\\y=y_i}} + \rho\mathbf{b}_2\Big|_{\substack{x=x_i\\y=y_i}} + \bar{\mathbf{t}}_2\Big|_{\substack{x=x_i\\y=y_i}}
\end{aligned} \tag{3.55}$$

where, for k=1,2 and for the k^{th} subdomain, the element matrices are

$$\mathbf{k}_{\mathbf{e}_k} = \int_{\Omega_k^e}\partial^{\mathrm{T}}\mathbf{E}_k\partial\mathbf{N}_i\Big|_{\substack{x=x_i\\y=y_i}}\mathrm{d}\Omega_k^e \;;\; \mathbf{m}_{\mathbf{e}_k} = \int_{\Omega_k^e}\rho\mathbf{N}_k\Big|_{\substack{x=x_i\\y=y_i}}\mathrm{d}\Omega_k^e$$

$$\mathbf{k}_{\mathbf{p}_k} = -\int_{\Gamma^{\mathrm{I}^e}}\mathbf{R}_k^{\mathrm{T}}\mathbf{N}_k\,\mathrm{d}\Gamma^{\mathrm{I}^e}\;,$$

$$\mathbf{k}_{\mathbf{s}_k} = -\mathbf{R}_k(x_i, y_i), \tag{3.56}$$

$$\mathbf{k}_{\mathrm{I}_k} = \int_{\Gamma^{\mathrm{I}^e}}\mathbf{T}^{\mathrm{T}}\mathbf{R}_k\,\mathrm{d}\Gamma^{\mathrm{I}^e},$$

and

$$\mathbf{f}_{e_k} = \partial^{\mathrm{T}}\mathbf{E}_k\boldsymbol{\varepsilon}_0^{(k)}\Big|_{\substack{x=x_i\\y=y_i}} - \partial^{\mathrm{T}}\boldsymbol{\sigma}_0^{(k)}\Big|_{\substack{x=x_i\\y=y_i}} + \rho\mathbf{b}_k\Big|_{\substack{x=x_i\\y=y_i}} + \rho\bar{\mathbf{t}}_k\Big|_{\substack{x=x_i\\y=y_i}} .$$

For both the finite element and the finite difference discretization strategies, assembling the element equations over the entire domain, enforcing continuity of the primary and secondary variables only within each subdomain and assembling the contributions along the element edges on the common subdomain boundary, and noting that $\mathbf{u}_{\mathbf{e}_1}$ and $\mathbf{u}_{\mathbf{e}_2}$, $\ddot{\mathbf{u}}_{\mathbf{e}_1}$ and $\ddot{\mathbf{u}}_{\mathbf{e}_2}$, $\mathbf{f}_{\mathbf{e}_1}$ and $\mathbf{f}_{\mathbf{e}_2}$, and $\boldsymbol{\alpha}_1$ and $\boldsymbol{\alpha}_2$ are completely uncoupled, yields the system of equations given by

$$\begin{bmatrix} \mathbf{M}_1 & \mathbf{0} & \mathbf{0} & \mathbf{0} & \mathbf{0} \\ \mathbf{0} & \mathbf{M}_2 & \mathbf{0} & \mathbf{0} & \mathbf{0} \\ \mathbf{0} & \mathbf{0} & \mathbf{0} & \mathbf{0} & \mathbf{0} \\ \mathbf{0} & \mathbf{0} & \mathbf{0} & \mathbf{0} & \mathbf{0} \\ \mathbf{0} & \mathbf{0} & \mathbf{0} & \mathbf{0} & \mathbf{0} \end{bmatrix} \begin{Bmatrix} \ddot{\mathbf{u}}_1 \\ \ddot{\mathbf{u}}_1 \\ \ddot{\mathbf{u}}_{\mathrm{I}} \\ \boldsymbol{\alpha}_1 \\ \boldsymbol{\alpha}_2 \end{Bmatrix} + \begin{bmatrix} \mathbf{K}_1 & \mathbf{0} & \mathbf{0} & \mathbf{K}_{\mathrm{s}_1} & \mathbf{0} \\ \mathbf{0} & \mathbf{K}_2 & \mathbf{0} & \mathbf{0} & \mathbf{K}_{\mathrm{s}_2} \\ \mathbf{0} & \mathbf{0} & \mathbf{0} & \mathbf{K}_{\mathrm{I}_1} & \mathbf{K}_{\mathrm{I}_2} \\ \mathbf{K}_{\mathrm{p}_1} & \mathbf{0} & \mathbf{K}_{\mathrm{I}_1}^{\mathrm{T}} & \mathbf{0} & \mathbf{0} \\ \mathbf{0} & \mathbf{K}_{\mathrm{p}_2} & \mathbf{K}_{\mathrm{I}_2}^{\mathrm{T}} & \mathbf{0} & \mathbf{0} \end{bmatrix} \begin{Bmatrix} \mathbf{u}_1 \\ \mathbf{u}_2 \\ \mathbf{u}_{\mathrm{I}} \\ \boldsymbol{\alpha}_1 \\ \boldsymbol{\alpha}_2 \end{Bmatrix} = \begin{Bmatrix} \mathbf{f}_1 \\ \mathbf{f}_2 \\ \mathbf{0} \\ \mathbf{0} \\ \mathbf{0} \end{Bmatrix} \quad (3.57)$$

or

$$\begin{bmatrix} \mathbf{M} & \mathbf{0} & \mathbf{0} \\ \mathbf{0} & \mathbf{0} & \mathbf{0} \\ \mathbf{0} & \mathbf{0} & \mathbf{0} \end{bmatrix} \begin{Bmatrix} \ddot{\mathbf{u}} \\ \ddot{\mathbf{u}}_{\mathrm{I}} \\ \boldsymbol{\alpha} \end{Bmatrix} + \begin{bmatrix} \mathbf{K} & \mathbf{0} & \mathbf{K}_{\mathrm{s}} \\ \mathbf{0} & \mathbf{0} & \mathbf{K}_{\mathrm{I}} \\ \mathbf{K}_{\mathrm{p}} & \mathbf{K}_{\mathrm{I}}^{\mathbf{T}} & \mathbf{0} \end{bmatrix} \begin{Bmatrix} \mathbf{u} \\ \mathbf{u}_{\mathrm{I}} \\ \boldsymbol{\alpha} \end{Bmatrix} = \begin{Bmatrix} \mathbf{f} \\ \mathbf{0} \\ \mathbf{0} \end{Bmatrix}$$

where **K**, **M**, **u**, and **f** are the assembled stiffness matrix, mass matrix displacement vector, and force vector for the entire structure, and $\mathbf{K}_{\mathrm{p}}$, $\mathbf{K}_{\mathrm{s}}$, $\mathbf{K}_{\mathrm{I}}$, $\mathbf{u}_{\mathrm{I}}$, and $\boldsymbol{\alpha}$ are the assembled $\mathbf{K}_{\mathrm{p}_k}$, $\mathbf{K}_{\mathrm{s}_k}$, $\mathbf{K}_{\mathrm{I}_k}$, $\mathbf{u}_{\mathrm{I}}$, and $\boldsymbol{\alpha}_k$ for all interfaces. The assembled stiffness and mass matrices, **K** and **M,** are block diagonal matrices containing the stiffness and mass matrices, $\mathbf{K}_k$ and $\mathbf{M}_k$, of each of the subdomains along its block diagonal. The interface "stiffness" matrix thus contains coupling terms that augment the stiffness matrices of the

subdomains along the interface. All of the interface "stiffness" terms appear in the stiffness matrix with none in the mass matrix. Similar results may be obtained when damping is included. As for the scalar-field problem, the three-approximation approach for vector-field problems yields systems of equations (see Eqs. (3.57)) of similar form and with the same attributes. Again, due to the generalization for the finite difference approximations, the system of equations is not necessarily symmetric due to the off-diagonal submatrices, $\mathbf{K}_{\mathrm{p}}$ and $\mathbf{K}_{\mathrm{s}}$, nor are they banded or positive definite. Therefore, standard Cholesky solvers may not be used, unless full pivoting is performed to obtain the solution. The upper diagonal submatrix blocks contain uncoupled stiffness matrices. The symmetry of the matrix is determined by the choice of the weight function, Φ. In general, due to the introduction of fictitious nodes for the imposition of boundary conditions and loads in the finite difference discretization, the stiffness matrices are not symmetric but are positive definite and sparse. The coupling is accomplished through the introduction of the coupling terms in the matrices $\mathbf{K}_{\mathrm{p}_k}$ and $\mathbf{K}_{\mathrm{s}_k}$ for both approaches. The number of additional degrees of freedom associated with the interface element is generally small in comparison with the total number of degrees of freedom in the subdomains. Thus, modeling flexibility is provided at a relatively small computational expense. The computational expense in this study may be reduced additionally as the efficiency of new solution algorithms for the system of equations in Eq. (3.57) is increased.

While it is convenient to represent the weighted residual form over the domain using a single equation, the system of equations, Eq. (3.57) is obtained from the individual weighted residual expressions over each of the subdomains and the constraint

integrals. The first two matrix equations of the system of equations, Eq. (3.57) are derived from the weighted residual statement for subdomain *k*. That is,

$$\int_{\Omega^e} \Phi_{i,j}^{(k)} \sigma_{ij}^{(k)} \, \mathrm{d}\Omega^e - \int_{\Omega^e} \Phi_i \rho (b_i^{(k)} - \dot{v}_i^{(k)}) \, \mathrm{d}\Omega^e - \int_{\Gamma^{s^e}} \Phi_i \bar{t}_i^{(k)} \, \mathrm{d}\Gamma^{s^e} = 0$$

The third matrix equation of the system results from the reciprocity statement of the secondary variables. That is,

$$\int_{\Gamma^{\mathrm{I}}} \hat{\lambda}_i \left(\hat{q}_i^{(1)} + \hat{q}_i^{(2)} \right) \mathrm{d}\Gamma^{\mathrm{I}} = 0 \quad \text{on} \quad \Gamma^{\mathrm{I}} .$$

The fourth and fifth matrix equations result from the continuity requirement for the primary variables, which is given by

$$\int_{\Gamma^{\mathrm{I}}} \lambda_i^{(k)} \left(v_i - u_i^{(k)} \right) \mathrm{d}\Gamma^{\mathrm{I}} = 0 \quad \text{on} \quad \Gamma^{\mathrm{I}}$$

$$\int_{\Gamma^{\mathrm{I}}} \lambda_i^{(2)} \left(v_i - u_i^{(2)} \right) \mathrm{d}\Gamma^{\mathrm{I}} = 0 \quad \text{on} \quad \Gamma^{\mathrm{I}}$$

Note that the forms of the coupling element matrices that are not in terms of the weight functions are independent of the method of discretization. That is,

$$\mathbf{k}_{\mathbf{p}_k} = - \int_{\Gamma^{\mathrm{I}^e}} \mathbf{R}_k^{\mathrm{T}} \mathbf{N}_k \, \mathrm{d}\Gamma^{\mathrm{I}^e} ,$$

and

$$\mathbf{k}_{\mathrm{I}_k} = \int_{\Gamma^{\mathrm{I}^e}} \mathbf{T}^{\mathrm{T}} \mathbf{R}_k \, \mathrm{d}\Gamma^{\mathrm{I}^e}$$

are of the same form for the finite element and finite difference discretizations. However, since the element shape functions, $\mathbf{N}_k$, differ for the two methods, the interface matrices, $\mathbf{k}_{\mathbf{p}_k}$, in general, are not identical.

Fluid Mechanics- finite element discretization

Substituting the approximations of Eq. (3.52) into Eq. (3.51) along with the constitutive equations and using the Galerkin method in which $\mathbf{\Phi} = \mathbf{N}$, yields

$$\left[\int_{\Omega_1^e} \rho \mathbf{N}_1^{\mathrm{T}} \mathbf{N}_1 \, \mathrm{d}\Omega_1^e\right] \dot{\mathbf{u}}_{e_1} + \left[\int_{\Omega_2^e} \rho \mathbf{N}_2^{\mathrm{T}} \mathbf{N}_2 \, \mathrm{d}\Omega_2^e\right] \dot{\mathbf{u}}_{e_2} + \left[\int_{\Omega_1^e} \rho \mathbf{N}_1^{\mathrm{T}} \left(\mathbf{N}_1 \mathbf{u}_{e_1}\right) \mathbf{N}_1 \, \mathrm{d}\Omega_1^e\right] \mathbf{u}_{e_1}$$
$$+ \left[\int_{\Omega_2^e} \rho \mathbf{N}_2^{\mathrm{T}} \left(\mathbf{N}_2 \mathbf{u}_{e_2}\right) \mathbf{N}_2 \, \mathrm{d}\Omega_2^e\right] \mathbf{u}_{e_2} + \left[\int_{\Omega_1^e} 2\mu \mathbf{B}_1^{\mathrm{T}} \mathbf{B}_{1_{\mathrm{f}}} \, \mathrm{d}\Omega_1^e\right] \mathbf{u}_{e_1} + \left[\int_{\Omega_2^e} 2\mu \mathbf{B}_2^{\mathrm{T}} \mathbf{B}_{2_{\mathrm{f}}} \, \mathrm{d}\Omega_2^e\right] \mathbf{u}_{e_2}$$
$$- \left[\int_{\Omega_1^e} \mathbf{B}_1^{\mathrm{T}} \hat{\mathbf{N}}_1 \mathbf{I} \, \mathrm{d}\Omega_1^e\right] \mathbf{P}_{e_1} - \left[\int_{\Omega_2^e} \mathbf{B}_2^{\mathrm{T}} \hat{\mathbf{N}}_2 \mathbf{I} \, \mathrm{d}\Omega_2^e\right] \mathbf{P}_{e_2}$$
$$- \left[\int_{\Gamma^{\mathrm{I}^e}} \mathbf{N}_1^{\mathrm{T}} \mathbf{R}_1 \, \mathrm{d}\Gamma^{\mathrm{I}^e}\right] \boldsymbol{\alpha}_1 - \left[\int_{\Gamma^{\mathrm{I}^e}} \mathbf{N}_2^{\mathrm{T}} \mathbf{R}_2 \, \mathrm{d}\Gamma^{\mathrm{I}^e}\right] \boldsymbol{\alpha}_2 + \left[\int_{\Gamma^{\mathrm{I}^e}} \mathbf{T}^{\mathrm{T}} \mathbf{R}_1 \, \mathrm{d}\Gamma^{\mathrm{I}^e}\right] \boldsymbol{\alpha}_1 + \left[\int_{\Gamma^{\mathrm{I}^e}} \mathbf{T}^{\mathrm{T}} \mathbf{R}_2 \, \mathrm{d}\Gamma^{\mathrm{I}^e}\right] \boldsymbol{\alpha}_2$$
$$+ \left[\int_{\Gamma^{\mathrm{I}^e}} \mathbf{R}_1^{\mathrm{T}} \mathbf{T} \, \mathrm{d}\Gamma^{\mathrm{I}^e}\right] \mathbf{u}_{\mathrm{I}} - \left[\int_{\Gamma^{\mathrm{I}^e}} \mathbf{R}_1^{\mathrm{T}} \mathbf{N}_1 \, \mathrm{d}\Gamma^{\mathrm{I}^e}\right] \mathbf{u}_{e_1} + \left[\int_{\Gamma^{\mathrm{I}^e}} \mathbf{R}_2^{\mathrm{T}} \mathbf{T} \, \mathrm{d}\Gamma^{\mathrm{I}^e}\right] \mathbf{u}_{\mathrm{I}} - \left[\int_{\Gamma^{\mathrm{I}^e}} \mathbf{R}_2^{\mathrm{T}} \mathbf{N}_2 \, \mathrm{d}\Gamma^{\mathrm{I}^e}\right] \mathbf{u}_{e_2}$$
$$= \int_{\Omega_1^e} \mathbf{N}_1^{\mathrm{T}} \rho \mathbf{b}_1 \mathrm{d}\Omega_1^e + \int_{\Gamma_1^{s^e}} \mathbf{N}_1^{\mathrm{T}} \bar{\mathbf{t}}_1 \, \mathrm{d}\Gamma_1^{s^e} + \int_{\Omega_2^e} \mathbf{N}_2^{\mathrm{T}} \rho \mathbf{b}_2 \mathrm{d}\Omega_2^e + \int_{\Gamma_2^{s^e}} \mathbf{N}_2^{\mathrm{T}} \bar{\mathbf{t}}_2 \, \mathrm{d}\Gamma_2^{s^e} \tag{3.58}$$

where $\mathbf{B}_k = \partial \mathbf{N}_k$ and $\mathbf{B}_{k\mathrm{f}} = \partial_{\mathrm{f}} \mathbf{N}_k$ for k=1,2 and the elemental matrices are

$$\mathbf{k}_{\mathbf{e}_k} = \int_{\Omega_k^e} 2\mu \mathbf{B}_k^{\mathrm{T}} \mathbf{B}_{k_{\mathrm{f}}} \, \mathrm{d}\Omega_k^e \; ; \; \mathbf{m}_{\mathbf{e}_k} = \int_{\Omega_k^e} \rho \mathbf{N}_k^{\mathrm{T}} \mathbf{N}_k \, \mathrm{d}\Omega_k^e \; ;$$

$$\mathbf{c}_{\mathbf{e}_k} = \int_{\Omega_k^e} \rho \mathbf{N}_k^{\mathrm{T}} \left(\mathbf{N}_k \mathbf{u}_{e_k}\right) \mathbf{N}_k \, \mathrm{d}\Omega_k^e \; ; \; \mathbf{q}_{\mathbf{e}_k} = \int_{\Omega_k^e} \mathbf{B}_k^{\mathrm{T}} \hat{\mathbf{N}}_k \mathbf{I} \, \mathrm{d}\Omega_k^e \; ;$$

$$\mathbf{k}_{\mathbf{p}k} = -\int_{\Gamma^{\mathrm{I}^e}} \mathbf{R}_k^{\mathrm{T}} \mathbf{N}_k \, \mathrm{d}\Gamma^{\mathrm{I}^e},$$

$$\mathbf{k}_{\mathbf{s}k} = -\int_{\Gamma^{\mathrm{I}^e}} \mathbf{N}_k^{\mathrm{T}} \mathbf{R}_k \, \mathrm{d}\Gamma^{\mathrm{I}^e},$$

$$\mathbf{k}_{\mathrm{I}k} = \int_{\Gamma^{\mathrm{I}^e}} \mathbf{T}^{\mathrm{T}} \mathbf{R}_k \, \mathrm{d}\Gamma^{\mathrm{I}^e},$$

and

$$\mathbf{f}_{ek} = \int_{\Omega_k^e} \mathbf{N}_k^{\mathrm{T}} \rho \mathbf{b}_k \mathrm{d}\Omega_k^e + \int_{\Gamma_k^{s^e}} \mathbf{N}_k^{\mathrm{T}} \bar{\mathbf{t}}_k \, \mathrm{d}\Gamma_k^{s^e}.$$

In addition to the element equations for momentum, Eq. (3.58), the element equations for continuity must be considered. Eq. (3.34) is used to provide the mathematical basis for the continuity equation for multiple domains. Using the Galerkin method, the weight function corresponding to the continuity equation is given by $\hat{\mathbf{\Phi}} = \hat{\mathbf{N}}$. Substituting the approximation for the weight function and the primary variable into Eq. (3.34) yields

$$\left(\int_{\Omega_1^e} \mathbf{B}_1^{\mathrm{T}} \hat{\mathbf{N}}_1 \, \mathrm{d}\Omega_1^e \right) \mathbf{u}_{e_1} + \left(\int_{\Omega_2^e} \mathbf{B}_2^{\mathrm{T}} \hat{\mathbf{N}}_2 \, \mathrm{d}\Omega_2^e \right) \mathbf{u}_{e_2} = 0$$

Fluid Mechanics- finite difference discretization

Substituting the approximations of Eq. (3.52) into Eq. (3.51) along with the constitutive equations and using the Dirac delta function as the weight function,

$\mathbf{\Phi}_k = \delta_k(x - x_i, y - y_i) = \delta_k(x_i, y_i)$,

$$\left[\rho\mathbf{N}_1\Big|_{\substack{x=x_i\\y=y_i}}\right]\dot{\mathbf{u}}_{e_1}+\left[\rho\mathbf{N}_2\Big|_{\substack{x=x_i\\y=y_i}}\right]\dot{\mathbf{u}}_{e_2}+\left[\rho\left(\mathbf{N}_1\mathbf{u}_{e_1}\right)\mathbf{N}_1\Big|_{\substack{x=x_i\\y=y_i}}\right]\mathbf{u}_{e_1}$$
$$+\left[\rho\left(\mathbf{N}_2\mathbf{u}_{e_2}\right)\mathbf{N}_2\Big|_{\substack{x=x_i\\y=y_i}}\right]\mathbf{u}_{e_2}+\left[2\mu\partial^{\mathrm{T}}\mathbf{T}\partial\mathbf{N}_1\Big|_{\substack{x=x_i\\y=y_i}}\right]\mathbf{u}_{e_1}+\left[2\mu\partial^{\mathrm{T}}\mathbf{T}\partial\mathbf{N}_2\Big|_{\substack{x=x_i\\y=y_i}}\right]\mathbf{u}_{e_2}$$
$$-\left[\partial^{\mathrm{T}}\mathbf{I}\hat{\mathbf{N}}_1\Big|_{\substack{x=x_i\\y=y_i}}\right]\mathbf{P}_{e_1}-\left[\partial^{\mathrm{T}}\mathbf{I}\hat{\mathbf{N}}_2\Big|_{\substack{x=x_i\\y=y_i}}\right]\mathbf{P}_{e_2}$$
$$-\left[\mathbf{R}_1(x_i,y_i)\right]\boldsymbol{\alpha}_1-\left[\mathbf{R}_2(x_i,y_i)\right]\boldsymbol{\alpha}_2+\left[\int_{\Gamma^{\mathrm{I}^e}}\mathbf{T}^{\mathrm{T}}\mathbf{R}_1\,\mathrm{d}\Gamma^{\mathrm{I}^e}\right]\boldsymbol{\alpha}_1+\left[\int_{\Gamma^{\mathrm{I}^e}}\mathbf{T}^{\mathrm{T}}\mathbf{R}_2\,\mathrm{d}\Gamma^{\mathrm{I}^e}\right]\boldsymbol{\alpha}_2$$
$$+\left[\int_{\Gamma^{\mathrm{I}^e}}\mathbf{R}_1^{\mathrm{T}}\mathbf{T}\,\mathrm{d}\Gamma^{\mathrm{I}^e}\right]\mathbf{u}_{\mathrm{I}}-\left[\int_{\Gamma^{\mathrm{I}^e}}\mathbf{R}_1^{\mathrm{T}}\mathbf{N}_1\,\mathrm{d}\Gamma^{\mathrm{I}^e}\right]\mathbf{u}_{e_1}+\left[\int_{\Gamma^{\mathrm{I}^e}}\mathbf{R}_2^{\mathrm{T}}\mathbf{T}\,\mathrm{d}\Gamma^{\mathrm{I}^e}\right]\mathbf{u}_{\mathrm{I}}-\left[\int_{\Gamma^{\mathrm{I}^e}}\mathbf{R}_2^{\mathrm{T}}\mathbf{N}_2\,\mathrm{d}\Gamma^{\mathrm{I}^e}\right]\mathbf{u}_{e_2}$$
$$=\rho\mathbf{b}_1(x_i,y_i)+\bar{\mathbf{t}}_1(x_i,y_i)+\rho\mathbf{b}_2(x_i,y_i)+\bar{\mathbf{t}}_2(x_i,y_i) \tag{3.59}$$

where, for k=1,2 and the elemental matrices are

$$\mathbf{k}_{\mathbf{e}_k}=2\mu\partial^{\mathrm{T}}\mathbf{T}\partial\mathbf{N}_k\Big|_{\substack{x=x_i\\y=y_i}};\ \mathbf{m}_{\mathbf{e}_k}=\rho\mathbf{N}_k\Big|_{\substack{x=x_i\\y=y_i}};$$

$$\mathbf{c}_{\mathbf{e}_k}=\rho\left(\mathbf{N}_k\mathbf{u}_e\right)\mathbf{N}_k\Big|_{\substack{x=x_i\\y=y_i}};\ \mathbf{q}_{\mathbf{e}_k}=\partial^{\mathrm{T}}\mathbf{I}\hat{\mathbf{N}}_k\Big|_{\substack{x=x_i\\y=y_i}};$$

$$\mathbf{k}_{\mathbf{p}_k}=-\int_{\Gamma^{\mathrm{I}^e}}\mathbf{R}_k^{\mathrm{T}}\mathbf{N}_k\,\mathrm{d}\Gamma^{\mathrm{I}^e},$$

$$\mathbf{k}_{\mathbf{s}_k}=-\mathbf{R}_k(x_i,y_i),$$

$$\mathbf{k}_{\mathrm{I}_k}=\int_{\Gamma^{\mathrm{I}^e}}\mathbf{T}^{\mathrm{T}}\mathbf{R}_k\,\mathrm{d}\Gamma^{\mathrm{I}^e},$$

and

$$\mathbf{f}_{e_k}=\rho\mathbf{b}_k(x_i,y_i)+\bar{\mathbf{t}}_k(x_i,y_i).$$

Considering continuity, and using the Dirac delta function as the weight function,

$\hat{\mathbf{\Phi}}_k = \delta_k(x - x_i, y - y_i) = \delta_k(x_i, y_i)$, the continuity equation is given by

$$\left[\partial^{\mathrm{T}}\mathbf{I}\hat{\mathbf{N}}_1\Big|_{\substack{x=x_i\\y=y_i}}\right]\mathbf{u}_{e_1} + \left[\partial^{\mathrm{T}}\mathbf{I}\hat{\mathbf{N}}_2\Big|_{\substack{x=x_i\\y=y_i}}\right]\mathbf{u}_{e_2} = \mathbf{0}$$

For both the finite element and the finite difference discretization strategies, assembling the element momentum equations, Eqs. (3.58) and (3.59) over the entire domain, enforcing continuity of the primary variable only within each subdomain, and noting that $\mathbf{u}_{\mathbf{e}_1}$ and $\mathbf{u}_{\mathbf{e}_2}$, $\dot{\mathbf{u}}_{\mathbf{e}_1}$ and $\dot{\mathbf{u}}_{\mathbf{e}_2}$, $\mathbf{P}_{\mathbf{e}_1}$ and $\mathbf{P}_{\mathbf{e}_2}$, $\mathbf{f}_{\mathbf{e}_1}$ and $\mathbf{f}_{\mathbf{e}_2}$, and $\boldsymbol{\alpha}_1$ and $\boldsymbol{\alpha}_2$ are completely uncoupled, yields the system of equations given by

$$\begin{bmatrix} \mathbf{M}_1 & \mathbf{0} & \mathbf{0} & \mathbf{0} & \mathbf{0} & \mathbf{0} & \mathbf{0} \\ \mathbf{0} & \mathbf{M}_2 & \mathbf{0} & \mathbf{0} & \mathbf{0} & \mathbf{0} & \mathbf{0} \\ \mathbf{0} & \mathbf{0} & \mathbf{0} & \mathbf{0} & \mathbf{0} & \mathbf{0} & \mathbf{0} \\ \mathbf{0} & \mathbf{0} & \mathbf{0} & \mathbf{0} & \mathbf{0} & \mathbf{0} & \mathbf{0} \\ \mathbf{0} & \mathbf{0} & \mathbf{0} & \mathbf{0} & \mathbf{0} & \mathbf{0} & \mathbf{0} \\ \mathbf{0} & \mathbf{0} & \mathbf{0} & \mathbf{0} & \mathbf{0} & \mathbf{0} & \mathbf{0} \\ \mathbf{0} & \mathbf{0} & \mathbf{0} & \mathbf{0} & \mathbf{0} & \mathbf{0} & \mathbf{0} \end{bmatrix} \begin{Bmatrix} \dot{\mathbf{u}}_1 \\ \dot{\mathbf{u}}_2 \\ \dot{\mathbf{u}}_{\mathrm{I}} \\ \mathbf{P}_1 \\ \mathbf{P}_2 \\ \boldsymbol{\alpha}_1 \\ \boldsymbol{\alpha}_2 \end{Bmatrix} + \begin{bmatrix} \mathbf{C}_1 & \mathbf{0} & \mathbf{0} & \mathbf{0} & \mathbf{0} & \mathbf{0} & \mathbf{0} \\ \mathbf{0} & \mathbf{C}_2 & \mathbf{0} & \mathbf{0} & \mathbf{0} & \mathbf{0} & \mathbf{0} \\ \mathbf{0} & \mathbf{0} & \mathbf{0} & \mathbf{0} & \mathbf{0} & \mathbf{0} & \mathbf{0} \\ \mathbf{0} & \mathbf{0} & \mathbf{0} & \mathbf{0} & \mathbf{0} & \mathbf{0} & \mathbf{0} \\ \mathbf{0} & \mathbf{0} & \mathbf{0} & \mathbf{0} & \mathbf{0} & \mathbf{0} & \mathbf{0} \\ \mathbf{0} & \mathbf{0} & \mathbf{0} & \mathbf{0} & \mathbf{0} & \mathbf{0} & \mathbf{0} \\ \mathbf{0} & \mathbf{0} & \mathbf{0} & \mathbf{0} & \mathbf{0} & \mathbf{0} & \mathbf{0} \end{bmatrix} \begin{Bmatrix} \mathbf{u}_1 \\ \mathbf{u}_2 \\ \mathbf{u}_{\mathrm{I}} \\ \mathbf{P}_1 \\ \mathbf{P}_2 \\ \boldsymbol{\alpha}_1 \\ \boldsymbol{\alpha}_2 \end{Bmatrix} +$$

$$- \begin{bmatrix} \mathbf{0} & \mathbf{0} & \mathbf{0} & \mathbf{Q}_1 & \mathbf{0} & \mathbf{0} & \mathbf{0} \\ \mathbf{0} & \mathbf{0} & \mathbf{0} & \mathbf{0} & \mathbf{Q}_2 & \mathbf{0} & \mathbf{0} \\ \mathbf{0} & \mathbf{0} & \mathbf{0} & \mathbf{0} & \mathbf{0} & \mathbf{0} & \mathbf{0} \\ \mathbf{0} & \mathbf{0} & \mathbf{0} & \mathbf{0} & \mathbf{0} & \mathbf{0} & \mathbf{0} \\ \mathbf{0} & \mathbf{0} & \mathbf{0} & \mathbf{0} & \mathbf{0} & \mathbf{0} & \mathbf{0} \\ \mathbf{0} & \mathbf{0} & \mathbf{0} & \mathbf{0} & \mathbf{0} & \mathbf{0} & \mathbf{0} \\ \mathbf{0} & \mathbf{0} & \mathbf{0} & \mathbf{0} & \mathbf{0} & \mathbf{0} & \mathbf{0} \end{bmatrix} \begin{Bmatrix} \mathbf{u}_1 \\ \mathbf{u}_2 \\ \mathbf{u}_{\mathrm{I}} \\ \mathbf{P}_1 \\ \mathbf{P}_2 \\ \boldsymbol{\alpha}_1 \\ \boldsymbol{\alpha}_2 \end{Bmatrix}$$

$$+ \begin{bmatrix} \mathbf{K}_1 & \mathbf{0} & \mathbf{0} & \mathbf{0} & \mathbf{0} & \mathbf{K}_{\mathrm{s}_1} & \mathbf{0} \\ \mathbf{0} & \mathbf{K}_2 & \mathbf{0} & \mathbf{0} & \mathbf{0} & \mathbf{0} & \mathbf{K}_{\mathrm{s}_2} \\ \mathbf{0} & \mathbf{0} & \mathbf{0} & \mathbf{0} & \mathbf{0} & \mathbf{0} & \mathbf{0} \\ \mathbf{0} & \mathbf{0} & \mathbf{0} & \mathbf{0} & \mathbf{0} & \mathbf{0} & \mathbf{0} \\ \mathbf{0} & \mathbf{0} & \mathbf{0} & \mathbf{0} & \mathbf{0} & \mathbf{K}_{\mathrm{I}_1} & \mathbf{K}_{\mathrm{I}_2} \\ \mathbf{K}_{\mathrm{p}_1} & \mathbf{0} & \mathbf{K}_{\mathrm{I}_1}^{\mathrm{T}} & \mathbf{0} & \mathbf{0} & \mathbf{0} & \mathbf{0} \\ \mathbf{0} & \mathbf{K}_{\mathrm{p}_2} & \mathbf{K}_{\mathrm{I}_2}^{\mathrm{T}} & \mathbf{0} & \mathbf{0} & \mathbf{0} & \mathbf{0} \end{bmatrix} \begin{Bmatrix} \mathbf{u}_1 \\ \mathbf{u}_2 \\ \mathbf{u}_{\mathrm{I}} \\ \mathbf{P}_1 \\ \mathbf{P}_2 \\ \boldsymbol{\alpha}_1 \\ \boldsymbol{\alpha}_2 \end{Bmatrix} = \begin{Bmatrix} \mathbf{f}_1 \\ \mathbf{f}_2 \\ \mathbf{0} \\ \mathbf{0} \\ \mathbf{0} \\ \mathbf{0} \\ \mathbf{0} \end{Bmatrix} \tag{3.60}$$

along with

$$\begin{bmatrix} \mathbf{Q}_1 & \mathbf{0} \\ \mathbf{0} & \mathbf{Q}_2 \end{bmatrix} \begin{Bmatrix} \mathbf{u}_1 \\ \mathbf{u}_2 \end{Bmatrix} = \begin{Bmatrix} \mathbf{0} \\ \mathbf{0} \end{Bmatrix}$$

or symbolically

$$\begin{bmatrix} \mathbf{M} & \mathbf{0} & \mathbf{0} & \mathbf{0} \\ \mathbf{0} & \mathbf{0} & \mathbf{0} & \mathbf{0} \\ \mathbf{0} & \mathbf{0} & \mathbf{0} & \mathbf{0} \\ \mathbf{0} & \mathbf{0} & \mathbf{0} & \mathbf{0} \end{bmatrix} \begin{Bmatrix} \dot{\mathbf{u}} \\ \dot{\mathbf{u}}_{\mathrm{I}} \\ \mathbf{P} \\ \boldsymbol{\alpha} \end{Bmatrix} + \begin{bmatrix} \mathbf{C(u)} + \mathbf{K} & \mathbf{0} & -\mathbf{Q} & \mathbf{K}_{\mathrm{s}} \\ \mathbf{0} & \mathbf{0} & \mathbf{0} & \mathbf{K}_{\mathrm{I}} \\ -\mathbf{Q}^{\mathbf{T}} & \mathbf{0} & \mathbf{0} & \mathbf{0} \\ \mathbf{K}_{\mathrm{p}} & \mathbf{K}_{\mathrm{I}}^{\mathbf{T}} & \mathbf{0} & \mathbf{0} \end{bmatrix} \begin{Bmatrix} \mathbf{u} \\ \mathbf{u}_{\mathrm{I}} \\ \mathbf{P} \\ \boldsymbol{\alpha} \end{Bmatrix} = \begin{Bmatrix} \mathbf{f} \\ \mathbf{0} \\ \mathbf{0} \\ \mathbf{0} \end{Bmatrix}$$

where **K**, **M**, **C, Q** are the assembled coefficient matrices for momentum and continuity, **u** and **f** are the displacement vector and force vector for the entire structure, and $\mathbf{K}_{\mathrm{p}}$, $\mathbf{K}_{\mathrm{s}}$, $\mathbf{K}_{\mathrm{I}}$, $\mathbf{u}_{\mathrm{I}}$, and $\boldsymbol{\alpha}$ are the assembled $\mathbf{K}_{\mathrm{p}_k}$, $\mathbf{K}_{\mathrm{s}_k}$, $\mathbf{K}_{\mathrm{I}_k}$, $\mathbf{u}_{\mathrm{I}}$, and $\boldsymbol{\alpha}_k$ for all interfaces.

The first two matrix equations of the system of equations, Eq. (3.60) are derived from the weighted residual statement for subdomain *k.* That is,

$$\int_{\Omega^e} \Phi_{i,j}^{(k)} \sigma_{ij}^{(k)} \, \mathrm{d}\Omega^e - \int_{\Omega^e} \Phi_i \rho (b_i^{(k)} - \dot{v}_i^{(k)}) \, \mathrm{d}\Omega^e - \int_{\Gamma^{s^e}} \Phi_i \bar{t}_i^{(k)} \, \mathrm{d}\Gamma^{s^e} = 0$$

The third matrix equation of the system results from the reciprocity statement of the secondary variables. That is,

$$\int_{\Gamma^{\mathrm{I}}} \hat{\lambda}_i \left(\hat{q}_i^{(1)} + \hat{q}_i^{(2)} \right) \mathrm{d}\Gamma^{\mathrm{I}} = 0 \quad \text{on} \quad \Gamma^{\mathrm{I}} .$$

The fourth and fifth matrix equations result from the continuity requirement for the primary variables, which is given by

$$\int_{\Gamma^{\mathrm{I}}} \lambda_i^{(1)} \left(v_i - u_i^{(1)} \right) \mathrm{d}\Gamma^{\mathrm{I}} = 0 \quad \text{on} \quad \Gamma^{\mathrm{I}}$$

$$\int_{\Gamma^{\mathrm{I}}} \lambda_i^{(2)} \left(v_i - u_i^{(2)} \right) \mathrm{d}\Gamma^{\mathrm{I}} = 0 \quad \text{on} \quad \Gamma^{\mathrm{I}}$$

Note that the forms of the coupling element matrices that are not in terms of the weight functions are independent of the method of discretization. That is,

$$\mathbf{k}_{\mathbf{p}_k} = -\int_{\Gamma^{\mathrm{I}^e}} \mathbf{R}_k^{\mathrm{T}} \mathbf{N}_k \, \mathrm{d}\Gamma^{\mathrm{I}^e} ,$$

and

$$\mathbf{k}_{\mathrm{I}_k} = \int_{\Gamma^{\mathrm{I}^e}} \mathbf{T}^{\mathrm{T}} \mathbf{R}_k \, \mathrm{d}\Gamma^{\mathrm{I}^e}$$

are of the same form for the finite element and finite difference discretizations. However, since the element shape functions, $\mathbf{N}_k$, differ for the two methods, the interface matrices, $\mathbf{k}_{\mathbf{p}_k}$, in general, are not identical.

In addition, for the penalty finite element model, the system of equations is of the same form as given in Eq. (3.60), except that penalty terms are included rather than the pressure terms. The resulting system of equations is given by

$$\begin{bmatrix} \mathbf{M}_1 & \mathbf{0} & \mathbf{0} & \mathbf{0} & \mathbf{0} \\ \mathbf{0} & \mathbf{M}_2 & \mathbf{0} & \mathbf{0} & \mathbf{0} \\ \mathbf{0} & \mathbf{0} & \mathbf{0} & \mathbf{0} & \mathbf{0} \\ \mathbf{0} & \mathbf{0} & \mathbf{0} & \mathbf{0} & \mathbf{0} \\ \mathbf{0} & \mathbf{0} & \mathbf{0} & \mathbf{0} & \mathbf{0} \end{bmatrix} \begin{Bmatrix} \dot{\mathbf{u}}_1 \\ \dot{\mathbf{u}}_2 \\ \dot{\mathbf{u}}_{\mathrm{I}} \\ \boldsymbol{\alpha}_1 \\ \boldsymbol{\alpha}_2 \end{Bmatrix} + \begin{bmatrix} \mathbf{C}_1 & \mathbf{0} & \mathbf{0} & \mathbf{0} & \mathbf{0} \\ \mathbf{0} & \mathbf{C}_2 & \mathbf{0} & \mathbf{0} & \mathbf{0} \\ \mathbf{0} & \mathbf{0} & \mathbf{0} & \mathbf{0} & \mathbf{0} \\ \mathbf{0} & \mathbf{0} & \mathbf{0} & \mathbf{0} & \mathbf{0} \\ \mathbf{0} & \mathbf{0} & \mathbf{0} & \mathbf{0} & \mathbf{0} \end{bmatrix} \begin{Bmatrix} \mathbf{u}_1 \\ \mathbf{u}_2 \\ \mathbf{u}_{\mathrm{I}} \\ \boldsymbol{\alpha}_1 \\ \boldsymbol{\alpha}_2 \end{Bmatrix} +$$

$$\begin{bmatrix} \mathbf{K}_1 & \mathbf{0} & \mathbf{0} & \mathbf{K}_{\mathrm{s}_1} & \mathbf{0} \\ \mathbf{0} & \mathbf{K}_2 & \mathbf{0} & \mathbf{0} & \mathbf{K}_{\mathrm{s}_2} \\ \mathbf{0} & \mathbf{0} & \mathbf{0} & \mathbf{K}_{\mathrm{I}_1} & \mathbf{K}_{\mathrm{I}_2} \\ \mathbf{K}_{\mathrm{p}_1} & \mathbf{0} & \mathbf{K}_{\mathrm{I}_1}^{\mathrm{T}} & \mathbf{0} & \mathbf{0} \\ \mathbf{0} & \mathbf{K}_{\mathrm{p}_2} & \mathbf{K}_{\mathrm{I}_2}^{\mathrm{T}} & \mathbf{0} & \mathbf{0} \end{bmatrix} \begin{Bmatrix} \mathbf{u}_1 \\ \mathbf{u}_2 \\ \mathbf{u}_{\mathrm{I}} \\ \boldsymbol{\alpha}_1 \\ \boldsymbol{\alpha}_2 \end{Bmatrix} + \begin{bmatrix} \mathbf{S}_1 & \mathbf{0} & \mathbf{0} & \mathbf{0} & \mathbf{0} \\ \mathbf{0} & \mathbf{S}_2 & \mathbf{0} & \mathbf{0} & \mathbf{0} \\ \mathbf{0} & \mathbf{0} & \mathbf{0} & \mathbf{0} & \mathbf{0} \\ \mathbf{0} & \mathbf{0} & \mathbf{0} & \mathbf{0} & \mathbf{0} \\ \mathbf{0} & \mathbf{0} & \mathbf{0} & \mathbf{0} & \mathbf{0} \end{bmatrix} \begin{Bmatrix} \mathbf{u}_1 \\ \mathbf{u}_2 \\ \mathbf{u}_{\mathrm{I}} \\ \boldsymbol{\alpha}_1 \\ \boldsymbol{\alpha}_2 \end{Bmatrix} = \begin{Bmatrix} \mathbf{f}_1 \\ \mathbf{f}_2 \\ \mathbf{0} \\ \mathbf{0} \\ \mathbf{0} \end{Bmatrix} \tag{3.61}$$

or symbolically

$$\begin{bmatrix} \mathbf{M} & \mathbf{0} & \mathbf{0} \\ \mathbf{0} & \mathbf{0} & \mathbf{0} \\ \mathbf{0} & \mathbf{0} & \mathbf{0} \end{bmatrix} \begin{Bmatrix} \dot{\mathbf{u}} \\ \dot{\mathbf{u}}_{\mathrm{I}} \\ \boldsymbol{\alpha} \end{Bmatrix} + \begin{bmatrix} \mathbf{C}(\mathbf{u}) + \mathbf{K} + \mathbf{S} & \mathbf{0} & \mathbf{K}_{\mathrm{s}} \\ \mathbf{0} & \mathbf{0} & \mathbf{K}_{\mathrm{I}} \\ \mathbf{K}_{\mathrm{p}} & \mathbf{K}_{\mathrm{I}}^{\mathrm{T}} & \mathbf{0} \end{bmatrix} \begin{Bmatrix} \mathbf{u} \\ \mathbf{u}_{\mathrm{I}} \\ \boldsymbol{\alpha} \end{Bmatrix} = \begin{Bmatrix} \mathbf{f} \\ \mathbf{0} \\ \mathbf{0} \end{Bmatrix}$$

where **K**, **M**, **C, S** are the assembled coefficient, mass, momentum, and penalty matrices, **u** and **f** are the displacement vector and force vector for the entire structure, and $\mathbf{K}_{\mathrm{p}}$, $\mathbf{K}_{\mathrm{s}}$, $\mathbf{K}_{\mathrm{I}}$, $\mathbf{u}_{\mathrm{I}}$, and $\boldsymbol{\alpha}$ are the assembled $\mathbf{K}_{\mathrm{p}_k}$, $\mathbf{K}_{\mathrm{s}_k}$, $\mathbf{K}_{\mathrm{I}_k}$, $\mathbf{u}_{\mathrm{I}}$, and $\boldsymbol{\alpha}_k$ for all interfaces. Recall that the element penalty matrix for the k^{th} subdomain is given by

$$\mathbf{s}_{\mathbf{e}_k} = \int_{\Omega_k^e} \left(\mathbf{N}_k^{\mathrm{T}}\right)_{,x_1} \left(\mathbf{N}_k\right)_{,x_2} \mathrm{d}\Omega_k^e$$

3.6.4. Multiple-Domain Modeling - Heterogeneous Discretization

The multifunctional weighted residual formulation of Eqs. (3.57) and (3.60) are used as the mathematical basis for multiple-domain modeling using heterogeneous discretization. Considering the two domains upon which this discussion is based, one subdomain is discretized using the finite element method, and the other subdomain is discretized using the finite difference method. Again, for the finite element development, the weight functions for the primary variables, **u** and **P**, are taken to be the finite element shape functions (*i.e.*, $\boldsymbol{\Phi}_k = \mathbf{N}_k$ and $\hat{\boldsymbol{\Phi}}_k = \hat{\mathbf{N}}_k$), and for the finite difference development, the weight functions are taken to be the Dirac delta function (*i.e.*, $\boldsymbol{\Phi}_k = \delta_k(x - x_i, y - y_i) = \delta_k(x_i, y_i)$). As expected, the set of element matrices becomes a hybrid of the matrices from the finite element method and the finite difference method. For completeness, these matrices are repeated here for the finite element and finite difference subdomains for solid mechanics as

$$\mathbf{k}_{\mathbf{e}_1} = \int_{\Omega_1^e} \mathbf{B}_1^{\mathrm{T}} \mathbf{E}_1 \mathbf{B}_1 \, \mathrm{d}\Omega_1^e \text{ and } \mathbf{k}_{\mathbf{e}_2} = \partial^{\mathrm{T}} \mathbf{E}_2 \partial \mathbf{N}_2 \Big|_{\substack{x=x_i \\ y=y_i}},$$

$$\mathbf{m}_{\mathbf{e}_1} = \int_{\Omega_1^e} \rho \mathbf{N}_1^{\mathrm{T}} \mathbf{N}_1 \, \mathrm{d}\Omega_1^e \text{ and } \mathbf{m}_{\mathbf{e}_2} = \rho \mathbf{N}_2 \Big|_{\substack{x=x_i \\ y=y_i}},$$

$$\text{and } \mathbf{f}_{e1} = \int_{\Omega_1^e} \mathbf{B}_1^{\mathrm{T}} \mathbf{E}_1 \boldsymbol{\varepsilon}_0^{(1)} \, \mathrm{d}\Omega_1^e - \int_{\Omega_1^e} \mathbf{B}_1^{\mathrm{T}} \boldsymbol{\sigma}_0^{(1)} \, \mathrm{d}\Omega_1^e + \int_{\Omega_1^e} \mathbf{N}_1^{\mathrm{T}} \rho \mathbf{b}_1 \mathrm{d}\Omega_1^e + \int_{\Gamma_1^{s^e}} \mathbf{N}_1^{\mathrm{T}} \bar{\mathbf{t}}_1 \, \mathrm{d}\Gamma_1^{s^e} \text{ and}$$

$$\mathbf{f}_{e2} = \partial^{\mathrm{T}} \mathbf{E}_2 \boldsymbol{\varepsilon}_0^{(2)} - \partial^{\mathrm{T}} \boldsymbol{\sigma}_0^{(2)} + \rho \mathbf{b}_2 \Big|_{\substack{x=x_i \\ y=y_i}} + \bar{\mathbf{t}}_2 \Big|_{\substack{x=x_i \\ y=y_i}}.$$

For fluid mechanics the element matrices are given by

$$\mathbf{k}_{\mathbf{e}_1} = \int_{\Omega_1^e} 2\mu \mathbf{B}_1^{\mathrm{T}} \mathbf{B}_{1_{\mathrm{f}}} \, \mathrm{d}\Omega_1^e \text{ and } \mathbf{k}_{\mathbf{e}_2} = 2\mu \partial^{\mathrm{T}} \mathbf{T} \partial \mathbf{N}_2 \Big|_{\substack{x=x_i \\ y=y_i}},$$

$$\mathbf{m}_{\mathbf{e}_1} = \int_{\Omega_1^e} \rho \mathbf{N}_1^{\mathrm{T}} \mathbf{N}_1 \, \mathrm{d}\Omega_1^e \text{ and } \mathbf{m}_{\mathbf{e}_2} = \rho \mathbf{N}_2 \Big|_{\substack{x=x_i \\ y=y_i}},$$

$$\mathbf{c}_{\mathbf{e}_1} = \int_{\Omega_1^e} \rho \mathbf{N}_1^{\mathrm{T}} \left(\mathbf{N}_1 \mathbf{u}_{e_1} \right) \mathbf{N}_1 \, \mathrm{d}\Omega_1^e \text{ and } \mathbf{c}_{\mathbf{e}_2} = \rho \left(\mathbf{N}_2 \mathbf{u}_{e_2} \right) \mathbf{N}_2 \Big|_{\substack{x=x_i \\ y=y_i}}$$

$$\mathbf{q}_{\mathbf{e}_1} = \int_{\Omega_1^e} \mathbf{B}_1^{\mathrm{T}} \hat{\mathbf{N}}_1 \mathbf{I} \, \mathrm{d}\Omega_1^e \text{ and } \mathbf{q}_{\mathbf{e}_2} = \partial^{\mathrm{T}} \mathbf{I} \hat{\mathbf{N}}_2 \Big|_{\substack{x=x_i \\ y=y_i}},$$

$$\text{and } \mathbf{f}_{e_1} = \int_{\Omega_1^e} \mathbf{N}_1^{\mathrm{T}} \rho \mathbf{b}_1 \mathrm{d}\Omega_1^e + \int_{\Gamma_1^{s^e}} \mathbf{N}_1^{\mathrm{T}} \bar{\mathbf{t}}_1 \, \mathrm{d}\Gamma_1^{s^e} \text{ and } \mathbf{f}_{e_2} = \rho \mathbf{b}_2 (x_i, y_i) + \bar{\mathbf{t}}_2 (x_i, y_i).$$

The coupling matrices at the element level are of the same form for both solid and fluid mechanics and these matrices are given by

$$\mathbf{k}_{\mathbf{s}_1} = -\int_{\Gamma^{\mathrm{I}^e}} \mathbf{N}_1^{\mathrm{T}} \mathbf{R} \, \mathrm{d}\Gamma^{\mathrm{I}^e} \text{ and } \mathbf{k}_{\mathbf{s}_2} = -\mathbf{R}(x_i, y_i),$$

and for the two domains, k=1,2,

$$\mathbf{k}_{\mathbf{p}_k} = -\int_{\Gamma^{I^e}} \mathbf{R}_k^{\mathrm{T}} \mathbf{N}_k \, d\Gamma^{I^e},$$

and

$$\mathbf{k}_{I_k} = \int_{\Gamma^{I^e}} \mathbf{T}^{\mathrm{T}} \mathbf{R}_k \, d\Gamma^{I^e}.$$

3.7. COMPUTATIONAL IMPLICATIONS

The multifunctional modeling approach for the vector field problem has been generalized such that it is applicable to solid and fluid mechanics as well as both homogeneous and heterogeneous discretization approaches. As such the computational implications are presented in this section for the generalized system of equations, Eqs. (3.57) and (3.60). Implications specific to a discipline or a discretization approach are highlighted, where appropriate.

The assembled coefficient matrices, **K**, **M, C,** and **Q,** are block diagonal matrices containing the matrices, $\mathbf{K}_k$, $\mathbf{M}_k$, $\mathbf{C}_k$, and $\mathbf{Q}_k$ of each of the subdomains along its block diagonal. The interface coupling matrix thus contains terms that augment the coefficient matrices of the subdomains along the interface. All of the interface coupling terms appear in the coefficient matrix associated with the primary variables with none in the matrix associated with the time derivative. Again, due to the generalization for the finite difference approximations, the system of equations is not necessarily symmetric due to the off-diagonal submatrices, $\mathbf{K}_{\mathrm{p}}$ and $\mathbf{K}_{\mathrm{s}}$, nor are they banded or positive definite. Note that, even for a single domain model, the mixed formulation results in a nonpositive definite matrix. Therefore, standard Cholesky solvers may not be used, unless full pivoting is performed to obtain the solution. The upper diagonal blocks contain

uncoupled fluid flow coefficient matrices. The symmetry of the matrix is determined by the choice of the weight function, Φ. For the finite element discretization, the subdomain matrices are symmetric. In general, due the imposition of boundary conditions and loads in the finite difference discretization, the coefficient matrices, $\mathbf{K}_k$, are not symmetric but are positive definite and sparse. The coupling is accomplished through the introduction of the coupling terms in the matrices $\mathbf{K}_{\mathrm{p}_k}$ and $\mathbf{K}_{\mathrm{s}_k}$ for both approaches and each of the disciplines discussed herein.

In addition, due to the generalization for the finite difference approximations, the system of equations is not necessarily symmetric due to the off-diagonal submatrices, $\mathbf{K}_{\mathrm{p}}$ and $\mathbf{K}_{\mathrm{s}}$. The system unknowns in Eq. (3.57) and (3.60) consist of both primary and secondary variables given by the displacements or velocities, $\mathbf{u}$, and the traction coefficients, $\boldsymbol{\alpha}$, respectively. Generally, the coupling matrices, $\mathbf{K}_{\mathrm{s}_k}$, are of the order of the length of the interdomain boundary, which results in a marked difference in the magnitude of the off-diagonal terms of the system matrix compared to its diagonal terms. This characteristic produces an ill-conditioned matrix whose solution can cause difficulties for some general-purpose solvers. Hence, the coupling matrix should be scaled such that it is of the same order as the subdomain stiffness.

The load transfer mechanism of the multifunctional approach may be interrogated for the vector-field problem by considering the first and second rows of Eqs. (3.57) and (3.60) for solid and fluid mechanics, respectively. In either case the matrix equations of interest are given for solid mechanics by

$$\mathbf{M}_1\ddot{\mathbf{u}}_1 + \mathbf{K}_1\mathbf{u}_1 + \mathbf{K}_{\mathrm{s}_1}\boldsymbol{\alpha}_1 = \mathbf{f}_1$$
$$\mathbf{M}_2\ddot{\mathbf{u}}_2 + \mathbf{K}_2\mathbf{u}_2 + \mathbf{K}_{\mathrm{s}_2}\boldsymbol{\alpha}_2 = \mathbf{f}_2$$

or for fluid mechanics by

$$\mathbf{M}_1\dot{\mathbf{u}}_1 + \mathbf{K}_1\mathbf{u}_1 + \mathbf{K}_{s_1}\boldsymbol{\alpha}_1 = \mathbf{f}_1$$
$$\mathbf{M}_2\dot{\mathbf{u}}_2 + \mathbf{K}_2\mathbf{u}_2 + \mathbf{K}_{s_2}\boldsymbol{\alpha}_2 = \mathbf{f}_2$$

These equations can be partitioned such that they correspond only to the primary variables, $\bar{\mathbf{u}}_k$ on the interdomain boundary

$$\begin{aligned} \overline{\mathbf{K}}_1\bar{\mathbf{u}}_1 + \mathbf{K}_{s_1}\boldsymbol{\alpha}_1 &= \mathbf{0} \\ \overline{\mathbf{K}}_2\mathbf{u}_2 + \mathbf{K}_{s_2}\boldsymbol{\alpha}_2 &= \mathbf{0} \end{aligned} \tag{3.62}$$

and $\overline{\mathbf{K}}_k$ denotes stiffness terms related to $\bar{\mathbf{u}}_k$ and there are no forces (including inertial forces $\mathbf{M}_k\ddot{\mathbf{u}}_k$) on the interdomain boundary and assuming steady fluid flow (*i.e.*, $\mathbf{M}_k\dot{\mathbf{u}}_k = \mathbf{0}$). The expressions given by $\overline{\mathbf{K}}_k\bar{\mathbf{u}}_k$ represent the internal fluxes at the interdomain boundary, and thus Eq. (3.62) may be written as

$$\bar{\mathbf{f}}_1 = -\mathbf{K}_{s_1}\boldsymbol{\alpha}_1 \quad \text{and} \quad \bar{\mathbf{f}}_2 = -\mathbf{K}_{s_2}\boldsymbol{\alpha}_2. \tag{3.63}$$

For homogeneous discretization using the finite element method, substituting for $\mathbf{K}_{s_i}$ from Eq. (3.54) into Eq. (3.63) gives

$$\bar{\mathbf{f}}_1 = -\int_{\Gamma^{I^e}} \mathbf{N}_1^{\mathrm{T}}\mathbf{R}_1 \, d\Gamma^{I^e} \; \boldsymbol{\alpha}_1 = -\int_{\Gamma^{I^e}} \mathbf{N}_1^{\mathrm{T}}\hat{\mathbf{t}}_1 \, d\Gamma^{I^e} \tag{3.64}$$

$$\bar{\mathbf{f}}_2 = \int_{\Gamma^{I^e}} \mathbf{N}_2^{\mathrm{T}}\mathbf{R}_2 \, d\Gamma^{I^e} \; \boldsymbol{\alpha}_2 = -\int_{\Gamma^{I^e}} \mathbf{N}_2^{\mathrm{T}}\hat{\mathbf{t}}_2 \, d\Gamma^{I^e} \tag{3.64}$$

Examining Eqs. (3.64) indicate that the evaluation of the internal forces is consistent with the evaluation of equivalent nodal forces in the presence of applied tractions on the boundary. In addition, Eq. (3.64) substantiates that the secondary variable along the interface is represented by distributed forces for each of the subdomains.

For homogeneous discretization using the finite difference method, substituting for $\mathbf{K}_{s_i}$ from Eq. (3.56) into Eq. (3.63) gives

$$\bar{\mathbf{f}}_1 = -\mathbf{R}_1\boldsymbol{\alpha}_1 = -\hat{\mathbf{t}}_1 \tag{3.65}$$

$$\bar{\mathbf{f}}_2 = -\mathbf{R}_2\boldsymbol{\alpha}_2 = -\hat{\mathbf{t}}_2$$

Examining Eq. (3.65) indicates that the evaluation of the internal forces is consistent with nodal forces evaluated at points in the presence of applied tractions on the boundary. In addition, Eq. (3.65) substantiates that the secondary variable along the interface for this approach is represented by nodal forces for each of the subdomains.

For heterogeneous discretization using the combined finite element and finite difference methods, substituting for $\mathbf{K}_{s_k}$ from Eq. (3.54) into Eq. (3.56) gives

$$\bar{\mathbf{f}}_1 = -\int_{\Gamma^{I^e}} \mathbf{N}_1^{\mathrm{T}}\mathbf{R}_1 \, \mathrm{d}\Gamma^{I^e} \; \boldsymbol{\alpha}_1 = -\int_{\Gamma^{I^e}} \mathbf{N}_1^{\mathrm{T}}\hat{\mathbf{t}}_1 \, \mathrm{d}\Gamma^{I^e} \tag{3.66}$$

$$\bar{\mathbf{f}}_2 = -\mathbf{R}_2\boldsymbol{\alpha}_2 = -\hat{\mathbf{t}}_2$$

Examining Eq. (3.66)) indicates, for subdomain 1, that the evaluation of the internal forces is consistent with the evaluation of equivalent nodal forces in the presence of applied tractions on the boundary, while for subdomain 2, the evaluation of the internal forces is consistent with nodal forces evaluated at points. This reveals that for this multiple domain approach, the secondary variable along the interface for subdomain 1 is represented by distributed forces, and for subdomain 2, the secondary variable along the interface is represented by nodal or point forces. Thus for this heterogeneous modeling approach, it is required to transform the interface secondary variables into equivalent quantities.

3.8. VERIFICATION TEST CASE

In this section, the multifunctional methodology for the vector-field problem is demonstrated on a verification test case. The application is described and the associated results and salient features are discussed. This application is considered a patch test for the formulation and verifies the applicability of the method for a configuration for which the solutions are known. Finite difference and finite element solutions for single- and multiple-domain configurations are presented to provide benchmark solutions for the multifunctional approach using heterogeneous discretization. Representative applications from the field of engineering science are presented in Chapter V.

3.8.1. Patch Test

As in the scalar-field problem, a patch test is used to determine the effectiveness of the multifunctional approach applied to a vector-field problem. A cantilevered plate is subjected to uniform inplane loading at the free end that yields a constant state of strain. In particular, this loading condition provides verification of the finite difference method for combinations of displacement and traction boundary conditions, and the method is validated for both the single- and multiple-domain models.

Problem Statement

The analysis domain and the boundary conditions are shown in Figure 3.1. The normal and tangential tractions are denoted by T_n and T_t, respectively, in the figure. This configuration has been used in the combined finite difference and finite element analysis reported by Dow et al.[20], and it is used here to provide a point of comparison. The length of the plate, L, is 20 in., the width, W, is 8 in., and the thickness, h, is 1 in. The material system is described by a Young's modulus of 30,000 psi and a Poisson's ratio of 0.3. An

applied displacement of 0.3 in. is applied at one end, and the opposite end is fixed. The other sides are free.

For the finite element method, four-node elements are used to discretize the domain for all applications. Homogeneous discretizations for single- and multiple-domain models for the finite element and finite difference methods are presented. For the finite element discretization of a single domain, a finite element mesh of 20 elements and 4 elements are used in the axial (*x*-direction) and transverse directions (*y*-direction) , respectively, of the plate. For multiple domains with compatible meshes (*i.e.*, nodal coincidence is maintained at the interface), two finite element meshes of 10 elements and 4 elements are used in the *x*- and *y*-directions, respectively. For the finite difference discretization of a single domain, a finite difference grid consistent with the finite element mesh was used. That is, a grid of 21 grid points and 5 grid points are used in the axial (*x*-direction) and transverse directions (*y*-direction), respectively, of the plate. Similarly, for multiple domains with compatible meshes, two finite difference meshes of 11 grid points and 5 grid points are used in the *x*-and *y*-directions, respectively. For multiple domains with incompatible finite element meshes, one domain is discretized with 10 elements in the *x*-direction and 4 elements in the *y*-direction. While the other domain is discretized with 20 elements in the *x*-direction and 8 elements in the *y*-direction. The multiple-domain discretization is shown in Figure 3.2. The finite difference discretization is consistent with the finite element mesh discretization.

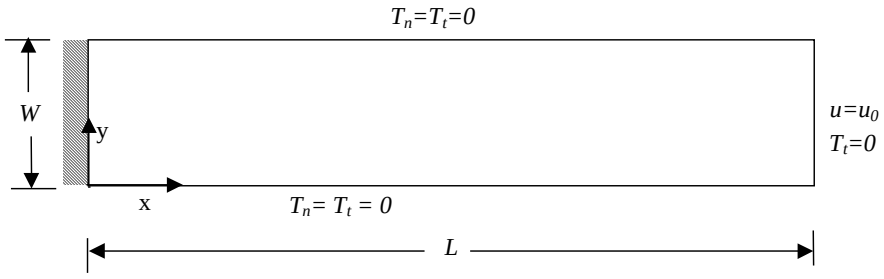

Figure 3.1. Analysis Domain and Boundary Conditions of Cantilevered Plate.

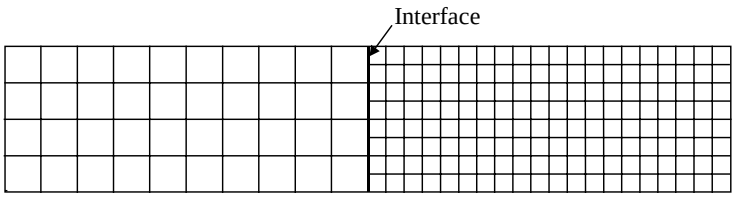

Figure 3.2. Multiple-Domain Discretization of Cantilevered Plate.

Boundary Conditions for Finite Difference Method

The finite difference method is extensively tested for the single- and multiple-domain configurations to assure that the boundary conditions are being applied correctly. Generally, for the vector-field problem, a 3×3 or nine-point central difference template is used to evaluate the momentum equation, Eq. (3.20). On the boundary of the domain, the template introduces fictitious nodes. In reference 43, the fictitious nodes are eliminated using traction conditions, T_n and T_t, and the constitutive equations. When the differential equation is evaluated at the corner of the domain boundary (see point i,j in Figure 3.3), a fictitious node (point $i+1,j+1$) is introduced for which there are no additional auxiliary equations. Thus, to eliminate the degrees of freedom associated with this fictitious node, non-physical higher-order derivatives of the constitutive equations are introduced that further complicate the approach. An alternative approach, used herein, is to apply the

momentum equation only to the nodes in the interior of the domain, while the differential equations representing the traction conditions are applied to the boundary nodes. Special forms[44] of the difference equations for grid points at the boundaries are used to avoid the use of fictitious nodes. These forms make use of higher-order forward or backward difference operators to express the differential forms in order to maintain the same order of accuracy as the central difference operator. For multiple-domain spatial modeling, the momentum equation is applied to nodes on the subdomain interface boundary. The higher-order backward or forward difference operators are used to introduce the unknown traction on the interface. This approach yields equations at the interface in terms of the unknown tractions at that specified interface node only. If a central difference scheme were used for the traction conditions, the equations on the interface would be in terms of the unknown tractions at the specified interface node and adjacent interface nodes. In the latter case, the resulting equations can not be derived from the generalized multifunctional formulation.

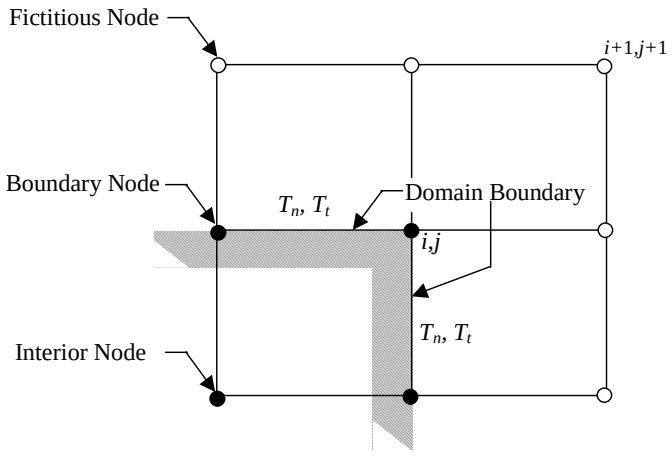

Figure 3.3. Central Difference Template Applied at a Corner.

Analysis Results

Several analyses have been performed: (1) two single-domain analyses, one with finite element discretization and one with finite difference discretization, respectively, (2) two multiple-domain analyses with homogeneous modeling, one with finite element discretization in each domain and one with finite difference discretization in each domain, and (3) one multiple-domain analysis with heterogeneous modeling with combined finite element and finite difference discretizations. All of the analyses yielded the exact solution within machine accuracy. Results for the internal forces or stresses along the interface for the analysis cases are shown in Table 3.1. The results are given at the locations along the width of the plate normalized by the plate width.

For the finite element domains, the internal forces, F_x and F_y, obtained from the multiple-domain analyses are normalized by the value of the force obtained from the exact solution multiplied by the element length along the edge of the interface. Thus, for a consistent load and for the finite elements used in this study, a normalized value of unity represents complete agreement with the exact solution at the interior nodes (*i.e.*, $1/8 \le y/W \le 7/8$). At the end nodes (*i.e.*, $y/W=0$ and $y/W=1$), a normalized value of one half represents complete agreement with the exact solution.

For the finite difference domains, the stresses, σ_x and τ_{xy}, obtained along the interface from the multiple-domain analyses are normalized by the value of the normal stress obtained from the exact solution. Thus, a normalized value of unity represents complete agreement with the exact solution. Values in Table 3.1 for the normalized distance along the interface, y/W, annotated with a superscript 'F' in parentheses denotes results obtained from the most refined subdomain (see Figure 3.2).

The single-domain analyses with either finite element discretization or finite difference discretization are in excellent agreement with the exact solution. Moreover, the interface force and stress results obtained with multiple-domain analyses using homogeneous modeling with either finite element discretization or finite difference discretization are in excellent agreement with the exact solution. For the heterogeneous modeling, the finite difference method was used in the coarsely discretized domain, and the finite element method was used in the more refined domain. Note that the stresses are used to compare the accuracy of the solution in the finite difference domain, and the internal forces are used to compare the accuracy in the finite element domain. The results obtained from this heterogeneous modeling approach are in overall good agreement with the exact solution.

Table 3.1. Results of the Multifunctional Approach for the Cantilevered Plate.

Location Along Interface, y/W	Analysis Type*									
	SD/FE		SD/FD		MD/FE		MD/FD		MD/HM	
	F_x	F_y	σ_x	τ_{xy}	F_x	F_y	σ_x	τ_{xy}	σ_x	F_x
0.	0.5	0.00	1.00	0.00	0.5	0.00	1.00	0.00	.999	.499
$1/8^{(F)}$	1.00	0.00	1.00	0.00	1.00	0.00	1.00	0.00	-	.999
1/4	1.00	0.00	1.00	0.00	1.00	0.00	1.00	0.00	.999	.999
$3/8^{(F)}$	1.00	0.00	1.00	0.00	1.00	0.00	1.00	0.00	-	.999
1/2	1.00	0.00	1.00	0.00	1.00	0.00	1.00	0.00	.999	1.00
$5/8^{(F)}$	1.00	0.00	1.00	0.00	1.00	0.00	1.00	0.00	-	1.00
3/4	1.00	0.00	1.00	0.00	1.00	0.00	1.00	0.00	1.00	1.00
$7/8^{(F)}$	1.00	0.00	1.00	0.00	1.00	0.00	1.00	0.00	-	1.00
1	0.5	0.00	1.00	0.00	0.5	0.00	1.00	0.00	1.00	.499

*SD/FE: Single-Domain with Finite Element discretization
SD/FD: Single-Domain with Finite Difference discretization
MD/FE: Multiple-Domain with Finite Element discretization
MD/FD: Multiple-Domain with Finite Difference discretization
MD/HM: Multiple-Domain with Heterogeneous Modeling (combined finite difference and finite element discretizations)

CHAPTER IV

REPRESENTATIVE SCALAR-FIELD APPLICATIONS

4.1. GENERAL

In this chapter, the multifunctional methodology is demonstrated on several representative scalar-field applications. The governing partial differential equation for the scalar-field problem is applicable to a variety of problems in engineering science. A sampling of these problems include a torsion problem, a heat conduction problem, and a two-dimensional flow problem. The applications are described, and the associated multifunctional analysis results and salient features are discussed. Finite difference and finite element solutions for single- and multiple-domain configurations are presented to provide benchmark solutions for the multifunctional approach using heterogeneous spatial discretizations. The finite element models use four-node Lagrange isoparametric finite elements, and the finite difference model uses a five-point template to approximate the governing differential equation. Stand-alone finite element software is used to generate the finite element stiffness matrices. The mathematical computing program MATLAB® is used to generate the finite difference matrices and the interface coupling matrices and to solve the resulting system of equations.

4.2. TORSION OF PRISMATIC BAR

The torsion of a prismatic bar with a rectangular cross-section is used to demonstrate the multifunctional capabilities for the Poisson problem. As mentioned in Section 2.2.1, the torsion problem reduces to the nonhomogeneous partial differential equation

$$\frac{\partial^2 \phi}{\partial x^2} + \frac{\partial^2 \phi}{\partial y^2} = -2G\theta$$

in which the stress function, ϕ, must be constant along the boundary of the cross-section, θ is the angle of twist per unit length of the bar, and G is the shear modulus. The configuration of the bar is shown in Figure 4.1, and the analysis domain and the boundary conditions, are shown in Figure 4.2.

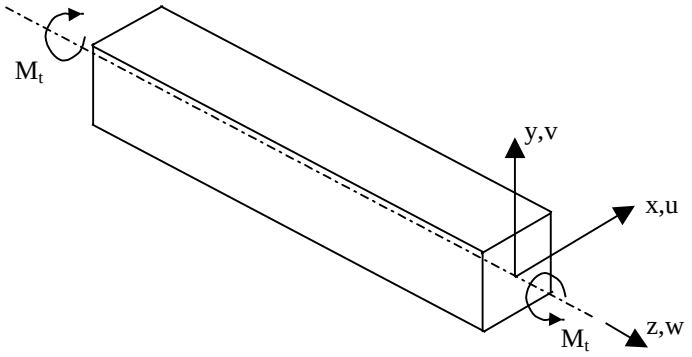

Figure 4.1. Prismatic Bar with Rectangular Cross-Section.

For a solid cross-section, the requirement of a stress-free boundary yields the boundary condition, $\phi = 0$, on all four bounding surfaces along the bar length. Because of the symmetries in the problem, only one quadrant of the rectangular cross-section needs to be considered. Moreover, this symmetric model is useful in verifying the application of mixed boundary conditions. That is, the application of boundary conditions in terms of both primary and secondary variables. The quadrant considered in the symmetric model is shown in Figure 4.3.

The shear stresses in the cross-section are

$$\tau_{zx} = \frac{\partial \phi}{\partial y}, \qquad \tau_{zy} = -\frac{\partial \phi}{\partial x}.$$

At the ends of the bar, the first moment integrated over the cross-sectional area must equal the twisting moment. This requirement gives

$$M_t = 2\int \phi \, dxdy$$

and the twisting moment is related to the angle of twist by

$$M_t = GJ\theta$$

where J is the torsional constant.

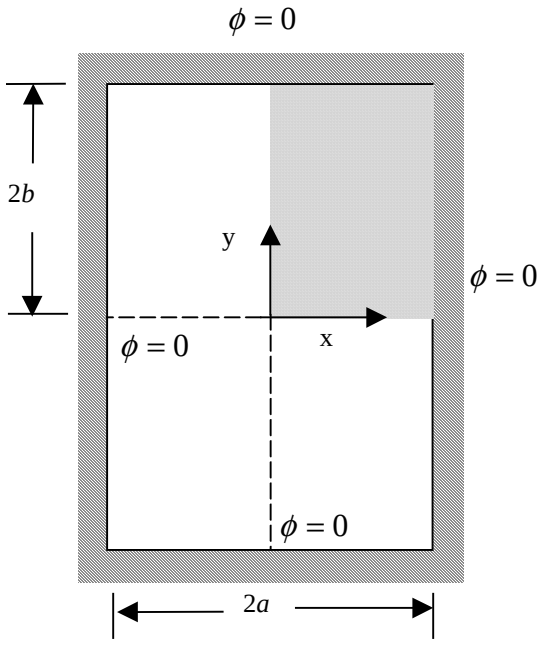

Figure 4.2. Analysis Domain and Boundary Conditions for Prismatic Bar with Rectangular Cross-Section.

The analytical solution[46] for the stress function is given by

$$\phi = \frac{32G\theta a^2}{\pi^3} \sum_{n=1,3,5,\ldots}^{\infty} \frac{1}{n^3}(-1)^{(n-1)/2}\left[1 - \frac{\cosh(n\pi y/2a)}{\cosh(n\pi b/2a)}\right]\cos\frac{n\pi x}{2a},$$

and by differentiating

$$\tau_{zx} = \frac{\partial \phi}{\partial y} = \frac{16G\theta a}{\pi^2} \sum_{n=1,3,5,\ldots}^{\infty} \frac{1}{n^2}(-1)^{(n-1)/2}\left[1 - \frac{\sinh(n\pi y/2a)}{\cosh(n\pi b/2a)}\right]\cos\frac{n\pi x}{2a}$$

and

$$\tau_{zy} = -\frac{\partial \phi}{\partial x} = \frac{16G\theta a}{\pi^2} \sum_{n=1,3,5,\ldots}^{\infty} \frac{1}{n^2}(-1)^{(n-1)/2}\left[1 - \frac{\cosh(n\pi y/2a)}{\cosh(n\pi b/2a)}\right]\sin\frac{n\pi x}{2a}.$$

Assuming that $b>a$, the maximum shearing stress corresponding to the maximum slope, is at the middle points ($y=0$) of the long sides $x=\pm a$ of the rectangular cross-section. Substituting $x=a$, $y=0$ and recognizing that

$$1 + \frac{1}{3^2} + \frac{1}{5^2} + \cdots = \frac{\pi^2}{8}$$

yields

$$\tau_{\max} = \left[2 - \frac{16}{\pi^2} \sum_{n=1,3,5,\ldots}^{\infty} \frac{1}{n^2 \cosh(n\pi b/2a)}\right] G\theta a.$$

In addition, the twisting moment, M_t, is given by

$$M_{\mathrm{t}} = \frac{1}{3} G\theta (2a)^3 (2b)\left(1 - \frac{192}{\pi^5}\frac{a}{b} \sum_{n=1,3,5,\ldots}^{\infty} \frac{1}{n^5} \tanh\frac{n\pi b}{2a}\right).$$

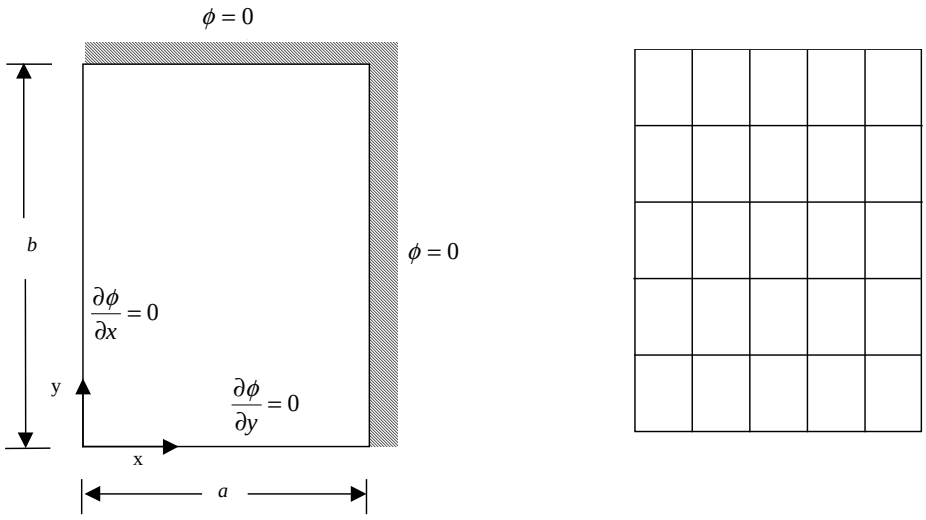

(a) Analysis Domain and Boundary Conditions (b) 6×6 Mesh of Grid Points

Figure 4.3. Analysis Domain, Boundary Conditions and Typical Mesh for One Quadrant of Prismatic Bar with Rectangular Cross-Section.

Spatial Modeling of Prismatic Bar

Analyses are performed for the case of *b=2a* (*i.e.*, rectangular cross-section), where *a* and *b* are dimensions of the cross-section shown in Figure 4.3(a). Three levels of grid refinement are used for the spatial modeling, namely meshes of (6×6), (11×11), and (21×21) grid points, each applied to one quadrant of the domain shown in Figure 4.3(a). A typical idealization for a (6×6) mesh of grid points is shown in Figure 4.3(b). Multiple-domain analyses with the spatial modeling of these three levels of grid refinement and with coincident nodes along the common subdomain boundary have been performed for comparison. For the multiple-domain spatial modeling with non-coincident nodes along the common boundary, the mesh discretization of the most refined domain is consistent with the discretization used in that same region for the single-domain analysis. The mesh in the less refined domain has half the "element"

density of that used in the refined domain. This mesh is referred to by the syntax $(11 \times 11)/(21 \times 21)$. The coarse and fine finite element models, shown in Figure 4.4, are used in the finite element homogeneous spatial modeling. For the finite difference homogeneous modeling and the heterogeneous modeling, a finite difference mesh is used that has the same number of grid points as the finite element mesh in the respective domain.

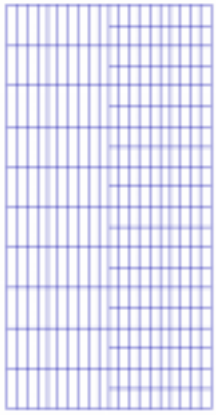

Figure 4.4. Multiple-Domain $(11 \times 11)/(21 \times 21)$ Idealization.

Twisting Moment for the Prismatic Bar

Having found the values of the stress function, ϕ, at the grid points in the solution domain by the respective spatial discretization approaches, the twisting moment may be found by repeated application of the trapezoidal rule for numerical integration. The computed twisting moment is then normalized by the analytical solution. The normalized twisting moment $\left(M_t / M_{t\,analytical}\right)$ obtained using the homogeneous and heterogeneous spatial modeling approaches are given in Table 4.1. A value of unity indicates perfect agreement with the analytical solution. Results in Table 4.1 indicate that all analyses are

in good agreement with the analytical solution. The maximum error in any of the computed solutions is less than 6%. The maximum error value for the multiple-domain analyses is less than 3% and is observed for the multiple-domain heterogeneous modeling analysis (MD/HM) using combined finite difference and finite element discretizations. Note that some of the error is intrinsic to the coarse approximation of the integral using the trapezoidal rule. The integration error decreases as the mesh refinement is increased. A more accurate integration rule such as Simpson's rule would produce results that are more accurate. Independent of the integral approximation, the solution accuracy for each of the modeling methods increases as the mesh refinement increases. For the same number of nodes or grid points, the finite element discretization yields more accurate solutions than the finite difference discretization. The results obtained for the single-domain modeling (*e.g.*, SD/FE and SD/FD) and the multiple-domain homogeneous modeling with coincident nodes along the subdomain boundary are identical or nearly identical (see the results for (6×6), (11×11) and (21×21) meshes in Table 4.1). These results validate the multifunctional approach for coincident grid points along the subdomain boundary. The results obtained for the multiple-domain heterogeneous modeling approach with coincident grid points along the subdomain boundary are less accurate than corresponding results obtained using homogeneous modeling but are in overall good agreement. In addition, with the heterogeneous modeling, the accuracy of the twisting moment increases as the mesh refinement increases. With multiple-domain modeling using finite element (MD/FE) discretization and with non-coincident nodes, the accuracy of the twisting moment is bounded by the accuracy of the less refined (11×11) and more refined (21×21) coincident meshes (see the results for the $(11 \times 11)/(21 \times$

21) mesh in Table 4.1). For the multiple-domain finite difference (MD/FD) discretization in both domains with non-coincident nodes, the twisting moment is slightly less accurate than the results obtained using the (11×11) coincident mesh, which is indicative of the error introduced by the finite difference interface constraints along the common boundary. For the heterogeneous modeling approach with coincident nodes along the interface boundary, the twisting moment is less accurate than the homogeneous approach with either finite element modeling or finite difference modeling. These results reveal the error introduced in the heterogeneous modeling approach for this problem due to the interface constraints. However, recall that the twisting moment is a secondary result, and the errors obtained are larger than those obtained for the primary variable, ϕ, the stress function. For the heterogeneous modeling approach with non-coincident nodes, the twisting moment is slightly more accurate than the (11×11) coincident mesh, which is indicative of the benefit gained (*i.e.,* more accurate field approximation and interface constraint) by the combination of the finite element and finite difference discretizations.

Table 4.1. Normalized Twisting Moment for the Prismatic Bar.

Analysis Type*	Normalized Twisting Moment, $M_t/(M_t)_{analytical}$			
	Mesh Density			
	(6×6)	(11×11)	(21×21)	$(11 \times 11)/(21 \times 21)$
SD/FE	0.9871	0.9944	0.9976	-
SD/FD	0.9743	0.9897	0.9964	-
MD/FE	0.9871	0.9944	0.9976	0.9959
MD/FD	0.9746	0.9898	0.9964	0.9834
MD/HM	0.9498	0.9738	0.9878	0.9749

* SD/FE: Single-Domain with Finite Element discretization
SD/FD: Single-Domain with Finite Difference discretization
MD/FE: Multiple-Domain with Finite Element discretization
MD/FD: Multiple-Domain with Finite Difference discretization
MD/HM: Multiple-Domain with Heterogeneous Modeling (combined finite difference and finite element discretizations)

Maximum Shear Stress for Prismatic Bar

The maximum shear stress, τ_{max}, occurs at $x=a$ and $y=0$ and is obtained by evaluating $\partial\phi/\partial x$ at that point. For the finite element method, the shear stress may be obtained from the element shape functions. However, a more general approximation is used herein to compare the finite element and finite difference computations. Generally, to determine this partial derivative, $\partial\phi/\partial x$, of the stress function, a smooth curve containing the stress function values at the grid points can be assumed to represent the function, ϕ. Newton's interpolation formula[47], used for fitting such a curve, can be used to define the function that is differentiated and evaluated at $x=a$ to give the value of maximum shear. However, due to errors introduced in the interpolation for large amounts of data, a simple backward-difference approximation with the error of the order of Δx^2 was used such that

$$\left(\frac{\partial\phi}{\partial x}\right)_{x=a,\,y=0} = \frac{1}{2\Delta x}\left(\phi_{i-2,\,j} - 4\phi_{i-1,\,j} + 3\phi_{i,\,j}\right)$$

where the subscripts, *i,j*, represent the location of the grid point at which the stress function is sampled (*i.e.*, $x=a$, $y=0$ in this case) and Δx is the distance between the i^{th} and the i-1^{th} grid point. The values for the maximum shear stress, τ_{max}, obtained using the multifunctional approach with single-domain (*e.g.*, SD/FE and SD/FD) and multiple-domain analyses are normalized by the analytical solution, and these normalized values are given in Table 4.2. A value of unity indicates perfect agreement with the analytical solution. The results indicate that all of the analyses are in excellent agreement with the analytical solution. The maximum error in any of the computed solutions is less than 2%. This maximum error value is obtained for the multiple-domain heterogeneous modeling

analysis (MD/HM). In general, the solution accuracy for each of the modeling methods increases as the mesh refinement increases. An exception to this characteristic is observed for the finite element discretization (see the results for the (11×11) and the (21×21) meshes in Table 4.2). In this case, the results are oscillating about the analytical solution. For the same number of nodes or grid points, the finite element discretization yields more accurate solutions than the finite difference discretization. The results obtained for the single-domain modeling and the homogeneous modeling with coincident nodes along the subdomain boundary are identical or nearly identical. As in the case for the twisting moment, this characteristic indicates that the multifunctional approach does not introduce error for the compatible meshes. The results obtained for the multiple-domain heterogeneous modeling approach with coincident grid points along the subdomain boundary are less accurate than corresponding results obtained using homogeneous modeling; however, the results are in overall good agreement. In addition, with the heterogeneous modeling, the accuracy of maximum shear stress increases as the mesh refinement increases. With multiple-domain modeling using finite element discretization and with non-coincident nodes, the accuracy of the twisting moment is bounded by the accuracy of the less refined (11×11) and more refined (21×21) coincident meshes (see the results for the (11×11)/(21×21) mesh in Table 4.2). For the finite difference discretization in both domains with non-coincident nodes, the twisting moment is slightly less accurate than the (6×6) coincident mesh, which is indicative of the error introduced by the finite difference interface constraints along the common boundary. However, the error for all of the finite difference homogeneous analyses is much less than 1%; thus, the difference in the homogeneous modeling is not appreciable.

For the heterogeneous modeling approach with non-coincident nodes, the twisting moment is slightly less accurate than the (11×11) coincident mesh, which, again, is indicative of the benefit gained (*i.e.,* more accurate field approximation and interface constraint) by the combination of the finite element and finite difference discretizations.

Table 4.2. Normalized Maximum Shear for the Prismatic Bar.

Analysis Type*	Normalized Maximum Shear, $\tau_{\max} / (\tau_{\max})_{analytical}$			
	Mesh Density			
	(6×6)	(11×11)	(21×21)	$(11 \times 11)/(21 \times 21)$
SD/FE	1.009	0.9997	0.9993	-
SD/FD	0.9940	0.9973	0.9986	-
MD/FE	1.009	0.9997	0.9993	0.9995
MD/FD	0.9942	0.9973	0.9986	0.9940
MD/HM	0.9842	0.9904	0.9948	0.9902

* SD/FE: Single-Domain with Finite Element discretization
SD/FD: Single-Domain with Finite Difference discretization
MD/FE: Multiple-Domain with Finite Element discretization
MD/FD: Multiple-Domain with Finite Difference discretization
MD/HM: Multiple-Domain with Heterogeneous Modeling (combined finite difference and finite element discretizations)

4.3. HEAT CONDUCTION PROBLEM

In this section, the basic equation of heat conduction is described briefly to provide a convenient reference for the fundamental concepts and equations governing conductive heat transfer. The starting point for heat conduction analysis is Fourier's law given in Cartesian vector form for an isotropic medium[48]

$$\mathbf{q} = -k\nabla T$$

where $\mathbf{q}$ is a vector whose components are the heat flow per unit area in the respective Cartesian directions, k is the thermal conductivity coefficient that may be a function of the temperature, T, and

$$\nabla = \frac{\partial}{\partial x}\mathbf{i} + \frac{\partial}{\partial y}\mathbf{j} + \frac{\partial}{\partial z}\mathbf{k} .$$

In an isotropic solid with temperature-dependent thermal conductivity, the law of conservation of energy with Fourier's law yields the thermal energy equation. The law of conservation of energy is given by

$$-\left(\frac{\partial q_x}{\partial x} + \frac{\partial q_y}{\partial y} + \frac{\partial q_z}{\partial z}\right) + Q = \rho c \frac{\partial T}{\partial t}$$

where Q is the internal heat generation rate per unit volume, ρ is the mass density, c is the specific heat, and t is time. For constant thermal properties and steady-state heat transfer, the heat conduction problem reduces to a nonhomogeneous partial differential equation of the form of Eq. (2.1) and is given by

$$-k\left(\frac{\partial^2 T}{\partial x^2} + \frac{\partial^2 T}{\partial y^2}\right) = Q$$

In this work, two-dimensional heat conduction in a square plate (see Figure 4.5) is used to demonstrate the multifunctional capabilities for thermal analysis. For this problem, the time-independent, heat conduction equation is

$$-\left(\frac{\partial^2 T}{\partial x^2} + \frac{\partial^2 T}{\partial y^2}\right) = \frac{Q}{k} \text{ in } \Omega = \{(\mathrm{x}, \mathrm{y}): \quad 0 < (x, y) < 1\}$$

subject to the boundary conditions

$$\begin{aligned} T &= 0 \text{ on } \Gamma^{\mathrm{p}} = \{\text{lines } x = 1 \text{ and } y = 1\} \\ \frac{\partial T}{\partial n} &= 0 \text{ on } \Gamma^{\mathrm{s}} = \{\text{lines } x = 0 \text{ and } y = 0\} \end{aligned}.$$

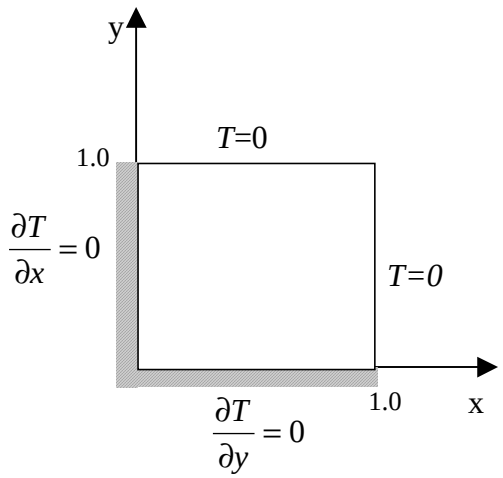

Figure 4.5. Analysis Domain and Boundary Conditions for the Steady-State Heat Conduction in a Square Plate.

Spatial Modeling of Square Plate

The spatial discretizations in the analyses were selected to be comparable to those reported by Reddy[32] for this problem. Coarse and fine models are used in each of the subdomains. The coarse model has a (2×3) nodal grid, and the fine model has a (3×5) nodal grid. The syntax $(m \times n)$ is used to denote spatial modeling with m grid points in the x-direction and n grid points in the y-direction. The number of grid points, rather than the number of elements, in the coordinate directions are used to describe the mesh densities to provide consistency when discussing the finite difference and finite element discretizations. Combinations of these mesh densities are used for comparative purposes where the letters C and F are used to denote the coarse and fine models, respectively. A multiple-domain model with finite element models discretized with a fine (3×5) nodal grid and a coarse (2×3) nodal grid is shown in Figure 4.6. Curves labeled C/C or F/F denote multiple-domain coarse or fine models, respectively, with coincident nodes along the common subdomain boundary. Multiple-domain analyses with finite element

discretization or finite difference discretization are denoted by MD/FE and MD/FD, respectively. Similarly, multiple-domain analyses using heterogeneous modeling with the combination of finite difference and finite element discretizations are denoted by MD/HM.

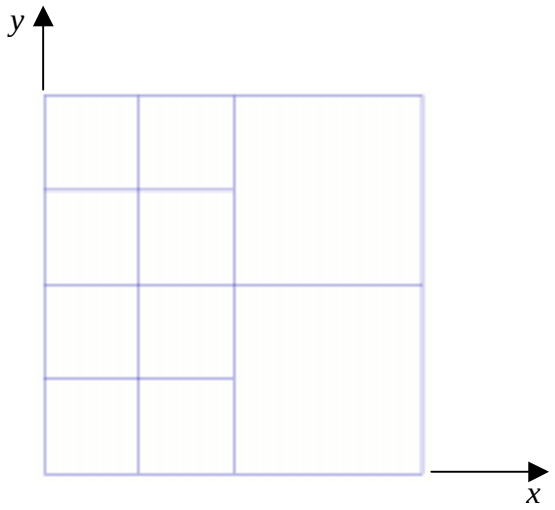

Figure 4.6. Homogeneous $(3 \times 5)/(2 \times 3)$ Idealization.

Temperature Distribution for Square Plate

The temperature distribution as a function of the distance along the *y=0* line is shown in Figure 4.7 for the different spatial discretizations and modeling approaches. The analytical solution for this problem is given by

$$T(x,y) = \frac{1}{2}\left\{\left(1-y^2\right) + \frac{32}{\pi^3}\sum_{n=1}^{\infty}\frac{(-1)^n \cos[(2n-1)\pi y/2]\cosh[(2n-1)\pi x/2]}{(2n-1)^3 \cosh[(2n-1)\pi/2]}\right\}$$

In addition, a 1-parameter Ritz approximation is given by

$$T(x,y) = \frac{5Q}{16k}\left(1-x^2\right)\left(1-y^2\right)$$

Results obtained using the multifunctional approach are compared to the analytical solution (solid line in the figure) and a Ritz approximation (dashed line in the figure). Finite element (see Figure 4.7(a)) and finite difference (see Figure 4.7(b)) solutions were obtained using a multiple-domain analysis with homogeneous spatial discretization and are in excellent agreement with the analytical solution. These results illustrate that the temperature at $x=y=0$ obtained with a coarse finite difference mesh is more accurate than that obtained with a comparable finite element mesh (see curves labeled MD/FE-C/C and MD/FD-C/C in Figure 4.7(a) and Figure 4.7(b)). This difference decreases as the meshes are refined, although the finite element model continues to produce a higher temperature value at $x=y=0$. The multiple-domain analyses with non-coincident nodes produce accurate results even at the subdomain common boundaries. The multiple-domain results for heterogeneous spatial discretization approaches are shown in Figure 4.7(c) and indicate the effectiveness of the multifunctional approach. The fine (3×5) nodal grid (see Figure 4.6) is discretized with the finite difference method, and the coarse (2×3) nodal grid is discretized with the finite element method. These results are in overall agreement with the results obtained with the homogeneous approaches. The homogeneous and heterogeneous results are compared in Figure 4.7(d) for models with non-coincident nodes with a fine model in the left domain and a coarse model in the right (see Figure 4.6). These results indicate that temperatures obtained with the heterogeneous approach are slightly lower than for the homogeneous approach with either finite element or finite difference discretizations. In addition, the results, obtained by using the finite difference discretization in one or both of the domains, illustrate the slight difference in the temperature at the interface from the

left and the right domains. However, note that the uniqueness of the solution along the interface boundary is satisfied only in an integral sense and this slight difference does not detract from the overall accuracy and effectiveness of the multifunctional approach for this Poisson problem.

An additional analysis has been performed to demonstrate the multifunctional capability for an inclined subdomain boundary (boundary not parallel to the *y*-axis). In this analysis, multiple-domain modeling with the finite element method is used. The finite element model used in the analysis has a (3×6) mesh of grid points in the left domain and a (2×3) mesh of grid points in the right domain as shown in Figure 4.8. The results for this multiple-domain finite element analysis are shown in Figure 4.9. These results (open squares) are compared to the analytical solution (solid line), the Ritz approximation (dashed line) and the multiple-domain finite element analysis (see Figure 4.6 for the model discretization) with a subdomain boundary parallel to the *y*-axis (open circles). The results indicate the effectiveness of the multifunctional approach for the inclined subdomain boundary.

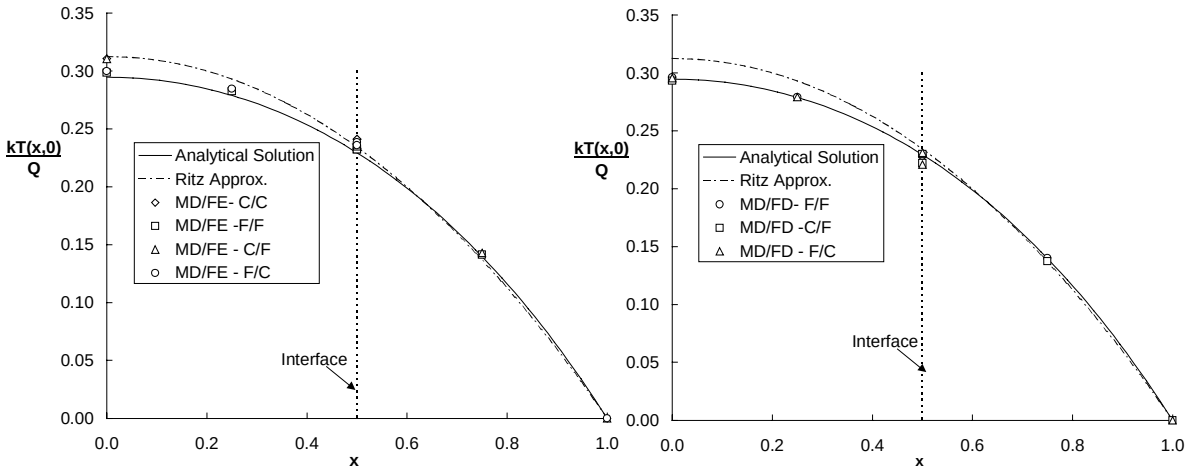

(a) Multiple-Domain Finite Element (MD/FE) Modeling

(b) Multiple-Domain Finite Difference (MD/FD) Modeling

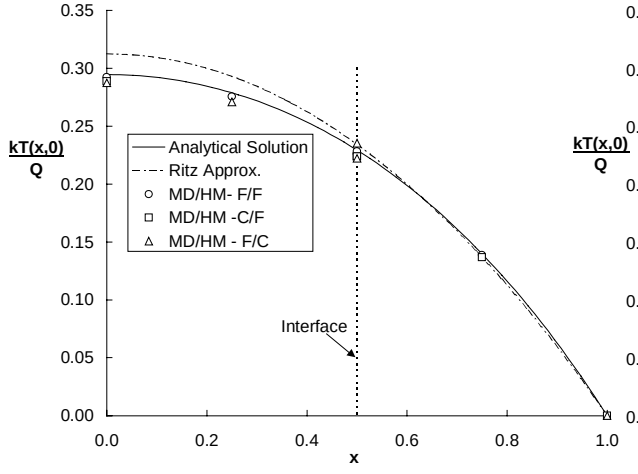

(c) Multiple-Domain Heterogeneous (MD/HM) Modeling

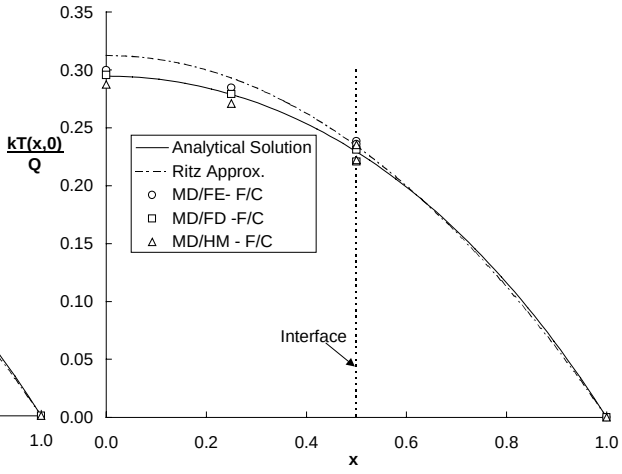

(d) Multiple-Domain Homogeneous and Heterogeneous Modeling

Figure 4.7. Temperature Distribution Along Insulated Edge of Square Plate.

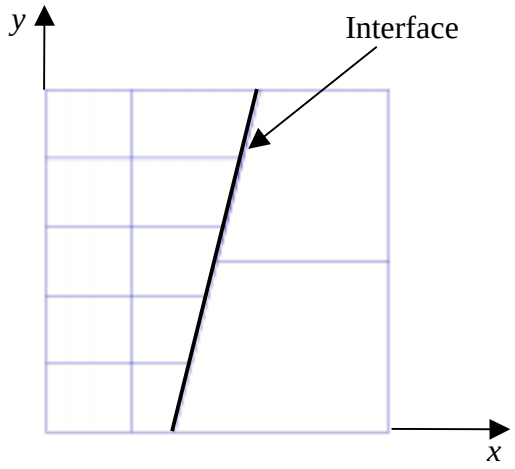

Figure 4.8. Spatial Discretization for Inclined Interface for Square Plate.

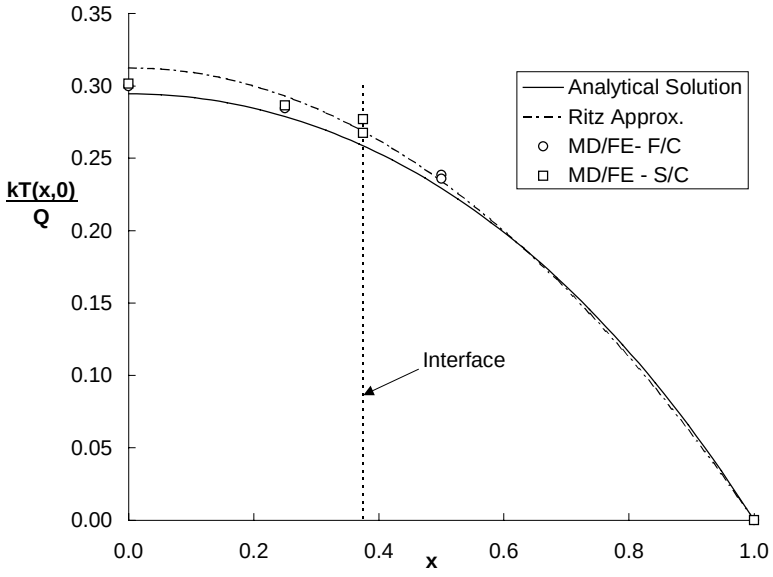

Figure 4.9. Temperature Distribution Along Insulated Edge of Square Plate with Inclined Interface.

4.4. POTENTIAL FLOW PROBLEM

A two-dimensional fluid flow problem is used to demonstrate the multifunctional capabilities for a fluid mechanics problem. As shown in Section 2.2.2, the equation governing irrotational fluid flow reduces to the Laplace equation

$$\frac{\partial^2 u}{\partial x^2} + \frac{\partial^2 u}{\partial y^2} = 0$$

where u can be either the stream function, ψ, or the velocity potential, ϕ. In this work, the two-dimensional, steady, inviscid flow between two infinite plates is considered. A rigid, infinite cylinder or radius, R, with an axis at a right angle to the flow is assumed to be in the passageway between the plates as shown in Figure 4.10. Far upstream from the cylinder there is a uniform flow field with a velocity of V_0. Because of the symmetries in this problem, only one quadrant of the domain is considered. The analysis domain and the boundary conditions on the velocity potential, ϕ, are shown in Figure 4.11.

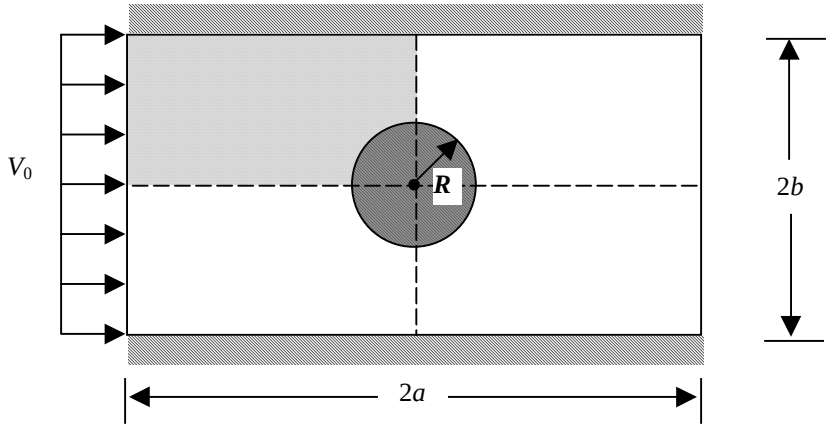

Figure 4.10. Domain of Flow Around Cylinder.

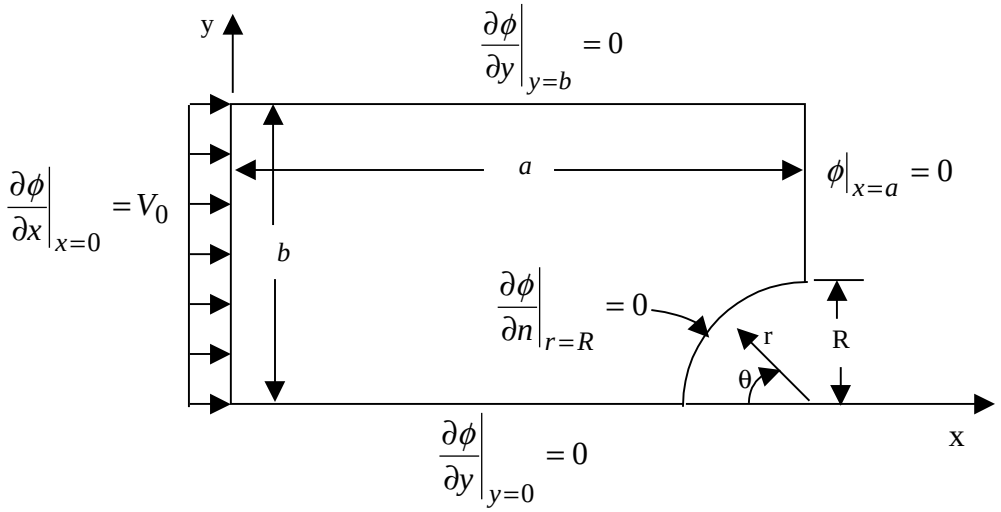

Figure 4.11. Analysis Domain of Flow Around Cylinder.

The finite element models used in this problem are shown in Figure 4.12. A reference solution is obtained using the finite element model shown in Figure 4.12(a). The local and global finite element models used in the homogeneous and heterogeneous spatial modeling approaches are shown in Figure 4.12(b). For the heterogeneous modeling, a finite difference mesh is used in the coarsely refined domain that has the same number of grid points as the finite element mesh used in the same domain. This discretization strategy illustrates the use of the finite element method to represent the complex geometry around the cylinder and the use of the finite difference method away from the curved boundary where it is most suitable.

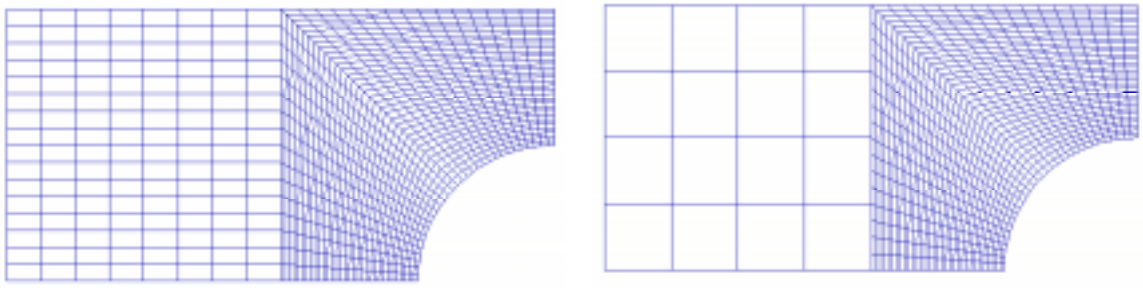

(a) Reference Model (b) Multiple Domain Model

Figure 4.12. Spatial Discretization for One Quadrant of Domain of Flow Around Cylinder.

Contour plots for the velocity potential, the horizontal velocity component and the transverse velocity component are shown in Figure 4.13, Figure 4.14, and Figure 4.15, respectively. In each of these figures, the results using the multifunctional approach are compared to results obtained from the single-domain analysis using the reference model (see Figure 4.12(a)). As shown in the figures, the velocity potential and the velocity components obtained using the multifunctional approach are in excellent agreement with the reference solution. In the multiple-domain analyses, the slight discontinuity in the horizontal and transverse velocity components at the interface (see Figure 4.14(b) and Figure 4.15(b)) is due in part to the difference in the computation of the velocity across the interface. Unlike in the single-domain analysis (*i.e.*, reference solution), in the multiple-domain analyses, the velocities are not averaged across the interface.

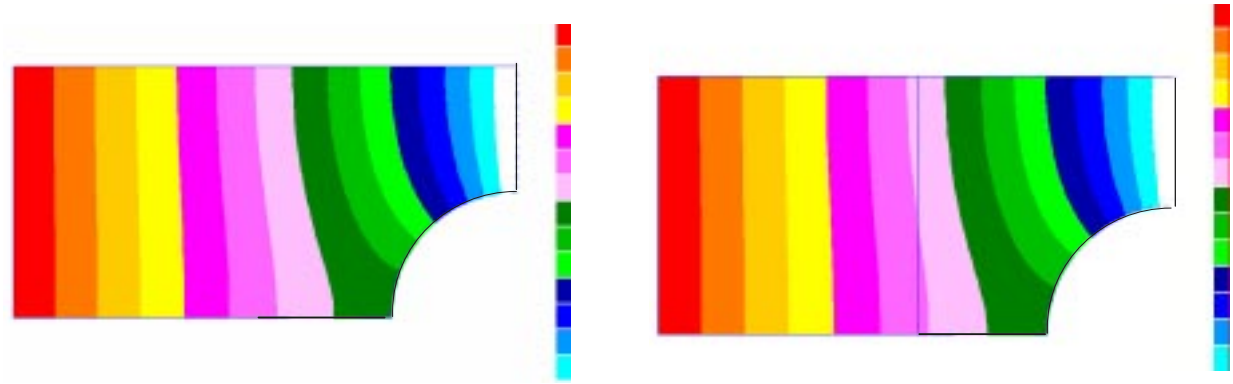

(a) Single-Domain Model (b) Multiple-Domain Model

Figure 4.13. Contour Plot of Velocity Potential for Flow Around Cylinder.

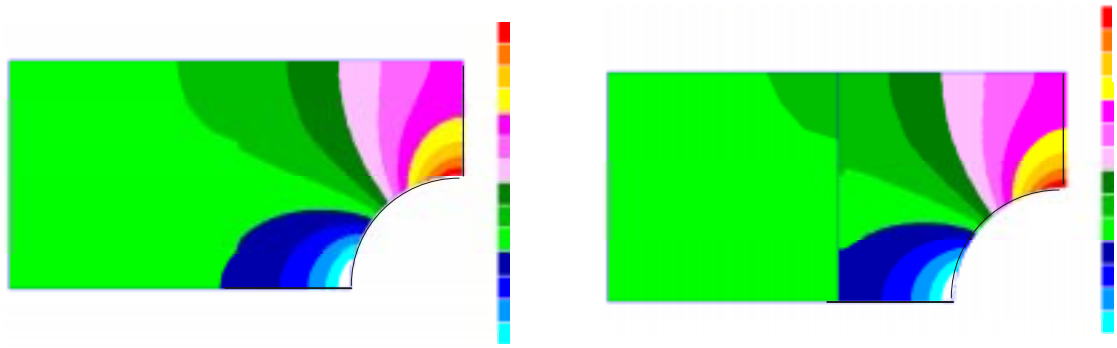

(a) Single-Domain Model (b) Multiple-Domain Model

Figure 4.14. Contour Plot of Horizontal Velocity Component for Flow Around Cylinder.

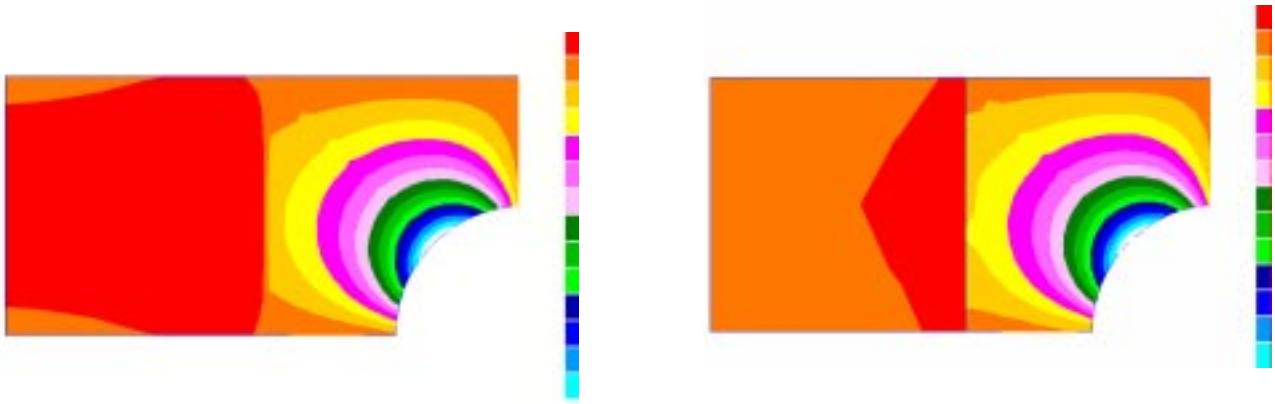

(a) Single-Domain Model (b) Multiple-Domain Model

Figure 4.15. Contour Plot of Transverse Velocity Component for Flow Around Cylinder.

The analytical potential solution for the tangential velocity around a cylinder in an infinite domain, valid on the cylinder surface, is given by

$$u_t = V_0\left(1+\frac{R^2}{r^2}\right)\sin\theta$$

where the angle, θ, radial distance, r, and the tangential velocity, u_t, can be computed from the relations

$$\theta = \tan^{-1}\left(\frac{y}{a-x}\right), \quad r = \left[(a-x)^2 + y^2\right]^{1/2}, \quad u_t = u_x \sin\theta + u_y \cos\theta.$$

The tangential velocity as a function of the angular distance along the cylinder surface is shown in Figure 4.16. Results are shown for the tangential velocity around a cylinder in an infinite domain for which an analytical solution is known and in a finite domain for which a reference solution is obtained using a refined single-domain finite element model. For the infinite domain configuration, the plate length to cylinder radius ratio,

$2a/R$, and the plate width to cylinder radius ratio, $2b/R$, are 40 and 20, respectively, and the domain can be considered as infinite. That is, the cylinder radius, *R*, is very small compared to the length, *2a*, and the width, *2b*. For the finite domain configuration, the plate length to cylinder radius ratio, $2a/R$, and the plate width to cylinder radius ratio, $2b/R$, are 4 and 2, respectively, and the domain is considered to be finite. The tangential velocity obtained for the multifunctional approach is in overall good agreement with the analytical solution for the infinite domain and with the reference solution (*i.e.*, single-domain analysis) for the finite domain. Results obtained with homogeneous multiple-domain analyses with finite element discretization in each domain are denoted by open circles in the figure. Results obtained with heterogeneous multiple-domain analyses with combined finite difference and finite element discretization are denoted by open squares in the figure. The tangential velocity obtained with the homogeneous modeling approach is in excellent agreement with the analytical and reference solutions for the infinite and finite domain configurations. The tangential velocity obtained with the heterogeneous modeling approach is more accurate for the infinite domain configuration than for the finite domain configuration. This characteristic is indicative of the performance of the finite difference approach, for this problem, in a gradient region.

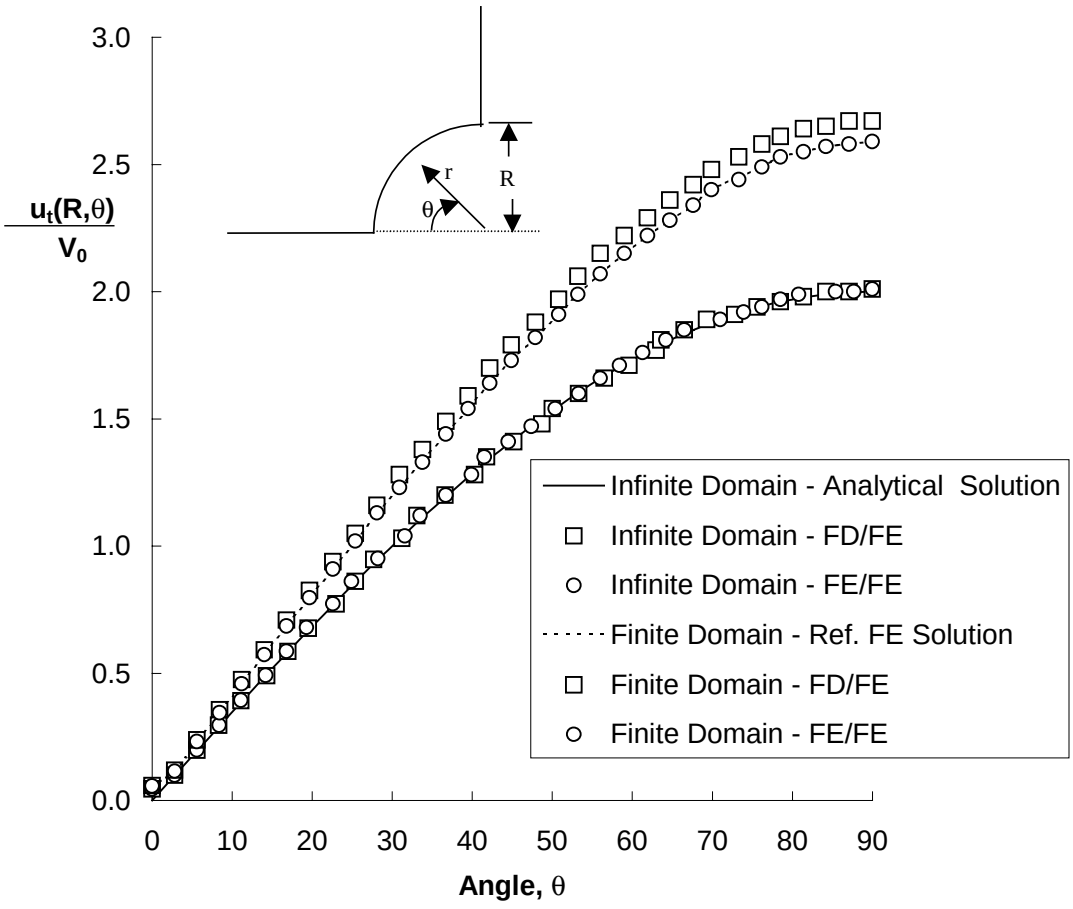

Figure 4.16. Tangential Velocity for Flow Around Cylinder.

4.5. SUMMARY

In this chapter, the multifunctional methodology has been described and demonstrated for a variety of problems in engineering science. These selected problems included second-order problems of solid mechanics, heat transfer, and fluid mechanics that can be formulated in terms of one dependent variable. The governing equation in each case is either the Laplace or the Poisson equation. The analyses performed have

demonstrated the effectiveness and accuracy of the solutions obtained for the respective problems. In all cases, the results obtained using the multifunctional methodology were in overall good agreement with the reported analytical or reference solution. In the next chapter, the multifunctional methodology is demonstrated for problems whose motion is described by coupled partial differential equations expressed in terms of two dependent variables -- vector-field problems.

CHAPTER V

REPRESENTATIVE VECTOR-FIELD APPLICATIONS AND EXTENSIONS

5.1. GENERAL

In this chapter, the multifunctional methodology is demonstrated on two representative vector-field applications. The applications are described and the associated results and salient features are discussed. The applications include a plane stress problem and a plane flow problem. Finite difference and finite element solutions for single- and multiple-domain configurations are presented to validate the multifunctional approach using heterogeneous discretization. The finite element models use four-node Lagrange isoparametric finite elements, and the finite difference model uses a nine-point template to approximate the governing differential equation. Stand-alone finite element software is used to generate the finite element stiffness matrices. The mathematical computing program MATLAB® is used to generate the finite difference matrices and the interface coupling matrices and to solve the resulting system of equations. In addition, extensions to multiple discipline analyses are discussed.

5.2. PLANE STRESS PROBLEM

A rectangular plate of uniform thickness subjected to a uniform tensile load and with a central circular cutout (shown in Figure 5.1) is an ideal example problem with which to verify the multifunctional approach. The example problem has a variety of practical applications (*i.e.,* rivet holes, aircraft door and window openings, etc.), and an exact solution is available[46]. The plate has been used by many researchers to verify

aspects of proposed computational methodologies. For example, the plate problem has been used by Ransom[8] to verify global/local analysis technology, by Aminpour et al.[25] to verify multiple-domain homogeneous modeling using the finite element method, and by Rose[10] to verify an adaptive geometry generator used with a multiple-domain finite element model. The plate configuration is such that the state of stress is represented by the condition of plane stress or plane strain. The membrane displacements, *u* and *v*, in the axial (*x*-direction) and transverse (*y*-direction) directions, respectively, represent the plate configuration in plane stress and plane strain.

Two configurations of this problem have been studied: an infinite plate and a finite-width plate. The infinite plate configuration has a central cutout that is very small relative to the length and width of the plate, and the exact solution for this problem was obtained by Timoshenko[46]. The stress distribution in the neighborhood of the cutout exhibits a stress concentration, but from Saint-Venant's principle, the stress distribution is essentially uniform at distances that are large compared with the radius of the cutout. The finite-width plate configuration has a larger central cutout relative to the length and width, and the stress distribution away from the cutout is not uniform. The finite-width plate with a central circular cutout has been discussed by Howland[49] and Peterson[50].

For the infinite plate configuration, herein, the length to radius ratio, $2a/R$, and the width to radius ratio, $2b/R$, are 40 and 20, respectively, and the plate can be considered as infinite. That is, the cutout radius, *R*, is very small compared to the length, *2a*, and the width, *2b*. The material system is aluminum with a Young's modulus of 10^7 psi, and a Poisson's ratio of 0.3, and the thickness of the plate, *h*, is 0.1 in. A uniform running load, $(N_x)_0$, is applied to each of its ends, and the other sides are free. The plate

example problem is used to verify the multifunctional approach for both homogeneous and heterogeneous spatial modeling. Because of the symmetry that exists, one quadrant of the domain (see Figure 5.2) is modeled. In addition, boundary conditions are shown in Figure 5.2 where T_n and T_t denote normal and tangential tractions, respectively. For the multiple-domain analysis, a refined model is used in the near-field subdomain (*i.e.*, the local region near the cutout), and a coarse, less-refined model is used in the remainder of the domain. A single-domain analysis using a finite element model that has the same number of nodes and elements in the near-field region as the multiple-domain model is used to obtain a reference solution with which to compare the solution obtained with the multifunctional approach. The single-domain model and the multiple-domain model (used in the homogeneous spatial modeling) are shown in Figure 5.3. For the homogeneous modeling, a finite element (FE) mesh is used in each region. For the heterogeneous modeling, a finite difference (FD) mesh is used in the far-field region that has the same number of grid points as the finite element mesh in that region. A finite element mesh is used in the region near the cutout.

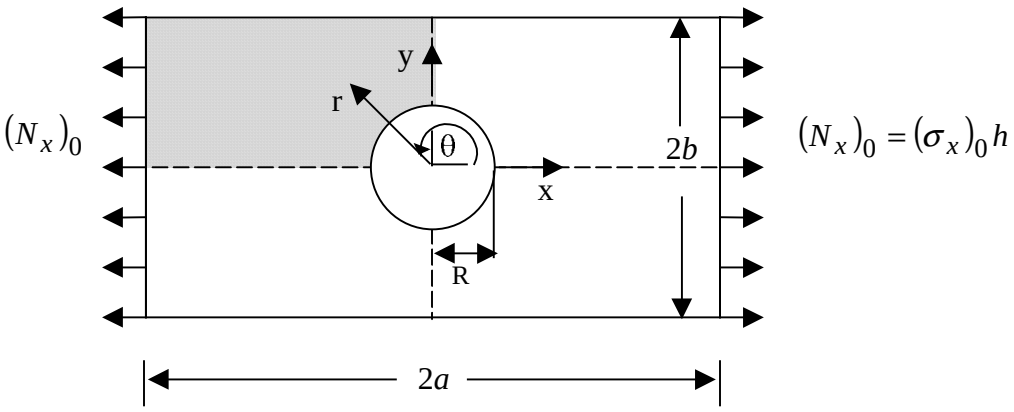

Figure 5.1. Domain of Plate with Central Circular Cutout.

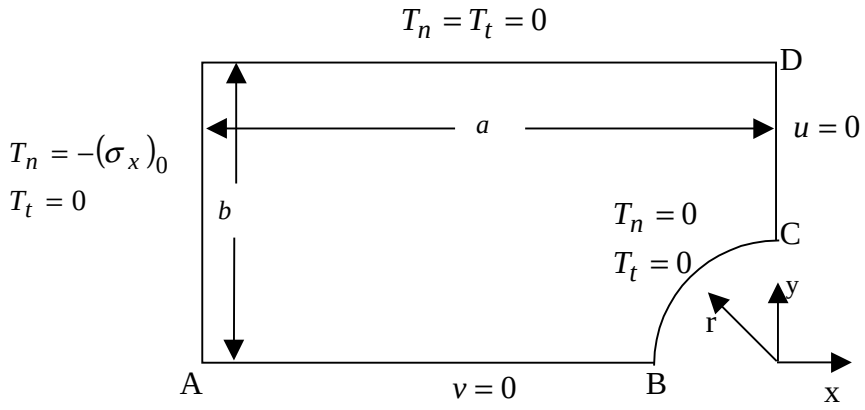

Figure 5.2. Geometric Configuration for One Quadrant of Plate with Central Circular Cutout.

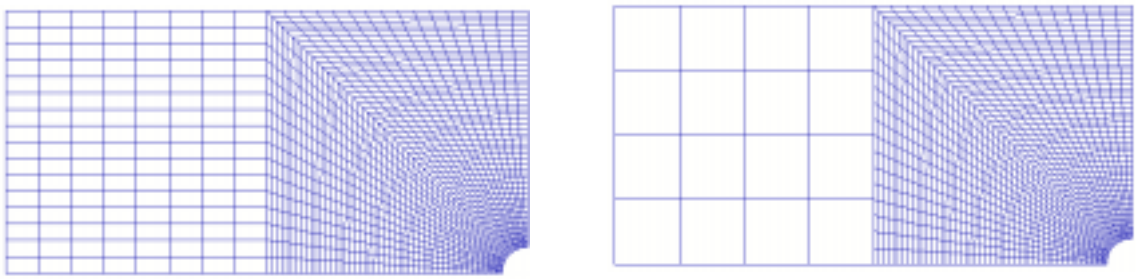

(a) Single-Domain Model (b) Multiple-Domain Model

Figure 5.3. Finite Element Models for One Quadrant of Infinite Plate with Central Circular Cutout.

The exact elasticity solution[46] for an infinite plate with a circular cutout loaded in tension indicates that the stress concentration factor, K_t, is 3.0 at the edge of the cutout and is given by

$$K_t = \frac{(N_x)_\theta\big|_{(R,\pi/2)}}{(N_x)_0}.$$

The stress concentration factor is defined as the ratio of the maximum stress resultant, $(N_x)_{max}$, to the uniform far-field stress resultant, $(N_x)_0$. Stress concentration factors

obtained using the multifunctional approach with homogeneous and heterogeneous modeling are 3.08 and 3.10, respectively, which is within 2.7% and 3.3% of the elasticity solution. The stress distributions of the hoop stress resultant $(N_x)_\theta$ along the midwidth, $\theta=\pi$, (denoted as line AB in Figure 5.2) and midlength, $\theta=\pi/2$, (denoted as line CD in Figure 5.2) normalized by the far-field stress resultant $(N_x)_0$, are shown in Figure 5.4 as a function of the distance from the plate center normalized by cutout radius, *R*. The elasticity solution for the stress distribution is given by

$$(N_x)_\theta = \frac{1}{2}(N_x)_0\left[\left(1+\frac{R^2}{r^2}\right)-\left(1+\frac{3R^4}{r^4}\right)\cos 2\theta\right]$$

and is shown by the solid lines in the figure. The stress distributions obtained from the multifunctional analyses using homogeneous modeling are indicated by the open circles in the figure. The stress distributions obtained from the multifunctional analyses using heterogeneous modeling are indicated by the open squares in the figure. Excellent correlation is observed for all analyses.

Contour plots of the magnitude, δ, of the displacement vector (*i.e.*, $\delta = \sqrt{u^2 + v^2}$) superimposed on the deformed shape and the longitudinal stress resultant, N_x, are shown in Figure 5.5 and Figure 5.6, respectively. The multiple-domain analysis results are shown for homogeneous modeling using finite element discretization in each of the subdomains. To aid visual comparison, the deformation has been magnified by 10% of the maximum domain dimension. The displacement contour plots reveal the nearly linear variation along the plate length in the far-field region of the plate with only local changes near the cutout. The stress resultant contour plots reveal the uniform stress state away from the cutout and the peak stress in the neighborhood of the

cutout. While not shown, the results for the multiple-domain heterogeneous modeling approach are nearly identical to those shown in Figure 5.5 and Figure 5.6, and thus have not been included. These contour plots illustrate further the excellent correlation among the multifunctional approach using homogeneous and heterogeneous modeling and the single-domain solution.

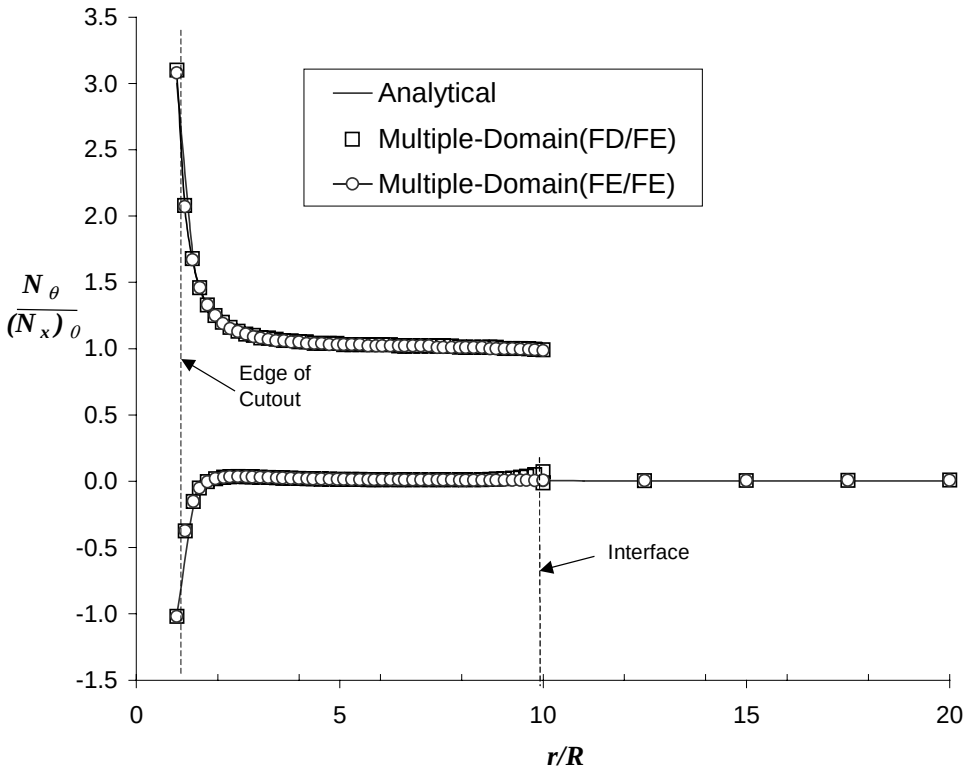

Figure 5.4. Longitudinal Stress Distribution along Midwidth and Midlength for Infinite Plate with Central Circular Cutout.

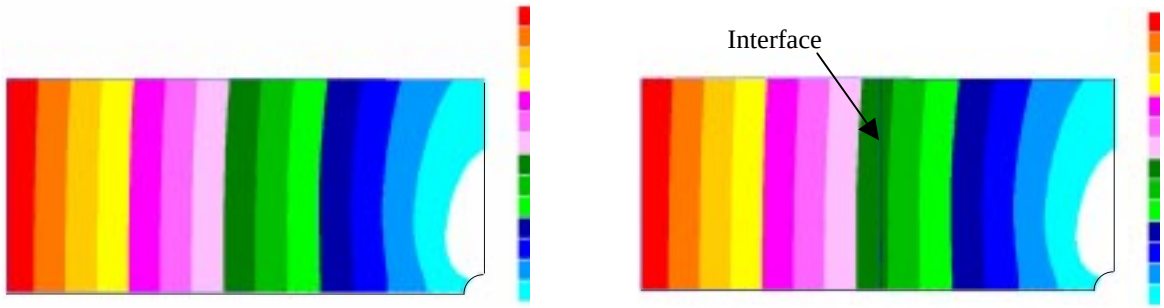

(a) Single-Domain Model (b) Multiple-Domain Model

Figure 5.5. Displacement Magnitude Distribution for Infinite Plate with Central Cutout.

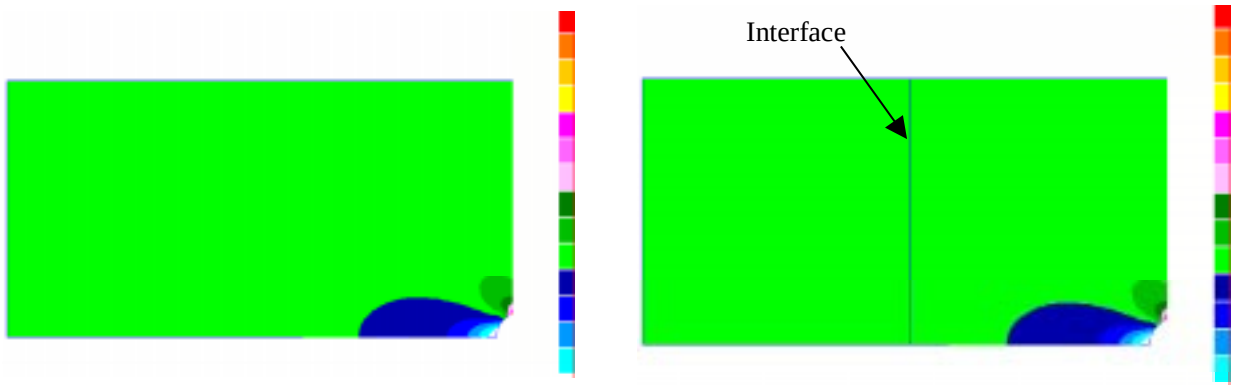

(a) Single-Domain Model (b) Multiple-Domain Model

Figure 5.6. Longitudinal Stress Resultant Distribution for Infinite Plate with Central Cutout.

While the infinite plate analyzed, herein, is an excellent test of the multifunctional approach, gradients in the deformation and the stress resultants, as indicated in Figure 5.5 and Figure 5.6, are well away from the subdomain interface boundary. Thus, to assess the accuracy of the approach when the subdomain interface is within a high gradient region, a second configuration is analyzed.

In the finite-width plate configuration, the length to radius ratio, $2a/R$, and the width to radius ratio, $2b/R$, are 4 and 2, respectively, and the plate is considered to be

finite. The aluminum material system and the thickness that was used for the infinite plate is used here for the finite-width plate. The finite-width effects on the stress concentration factor for isotropic plates with cutouts have been reported by Peterson[50]. By including finite-width effects, the stress concentration factor is reduced from the value of three for an infinite plate. The stress concentration factor should be applied to the nominal stresses, which are based on the net cross-sectional area associated with the load application. For the case of a finite-width plate with a cutout, the net cross-sectional area corresponds to

$$A_{net} = (2b - 2R_0)h = 2bh\left(1 - \frac{R}{b}\right)$$

where h is the plate thickness, and the nominal longitudinal stress for an uniaxial load, P, can be expressed as

$$(\sigma_x)_{nom} = \frac{P}{A_{net}} \text{ and } (N_x)_{nom} = (\sigma_x)_{nom} h \,.$$

The geometry definition for the finite-width plate, herein, gives a stress concentration factor of 2.16 reported by Peterson.

Multiple-domain homogeneous and heterogeneous modeling approaches are used for the finite-width plate. A refined model is used in the near-field domain, and a less-refined model is used in the far-field domain. The single-domain model and the multiple-domain model are shown in Figure 5.7. In the multiple-domain homogeneous modeling approach, finite element (FE) discretization is used in each domain. In the multiple-domain heterogeneous modeling approach, finite difference (FD) discretization is used in the far-field domain, and finite element (FE) discretization is used in the near-field domain around the cutout.

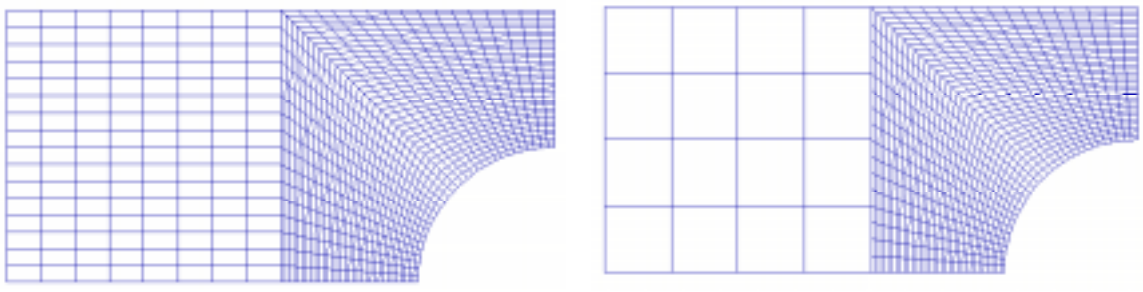

(a) Single-Domain Model (b) Multiple-Domain Model

Figure 5.7. Finite Element Models for One Quadrant of Finite-Width Plate with Central Cutout.

Stress concentration factors obtained using the multifunctional approach with homogeneous (multiple-domain FE/FE) and heterogeneous (multiple-domain FD/FE) modeling are 2.19 and 2.73, respectively. These factors are higher by 1.4% and 26.4%, respectively, than the values given in Peterson[46]. Note that the solution obtained using the heterogeneous modeling approach with finite difference and finite element discretizations is nearly 30% in error. This error is likely due to the inaccuracy of the finite difference method in the high gradient region and to the constraint conditions along the interface.

To delineate this error, additional heterogeneous analyses are performed using finite difference domains with grid spacing in the transverse direction of one half (*i.e.*, 9×9 mesh of grid points) and one fourth (*i.e.*, 17×17 mesh of grid points) the grid spacing in the initial finite difference domain (*i.e.*, 5×5 mesh of grid points) (see Figure 5.7(b)). The stress concentration factors obtained with these more refined finite difference discretizations are 2.42 and 2.31, which are within 12% and 7% of the

Peterson's solution[46]. The stress distributions of the hoop stress resultant $(N_x)_\theta$ midlength, $\theta=\pi/2$, (denoted as line CD in Figure 5.2) normalized by the nominal stress resultant $(N_x)_{nom}$, are shown in Figure 5.8 as a function of the distance from the plate center normalized by cutout radius, *R*. The analytical solution reported by Howland[49] is denoted by the thick solid line. The stress distribution obtained using 5×5, 9×9 and 17×17 mesh of grid points are denoted by the short dashed line, the thin solid line, and the dashed and dotted line, respectively. The results shown in Figure 5.8 indicate that the error decreases as the finite difference grid density increases, and the error decreases away from the edge of the cutout.

The stress distributions of the hoop stress resultant $(N_x)_\theta$ along the midwidth, $\theta=\pi$, (denoted as line AB in Figure 5.2) and midlength, $\theta=\pi/2$, (denoted as line CD in Figure 5.2) normalized by the nominal stress resultant $(N_x)_{nom}$, are shown in Figure 5.8 as a function of the distance from the plate center normalized by cutout radius, *R*. The analytical solution reported by Howland[49] is denoted by the solid lines. This analytical solution is valid for distances, *r*, away from the cutout of less than the plate half-width, *b*. Thus, for this configuration the solution along the midwidth is valid only for $r \leq 2R$. The stress distribution for the multifunctional analysis using homogeneous modeling with finite element discretization in each of the domains is denoted by the open circles in the figure. The stress distribution for the multifunctional analysis using heterogeneous modeling with combined finite difference and finite element discretizations is denoted by the open squares in the figure. For the heterogeneous modeling approach, the distribution is given for the most refined finite difference discretization (*i.e.*, 17×17 mesh of grid points). The stress distributions obtained with the multifunctional approach using

homogeneous and heterogeneous discretization are in excellent agreement with the reported solution.

Contour plots of the magnitude of the displacement vector superimposed on the deformed shape and the longitudinal stress resultant, N_x, are shown in Figure 5.10 and Figure 5.11, respectively. Results for the multiple-domain homogeneous modeling approach using finite element discretization in each of the subdomains are shown in the figures. While not shown, the results for the multiple-domain heterogeneous modeling approach are nearly identical to those shown in Figure 5.10 and Figure 5.11, and thus have not been included. Note that the deformation has been magnified by 10% of the maximum domain dimension. The displacement contour plots reveal a deviation from the nearly linear variation observed in the far-field region of the infinite plate, and the deformation at the cutout is more pronounced. The contour plots illustrate further the excellent correlation of the deformation (primary variable) patterns predicted using the multifunctional approach with the single-domain solution even with the interface boundary domain in a high-gradient region. The stress resultant (secondary variable) patterns predicted using the multifunctional approach are also in excellent agreement. The slight discontinuity in the stress resultant at the subdomain boundary (*i.e.*, interface) is due to the derivation of the nodal stress resultant values from the element quantities. The stress resultants are recovered at the finite element nodes by extrapolating the stresses at the integration points to the nodes. A single nodal value of the stress resultant is obtained by averaging the stress resultants of the adjacent elements. In the multiple-domain analyses, the stress is not averaged across the subdomain boundary; thus, any gradient across the interface is not considered.

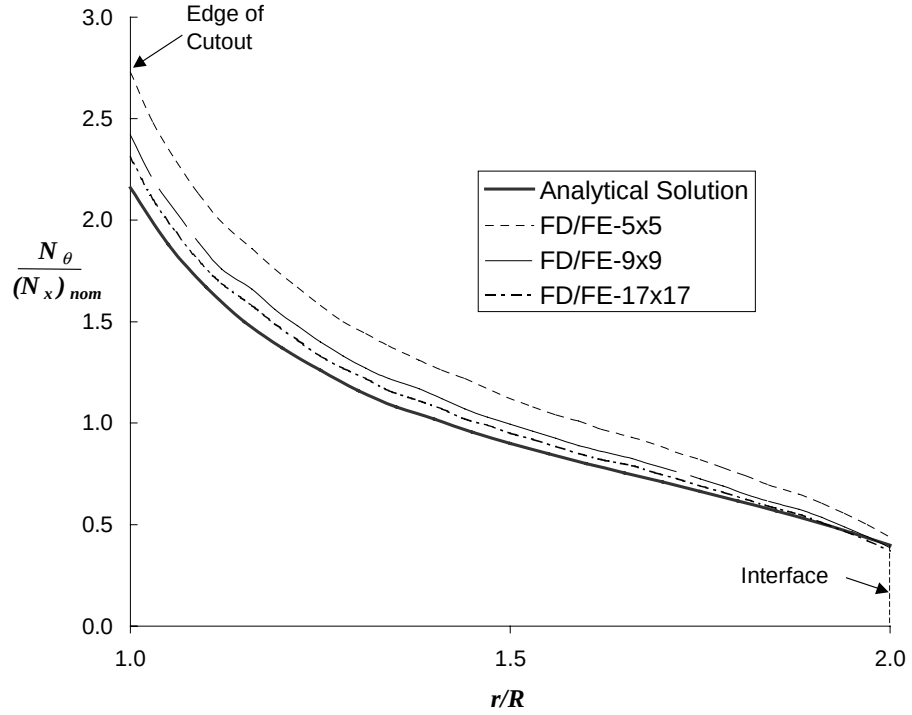

Figure 5.8. Convergence of Longitudinal Stress Distribution along Midlength for Finite-Width Plate with Central Circular Cutout.

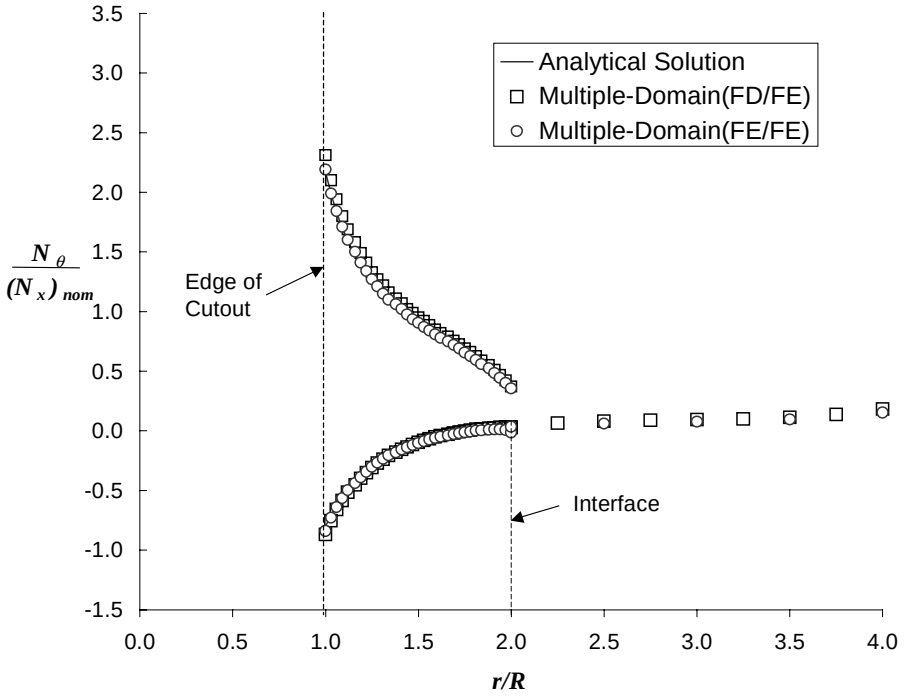

Figure 5.9. Longitudinal Stress Distribution along Midwidth and Midlength for Finite- Width Plate with Central Circular Cutout.

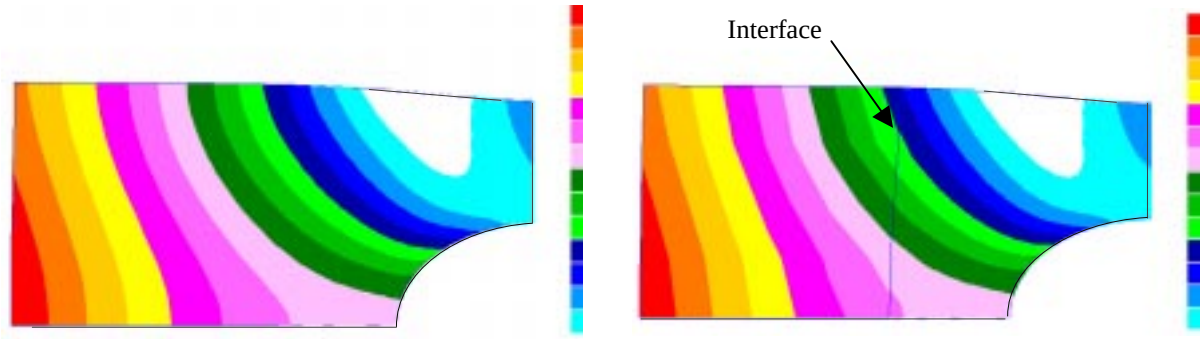

(a) Single-Domain Model (b) Multiple-Domain Model

Figure 5.10. Displacement Magnitude Distribution for Finite-Width Plate with Central Circular Cutout.

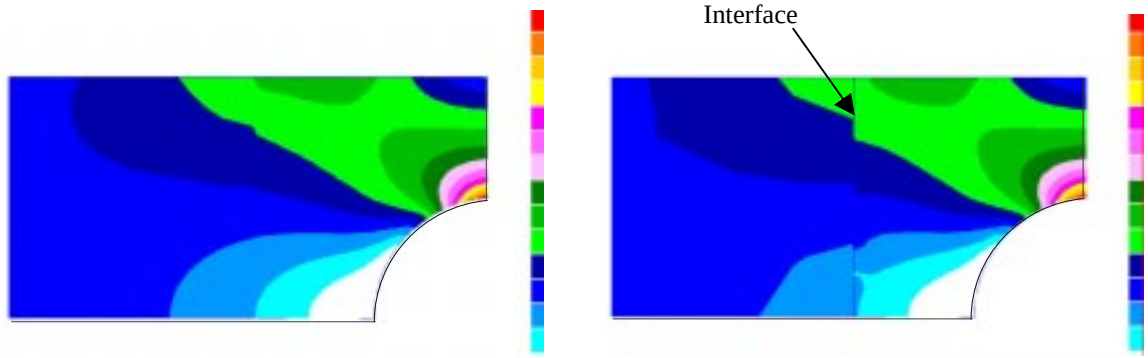

(a) Single-Domain Model (b) Multiple-Domain Model

Figure 5.11. Longitudinal Stress Resultant Distribution for Finite-Width Plate with Central Circular Cutout.

5.3. PLANE FLOW PROBLEM

The flow of a viscous incompressible material squeezed between two long parallel plates[41] is considered to illustrate the applicability and performance of the multifunctional approach to a representative vector-field problem in fluid mechanics.

The geometric configuration and the associated boundary conditions of the problem are indicated in Figure 5.12.

A state of plane flow exists when the length of the bounding plates is very large compared to the width of and distance between the plates. Assuming the conditions of plane flow, the velocity and pressure fields are determined for a fixed distance between the plates. The plates are moving toward each other with a velocity, v_0, and the width of and distance between the two plates is given by $2a$ and $2b$, respectively. For this configuration, the ratio of the plate width and the distance between the plates, $2a/2b$, is 3. Due to the double symmetry present in the problem, one quadrant of the domain was analyzed. The viscosity, μ, of the fluid is 1 lb-sec/in^2. The penalty finite element model[32] is used in the analysis. The penalty function formulation (see Eq. (3.61)) involves treating the continuity equation as a constraint among velocity components. A 10×6 nonuniform mesh (10 elements in the x-direction and 6 elements in the y-direction) of four-node bilinear elements is used for the single-domain analysis (*i.e.*, reference model in Figure 5.13(a)). The nonuniform mesh, with smaller elements near the free surface at $x=a$, is used to delineate the singularity in the shear stress at the point, $x=a, y=b$. This singularity and the associated necessity for nonuniform mesh refinement make this problem ideal for demonstrating the multifunctional approach with detailed local modeling. The finite element models for the single- and multiple-domain analyses are shown in Figure 5.13(a) and Figure 5.13(b), respectively. In the multiple-domain analysis, homogeneous spatial modeling with finite element discretization is used. In this analysis, more elements are used in the region near $x=a, y=b$ than in the single-domain analysis (see Figure 5.13). This local modeling yields a more complex configuration of

the subdomain common boundary. That is, the interface between the subdomains consists of two non-collateral segments.

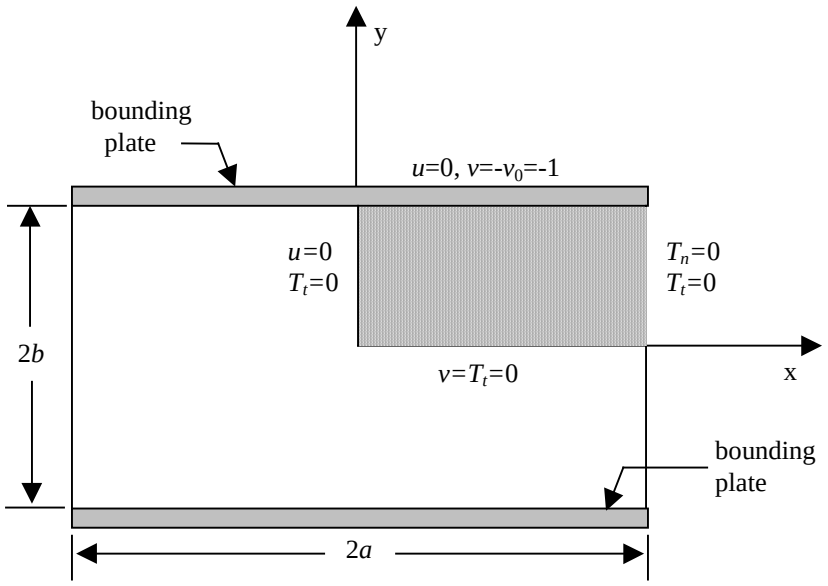

Figure 5.12. Geometric Configuration for Fluid Squeezed Between Parallel Plates.

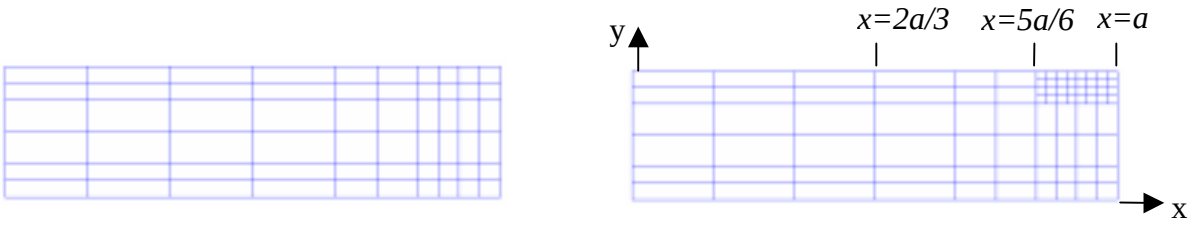

(a) Single-Domain Model (b) Multiple-Domain Model

Figure 5.13. Finite Element Models for Fluid Squeezed Between Two Parallel Plates.

An approximate analytical solution to this two-dimensional problem is provided by Nadai[51] and is given by

$$u = \frac{3v_0 x}{2b}\left(1-\frac{y^2}{b^2}\right); \quad v = -\frac{v_0 y}{2b}\left(3-\frac{y^2}{b^2}\right)$$

$$P = \frac{P_0}{a^2}\left(a^2 - y^2 - x^2\right); \quad P_0 = -\frac{3\mu v_0 a^2}{2b^3}$$

$$\sigma_x = 2\mu\frac{\partial u}{\partial x} - P = \frac{P_0}{a^2}\left(x^2 - 3y^2 - a^2 + 2b^2\right)$$

$$\sigma_y = 2\mu\frac{\partial v}{\partial y} - P = \frac{P_0}{a^2}\left(x^2 + y^2 - a^2 - 2b^2\right)$$

and

$$\tau_{xy} = \mu\left(\frac{\partial u}{\partial y} + \frac{\partial v}{\partial x}\right) = \frac{-2P_0 xy}{a^2}.$$

Note that this approximate solution does not satisfy the traction-free conditions ($T_n=\sigma_x=0$ and $T_t = \tau_{xy}=0$) on the free edge (*i.e.*, $x=a$). Likewise, these traction-free conditions are not imposed in the finite element analysis; thus, the conditions are not identically satisfied. The horizontal velocity, u, as a function of y, at three representative locations, $x=2a/3$, $x=5a/6$ (along the vertical interface), and $x=a$, is shown in Figure 5.14(a), Figure 5.14(b), and Figure 5.14(c), respectively. The analytical solution of Nadai[51] is represented by the solid line in the figure. Finite element solutions obtained using a single-domain spatial discretization are represented by the dashed lines in the figure. The multiple-domain results for the homogeneous spatial modeling approach using finite element discretization in each of the subdomains are also shown in the figures, and these results are represented by the open circles. The results for the horizontal velocity component obtained from the single- and multiple-domain analyses are in excellent

agreement with each other, and the results are in overall good agreement with the analytical solution.

The pressure, *P*, as a function of *x*, near the centerline for the flow (*i.e., y = b/16* - the centroids of the first row of finite elements in Figure 5.13), is shown in Figure 5.15. The analytical solution is denoted by the solid line. The solutions obtained from the single- and multiple-domain analyses are denoted by the dashed line and open circles, respectively. The results obtained from the multiple-domain analysis are in excellent agreement with those from the single-domain analysis. These finite element results are also consistent with the results published in the literature[32]. However, the finite element models predict a higher pressure in the center of the flow field (*i.e., x*=0) than predicted by the analytical solution.

While the velocity components and pressure field characterize the flow through the plates, the shear stress distribution illustrates the significance of using a graded single-domain mesh and a locally-refined multiple-domain mesh. The shear stress, τ_{xy}, as a function of *x*, near the upper bounding plate (*i.e., y = 15b/16* - the centroids of the last row of finite elements in Figure 5.13), is computed at the center of the finite elements and is shown in Figure 5.16. Again, the single-domain (dashed line in the figure) and multiple-domain (open circles in the figure) results are in excellent agreement with the approximate solution of Nadai[51] (solid line in the figure) away from the free-edge. In addition, because of the local refinement at the free edge, the multiple-domain results for $x \geq 5a/6$ correspond to the shear stress located at $y = 31b/32$ (the centroids of the last row of elements in the refined region). These results illustrate the better representation of the gradient in the shear stress at the free edge than either the single-domain analysis or the

analytical solution. The approximate nature of the analytical solution is highlighted by these results since the solution given does not delineate the gradient on the boundary.

For completeness, the longitudinal, σ_x, and transverse stress, σ_y, distributions are shown at $y = 15b/16$ and $y = 31b/32$, respectively, in Figure 5.17 and Figure 5.18. In general, the stresses predicted by the single- and multiple-domain finite element analyses have a larger value than those obtained by the analytical solution. However, the analytical solution is an approximate solution, and the finite element solutions predict the same overall trends in the stress distributions. The longitudinal stress distribution, σ_x, reveals the oscillatory nature of the finite element solution at the free-edge. The wavelength of the oscillations decreases as the mesh is increased in the local region at the free edge as indicated by the results from the multiple-domain analysis. In addition, the value of the peak stress at the free edge increases as the finite element mesh is refined.

Overall, the results obtained with the multifunctional discretization approach are in excellent agreement with the single-domain analysis results and with the analytical solution given in the literature. These successful comparisons indicate the effectiveness of the method and its applicability to the vector-field problem, specifically that of the fluid flow problem.

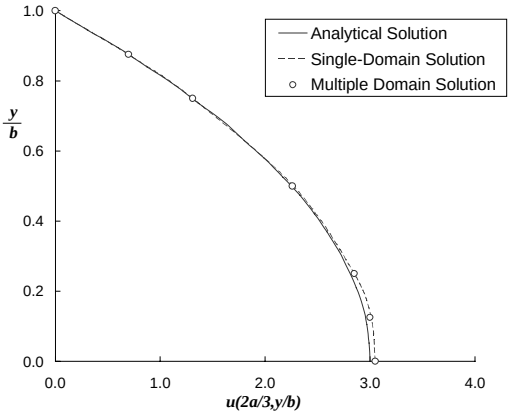

(a) Velocity, u, at $x=2a/3$

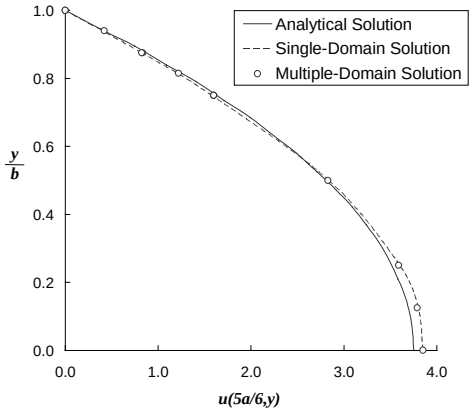

(b) Velocity, u, at $x=5a/6$

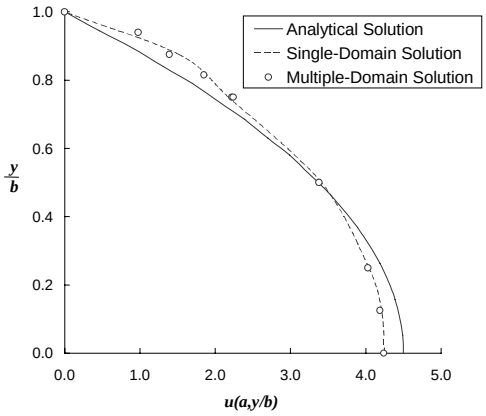

(c) Velocity, u, at $x=a$

Figure 5.14. Horizontal Velocity for the Flow Between Two Parallel Plates.

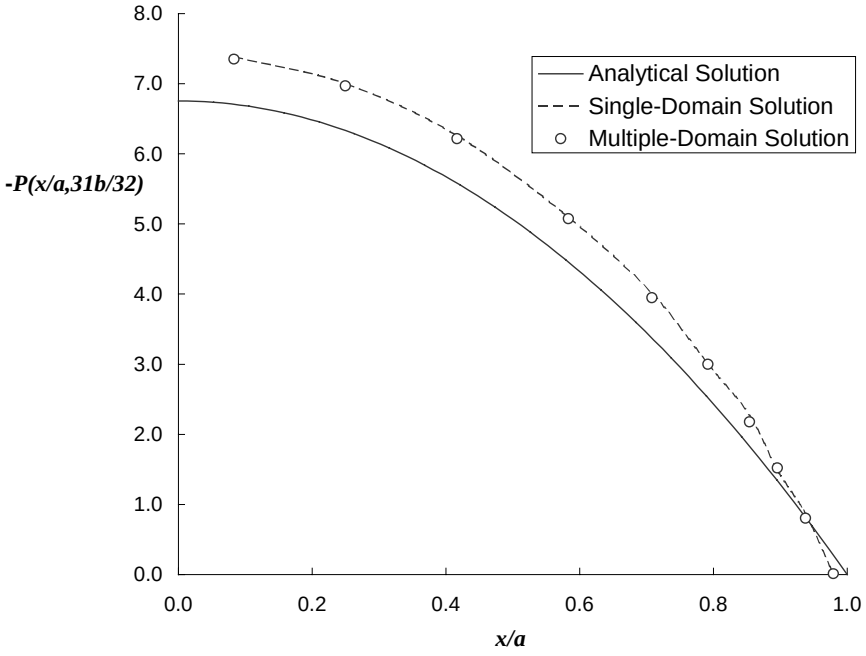

Figure 5.15. Pressure Distribution Near Centerline for the Flow Between Two Parallel Plates.

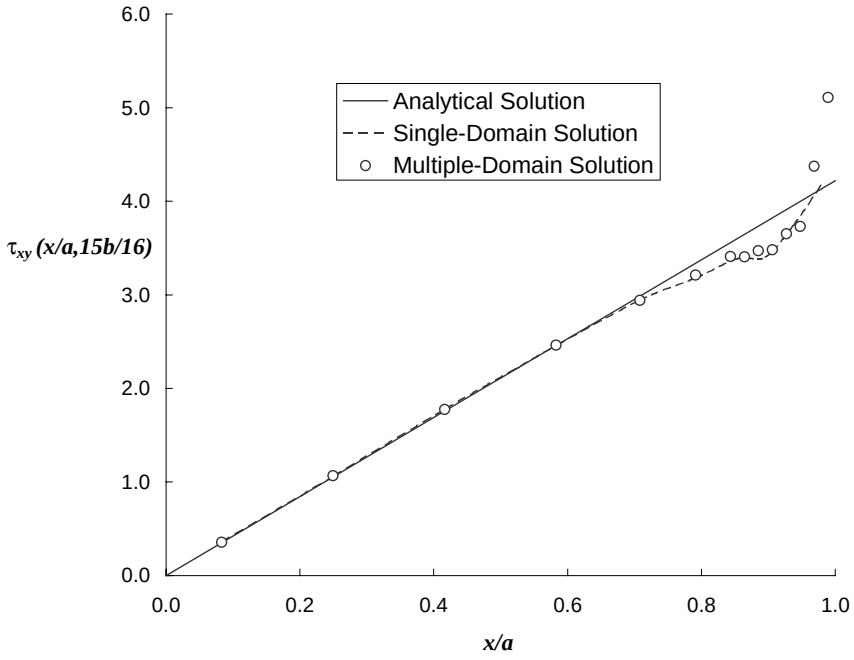

Figure 5.16. Shear Stress Distribution Near Plate Boundary for the Flow Between Two Parallel Plates.

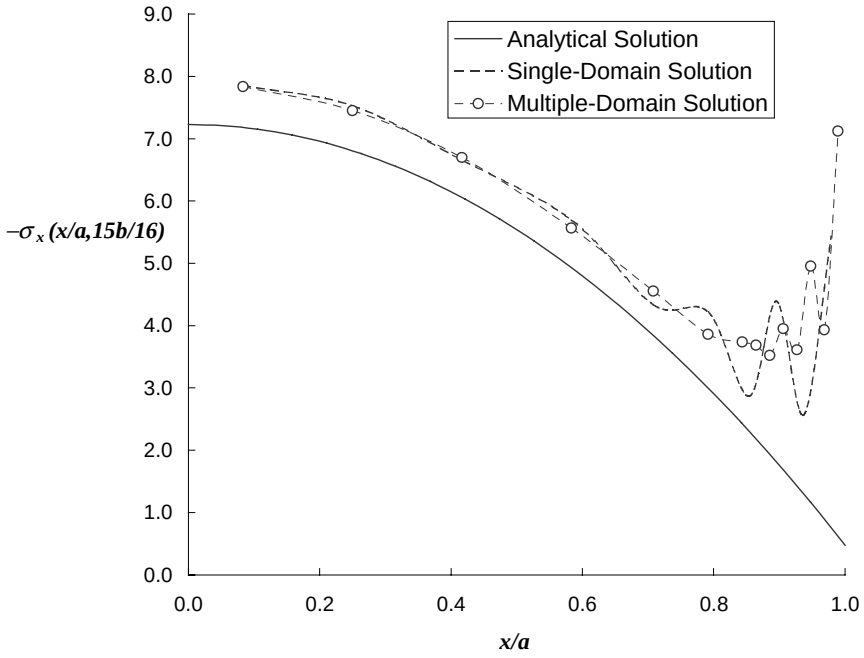

Figure 5.17. Longitudinal Stress Distribution Near Plate Boundary for the Flow Between Two Parallel Plates.

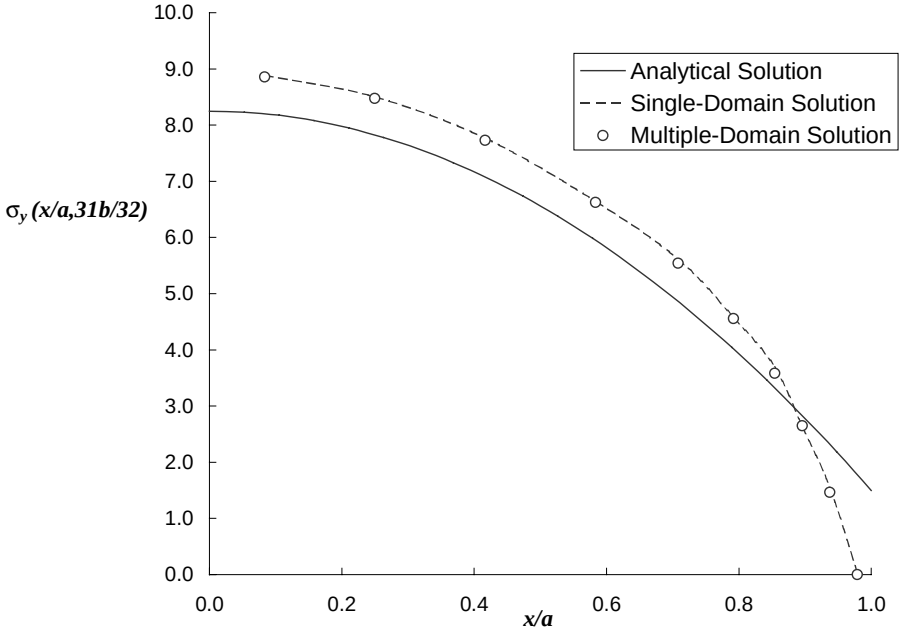

Figure 5.18. Transverse Stress Distribution Near Centerline for the Flow Between Two Parallel Plates.

5.4. EXTENSIONS TO MULTIPLE DISCIPLINES

In the present work, the multifunctional capability has been demonstrated on scalar- and vector-field problems applicable to the general field of engineering science and mechanics. While the demonstrations have illustrated the capability within different disciplines (*i.e.*, solid mechanics, fluid mechanics, and heat transfer), the method's use has not been demonstrated for multidisciplinary analysis. Extensions to simultaneous multiple disciplines are discussed here.

The term multidisciplinary or coupled systems refers to two or more systems that interact with each other, with the independent solution of any one system being impossible without simultaneous solution of the others[52]. In general, coupled systems and formulations, such as the multifunctional methodology presented in this work, are those applicable to multiple domains and dependent variables which usually describe different physical phenomena, and in which (1) neither domain can be analyzed independently; and (2) neither set of dependent variables can be explicitly eliminated at the differential equation level. The class of coupling problems that are the focus of this work can be categorized by coupling that occurs on domain interfaces via the boundary conditions imposed on that interface. Generally, the domains describe different physical situations, but it is possible to consider coupling between domains that are physically similar in which different discretization strategies have been used. Fluid-structure and thermal-structure interaction problems are typical examples that involve different disciplines in different but adjacent domains. Structure-structure or fluid-fluid interaction problems are examples where the interface divides arbitrarily chosen regions in which different mathematical approximations and/or spatial discretization procedures are used.

Single discipline interaction problems have been demonstrated extensively in this work. The extension of the multifunctional approach to multiple disciplines is illustrated using the fluid-structure interaction problem.

Different methodologies have been developed for the computational analysis of the fluid-structure interaction problem, and different terminology has been used to describe the extent to which the disciplines are coupled. In this work, two classes of coupling are outlined; namely, fully coupled and loosely coupled methods. Fully coupled methods reformulate the governing equations so both the fluid and structural equations are combined into one set of equations, coupling the solutions only at the boundary interfaces between the fluid and the structure[36]. These new governing equations are solved and integrated in time simultaneously. Loosely coupled methods make use of independent computational fluid dynamic (CFD) and computational structural mechanics (CSM) software modules. The coupling is accounted for by the exchange of data at the interface between the fluid and the structure. This coupling approach takes full advantage of the numerical procedures of individual disciplines such as finite difference approximations for fluids and finite element approximations for structures. In addition, software development efforts are simplified and software modularity is preserved. An alternate to the coupling approaches is to solve both the structures and fluids problems in a single computational domain. The major disadvantage of this methodology is the ill-conditioned matrices associated with the two physical domains. A secondary disadvantage is the inability to use existing CFD codes because they do not account for the interaction with the structure. In addition, the codes can not be readily extended to include this interaction. Thus, the method does not take full advantage of these

specialized and well-trusted programs. The extensions of the multifunctional capability will focus on the loosely coupled method.

The procedure for a loosely coupled method is given by (1) advance the structural system under the fluid-induced load, (2) transfer the motion on the wet boundary (*e.g.*, the fluid-structure interface) of the structure to the fluid system, (3) update the fluid dynamic mesh accordingly, (4) advance the fluid system and compute new pressure and fluid stress fields, and (5) convert the pressure and stresses into structural loads. The multifunctional approach is applicable to steps two and five in the procedure outlined. These steps are concerned with the transfer of data from a CFD grid to a CSM grid. Data transfer is complicated by the fact that there are basic differences between the nature of the solution methods. CFD analyses are concerned with the flow field surrounding the surface exposed to the flow. Thus, a CFD grid is very fine around the exterior of an airfoil, wherever changes in the flow field characteristics (*i.e.*, boundary layer effects) are expected to be maximum. Conversely, CSM methods examine airloads on the surface and how these loads affect the internal structure. CSM grids lie on the surface within the airfoil and are oriented to the structural components. Thus, CFD and CSM grids differ in grid density and data transfer requires extrapolation and interpolation of discipline-specific field variables.

Smith et al.[53] evaluated computational algorithms to interface CFD and CSM grids. In this reference, several candidate algorithms for passing information from the fluid regime to the structural regime were evaluated and the disadvantages of each were discussed. In addition, a load and motion transfer method based on the conservation of momentum and energy has been developed by Farhat[54]. In this reference, a conservative

algorithm for computing the loads induced by a fluid on a structure is discussed. This algorithm was shown to be accurate, robust and reliable for transferring data from a CFD grid to a CSM grid not only when the discretization differed, but also when the grids did not share the same geometry as in beam or wing-box geometric models (see Figure 5.19). In the figure, the structural surface is denoted by Γ_S and the fluid surface is denoted by Γ_F. The beam model is representative of the use of a beam finite element model to idealize the structural component within the airflow. The wing-box model is representative of a plate and shell finite element model to idealize the component in the flow. The multifunctional methodology developed herein provides an alternate conservative algorithm for transferring data from the CFD grid to a CSM grid. In general, the methodology can be used to transfer data among many different disciplines. Further development of the methodology to a two-dimensional (surface) interface is required. This development follows the approach presented by Aminpour et al.[55] for coupling three-dimensional finite element meshes.

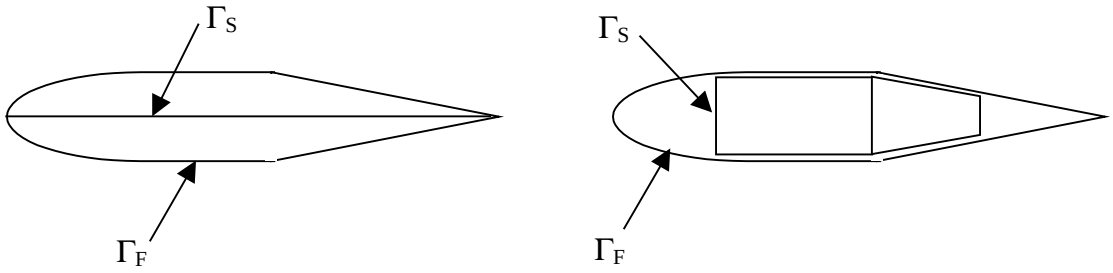

Figure 5.19. Beam and Wing-box Structural Models.

The governing equations for multifunctional analysis of vector-field problems have been developed in Chapter III and are given in Eqs. (3.32) and (3.34). Discretized

equations are given for solid mechanics in Eq. (3.57) and for fluid mechanics in Eqs. (3.60) and (3.61). In these systems of equations, the third equation represents the subdomain discretization mapping from one subdomain to another subdomain. This equation is given by

$$\mathbf{K}_{\mathrm{I}}\boldsymbol{\alpha} = \mathbf{0} \quad \text{or} \quad \begin{bmatrix}\mathbf{K}_{\mathrm{I}_1} & \mathbf{K}_{\mathrm{I}_2}\end{bmatrix}\begin{Bmatrix}\boldsymbol{\alpha}_1 \\ \boldsymbol{\alpha}_2\end{Bmatrix} = \mathbf{0} \tag{5.1}$$

where the variables with a subscript 1 represent a solid subdomain and the variables with a subscript 2 represent a fluid subdomain. At this point, consider that the loads, $\boldsymbol{\alpha}_2$, on the CFD grid are known. Eq. (5.1) can be used to solve for the unknown structural loads, $\boldsymbol{\alpha}_1$, provided that matrix $\mathbf{K}_{\mathrm{I}_1}$ is square and invertible (*i.e.*, the number of pseudo nodes used to describe the generalized displacement along the interface is equal to the number of Lagrange multipliers). Therefore,

$$\boldsymbol{\alpha}_1 = -\mathbf{K}_{\mathrm{I}_1}^{-1}\mathbf{K}_{\mathrm{I}_2}\boldsymbol{\alpha}_2 \tag{5.2}$$

and

$$\boldsymbol{\alpha} = \begin{Bmatrix}\boldsymbol{\alpha}_1 \\ \boldsymbol{\alpha}_2\end{Bmatrix} = \begin{Bmatrix}-\mathbf{K}_{\mathrm{I}_1}^{-1}\mathbf{K}_{\mathrm{I}_2} \\ \mathrm{I}\end{Bmatrix}\boldsymbol{\alpha}_2 = \mathbf{A}\boldsymbol{\alpha}_2 .$$

Moreover, it can be shown that $\mathbf{K}_{\mathrm{I}}\mathbf{A} = \mathbf{0}$ [56]. That is, the matrix $\mathbf{A}$ spans the null space of matrix $\mathbf{K}_{\mathrm{I}}$.

The fourth and fifth partitioned equations of the system of equations, given in Eqs. (3.57), (3.60) and (3.61), may be used to interpolate the structural deformations to the fluid grid. Recall that these equations are associated with the generalized displacements on the interface and thus, the generalized displacement vector may be partitioned as

$$\mathbf{u}_1 = \begin{Bmatrix} \mathbf{u}_1^o \\ \mathbf{u}_1^i \end{Bmatrix} \text{and similarly } \mathbf{u}_2 = \begin{Bmatrix} \mathbf{u}_2^o \\ \mathbf{u}_2^i \end{Bmatrix}$$

where the subscripts, *i* and *o*, represent generalized deformations on the interface and within subdomain 1 or 2 (*e.g.*, not on the interface). As such, the fourth and fifth equations are given as

$$\mathbf{K}_{\mathrm{p}_1}\mathbf{u}_1^i + \mathbf{K}_{\mathrm{I}_1}^{\mathrm{T}}\mathbf{u}_{\mathrm{I}} = \mathbf{0} \text{ and } \mathbf{K}_{\mathrm{p}_2}\mathbf{u}_2^i + \mathbf{K}_{\mathrm{I}_2}^{\mathrm{T}}\mathbf{u}_{\mathrm{I}} = \mathbf{0}$$

or

$$\mathbf{K}_{\mathrm{p}}\mathbf{u}^i + \mathbf{K}_{\mathrm{I}}^{\mathrm{T}}\mathbf{u}_{\mathrm{I}} = \mathbf{0} \ .$$

Premultiplying this equation by $\mathbf{A}^{\mathrm{T}}$ yields

$$\mathbf{A}^{\mathrm{T}}\mathbf{K}_{\mathrm{p}}\mathbf{u}^i + \mathbf{A}^{\mathrm{T}}\mathbf{K}_{\mathrm{I}}^{\mathrm{T}}\mathbf{u}_{\mathrm{I}} = \mathbf{0}$$

Since $\mathbf{A}^{\mathrm{T}}\mathbf{K}_{\mathrm{I}}^{\mathrm{T}} = \mathbf{0}$,

$$\mathbf{A}^{\mathrm{T}}\mathbf{K}_{\mathrm{p}}\mathbf{u}^i = \mathbf{0} \text{ and } \mathbf{A}^{\mathrm{T}}\mathbf{K}_{\mathrm{p}_1}\mathbf{u}_1^i + \mathbf{A}^{\mathrm{T}}\mathbf{K}_{\mathrm{p}_2}\mathbf{u}_2^i = \mathbf{0}$$

or

$$\overline{\mathbf{K}}_1\mathbf{u}_1^i + \overline{\mathbf{K}}_2\mathbf{u}_2^i = \mathbf{0} \tag{5.3}$$

The variables, $\mathbf{u}_1^i$, are associated with the known structural deformations from the structures grid, and the variables, $\mathbf{u}_2^i$, are associated with the unknown deformations to be imposed on the fluid grid. Given that the matrix $\overline{\mathbf{K}}_2$ is square and invertible, Eq. (5.3) can be solved to obtain the unknown deformations. Therefore,

$$\mathbf{u}_2^i = -\overline{\mathbf{K}}_2^{-1}\overline{\mathbf{K}}_1\mathbf{u}_1^i \tag{5.4}$$

The values, $\mathbf{u}_2^i$, can now be used in the CFD code to update the surface deformation and to calculate a new set of surface loads. With Eqs. (5.2) and (5.4), the multifunctional methodology described herein may be extended to the multiple-domain analyses of different disciplines.

5.5. SUMMARY

In this chapter, the multifunctional methodology has been described and demonstrated for vector-field problems in engineering science. The selected problems included problems of solid mechanics and fluid mechanics. The governing equation in each case is the equation of linear momentum. In addition, for fluid mechanics, continuity conditions are required. The analyses performed have demonstrated the effectiveness and accuracy of the solutions obtained for the respective problems. In all cases, the results obtained using the multifunctional methodology were in overall good agreement with the reported analytical or reference solution.

Based on the findings for the vector-field problems, extensions of the multifunctional collaborative methodology to multiple-domain analyses of different disciplines have been briefly investigated. An exploratory examination of the extensions illustrates the applicability of the methodology to loosely coupled multiple-discipline applications.

CHAPTER VI

CONCLUSIONS AND RECOMMENDATIONS

6.1. GENERAL

Multifunctional methodologies and analysis procedures have been formulated for interfacing diverse domain idealizations including multi-fidelity modeling methods and multiple-discipline analysis methods. The methods, based on the method of weighted residuals, ensure accurate compatibility of primary and secondary variables across the domain interfaces. Methods have been developed for scalar-field and vector-field problems. The methods have been rigorously developed for multiple-domain applications, and the robustness and accuracy has been illustrated. Multi-fidelity modeling approaches have been developed that include both homogeneous (*i.e.,* the same discretization method in each domain) and heterogeneous (*i.e.,* different discretization methods in each domain) discretization approaches. Results have been presented for the scalar- and vector-field multifunctional formulation using representative test problems. Associated computational issues are also discussed. In addition, the extension to multiple-domain analysis with different disciplines has been discussed.

6.2. CONCLUSIONS

The multi-fidelity modeling of domains has been developed for homogeneous and heterogeneous discretization approaches for both scalar- and vector-field problems. The finite element and finite difference methods and combinations thereof have been used in each of the discretization approaches.

Multi-fidelity modeling

Several general conclusions regarding the multi-fidelity modeling approaches can be made. First, each of the multiple-domain approaches leads to a non-positive definite system of equations, which impacts the solution strategy. Second, modeling flexibility in the multiple-domain method is increased at the expense of additional degrees of freedom introduced to the system of equations. However, the modeling advantage gained outweighs the computational expense due to the additional degrees of freedom, and the impact of the increased number of degrees of freedom due to the interface constraints is reduced as the overall problem size is increased. Third, while the multifunctional method encompasses heterogeneous discretization approaches using the finite difference method, the limitations regarding its use in the presence of complex boundary conditions and configurations restrict the method's general-purpose use. Fourth, in general, the homogeneous and heterogeneous multiple-domain approaches using the finite difference discretization in one or both domains yield systems of equations that are not symmetric. This lack of symmetry is due to the use of the Dirac delta function as the weight function in the formulation. This function is introduced in the constraint integral used to form the coupling matrix in the upper triangular part of the system matrix. The finite difference "shape function" is used in the corresponding constraint integral used to form the coupling matrix in the lower triangular part of the system matrix. In fact, in the finite difference method, there may be a lack of symmetry in each of the independent subdomain "stiffness" matrices due to the imposition of the boundary conditions.

Scalar-field problems

Conclusions regarding the multiple-domain modeling approach for the scalar-field problem include the following statements. First, scalar-field problems introduce many of the computational issues associated with the multifunctional approach. Second, satisfaction of the boundary conditions for the scalar-field problem using finite difference discretization is more straightforward than for the vector-field problem. The five-point template used to approximate the derivatives does not introduce difficulties at the corners of the domain, as is the case with the nine-point template used in the vector-field problem. Third, fictitious nodes are avoided by evaluating the governing equations only at the interior grid points of the domain. The essential and natural boundary conditions are applied at the boundary nodes with higher-order forward and backward difference approximations used for the first derivatives present in the natural boundary condition equations. Fourth, the governing equation is evaluated at the nodes along the subdomain common boundary. Straightforward central difference approximations are used at the interface to represent the interface tractions, which in turn are used to eliminate the fictitious nodes at the common boundary.

Vector-field problems

Based on the studies of the multiple-domain modeling approach for the vector-field problem, the following conclusions are drawn. First, the use of the finite difference method for the vector-field problem (*e.g.*, plane stress problem) was far more complicated than for the scalar-field problem. The traction and displacement boundary conditions and the necessity to introduce and eliminate fictitious nodes outside the domain boundary greatly complicate the development. Second, the nine-point template

required in the finite difference approximation of the governing equations of the continuum introduces the need for alternative higher-order forward and backward difference approximations of the cross-derivatives present in the equations. Third, because of the difficulties associated with the first and second conclusions, the homogeneous and heterogeneous modeling approach using the finite difference method in one or both subdomains is not as attractive for vector-field problems as for scalar-field problems. Fourth, the governing equation is evaluated at the nodes along the subdomain common boundary. Complex manipulation of the nine-point template is required using forward and backward difference approximations of the cross-derivatives in order to limit the introduction of the fictitious nodes to the node along the common boundary at which the governing equation is being evaluated. This requirement is automatically satisfied in the scalar-field problem by the five-point template. The interface tractions are used to eliminate the fictitious nodes at the common boundary.

Limitations

While a rigorous multifunctional formulations has been presented, there are limitations in the implementation. Note that the purpose of the implementation described herein was to demonstrate the capabilities of the multifunctional approach on a set of representative benchmark problems. With this in mind, the limitations of the current implementation are as follows:

- The nodes or grid points at the ends of the common subdomain boundary of each of the subdomains must coincide.
- In the finite difference method used, at least three nodes are required in each of the coordinate directions where traction boundary conditions are imposed.

- Extreme care must be taken to perform accurate input and output using data-exchange files (in this work, double-precision floating-point accuracy).
- The development of the interface routines in MATLAB® limits the size of problem that may be analyzed.
- Cubic splines are used on the subdomain common boundary, which requires at least four unique nodes along this boundary.
- The implementation is limited to one-dimensional straight or curved common subdomain boundaries.
- The geometry is assumed to be conforming. That is, each of the subdomains describe the same geometry along the common boundary.

In this work, the benchmark vector-field problems illustrated require only C^0 continuity (continuity of the primary variable). Thus, continuity of the primary variable is maintained along the subdomain common boundary through the interface constraint. For plate bending problems using classical plate theory, C^1 continuity is required. In this case, continuity of the primary variable and its derivative is maintained along the common subdomain boundary. Here, the derivatives are approximated in the same manner as the primary variable. That is, cubic spline functions are used to approximate the generalized variables along the common subdomain boundary. Results for a wider range of problems including a plate bending problem have been given in reference 25.

Summary of Results

Results were presented for the scalar- and vector-field developments using example patch test problems. In addition, results for torsion, heat conduction and potential flow problems have been presented to demonstrate further the effectiveness of

the scalar-field development. Results for plane stress and plane flow problems have been presented for the vector-field development. Results for all problems presented are in overall good agreement with the exact or reference configuration by which they were evaluated.

The multifunctional methodology presented provides an effective mechanism by which domains with diverse idealizations can be interfaced. This capability promises to provide rapidly the high-fidelity data needed in the early design phase. Moreover, the capability is applicable to the problems in the general field of engineering science and mechanics. Hence, the methodology provides a collaborative capability that accounts for discipline interactions among many disciplines.

6.3. RECOMMENDATIONS FOR FUTURE WORK

Future studies related to the present work are recommended. The present work provides a starting point for the following additional studies:

1. Explore the use of a finite difference energy method, which alleviates many of the issues associated with the proper identification of boundary conditions and the use of irregular grids.
2. Evaluate the performance of the methodology for the analysis of more complex structures and fluid flow problems.
3. Extend and implement the multiple-discipline capability.
4. Develop other analysis capabilities including thermal analysis, modal and buckling analysis, dynamic analysis, and nonlinear analysis.
5. Develop other heterogeneous multiple-domain discretization approaches such as the use of the finite element and boundary element methods.

6. Develop strategy to exploit massively parallel processing (MPP) computer systems.
7. Incorporate computationally intelligent strategies to identify where and when homogeneous or heterogeneous approaches should be used.

APPENDIX A

OVERVIEW OF STEPS IN ANALYSIS AND SIMULATION

Multifunctional collaborative methods should address four typical steps of analysis and design, namely, (1) representation or modeling of the geometry, (2) knowledge-based selection and development of appropriate mathematical models (*i.e.*, idealization/discretization), (3) solution of the mathematical model (continuous and/or discrete), and (4) interrogation/assessment of the results. These steps provide the foundation for enhanced integrated design and analysis tools, and the steps are briefly outlined in this appendix.

Geometry Modeling

To represent the structural geometry (geometry modeling) a geometric model is created to represent the size and shape of a system component. In aerodynamic and structural analyses, a common three-dimensional parameterized description of the airframe is shared. Geometry modeling is the starting point of the product design and manufacture process and is the first step in using a computer-aided design/computer-aided manufacturing (CAD/CAM) system[57.] The accuracy of the geometric model and the way in which it is structured has far-reaching effects on other CAD functions such as finite element analysis, drafting, and numerical control (NC) part programming. CAD/CAM systems can be utilized to develop a design and monitor and control the manufacturing process from start to finish. Numerous CAD software packages[58] for defining the geometry of structural systems are commercially available.

Computer-aided engineering (CAE) has facilitated the assimilation of the engineer/analyst earlier in the design stage as an engineer in-the-loop. Typically, this

cycle leads from the design engineer to the analyst and back to the designer. A critical aspect of this cycle is the time required to generate analysis models, perform the analysis and decide if changes are needed. However, new trends in modeling and simulation are redefining the roles of the designer and the analyst. Many companies are now turning designers into analysts. The underlying philosophy guiding this paradigm shift is the desire to give designers the tools needed to predict a design's performance early in the process, rather than just to define its geometry. These tools also embody a knowledge base to guide the designer through various analysis steps. Moreover, this new paradigm allows the highly specialized analysts to impact the design by performing more complex analyses to determine the structural integrity, the potential failure mechanisms and the complex response characteristics (*i.e.*, material or geometric nonlinearity), and multidisciplinary characteristics of the design.

This role redefinition can succeed only if enough analyses are performed early in the design process to identify critical design parameters, evaluate their interactions, and determine the best overall design. To expedite this process developers of computer-aided design (CAD) and analysis software have integrated the CAD and analysis functions. Such software integration and database coupling frequently enables designers to perform analyses directly on geometry, thus reducing the time required to prepare analysis models.

Idealization/Discretization

To develop discretized mathematical models of aerospace systems, several approximate numerical analysis methods have evolved over the years. The most commonly used discretization methods are the finite difference method and the finite

element method. The finite difference method of a configuration gives a pointwise approximation to the governing equations. While finite difference techniques are widely used in fluid dynamics and can treat fairly complex problems, they become hard to use when irregular geometrical shapes or unusual boundary conditions are encountered. This adverse attribute is particularly significant in structural analysis. In contrast, the finite element method is widely used for the analysis of many engineering problems involving static, dynamic and thermal stresses of structures. Typical input for a finite element analysis program consists of the geometric idealization, the material properties, the loading, and boundary conditions. The area of greater difficulty in the finite element technique lies in the geometric idealization, that is, representing the geometry of the structure by a suitable finite element mesh. Element aspect ratio, taper, and skew are characteristics that adversely affect the performance of many finite elements in use today and thus are factors in determining the suitability of a mesh. As the complexity of structural configurations and material systems being modeled with the finite element method has increased, manual mesh generation has become extremely tedious, time-consuming, expensive and consequently, intractable. This limitation is alleviated through the development of automatic mesh generators, which are typically integrated within the finite element modeling software and often integrated within the CAD system. These mesh generators are powerful tools for discretizing complex structural configurations. Issues associated with idealization still arise such as whether to use solid finite elements or shell finite elements. However, if the CAD and analysis engines are not driven from the same geometry, the translation of geometry may introduce errors in analytical models. In addition, due to the geometric complexity of such configurations, even the most robust

automatic mesh generator can often require analyst interaction to establish a suitable mesh and to provide engineering insight into the proper finite element to be used in the analysis. For example, some automatic mesh generators place three-dimensional models where two-dimensional shells should be used, which may distort the results.

Response Prediction

To solve the discrete system of simultaneous equations resulting from the discretization process and subsequent finite element assembly operations, myriad solution strategies have been developed for obtaining efficiently the unknown nodal values of the field variable or the primary unknowns. Two families of methods for solving linear systems of algebraic equations can be distinguished: direct and iterative equation solvers. The former can be defined as leading to the solution of a linear system in one step, while the latter will require many iterative steps. If the equations are linear, a number of standard solution techniques may be used which generally include either an iterative or direct solver. If the equations are nonlinear, their solution is more difficult to obtain. All approaches will necessarily be repeated solution of linearized equations. A common solution method used to solve nonlinear systems of equations is the Newton-Raphson incremental-iterative solution procedure, which is accurate and converges for highly nonlinear behavior. High-performance equation solvers are a key component of solution strategies for linear and nonlinear structural response calculations for static, dynamic and eigenvalue problems in finite element analysis. There has been a plethora of research in the area of equation solvers for large-scale aerospace structures with only representative works referenced herein. Matrices resulting from discretization of structural systems are generally real, symmetric, positive definite, banded, and sparse. The performance of

iterative and direct equation solvers has been compared to identify the most appropriate tool for the solution of equations arising from structures systems[59]. This work identified advantages and disadvantages of both types of solvers. The study concluded that the relative performance of solvers depends on the amount of computations as well as the rate at which operations can be carried out on a given computer.

Direct sparse solvers were found to be most attractive for models composed of higher-order finite elements, where they benefit most from a greatly reduced operation count. Sparse direct techniques are efficient improvements over first-generation direct methods that require more operation counts and larger memory capacity[60]. The number of operations in a sparse method are significantly reduced through reordering and storage strategies that effectively compress the global stiffness matrix into a format that exhibits a greater degree of nonsparsity prior to factorization and thus substantially reduces the associated computational costs. Iterative methods require much less memory than direct solvers, but their effective use depends on a fast convergence rate, which has been found to be best for finite elements with low aspect ratios. Skyline and variable band linear equation solvers have been developed to exploit the matrix characteristics of structural systems and to exploit the full capabilities of parallel and vector supercomputers[61]. More recently, general-purpose equation solvers have been developed for complex, nonsymmetric, indefinite, and dense matrix characteristics, which are prevalent in disciplines such as electromagnetic and acoustic analysis[62]. Over the years, equation solvers have been developed to take advantage of the rapidly increasing computational power afforded by vector and parallel high-performance computers. These ultra-rapid equation solvers coupled with the major advances in computational power now available

in desktop personal computers and workstations have made it feasible to perform high-fidelity analyses in the preliminary design stage. However, additional developments are required to perform real-time large-scale analyses within an interactive virtual reality analysis and design environment. More intensive reviews of equation solvers may be found in the open literature (*e.g.*, references 63, 64, and 65).

Assessment of Results

The fourth and final step in the analysis and simulation process is the interrogation of the results. In years past, the engineer would spend an enormous amount of time plowing through pages of computer output while waiting for results from additional analyses. With the increased speed and efficiency of today's equation solvers, the rapid interrogation of results becomes decidedly more significant. It is at this step of interpretation of results that the engineer must be integrally involved. Powerful pre- and post-processing tools coupled with state-of-the-art computational technology provide the engineer with a comprehensive tool set for creating and discretizing complex geometries, performing analyses and visualizing results. Some software provide novel capability to enhance the designer-computer interaction while interrogating results. Engineers can view the results of parametric studies in a series of windows to identify or compare important design parameters. In addition, analysis results from different design approaches may be viewed in different windows and assessed to determine the most feasible design. This and other such visualization capabilities facilitate the rapid interpretation of analysis results, thus improving productivity of higher-order analyses and providing an opportunity for the engineer/analyst to be an integral part of the design process from concept to manufacture. Recently, immersive virtual reality environments

for visualization and interpretation of geographically dispersed results have been proposed as part of the NASA Intelligent Synthesis Environment (ISE) Initiative that promises to revolutionize the design process[66, 67]. Immersive environments are human-scale computer-generated projection systems that allow users to interact directly with their data in three spatial dimensions. Emerging advanced engineering environments[68] will provide visual, auditory, and haptic feedback to further aid the engineer in detailed assessment of results.

APPENDIX B

CUBIC SPLINE INTERPOLATION MATRICES

The interpolation matrices used in the deformation and geometry assumptions of the multifunctional approach are outlined in this appendix. Given a series of points x_i $(i = 0,1,\ldots,n)$ which are generally not evenly spaced, and the corresponding function values $f(x_i)$, the cubic spline function denoted $g(x)$ may be written as

$$g(x) = \frac{g_{,xx}(x_i)}{6}\left[\frac{(x_{i+1}-x)^3}{\Delta x_i} - \Delta x_i (x_{i+1}-x)\right] + \frac{g_{,xx}(x_{i+1})}{6}\left[\frac{(x-x_i)^3}{\Delta x_i} - \Delta x_i (x-x_i)\right] + f(x_i)\left[\frac{(x_{i+1}-x)}{\Delta x_i}\right] + f(x_{i+1})\left[\frac{(x-x_i)}{\Delta x_i}\right] \tag{B.1}$$

where $\Delta x = x_{i+1} - x_i$ and $g_{,xx}$ denotes differentiation twice with respect to x. This equation provides the interpolating cubics over each interval for $i = 0,1,\ldots,n-1$ and may be given in matrix form as

$$\mathbf{g} = \hat{\mathbf{T}}_1 \mathbf{g}_{,xx} + \hat{\mathbf{T}}_2 \mathbf{f} \tag{B.2}$$

For each of the k values of x at which the spline function is to be evaluated, $x_i \leq x_k \leq x_{i+1}$, $k = 1,2 \ldots p$, and p is the number of evaluation points. The $\hat{\mathbf{T}}_1$ and $\hat{\mathbf{T}}_2$ matrices may be written in the form

$$\hat{\mathbf{T}}_1 = \begin{bmatrix} (\hat{t}1)_{1,1} & (\hat{t}1)_{1,2} & \cdots & (\hat{t}1)_{1,n+1} \\ (\hat{t}1)_{2,1} & (\hat{t}1)_{2,2} & \cdots & (\hat{t}1)_{2,n+1} \\ \vdots & \vdots & \ddots & \vdots \\ (\hat{t}1)_{p,1} & (\hat{t}1)_{p,2} & \cdots & (\hat{t}1)_{p,n+1} \end{bmatrix} \quad \text{and} \quad \hat{\mathbf{T}}_2 = \begin{bmatrix} (\hat{t}2)_{1,1} & (\hat{t}2)_{1,2} & \cdots & (\hat{t}2)_{1,n+1} \\ (\hat{t}2)_{2,1} & (\hat{t}2)_{2,2} & \cdots & (\hat{t}2)_{2,n+1} \\ \vdots & \vdots & \ddots & \vdots \\ (\hat{t}2)_{p,1} & (\hat{t}2)_{p,2} & \cdots & (\hat{t}2)_{p,n+1} \end{bmatrix}$$

where

$$\left(\hat{t}_1\right)_{k,j} = \begin{cases} 0 & \text{for } x_k < x_i \quad \text{or } x_k > x_{i+1} \\ \left[\dfrac{\left(x_{i+1}-x_k\right)^3}{\Delta x_i} - \Delta x_i\left(x_{i+1}-x_k\right)\right] & \text{for } x_i \le x_k \le x_{i+1} \quad \text{and} \quad j = i+1 \\ \left[\dfrac{\left(x_k-x_i\right)^3}{\Delta x_i} - \Delta x_i\left(x_k-x_i\right)\right] & \text{for } x_i \le x_k \le x_{i+1} \quad \text{and} \quad j = i+2 \end{cases},$$

$$\left(\hat{t}_2\right)_{k,j} = \begin{cases} 0 & \text{for } x_k < x_i \quad \text{or } x_k > x_{i+1} \\ \dfrac{\left(x_{i+1}-x_k\right)}{\Delta x_i} & \text{for } x_i \le x_k \le x_{i+1} \quad \text{and} \quad j = i+1 \\ \dfrac{\left(x_k-x_i\right)}{\Delta x_i} & \text{for } x_i \le x_k \le x_{i+1} \quad \text{and} \quad j = i+2 \end{cases},$$

and

$$\mathbf{g}_{,xx} = \begin{Bmatrix} g_{,xx}(x_0) \\ g_{,xx}(x_1) \\ \vdots \\ g_{,xx}(x_n) \end{Bmatrix}, \text{ and } \quad \mathbf{f} = \begin{Bmatrix} f(x_0) \\ f(x_1) \\ \vdots \\ f(x_n) \end{Bmatrix} = \begin{Bmatrix} f_0 \\ f_1 \\ \vdots \\ f_n \end{Bmatrix}.$$

Note that there are, at most, two nonzero coefficients in each row of the $\hat{\mathbf{T}}_1$ and $\hat{\mathbf{T}}_2$ matrices given above.

Applying additional smoothness conditions (*i.e.*, equating the first and second derivatives of adjacent interpolating cubics at x_i) yields a set of simultaneous equations of the form

$$\begin{aligned} &\left[\frac{\Delta x_{i-1}}{\Delta x_i}\right] g_{,xx}(x_{i-1}) + \left[\frac{2\left(x_{i+1}-x_i\right)}{\Delta x_i}\right] g_{,xx}(x_i) + [1]\, g_{,xx}(x_{i+1}) \\ &= 6\left[\frac{f(x_{i+1})-f(x_i)}{(\Delta x_i)^2} - \frac{f(x_i)-f(x_{i-1})}{(\Delta x_i)(\Delta x_{i-1})}\right] \end{aligned} \qquad i = 1,2,\ldots,n-1. \qquad \text{(B.3)}$$

If the x_i are evenly separated with spacing Δx, then the Eq. (B.3) becomes

$$[1]g_{,xx}(x_{i-1})+[4]g_{,xx}(x_i)+[1]g_{,xx}(x_{i+1}) = 6\left[\frac{f(x_{i+1})-2f(x_i)+f(x_{i-1})}{(\Delta x)^2}\right] \quad . \tag{B.4}$$

Eqs. (B.3) and (B.4) may be written as

$$\mathbf{A}g_{,xx} = \mathbf{P}f \tag{B.5}$$

The coefficients of matrices **A** and **P** are dependent upon the end conditions, which are discussed in the following section.

End Conditions

Whether the equations are of the form of Eq. (B.3) or Eq. (B.4), there are *n*-1 equations in the *n*+1 unknowns $g_{,xx}(x_0),\ g_{,xx}(x_1), \ldots, g_{,xx}(x_n)$. The two necessary additional equations are obtained by specifying conditions on $g_{,xx}(x_0)$ and $g_{,xx}(x_n)$. For a *natural spline*, $g_{,xx}(x_0) = g_{,xx}(x_n) = 0$. However, in this work, these second derivatives are calculated by differentiating (twice) a cubic function which passes through the first four pseudo-nodes along the interface path and another cubic function that passes through the last four pseudo-nodes along the interface path. Evaluating this cubic function, $g(x) = a_0 + a_1 x + a_2 x^2 + a_3 x^3$, and at the first four points gives

$$\begin{Bmatrix} g(x_0) \\ g(x_1) \\ g(x_2) \\ g(x_3) \end{Bmatrix} = \begin{bmatrix} 1 & x_0 & x_0^2 & x_0^3 \\ 1 & x_1 & x_1^2 & x_1^3 \\ 1 & x_2 & x_2^2 & x_2^3 \\ 1 & x_3 & x_3^2 & x_3^3 \end{bmatrix} \begin{Bmatrix} a_0 \\ a_1 \\ a_2 \\ a_3 \end{Bmatrix} \quad \text{or} \quad \mathbf{Na} = \mathbf{g} \tag{B.6}$$

Solving for the coefficients yields $\mathbf{a} = \mathbf{N}^{-1}\mathbf{g}$ or

$$\begin{Bmatrix} a_0 \\ a_1 \\ a_2 \\ a_3 \end{Bmatrix} = \begin{bmatrix} n_{11} & n_{12} & n_{13} & n_{14} \\ n_{21} & n_{22} & n_{23} & n_{24} \\ n_{31} & n_{32} & n_{33} & n_{34} \\ n_{41} & n_{42} & n_{43} & n_{44} \end{bmatrix} \begin{Bmatrix} g(x_0) \\ g(x_1) \\ g(x_2) \\ g(x_3) \end{Bmatrix} \tag{B.7}$$

From the cubic function, $g_{,xx}(x) = 2a_2 + 6a_3 x$ where a_2 and a_3 are determined from Eq. (B.7). Equation (B.7) is valid for evenly spaced as well as arbitrarily spaced points. Similar expressions are obtained for the cubic function passing through the last four points where coefficients of the inverted matrix similar to those in Eq. (B.7) are denoted $\bar{n}_{kl}$ for k,l =1,...,4. With these end conditions, the matrices of Eq. (B.5) are given for equally-spaced points as

$$\mathbf{A} = \begin{bmatrix} 1 & 0 & 0 & \cdots & & \\ 1 & 4 & 1 & \cdots & & \\ & 1 & 4 & 1 & & \\ & & & \ddots & & \\ & & \cdots & 1 & 4 & 1 \\ & & \cdots & 0 & 0 & 1 \end{bmatrix}_{(n+1 \text{ x } n+1)}$$

and

$$\mathbf{P} = \begin{bmatrix} p_1 & p_2 & p_3 & p_4 & \cdots & \\ \dfrac{6}{\Delta x} & \dfrac{-12}{\Delta x} & \dfrac{6}{\Delta x} & & \cdots & \\ & \dfrac{6}{\Delta x} & \dfrac{-12}{\Delta x} & \dfrac{6}{\Delta x} & \cdots & \\ & & & \ddots & & \\ & & \cdots & & \ddots & \\ & \cdots & \bar{p}_1 & \bar{p}_2 & \bar{p}_3 & \bar{p}_4 \end{bmatrix}_{(n+1 \text{ x } n+1)}$$

where $p_k = 2n_{3k} + 6n_{4k}$ and $\bar{p}_k = 2\bar{n}_{3k} + 6\bar{n}_{4k}$ for k,l =1,...,4. For unevenly spaced points, the tridiagonal **A** and **P** matrices may readily be obtained from Eq. (B.3).

Expressing $g(x)$ in Terms of Functional Values $f(x_i)$

In Eq. (B.2), the spline function g(x) is expressed in terms of the functional values $f(x_i)$ as well as second derivatives of the spline function, $g_{,xx}(x_i)$. However, it is desirable to express $g(x)$ in terms of the function values $f(x_i)$ only. This manipulation is done by solving for $g_{,xx}(x_i)$ in Eq. (B.5) yielding

$$\mathbf{g}_{,xx} = \mathbf{A}^{-1}\mathbf{P}\mathbf{f} \tag{B.8}$$

Substituting in Eq. (B.2) yields

$$\mathbf{g}(x) = \hat{\mathbf{T}}_1\mathbf{A}^{-1}\mathbf{P}\mathbf{f} + \hat{\mathbf{T}}_2\mathbf{f} = \left(\hat{\mathbf{T}}_1\mathbf{A}^{-1}\mathbf{P} + \hat{\mathbf{T}}_2\right)\mathbf{f} = \mathbf{T}\mathbf{f}\,. \tag{B.9}$$

Derivatives of the spline function are obtained by differentiating Eq. (B.9) yielding

$$g_{,x}(x) = \left(\hat{\mathbf{T}}_1\right)_{,x}\mathbf{A}^{-1}\mathbf{P}\mathbf{f} + \left(\hat{\mathbf{T}}_2\right)_{,x}\mathbf{f} = \left[\left(\hat{\mathbf{T}}_1\right)_{,x}\mathbf{A}^{-1}\mathbf{P} + \left(\hat{\mathbf{T}}_2\right)_{,x}\right]\mathbf{f} = \mathbf{T}_{,x}\mathbf{f} \tag{B.10}$$

where

$$\left(\hat{\mathbf{T}}_1\right)_{,x} = \begin{bmatrix} \left(\hat{t}_1'\right)_{1,1} & \left(\hat{t}_1'\right)_{1,2} & \cdots & \left(\hat{t}_1'\right)_{1,n+1} \\ \left(\hat{t}_1'\right)_{2,1} & \left(\hat{t}_1'\right)_{2,2} & \cdots & \left(\hat{t}_1'\right)_{2,n+1} \\ \vdots & \vdots & \ddots & \vdots \\ \left(\hat{t}_1'\right)_{p,1} & \left(\hat{t}_1'\right)_{p,2} & \cdots & \left(\hat{t}_1'\right)_{p,n+1} \end{bmatrix} \quad \text{and} \quad \left(\hat{\mathbf{T}}_2\right)_{,x} = \begin{bmatrix} \left(\hat{t}_2'\right)_{1,1} & \left(\hat{t}_2'\right)_{1,2} & \cdots & \left(\hat{t}_2'\right)_{1,n+1} \\ \left(\hat{t}_2'\right)_{2,1} & \left(\hat{t}_2'\right)_{2,2} & \cdots & \left(\hat{t}_2'\right)_{2,n+1} \\ \vdots & \vdots & \ddots & \vdots \\ \left(\hat{t}_2'\right)_{p,1} & \left(\hat{t}_2'\right)_{p,2} & \cdots & \left(\hat{t}_2'\right)_{p,n+1} \end{bmatrix}$$

$$\left(\hat{t}_1'\right)_{k,j} = \begin{cases} 0 & \text{for } x_k < x_i \quad \text{or } x_k > x_{i+1} \\ \left\{\dfrac{-3(x_{i+1}-x_k)^2}{\Delta x_i} + \Delta x_i\right\} & \text{for } x_i \le x_k \le x_{i+1} \quad \text{and} \quad j = i+1 \\ \left\{\dfrac{3(x_k-x_i)^2}{\Delta x_i} - \Delta x_i\right\} & \text{for } x_i \le x_k \le x_{i+1} \quad \text{and} \quad j = i+2 \end{cases},$$

and

$$\left(\hat{t}_2'\right)_{k,j} = \begin{cases} 0 & \text{for } x_k < x_i \quad \text{or } x_k > x_{i+1} \\ \dfrac{-1}{\Delta x_i} & \text{for } x_i \le x_k \le x_{i+1} \quad \text{and} \quad j = i+1 \\ \dfrac{1}{\Delta x_i} & \text{for } x_i \le x_k \le x_{i+1} \quad \text{and} \quad j = i+2 \end{cases} ,$$

Again, note that there are, at most, two nonzero coefficients in the $\left(\hat{\mathbf{T}}_1\right)_{,x}$ and $\left(\hat{\mathbf{T}}_2\right)_{,x}$ matrices. In this derivation, *x* has been used as the independent variable. However, in the context of the interface definition herein, *s* is the independent variable and is substituted for *x* in the derivation in Appendix C. For the displacement assumption, the matrices developed for equally spaced points were used. For the geometry assumption, matrices for unequally spaced points were used.

APPENDIX C

DERIVATION OF INTERFACE GEOMETRY

C.1. GENERAL

In the initial development outlined in reference 25, the interface path, Γ^I, was defined by piecewise linear segments. For curved interfaces, this definition only approximates the true curved geometry. The error in this approximation is a function of the interface path curvature and the number and location of the subdomain nodes along the interface. In addition, the interface path was computed along each subdomain independently, thus producing two different interface geometry definitions. For a structure with mild curvature, the error in the interface path definition did not influence the accuracy of the solution obtained in the analysis[25]. However, for problems with moderate to large curvature, this error may be large and adversely influence the accuracy of the interface element analysis.

In the present work, the element interface geometry is determined in one of two ways: (1) by specifying the function that represents the exact geometry of the interface (i.e., the linear interface is the trivial case) or (2) by passing a spline of the desired order (typically a cubic spline) through the specified coordinate data points to determine the function representing the geometry. In either case, the specified or computed function is parameterized and its first derivative is used to determine the arc length along the interface geometry of the subdomains as well as the interface boundary. Thus, in contrast to the earlier work, the interface geometry definition is a more accurate representation of

an arbitrarily curved geometry. In addition, only one interface path geometry is defined, and all the finite element nodes along that interface lie on that geometry.

For a curved geometry, the most general way of determining the interface path of the two approaches mentioned previously is by using the latter approach (i.e., passing a cubic spline through the specified coordinates). In this case, a smooth curve is fit to the set of spatial coordinates by computing three cubic spline functions (one for each coordinate direction) expressing the coordinates as functions of a chordal distance parameter. The derivatives of these functions are obtained by differentiating the interpolating function. These derivatives are used in the parametric definition for the length of the arc between two points to compute the arc length between each of the specified coordinates. The spatial coordinates of the finite element nodes along each subdomain boundary provide the input for the interface geometry definition. These nodal coordinates are used to construct the function representing the curved geometry and to determine the arc length of the path. The associated variable, *s*, is computed along the subdomain boundaries. The number of evenly-spaced pseudo-nodes is determined internally or from the used-specified value after which the path variable, *s*, is computed along the interface path. See Appendix B for a brief discussion of the cubic spline used as the basis for the geometry representation.

C.2. GEOMETRY REPRESENTATION

The arc length or interface path is derived in this appendix. The spatial coordinates of finite element node *i* are given by x_i, y_i, and z_i. The curve may be represented parametrically by

$$x = x(r)$$
$$y = y(r)$$
$$z = z(r)$$

where $r_i = \sqrt{(x_{i+1} - x_i)^2 + (y_{i+1} - y_i)^2 + (z_{i+1} - z_i)^2}$. Smooth cubic splines are fit through each of these coordinate functions. These coordinate functions are then expressed as

$$x(r) = \mathbf{T}\mathbf{x}_s$$
$$y(r) = \mathbf{T}\mathbf{y}_s$$
$$z(r) = \mathbf{T}\mathbf{z}_s$$

where **T** is a matrix of interpolation functions (see Eq. B.9 in Appendix B) and is evaluated at the points r_i. The vectors $\mathbf{x}_s$, $\mathbf{y}_s$, and $\mathbf{z}_s$ contain the sorted nodal coordinates, x_i, y_i, and z_i, along the interface (*i.e.*, the concatenation of the nodes from each of the subdomains to which the interface element is attached).

The length of the arc between each of the points along the interface may be calculated immediately as

$$s(r_i) = \int_{r_{i-1}}^{r_i} \sqrt{\left(\frac{dx}{dr}\right)^2 + \left(\frac{dy}{dr}\right)^2 + \left(\frac{dz}{dr}\right)^2}$$

and

$$\frac{dx}{dr} = x_{,r}(r) = \mathbf{T}_{,r}\,\mathbf{x}_s$$
$$\frac{dy}{dr} = y_{,r}(r) = \mathbf{T}_{,r}\,\mathbf{y}_s$$
$$\frac{dz}{dr} = z_{,r}(r) = \mathbf{T}_{,r}\,\mathbf{z}_s$$

where $\mathbf{T}_{,r}$ is obtained by differentiation of the interpolation matrix **T** with respect to the independent variable, *r*, (see Eq. B.10 in Appendix B) and is evaluated at points, r_i. The variable, *s*, is called the parameter of the arc length or the path variable herein. This variable measures the distance along the curve given by the parametric equations above. Thus, the arc length, $s(r_i)$ is obtained by numerical integration using Gaussian quadrature with four quadrature points. The path variable, as previously defined, is associated with the coordinates of the finite element nodes along the interface. The path variable, *s*, for the pseudo-nodes is computed by dividing the total arc length into equal segments. This total arc length is determined by summing the arc length between each set of two points, $r_{i\text{-}1}$ and r_i, over the total interface path to obtain the total arc length. In addition to the path variable, *s*, at the *j* pseudo-nodes, the coordinate location of these pseudo-nodes is also desired.

Moreover, in general, a computational coordinate frame is established along the interface; thus, the tangent to the interface path is desired. These calculations are addressed in the following discussion.

Upon obtaining the path variable at the finite element nodes along the interface, the coordinate functions may now be expressed as

$$x = x(s) = \mathbf{T}\mathbf{x}_s$$
$$y = y(s) = \mathbf{T}\mathbf{y}_s$$
$$z = z(s) = \mathbf{T}\mathbf{z}_s$$

Here, the interpolation matrix **T** is evaluated at the path coordinates, *s*, of the pseudo-nodes yielding desired *x*, *y*, and *z* coordinates. The unit tangent vector to the interface

path is obtained by differentiating the coordinate functions with respect to the path variable, *s*, and is given by

$$x_{,s}(s) = \mathbf{T}_{,s}\,\mathbf{x}_s$$
$$y_{,s}(s) = \mathbf{T}_{,s}\,\mathbf{y}_s$$
$$z_{,s}(s) = \mathbf{T}_{,s}\,\mathbf{z}_s$$

where $\mathbf{T}_{,s}$ is evaluated at the path coordinate, *s*, of the pseudo-nodes and the finite element nodes. The tangent vector is then given by

$$\mathbf{t}_{\mathrm{V}} = \frac{x_{,s}(s)}{\bar{r}}\hat{i} + \frac{y_{,s}(s)}{\bar{r}}\hat{j} + \frac{z_{,s}(s)}{\bar{r}}\hat{k}$$

where $\bar{r} = \sqrt{(x_{,s}(s))^2 + (y_{,s}(s))^2 + (z_{,s}(s))^2}$.

REFERENCES

1. Eringen, A. C., *Mechanics of Continua*, John Wiley & Sons, Inc., New York, 1967.

2. Frederick, D. and Chang, T. S., *Continuum Mechanics*, Scientific Publishers, Inc., Cambridge, Massachusetts, 1972.

3. Chadwick, P., *Continuum Mechanics - Concise Theory and Problems*, John Wiley & Sons, New York, 1976.

4. Hirch, C., *Numerical Computation of Internal and External Flows, Volume 1: Fundamentals of Numerical Discretization*, John Wiley & Sons, Inc., New York, 1988.

5. Ross, S. L., *Differential Equations*, Xerox College Publishing, Lexington, Massachusetts, 1964.

6. Malvern, L. E., *Introduction to the Mechanics of a Continuous Medium*, Prentice-Hall, Inc., Englewood Cliffs, New Jersey, 1969.

7. Finlayson, B. A., *The Method of Weighted Residuals and Variational Principles - With Application in Fluid Mechanics, Heat and Mass Transfer*, Academic Press, Inc, New York, 1972.

8. Ransom, J. B., *Global/Local Stress Analysis of Composite Structures*, M.S. Thesis, Department of Mechanical Engineering and Mechanics, Old Dominion University, 1989.

9. Ransom, J. B. and Knight, N. F., Jr., "Global/Local Stress Analysis of Composite Panels," *Computers and Structures*, Vol. 37, No. 4, 1990, pp. 375-395.

10. Rose, O. J., *Curvilinear Interface Methodology for Finite-Element Applications*, Ph.D. Dissertation, Department of Aerospace Engineering, Old Dominion University, 2000.

11. Wang, J. T., Housner, J. M., and Szewczyk, Z. P., "A Feasibility Study of Synthesizing Substructures Modeled with Computational Neural Networks," AIAA Paper No. 98-1778. *Proceedings of the AIAA/ASME/ASCE/AHS/ASC 39th Structures, Structural Dynamics, and Materials Conference*, April 20-23, 1998, Los Angeles, CA.

12. Whitcomb, J. D. and Kyeongsik, W., "Application of Iterative Global/Local Finite Element Analysis, Part 1: Linear Analysis," *Communications in Numerical Methods in Engineering*, Vol. 9, 1993, pp. 745-756.

13. Whitcomb, J. D. and Kyeongsik, W., "Application of Iterative Global/Local Finite Element Analysis, Part 2: Geometrically Nonlinear Analysis," *Communications in Numerical Methods in Engineering*, Vol. 9, 1993, pp. 757-766.

14. Knight, N. F., Jr., Ransom, J. B., Griffin, O. H., Jr., and Thompson, D. M., "Global/Local Methods Research Using a Common Structural Analysis Framework," *Finite Elements in Analysis and Design*, Vol. 9, 1991, pp. 91-112.

15. Krishnamurthy, T. and Raju, I. S., "Coupling Finite and Boundary Element Methods for Two-Dimensional Potential Problems," AIAA Paper No. 92-2240, *Proceedings of the AIAA/ASME/ASCE/AHS/ASC 33rd Structures, Structural Dynamics, and Materials Conference*, 1992, pp. 148-162.

16. Krishnamurthy, T. and Raju, I. S., "Coupling Finite and Boundary Element Methods for 2-D Elasticity Problems," AIAA Paper No. 93-1451, *Proceedings of the AIAA/ASME/ASCE/AHS/ASC 34th Structures, Structural Dynamics, and Materials Conference*, 1993, pp. 1274-1290.

17. Pates, C. S., Mei, C., and Shirahatti, U., "Coupled Boundary/Finite Element Methods for Random Structural-Acoustic Vibrations," AIAA Paper No. 95-1346, *Proceedings of the AIAA/ASME/ASCE/AHS/ASC 36th Structures, Structural Dynamics, and Materials Conference*, 1995, pp. 1569-1579.

18. Kao, P., "Coupled Rayleigh-Ritz/Finite Element Structural Analysis Using Penalty Function Method," AIAA Paper No. 92-2238, *Proceedings of the AIAA/ASME/ASCE/AHS/ASC 33rd Structures, Structural Dynamics, and Materials Conference*, 1992, pp. 135-139.

19. Holt, M. and Meade, A. J., Jr., "Flight Vehicle Aerodynamics Calculated by a Galerkin Finite Element/Finite Difference Method," *Computing Systems in Engineering*, Vol. 3, Nos. 1-4, 1992, pp. 413-421.

20. Dow, J. O., Hardaway, J. L., and Hamernik, J. D., "Combined Application of the Finite Element/Finite Difference Methods," AIAA Paper No. 92-2237, *Proceedings of the AIAA/ASME/ASCE/AHS/ASC 33rd Structures, Structural Dynamics, and Materials Conference*, 1992, pp. 129-134.

21. Rao, A. K., Raju, I. S., and Murty, A. V. K., "A Powerful Hybrid Method in Finite Element Analysis," *International Journal for Numerical Methods in Engineering*, Vol. 3, 1971, pp. 389-403.

22. Giles, G. L. and Norwood, R. K., "Coupling Equivalent Plate and Finite Element Formulations in Multiple-Method Structural Analyses," *AIAA Journal of Aircraft*, Vol. 31, No. 5, 1994, pp. 1189-1196.

23. Zienkiewicz, O. C., Kelly, D. W., and Peters, P., "The Coupling of the Finite Element Method and Boundary Solution Procedures," *International Journal for Numerical Methods in Engineering*, Vol. 11, 1977, pp. 355-375.

24. Housner, J. M. and Aminpour, M. A. , "Multiple Methods Integration for Structural Mechanics Analysis and Design," *First NASA Advanced Composites Technology Conference*, NASA CP 3104, Part 2, 1991, pp. 875-889.

25. Aminpour, M. A., Ransom, J. B., and McCleary, S. L., "A Coupled Analysis for Structures with Independently Modeled Finite Element Subdomains," *International Journal for Numerical Methods in Engineering*, Vol. 38, 1995, pp. 3695-3718.

26. Ransom, J. B., McCleary, S. L., and Aminpour, M. A., "A New Interface Element for Connecting Independently Modeled Substructures," AIAA Paper No. 93-1503, *Proceedings of the AIAA/ASME/ASCE/AHS/ASC 34th Structures, Structural Dynamics, and Materials Conference*, 1993, pp. 1693-1703.

27. Schiermeier, J. E., Housner, J. M., Ransom, J. B., Aminpour, M. A., and Stroud, W. J, "The Application of Interface Elements to Dissimilar Meshes in Global/Local Analysis," *Proceedings of the 1996 World MSC User's Conference, June 3-7, 1996*, Newport Beach, California.

28. Davilá, C. G., Ransom, J. B., and Aminpour, M. A., *Cross-Surface Interface Element for Coupling Built-up Structural Subdomains*, NASA TM-109125, 1994.

29. Ransom, J. B., "Interface Technology for Geometrically Nonlinear Analysis of Multiple Connected Subdomains," AIAA Paper No. 97-1298, *Proceedings of the AIAA/ASME/ASCE/AHS/ASC 38th Structures, Structural Dynamics, and Materials Conference*, 1997, pp. 1862-1872 .

30. Aminpour, M. A. and Krishnamurthy, T., "A Two-Dimensional Interface Element for Multi-Domain Analysis of Independently Modeled Three-Dimensional Finite Element Meshes," AIAA Paper No. 97-1297, *Proceedings of the AIAA/ASME/ASCE/AHS/ASC 38th Structures, Structural Dynamics, and Materials Conference*, 1997, pp. 1853-1861.

31. Schiermeier, J. E., Housner, J. M., Ransom, J. B., Aminpour, M. A., and Stroud, W. J, "Interface Elements in Global/Local Analysis - Part 2: Surface Interface Elements," *Proceedings of the 1997 World MSC User's Conference*, November 17-20, 1997, Newport Beach, California.

32. Reddy, J. N., *An Introduction to the Finite Element Method*, McGraw-Hill Book Company, New York, 1984.

33. Zienkiewicz, O. C, and Taylor, R. L., *The Finite Element Method-Volume 1: Basic Formulation and Linear Problems*, Third Edition, McGraw-Hill Book Company, UK, Vol. 1, 1989.

34. Cook, R. D., Malkus, D. S., and Plesha, M. E., *Concepts and Applications of Finite Element Analysis*, Third Edition, John Wiley & Sons, New York, 1989.

35. Zienkiewicz, O. C. and Onate, E., "Finite Volumes vs. Finite Elements. Is There Really a Choice?," *Nonlinear Computational Mechanics, State-of-the-Art*, P. Wriggers and W. Wagner (eds.), Springer-Verlag, Berlin, 1991, pp. 240-254.

36. Guruswamy, G. P., "Coupled Finite Difference/Finite Element Approach for Wing-Body Aeroelasticity," AIAA Paper No. 92-4680, *Proceedings of the Fourth AIAA/USAF/NASA/OIA Symposium on Multidisciplinary Analysis and Optimization*, 1992, pp. 1-12.

37. Zienkiewicz, O. C. and Morgan, K., *Finite Elements and Approximation*, John Wiley & Sons, New York, 1983.

38. Bracewell, R.N., *The Fourier Transform and Its Applications*, McGraw-Hill Book Company, New York, 1965, pp. 69-97.

39. Reissner, E., "Note on the Theorem of the Symmetry of the Stress Tensor," *Journal of Mathematics and Physics*, Vol. 23, 1944, pp. 192-194.

40. Carroll, M. M., "Foundations of Solid Mechanics," *Applied Mechanics Reviews*, Vol. 38, No. 10, 1985, pp. 1301-1308.

41. Reddy, J. N. and Gartling, D. K., *The Finite Element Method in Heat Transfer and Fluid Dynamics*, Boca Raton, FA, CRC Press, 1994.

42. Zienkiewicz, O.C., "The Finite Element Method: From Intuition to Generality," *Applied Mechanics Reviews*, Vol. 23, No. 3, 1970, pp. 249-256.

43. Dow, J. O., Jones, M. S., and Harwood, S. A, "A New Approach to Boundary Modelling for Finite Difference Applications in Solid Mechanics," *International Journal for Numerical Methods in Engineering*, Vol. 30, 1990, pp. 99-113.

44. Fenner, R.T., *Engineering Elasticity - Application of Numerical and Analytical Techniques*, Halstead Press, New York, 1986.

45. Dow, J. O., Jones, M. S., and Harwood, S. A., "A Generalized Finite Difference Method for Solid Mechanics," *Numerical Methods for Partial Differential Equations.* Vol. 6, No. 2, 1990, pp. 137-152.

46. Timoshenko, S. P. and Goodier, J. N., *Theory of Elasticity*, Third Edition, McGraw-Hill, New York, 1970.

47. Sololnikoff, I. S. and Redheffer, R. M., *Mathematics and Physics and Modern Engineering*, McGraw-Hill, New York, 1966.

48. Chapman, A. J., *Heat Transfer*, Third Edition, Macmillan, New York, 1974.

49. Howland, R. C. J., "On the Stresses in the Neighborhood of a Circular Hole in a Strip under Tension," *Philosophical Transactions of the Royal Society*, Series A, Vol. 229, 1930, pp. 49-86.

50. Peterson, R. E., *Stress Concentration Design Factors*, Wiley-International, New York, 1953, pp. 77-88.

51. Nadai, A., *Theory of Flow and Fracture of Solids*, Vol. 2, McGraw-Hill, New York, 1963.

52. Zienkiewicz, O. C and Taylor, R. L., *The Finite Element Method - Volume 2: Solid and Fluid Mechanics, Dynamics, and Nonlinearity*, Fourth Edition, McGraw-Hill Book Company, UK, 1991.

53. Smith, M. J., Cesnik, C. E., and Hodges, D. H., "An Evaluation of Computational Algorithms to Interface Between CFD and CSM Methodologies," AIAA Paper No. 96-1400, *Proceedings of the AIAA/ASME/ASCE/AHS/ASC 37th Structures, Structural Dynamics, and Materials Conference*, 1996, pp. 745-755.

54. Farhat, C., Lesoinne, M., and LeTallec, P., "Load and Motion Transfer Algorithms for Fluid/Structure Interaction Problems with Non-matching Discrete Interfaces: Momentum and Energy Conservation, Optimal Discretization and Application to Aeroelasticity," *Computer Methods in Applied Mechanics and Engineering*, Vol. 157, 1998, pp. 95-114.

55. Aminpour, M. A., Krishnamurthy, T., and Shin, Y., "Coupling of Independently Modeled Three-Dimensional Finite Element Meshes with Non-Matching Arbitrary Shape Interface Boundaries," AIAA Paper No. 99-1286, *Proceedings of the AIAA/ASME/ASCE/AHS/ASC 40th Structures, Structural Dynamics, and Materials Conference*, 1999, pp. 856-865.

56. Aminpour, M. A., Pageau, S., and Shin, Y., "An Alternative Method for Interface Modeling Technology," AIAA Paper No. 2000-1352, *Proceedings of the AIAA/ASME/ASCE/AHS/ASC 41st Structures, Structural Dynamics, and Materials Conference*, 2000, pp. 1-13.

57. Besant, C. B. and Lui, C. W., *Computer Aided Design and Manufacture*, Ellis Horwood Limited Publishing, West Sussex, England, 1986.

58. Deitz, D., "The Convergence of Design and Analysis," *Mechanical Engineering*, Vol. 119, No. 3, March 1997, pp. 93-100.

59. Poole, E. L., Knight, N. F., Jr.; and Davis, D. D., "High Performance Equation Solvers and Their Impact on the Finite Element Analysis," *International Journal for Numerical Methods in Engineering*, Vol. 33, No. 4, 1992, pp. 855-868.

60. Brussino, G. and Walczak, J., "Re-engineering CAE," *Mechanical Engineering*, Vol. 118, No. 7, July 1996, pp. 70-73.

61. Storaasli, O. O., Poole, E. L., Ortega, J., Cleary, A., and Vaughan, C., "Solution of Structural Analysis Problems on a Parallel Computer," AIAA Paper No. 88-2287, *Proceedings of the AIAA/ASME/ASCE/AHS/ASC 29th Structures, Structural Dynamics, and Materials Conference*, 1988, pp. 596-605.

62. Storaasli, O. O., "Performance of NASA Equation Solvers on Computational Mechanics Applications," AIAA Paper No. 96-1505, *Proceedings of the AIAA/ASME/ASCE/AHS/ASC 37th Structures, Structural Dynamics, and Materials Conference*, 1996, pp. 1680-1685.

63. Duff, I. S., "A Survey of Sparse Matrix Research," *Proceedings of the IEEE*, Vol. 65, No. 4, April 1977, pp. 500-535.

64. Golub, G. H. and Van Loan, C. F., *Matrix Computations*, The Johns Hopkins University Press, Maryland, 1989.

65. Ortega, J. M., *Introduction to Parallel and Vector Solution of Linear Systems*, Plenum Press, New York, 1988.

66. Noor, A., K., Venneri, S. L., Housner, J. M., and Peterson, J.C., "A Virtual Environment for Intelligent Design," *Aerospace America*, Vol. 35, No. 4, April 1997, pp. 28-30, 33-35.

67. Goldin, D. S., Venneri, S. L., and Noor, A. K., "A New Frontier in Engineering," *Mechanical Engineering*, Vol. 120, No. 2, February 1998, pp. 63-69.

68. National Research Council (NRC), *Advanced Engineering Environments: Achieving the Vision (Phase 1)*, Committee on Advanced Engineering Environments, National Academy Press, Washington, D.C., 1999.

REPORT DOCUMENTATION PAGE

Form Approved
OMB No. 0704-0188

Public reporting burden for this collection of information is estimated to average 1 hour per response, including the time for reviewing instructions, searching existing data sources, gathering and maintaining the data needed, and completing and reviewing the collection of information. Send comments regarding this burden estimate or any other aspect of this collection of information, including suggestions for reducing this burden, to Washington Headquarters Services, Directorate for Information Operations and Reports, 1215 Jefferson Davis Highway, Suite 1204, Arlington, VA 22202-4302, and to the Office of Management and Budget, Paperwork Reduction Project (0704-0188), Washington, DC 20503.

1. AGENCY USE ONLY (*Leave blank*)	2. REPORT DATE	3. REPORT TYPE AND DATES COVERED
	September 2001	Technical Memorandum

4. TITLE AND SUBTITLE
On Multifunctional Collaborative Methods in Engineering Science

5. FUNDING NUMBERS
WU 706-85-10-01

6. AUTHOR(S)
Jonathan B. Ransom

7. PERFORMING ORGANIZATION NAME(S) AND ADDRESS(ES)
NASA Langley Research Center
Hampton, VA 23681-2199

8. PERFORMING ORGANIZATION REPORT NUMBER
L-18104

9. SPONSORING/MONITORING AGENCY NAME(S) AND ADDRESS(ES)
National Aeronautics and Space Administration
Washington, DC 20546-0001

10. SPONSORING/MONITORING AGENCY REPORT NUMBER
NASA/TM-2001-211046

11. SUPPLEMENTARY NOTES
Dissertation submitted in partial fulfillment of the requirements for the degree of Doctor of Philosophy in Engineering Mechanics, Old Dominion University, Norfolk, Virginia, May 2001.

12a. DISTRIBUTION/AVAILABILITY STATEMENT
Unclassified-Unlimited
Subject Category 39 Distribution: Standard
Availability: NASA CASI (301) 621-0390

12b. DISTRIBUTION CODE

13. ABSTRACT *(Maximum 200 words)*
Multifunctional methodologies and analysis procedures are formulated for interfacing diverse subdomain idealizations including multi-fidelity modeling methods and multi-discipline analysis methods. These methods, based on the method of weighted residuals, ensure accurate compatibility of primary and secondary variables across the subdomain interfaces. Methods are developed using diverse mathematical modeling (i.e., finite difference and finite element methods) and multi-fidelity modeling among the subdomains. Several benchmark scalar-field and vector-field problems in engineering science are presented with extensions to multidisciplinary problems. Results for all problems presented are in overall good agreement with the exact analytical solution or the reference numerical solution. Based on the results, the integrated modeling approach using the finite element method for multi-fidelity discretization among the subdomains is identified as most robust. The multiple-method approach is advantageous when interfacing diverse disciplines in which each of the method's strengths are utilized.

14. SUBJECT TERMS
Global/Local Analysis; Multiple Domain Analysis; Engineering Science; Multidisicplinary Analysis; Finite Element and Finite Difference Methods

15. NUMBER OF PAGES
245

16. PRICE CODE
A11

17. SECURITY CLASSIFICATION OF REPORT	18. SECURITY CLASSIFICATION OF THIS PAGE	19. SECURITY CLASSIFICATION OF ABSTRACT	20. LIMITATION OF ABSTRACT
Unclassified	Unclassified	Unclassified	UL